博士論文

論文題目　Mathematical analysis and numerical methods for phase transformation and anomalous diffusion

（相転移と特異拡散に対する数学解析と数値解法について）

氏　　名　劉　逸侃（Yikan LIU）

Preface

Over the last few decades, numerous topics from industrious applications and issues on environmental protections have witnessed the increasing significance of underlying mathematical models. A considerable number among them can be expressed by partial differential equations, and the related fields such as system control and black box inference are mostly reduced to the corresponding inverse problems. The present dissertation concentrates on two kinds of evolution equations originating from respective backgrounds, that is,

- the multiple hyperbolic equations for phase transformation kinetics, and
- the multi-term time-fractional diffusion equations for anomalous diffusion phenomena.

Since both governing equations are recent generalizations of their hyperbolic and parabolic prototypes, we carry out systematic analysis from various viewpoints and develop the related numerical methods. The present researches are not only motivated by the theoretical interests, but also root in their direct applications in practices. The study of phase transformation is essential for understanding the material properties and controlling the manufacturing processes, and that of anomalous diffusion contributes to the modeling of the pollution mechanism as well as source identification and purification. Especially, by treating both topics simultaneously we will be able to investigate a series of complex phenomena of contaminants in heterogeneous medias, including dissolution, diffusion and accumulation.

Part I

Phase transformation phenomena occur extensively in many spontaneous and artificial processes, in which nucleation and crystallization greatly dominate the final mechanical properties. Part I is devoted to the reformulation and thorough analysis of the hyperbolic-type equations derived from Cahn's time cone model (see [17])

$$u(x,t) = \int_{\Omega_\rho(x,t)} \Psi(y,s)\,\mathrm{d}y\mathrm{d}s \quad (x \in \mathbb{R}^d,\ t \geq 0), \quad \text{where} \tag{0.1}$$

$$\Omega_\rho(x,t) := \{(y,s);\, 0 < s < t,\ |y-x| < R(t) - R(s)\}, \quad R(t) := \int_0^t \rho(s)\,\mathrm{d}s. \tag{0.2}$$

Here u, ρ and Ψ denote the expectation of transformation events, the growth speed and the nucleation rate, respectively. In Chapters 1–4, we shall investigate the forward problem and the reconstructions of ρ and Ψ from both theoretical and numerical aspects.

Chapter 1

The time cone model (0.1) involves multiple integrals, preventing us from smooth arguments on both forward and inverse problems. Hinted by d'Alembert's formula in the one-dimensional

case and the combination of Poisson's integral formula and Duhamel's principle in the three-dimensional case, in Chapter 1 we derive a class of equivalent formulations of (0.1) in all odd spatial dimensions.

Theorem 0.1 *Let the spatial dimensions $d = 2m+1$ $(m = 0, 1, \ldots)$ and $u(x,t)$ satisfy (0.1)–(0.2). Assume that $u(x,t)$, $\Psi(x,t)$ and $\rho(t)$ $(x \in \mathbb{R}^d,\ t \geq 0)$ are sufficiently smooth functions, and $\rho(t)$ is strictly positive for $t \geq 0$. Then $u(x,t)$ solves the following initial value problem for the multiple hyperbolic equation*

$$\begin{cases} \mathcal{H}_\rho^{m+1} u(x,t) = c_m\, \Psi(x,t)/\rho(t) & (x \in \mathbb{R}^d,\ t > 0), \\ \partial_t^\ell u(x,0) = 0 & (x \in \mathbb{R}^d,\ \ell = 0, 1, \ldots, d), \end{cases} \quad \textit{where} \tag{0.3}$$

$$\mathcal{H}_\rho w(x,t) := \frac{1}{\rho(t)}\, \partial_t \left(\frac{\partial_t w(x,t)}{\rho(t)} \right) - \triangle w(x,t), \quad c_m := (2m)!!\, 2^{m+1} \pi^m.$$

The above result is an immediate corollary to the governing equations of the auxiliary function $U(x,\tau) := u(x, R^{-1}(\tau))$ after the change of variable $\tau := R(t) (= \int_0^t \rho(s)\, \mathrm{d}s)$, which reads

$$\begin{cases} (\partial_\tau^2 - \triangle)^{m+1} U(x,\tau) = c_m \underbrace{\Psi(x, R^{-1}(\tau))/\rho(R^{-1}(\tau))}_{=:F(x,\tau)} & (x \in \mathbb{R}^{2m+1},\ \tau > 0), \\ \partial_\tau^\ell U(x,0) = 0, \quad \ell = 0, 1, \ldots, 2m+1 & (x \in \mathbb{R}^{2m+1}). \end{cases} \tag{0.4}$$

The derivations of (0.3) and (0.4) provide remarkable convenience in the quantitative analysis of the time cone model, and we outline the general strategy.

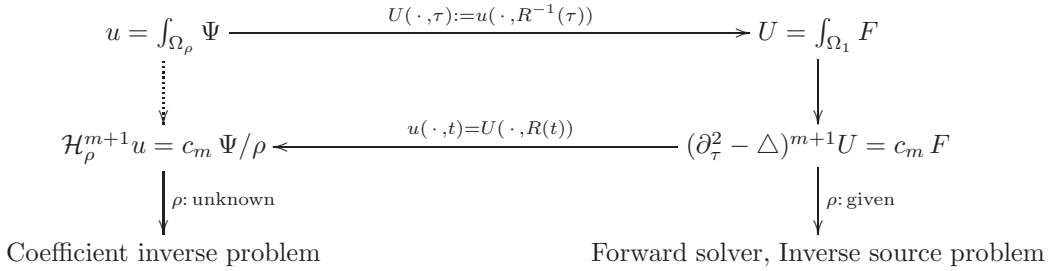

As the first application, we implement numerical simulations of forward problem for $d = 1, 3$ with satisfactory accuracy and efficiency by means of the alternating direction implicit method.

Chapter 2

In Chapter 2, we investigate an inverse problem of determining the growth speed $\rho(t)$ in the one-dimensional time cone model by the final observation data. By imposing the homogeneous Dirichlet boundary condition, the problem turns out to be the following coefficient inverse problem in view of the hyperbolic governing equation (0.3) with $m = 0$.

Problem 0.1 *Let $L > 0$, $T > 0$ be given, and u satisfy*

$$\begin{cases} \dfrac{1}{\rho(t)}\, \partial_t \left(\dfrac{\partial_t u(x,t)}{\rho(t)} \right) = \triangle u(x,t) + \dfrac{2\, \Psi(x,t)}{\rho(t)} & (0 < x < L,\ 0 < t \leq T), \\ u(x,0) = \partial_t u(x,0) = 0 & (0 < x < L), \\ u(0,t) = u(L,t) = 0 & (0 < t \leq T). \end{cases}$$

Provided that the nucleation rate Ψ is known, determine the growth speed ρ by the final measurements $y^\delta \in L^2(0,L)$ satisfying $\|y^\delta - u(\,\cdot\,, T)\|_{L^2(0,L)} \leq \delta$, where $\delta > 0$ is the noise level.

Using the eigensystem of $-\triangle$, we can write $u(\,\cdot\,,T)$ in form of $R(t)$ defined in (0.2). Since $\rho(t)=R'(t)$, this suggests a two-step reconstruction. First, we reconstruct $R(t)$ by the truncated Tikhonov-type regularization

$$R_\alpha^{M,N}:=\mathop{\arg\min}_{R\in\mathcal{P}_M}\frac{2}{L}\sum_{n=1}^{N}\left(\int_0^L\big(y^\delta(x)-u(x,T)\big)\sin\Big(\frac{\pi nx}{L}\Big)\,\mathrm{d}x\right)^2+\alpha\|R\|^2_{L^2(0,T)},$$

where $\alpha>0$ is the regularization parameter and $\mathcal{P}_M$ collects all polynomials with orders no higher than M. To seek for a minimizer, we solve the Euler equation by the pseudo-spectral method. Second, since the numerical differentiation is also ill-posed, we employ another regularization method to reconstruct the growth speed $\rho(t)$. Numerical prototype examples are presented to illustrate the validity and effectiveness of the proposed scheme.

Chapter 3

In view of the multiple hyperbolic equation (0.3) for phase transformation, the reconstruction of the nucleation rate $\Psi(x,t)$ turns out to be an inverse source problem. However, existing works on the related numerical methods are absent even for the single hyperbolic case. As a preparation, in Chapter 3 we develop an iterative method for the following problem.

Problem 0.2 *Let $\Omega\subset\mathbb{R}^d$ $(d=1,2,3)$ be open bounded with a smooth boundary, $\omega\subset\Omega$ and $T>0$ be suitably given, and $u(f)$ satisfy*

$$u(f)\begin{cases}\partial_t^2u(x,t)-\triangle u(x,t)=f(x)\,h(x,t) & (x\in\Omega,\ 0<t\le T),\\ u(x,0)=\partial_tu(x,0)=0 & (x\in\Omega),\\ \partial_\nu u(x,t)=0 & (x\in\partial\Omega,\ 0<t\le T).\end{cases}$$

Provided that h is known, determine f by the measurements of $u(f)$ in $\omega\times(0,T)$.

Under certain conditions on ω and T due to the finite wave speed and regularity assumptions on f and h, a global Lipschitz stability for the above problem is guaranteed (see [31]).

Numerically, we formulate the reconstruction as the following minimization problem

$$\min_{f\in L^2(\Omega)}J(f),\quad J(f):=\|u(f)-u^\delta\|^2_{L^2(\omega\times(0,T))}+\alpha\|f\|^2_{L^2(\Omega)},\tag{0.5}$$

where $\alpha>0$ is the regularization parameter and u^δ denotes the noisy data. By investigating the Euler equation for the minimizer, we propose the iteration

$$f_{m+1}=\frac{K}{K+\alpha}f_m-\frac{1}{K+\alpha}\int_0^T h\,z(f_m)\,\mathrm{d}t\quad(K>0,\ m=0,1,\ldots),\tag{0.6}$$

where $z(f_m)$ is the solution to the corresponding backward system. Abundant amounts of numerical experiments are presented to demonstrate the accuracy and efficiency of the algorithm.

Chapter 4

Chapter 4 establishes both theoretical stability and numerical method for the reconstruction of the nucleation rate Ψ in the three-dimensional time cone model, which is an inverse source problem for (0.3) with $m=1$. Assuming $\Psi(x,t)=f(x)\,g(x,t)$ and imposing the homogeneous Neumann boundary conditions, we formulate the problem as follows.

Problem 0.3 *Let $\Omega \subset \mathbb{R}^3$ be open bounded with a smooth boundary, $\omega \subset \Omega$ and $T > 0$ be suitably given, and $u(f)$ satisfy*

$$u(f)\begin{cases} \mathcal{H}_\rho^2 u(x,t) = f(x)\,h(x,t) & (x \in \Omega,\ 0 < t \le T), \\ \partial_t^\ell u(x,0) = 0 & (x \in \Omega,\ \ell = 0,1,2,3), \\ \partial_\nu u(x,t) = \partial_\nu \triangle u(x,t) = 0 & (x \in \partial\Omega,\ 0 < t \le T), \end{cases} \quad \text{where } h(x,t) := \frac{8\pi\, g(x,t)}{\rho(t)}. \tag{0.7}$$

Provided that g and ρ are known, determine f by the measurements of $u(f)$ in $\omega \times (0,T)$.

By a Carleman estimate in [31], we prove the following global Lipschitz stability.

Theorem 0.2 *Let $\partial\Omega$ be of C^3 class and u be the solution to (0.7), where $f \in L^2(\Omega)$,*

$$\begin{aligned} &g \in H^1(0,T;L^\infty(\Omega)) \text{ and } \exists\, g_0 > 0 \text{ such that } |g(\,\cdot\,,0)| \ge g_0 \text{ a.e. in } \Omega, \\ &\rho \in C^3[0,T] \text{ and } \exists\, \rho_0 > 0 \text{ such that } \rho \ge \rho_0 \text{ in } [0,T]. \end{aligned}$$

Suppose that ω is a subdomain of Ω such that

$$\begin{aligned} &\{x \in \partial\Omega;\, (x - x_0)\cdot\nu(x) \ge 0\} \subset \partial\omega \text{ for some } x_0 \notin \overline{\Omega \setminus \omega}\,, \quad \text{and} \\ &R(T) = \int_0^T \rho(t)\,\mathrm{d}t > \sup_{x\in\Omega} |x - x_0|. \end{aligned}$$

Then there exists a constant $C = C(\Omega,\omega,T,g,\rho) > 0$ such that

$$\|f\|_{L^2(\Omega)} \le C\left(\|\partial_t^4 u - \rho^2 \partial_t^2 \triangle u\|_{L^2(\omega\times(0,T))} + \|\partial_t u\|_{L^2(0,T;H^2(\omega))} + \sum_{k=2}^{3} \|\partial_t^k u\|_{L^2(\omega\times(0,T))} \right).$$

Based on the preparation in the previous chapter, without lose of generality we suppose $\rho(t) \equiv 1$ and propose the same minimization problem (0.5) for numerical treatments, which leads to a parallel iteration as (0.6). Extensive numerical experiments up to three spatial dimensions show the feasibility of the iteration, and detailed analysis of the computational performance are also provided.

Part II

Regarding the diffusion phenomena in highly heterogeneous medias, field experiments indicate a remarkable deviation from that described by the classical diffusion equation. As one candidate for modeling, the time-fractional diffusion equation with a Caputo derivative, for example,

$$\partial_t^\alpha u = \triangle u (+F) \quad \text{with} \quad \partial_t^\alpha f(t) := \frac{1}{\Gamma(1-\alpha)} \int_0^t \frac{f'(s)}{(t-s)^\alpha}\,\mathrm{d}s \ (0 < \alpha < 1),$$

has been studied intensively from various aspects (see, e.g., [121]). To improve the modeling accuracy, we generalize the above formulation to consider the following initial-boundary value problem for the multi-term time-fractional diffusion equation

$$\begin{cases} \displaystyle\sum_{j=1}^{m} q_j \partial_t^{\alpha_j} u(x,t) + \mathcal{A}u(x,t) = F(x,t) & (x \in \Omega,\ 0 < t \le T), \\ u(x,0) = a(x) & (x \in \Omega), \\ u(x,t) = 0 & (x \in \partial\Omega,\ 0 < t \le T), \end{cases} \tag{0.8}$$

where $\Omega \subset \mathbb{R}^d$ is open bounded with a smooth boundary, α_j, q_j $(j = 1, \dots, m)$ are positive constants such that $1 > \alpha_1 > \cdots > \alpha_m > 0$ and $q_1 = 1$, and $\mathcal{A}$ is a symmetric uniformly elliptic operator. Chapter 5 is devoted to the strong maximum principle and a related inverse source problem for $m = 1$, and Chapters 6–7 are concerned with the theoretical well-posedness and the numerical treatment for $m \geq 2$, respectively.

Chapter 5

The strong maximum principle is one of the remarkable characterizations of parabolic equations, which is expected to be partly inherited by fractional diffusion equations. Based on the corresponding weak maximum principle, in Chapter 5 we establish the following strong maximum principle for single-term time-fractional diffusion equations (i.e., (0.8) with $m = 1$), which is slightly weaker than that for the parabolic case.

Theorem 0.3 *Let $a \in L^2(\Omega)$ satisfy $a \geq 0$ and $a \not\equiv 0$, $F = 0$, and u be the solution to (5.1)–(5.3) with $m = 1$. Then for any $x \in \Omega$, the set $\{t > 0;\, u(x,t) \leq 0\}$ is at most a countable set which admits only ∞ as its possible accumulation point.*

Next, we consider an inverse source problem for (0.8) under the assumption that the inhomogeneous term F is in form of separation of variables.

Problem 0.4 *Let $x_0 \in \Omega$ and $T > 0$ be arbitrarily given, and u be the solution to (0.8) with $m = 1$, $a = 0$ and $F(x,t) = \rho(t)\, g(x)$, where $\rho \in C^1[0,T]$ and $g \in C_0^\infty(\Omega)$. Provided that g is known, determine $\rho(t)$ $(0 \leq t \leq T)$ by the single point observation data $u(x_0,t)$ $(0 \leq t \leq T)$.*

As a direct application of the obtained strong maximum principle, we give a uniqueness result for the above problem by assuming the positivity of the spatial component in the source term.

Theorem 0.4 *Under the same settings in the above problem, we further assume that $g \geq 0$ and $g \not\equiv 0$. Then $u(x_0,t) = 0$ $(0 \leq t \leq T)$ implies $\rho(t) = 0$ $(0 \leq t \leq T)$.*

Chapter 6

In Chapter 6, we investigate the well-posedness and the long-time asymptotic behavior of the solution to (0.8) for $m \geq 2$. First, by exploiting several important properties of multinomial Mittag-Leffler functions, various estimates follow from the explicit solution in form of these special functions.

Theorem 0.5 *Define the fractional power $\mathcal{A}^\gamma$ and spaces $\mathcal{D}(\mathcal{A}^\gamma)$ with $\gamma \geq 0$.*

(1) *Let $F = 0$ and $a \in \mathcal{D}(\mathcal{A}^\gamma)$ with $\gamma \in [0,1]$. Then there exist a unique solution to (0.8) and a constant $C > 0$ such that*

$$\begin{aligned} \|u(\,\cdot\,,t)\|_{H^2(\Omega)} &\leq C\|a\|_{\mathcal{D}(\mathcal{A}^\gamma)} t^{\alpha_1(\gamma-1)}, \\ \|\partial_t u(\,\cdot\,,t)\|_{L^2(\Omega)} &\leq C\|a\|_{\mathcal{D}(\mathcal{A}^\gamma)} t^{\alpha_1\gamma-1}, \end{aligned} \qquad 0 < t \leq T.$$

Moreover, if $\gamma > 0$, there holds for $0 < \beta < 1$ that

$$\|\partial_t^\beta u(\,\cdot\,,t)\|_{L^2(\Omega)} \leq C\|a\|_{\mathcal{D}(\mathcal{A}^\gamma)} t^{\alpha_1\gamma-\beta}, \quad 0 < t \leq T.$$

(2) *Let $a = 0$ and $F \in L^p(0,T;\mathcal{D}(\mathcal{A}^\gamma))$ with $p \in [1,\infty]$ and $\gamma \in [0,1]$. Then there exists a unique solution to (0.8) and a constant $C > 0$ such that*

$$\|u\|_{L^2(0,T;\mathcal{D}(\mathcal{A}^{\gamma+1}))} \leq C\|F\|_{L^2(0,T;\mathcal{D}(\mathcal{A}^\gamma))} \quad \text{if } p = 2,$$

$$\|u\|_{L^p(0,T;\mathcal{D}(\mathcal{A}^{\gamma+1-\epsilon}))} \le \frac{C}{\epsilon}\|F\|_{L^p(0,T;\mathcal{D}(\mathcal{A}^\gamma))} \quad \textit{for each } \epsilon \in (0,1] \textit{ if } p \neq 2.$$

Based on the above theorem, we further verify the Lipschitz continuous dependency of the solution to (0.8) with respect to $(\alpha_1, \ldots, \alpha_m)$, $(q_1, \ldots, q_m)$ and the diffusion coefficient in $\mathcal{A}$, which is fundamental for the optimization approach to the related coefficient inverse problem.

Second, by a Laplace transform argument, we show that the decay rate of the solution as $t \to \infty$ is given by the minimum order α_m.

Theorem 0.6 *Let u be the unique solution to (0.8) with $F = 0$ and $a \in L^2(\Omega)$. Then there exists a constant $C > 0$ such that*

$$\left\| u(\cdot\,, t) - \frac{q_m}{\Gamma(1-\alpha_m)} \frac{\mathcal{A}^{-1}a}{t^{\alpha_m}} \right\|_{H^2(\Omega)} \le \frac{C\|a\|_{L^2(\Omega)}}{t^{\min\{\alpha_{m-1}, 2\alpha_m\}}} \quad \textit{as } t \to \infty.$$

Chapter 7

Based on the results obtained in the previous chapter, in Chapter 7 we develop both semidiscrete and fully discrete Galerkin finite element methods (FEM) for problem (0.8) with $\mathcal{A} = -\triangle$.

Let X_h be a finite element space over a triangulation of Ω with a maximum diameter h. The semidiscrete Galerkin FEM for problem (0.8) is to find $\{u_h(t)\}_{0\le t\le T} \subset X_h$ such that

$$\begin{cases} \displaystyle\sum_{j=1}^{m} q_j \left(\partial_t^{\alpha_j} u_h(t), v_h\right) + (\nabla u_h(t), \nabla v_h) = (F_h(t), v_h), \quad \forall\, v_h \in X_h,\ 0 < t \le T, \\ u_h(0) = a_h, \end{cases} \tag{0.9}$$

where a_h and F_h stand for appropriate approximations of a and F according to their smoothness. By the discrete counterparts of refined estimates for the solution to (0.8), we deduce nearly optimal error estimates for the scheme (0.9).

Theorem 0.7 *Let u and u_h be the solutions to (0.8) and (0.9), respectively.*

(1) *Let $F = 0$ and $a \in \mathcal{D}(\mathcal{A}^\gamma)$ with $-1/2 < \gamma \le 1$. Then there exists a constant $C > 0$ such that for $0 < t \le T$,*

$$\begin{aligned} &\|u_h(t) - u(t)\|_{L^2(\Omega)} + h\|\nabla(u_h(t) - u(t))\|_{L^2(\Omega)} \\ &\le \begin{cases} C\,h^2\|a\|_{\mathcal{D}(\mathcal{A})}, & \gamma = 1, \\ C\,h^{2(1+\min(\gamma,0))}|\ln h|\|a\|_{\mathcal{D}(\mathcal{A}^\gamma)} t^{\alpha_1(\max(\gamma,0)-1)}, & -1/2 < \gamma \le 1/2. \end{cases} \end{aligned}$$

(2) *Let $a = 0$ and $F \in L^\infty(0,T;\mathcal{D}(\mathcal{A}^\gamma))$ with $-1/2 < \gamma \le 0$. Then there exists a constant $C > 0$ such that for $0 < t \le T$,*

$$\|u_h(t) - u(t)\|_{L^2(\Omega)} + h\|\nabla(u_h(t) - u(t))\|_{L^2(\Omega)} \le C\,h^{2(1+\gamma)}|\ln h|^2\|F\|_{L^\infty(0,t;\mathcal{D}(\mathcal{A}^\gamma))}.$$

By discretizing the Caputo derivatives in (0.9) with a step size $\tau > 0$, the fully discrete Galerkin FEM is to approximate the solution to (0.8) at knots $\{t_\ell\}_{\ell=0}^{N_t}$ in time.

Theorem 0.8 *Let $a \in \mathcal{D}(\mathcal{A})$, $F \in L^\infty(0,T;\mathcal{D}(\mathcal{A}^{1/2}))$ and $\{u_h^\ell\}_{\ell=0}^{N_t} \subset X_h$ be the solution to the fully discrete scheme. Suppose that the solution u to (0.8) is sufficiently smooth. Then there exists a constant $C > 0$ such that*

$$\begin{aligned} \|u_h^\ell - u(t_\ell)\|_{L^2(\Omega)} \le C \Bigg\{ & h^2 \left(\|a\|_{\mathcal{D}(\mathcal{A})} + \|F\|_{L^\infty(0,t_\ell;\mathcal{D}(\mathcal{A}^{1/2}))} + \max_{0\le t\le t_\ell} \|\partial_t u(t)\|_{\mathcal{D}(\mathcal{A})} \right) \\ & + \tau^{2-\alpha_1} \max_{0\le t\le t_\ell} \|\partial_t^2 u(t)\|_{L^2(\Omega)} \Bigg\}, \quad \ell = 1, \ldots, N_t. \end{aligned}$$

Finally, abundant numerical experiments for one- and two-dimensional problems confirm the above convergence rates.

January 9, 2015
The University of Tokyo

Yikan Liu

Acknowledgements

First, the author would like to attribute his sincerest gratitude to Prof. Masahiro Yamamoto, his supervisor as well as mentor, who has furnished selfless instructions and successive encouragements to the author in spite of his business. The author has benefited a lot not only from his conviction and attitude toward academic researches, but also from his foresight and enthusiasm on multidisciplinary collaborations. The inculcation of Prof. Yamamoto will definitely become invaluable treasures that the author should cherish forever in order to be a decent researcher in mathematics.

Second, I am grateful to the faculty members of Graduate School of Mathematical Sciences, The University of Tokyo, whose profound erudition on various branches of mathematics has kept impressing the author during his master's and doctoral programs. The author also appreciates the instructive discussions and helpful communications with those related to Prof. Yamamoto's laboratory, especially Dr. Kenichi Sakamoto, Dr. Masaaki Uesaka, Dr. Atsushi Kawamoto, Mr. Kenichi Fujishiro and Mr. Yuta Fukasawa.

Next, the author would like to give heartfelt thanks to his colleagues, who share their expertise and diligence in pursuit of high qualities of the joint works. Chapter 2 is based on the joint paper [48] with Dr. Xiang Xu (Zhejiang University). Chapters 3–4 are based on yet unpublished works with Dr. Daijun Jiang (Central China Normal University). Chapter 6 is based on the joint paper [88] with Mr. Zhiyuan Li (The University of Tokyo). Chapter 7 is based on the joint paper [78] with Dr. Bangti Jin (University College London), Prof. Raytcho Lazarov and Mr. Zhi Zhou (Texas A&M University). Also, special thanks should go to Prof. Jin Cheng (Fudan University), the author's former supervisor, who provided him with the opportunity to study in Japan and has given consistent cares. The author also thanks members of the inverse problem group in Fudan University, especially Prof. Wenbin Chen and Prof. Shuai Lu, for valuable discussions.

The author has been financially supported by China Scholarship Council and Program for Leading Graduate Schools (MEXT, Japan). Thanks to the long-term overseas visits supported by the latter, the author benefited a lot from Prof. William Rundell (Texas A&M University), Prof. Dr. Dietmar Hömberg (WIAS) and Prof. Dr. Yuri Luchko (Beuth Hochschule für Technik Berlin). The author also appreciates the discussions with Prof. Dr. Matthias Hieber and Prof. Dr. Herbert Egger during his visit to TU Darmstadt supported by Japanese-German Graduate Externship. The author thanks Prof. Yoshihiro Shibata (Waseda University) and Prof. Yoshikazu Giga (The University of Tokyo) for arranging the stay in Darmstadt by the program.

Last but not least, the author is deeply indebted to his beloved family, especially his parents, for their warm considerations and great supports all through these years regardless of the distance. They have raised up the author to overcome difficulties and obstacles on his road to advance.

Contents

Part I

Multiple Hyperbolic Equations for Phase Transformation

Chapter 1

Derivation and Numerical Simulations of the Multiple Hyperbolic Equations

We discuss Cahn's time cone method modeling phase transformation kinetics. The model equation by the time cone method is an integral equation in the space-time region. First we reduce it to a class of hyperbolic equations, and in the case of odd spatial dimensions, the reductions turn out to be initial value problems for multiple hyperbolic equations. Next we propose a numerical method for these hyperbolic-type equations. By means of the alternating direction implicit method, numerical simulations for practical forward problems are implemented with satisfactory accuracy and efficiency. In particular, in the three-dimensional case, our numerical method is extremely fast on the basis of the reduced double hyperbolic equation.

1.1 Introduction

Phase transformations such as the crystallization of liquids and materials are important kinetics arising in both spontaneous phenomena and artificial processes. In such transformations, nucleation and structure growth consist of the most determinant kinetics which greatly characterize the final mechanical properties. In retrospect, the earliest stochastic modeling of the phase transformation can trace back to Johnson-Mehl-Avrami-Kolmogorov theory (usually abbreviated as JMAK theory, see Kolmogorov [43], Johnson and Mehl [39] and Avrami [2–4]). These pioneering works were concerned with an infinite specimen without transformation initially, in which the random events of generation were expected to follow the Poisson distribution. Hence the fraction of phase transformations reads

$$P = 1 - \mathrm{e}^{-u}, \tag{1.1}$$

where u denotes the expectation of the generation events. More importantly, newborn nuclei were assumed to appear randomly in the remaining untransformed space with a constant expected nucleation rate, and each nucleus was supposed to grow radially at a constant speed until impingement.

Efforts on extending the original JMAK theory have then been devoted extensively in the last several decades (see, e.g., [16,36,37]), and one of the most remarkable works should be attributed to Cahn [17], which inherits the Poisson distribution assumption on generation events but

greatly polishes the model of nuclei growth. More precisely, instead of constants the nucleation rate is allowed to be time- and space-dependent while the growth speed can be time-dependent, written as $\Psi(x,t)$ and $\rho(t)$ respectively. With these settings, in general spatial dimensions the expectation of generation events is modeled as

$$u(x,t) = \int_{\Omega_\rho(x,t)} \Psi(y,s)\,\mathrm{d}y\mathrm{d}s \quad (x \in \mathbb{R}^d,\ t \geq 0), \tag{1.2}$$

where $\Omega_\rho(x,t)$ denotes the so-called "time cone" defined as

$$\Omega_\rho(x,t) := \{(y,s);\, 0 < s < t,\ |y-x| < R(t) - R(s)\}, \quad R(t) := \int_0^t \rho(s)\,\mathrm{d}s. \tag{1.3}$$

Obviously, $R(t) - R(s) = \int_s^t \rho(\tau)\,\mathrm{d}\tau$ stands for the radius of a transformed domain at time t generated by a nucleus which was born at time s without impingement. Therefore, a time cone $\Omega_\rho(x,t)$ can be physically interpreted as the ensemble of all pairs (y,s) which would have caused transformation at (x,t). Especially, when Ψ, ρ are positive constants and $d = 3$, the phase transformation fraction can be easily calculated from (1.2) and (1.1), yielding the well-known JMAK equation

$$P(x,t) = 1 - \exp\left(-\pi\Psi\rho^3 t^4/3\right). \tag{1.4}$$

For an intuitive understanding of time cones, see Figure 1.1. As subsequent researches after Cahn's time cone method, we refer to [5, 54].

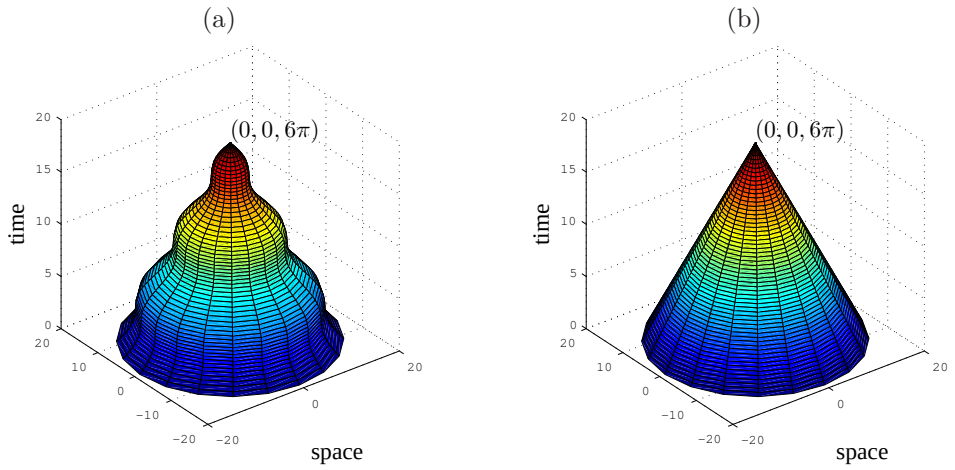

Figure 1.1: Examples of the two-dimensional time cones $\Omega_\rho(x,t)$ with $x = (0,0)$ and $t = 6\pi$, generated by different growth speeds. (a) $\rho(t) = 1 + 0.9\cos t$. (b) $\rho(t) \equiv 1$.

Although models on phase transformation kinetics have been well established and have been widely utilized in industry, mathematical considerations on related forward and inverse problems are limited. To the best of our knowledge, only a similar but parallel concept named "causal cone" approach was proposed to study the morphology of crystalline polymeric systems, upon which several forward problems were investigated (see [12, 13, 15, 21, 24, 26, 50]). For a comprehensive collection of mathematical topics on the polymer processing, we refer to Capasso [19].

As will be explained later, the time cone model (1.2)–(1.3) in its original expression is difficult to handle because it involves multiple integrations. Therefore, the purpose of this chapter is to develop an alternative formulation describing Cahn's model which provides convenient methods

for the discussion of both forward and inverse problems. Here by forward problems we mainly refer to finding u by (1.2) with given Ψ and ρ as well as suitable initial and boundary values, while inverse problems stand for the determination of Ψ or ρ by partial observations of u. The derived equivalent representations turn out to be a class of multiple hyperbolic systems, in the most concise forms only in odd spatial dimensions. Consequently, such treatment allows direct applications of abundant existing results concerning hyperbolic equations. We shall demonstrate the dramatically efficient forward solver in this chapter and deal with several inverse problems in the forthcoming chapters.

The rest of this chapter is organized as follows. In Section 1.2, we briefly mention the motivation to find hyperbolic alternatives of Cahn's model (1.2)–(1.3) and state the main result, which proof is given in Section 1.3. Section 1.4 shows numerical simulations of the forward problem in practical dimensions, and Section 1.5 gives concluding remarks and prospections of future works. Finally, proofs of technical lemmata are postponed to Appendix 1.A.

1.2 Motivation and the main result

From now on we concentrate on Cahn's time cone model (1.2)–(1.3), which takes the form of an integral equation. More precisely, the nucleation rate $\Psi(x,t)$ acts as the integrand function, and the growth speed $\rho(t)$ is embedded in the domain of integration. Therefore, although the solution u is explicitly expressed in (1.2), in view of numerical treatments of forward problems it involves a $(d+1)$-dimensional numerical integration to approximate u only for a single pair (x,t), not to mention the tremendous computational complexity in practice. On the other hand, note that the profile of a time cone $\Omega_\rho(x,t)$ becomes irregular when the growth speed is no longer a constant (compare Figure 1.1(a) and Figure 1.1(b)). Thus it is also inconvenient to investigate corresponding inverse problems based on such an integral equation with a complicated domain of integration. These difficulties indicate the necessity to replace the original formulation by an equivalent time-evolutionary governing system, where Ψ and ρ are directly attainable.

In fact, such consideration is motivated by a first observation when $d = 1$ and ρ is a constant, in which case equation (1.2) takes the exact form of d'Alembert's formula

$$u(x,t) = \int_0^t \int_{x-\rho(t-s)}^{x+\rho(t-s)} \Psi(y,s)\,\mathrm{d}y\mathrm{d}s.$$

In other words, providing certain regularity $\Psi \in C^{0,1}(\mathbb{R}\times\mathbb{R}_+)$, the function $u(x,t)$ should satisfy an inhomogeneous wave equation with homogeneous initial condition

$$\begin{cases} (\partial_t^2 - \rho^2\,\partial_x^2)u(x,t) = 2\rho\,\Psi(x,t) & (x\in\mathbb{R},\ t>0), \\ u(x,0) = \partial_t u(x,0) = 0 & (x\in\mathbb{R}). \end{cases}$$

Furthermore, obviously the growth speed and the nucleation rate play the roles of the propagation speed of wave and the source term (up to a multiplier) respectively. As a result, there is sufficient evidence to expect hyperbolic-type governing equations with respect to u with time-dependent ρ in higher spatial dimensions.

Now we state the main conclusion of the derived systems.

Theorem 1.1 (Multiple hyperbolic equations) *Let the spatial dimensions $d = 2m+1$ ($m = 0,1,\ldots$) and $u(x,t)$ satisfy (1.2)–(1.3). Assume that $u(x,t)$, $\Psi(x,t)$ and $\rho(t)$ ($x\in\mathbb{R}^d$, $t\geq 0$) are sufficiently smooth functions, and $\rho(t)$ is strictly positive for $t\geq 0$. Introduce the hyperbolic*

operator

$$\mathcal{H}_\rho w(x,t) := \frac{1}{\rho(t)}\,\partial_t\left(\frac{\partial_t w(x,t)}{\rho(t)}\right) - \triangle w(x,t).$$

Then $u(x,t)$ solves the following initial value problem for the multiple hyperbolic equation

$$\begin{cases} \mathcal{H}_\rho^{m+1} u(x,t) = (2m)!!\, 2^{m+1}\pi^m\, \Psi(x,t)/\rho(t) & (x\in\mathbb{R}^d,\ t>0), \\ \partial_t^\ell u(x,0) = 0, \quad \ell = 0,1,\dots,d & (x\in\mathbb{R}^d). \end{cases} \tag{1.5}$$

Remark 1.1 (a) From the physical interpretation of the nucleation rate, we have $\Psi(x,t)\ge 0$ and thus $u(x,t)$ should be non-negative by (1.2). However such non-negativity is not used in this chapter.

(b) On the other hand, for simplicity we assume that Ψ, ρ and u are sufficiently smooth. In fact, if $\rho\in C^d[0,T]$ and $\Psi\in L^2(\mathbb{R}^d\times(0,T))$ for some $T>0$, then by a priori estimates (e.g., Lions and Magenes [47]) and the multiple hyperbolic system (1.5), we can establish the corresponding regularity of u in Sobolev spaces, but here we do not discuss the details.

It is readily seen that $\mathcal{H}_\rho$ is a hyperbolic operator with a damping term and the propagation speed of wave is indeed $\rho(t)$. Actually, in the next section we can find a change of variable in time by which $\mathcal{H}_\rho$ corresponds to the d'Alembertian with respect to the new time axis. For any odd d, the above theorem indicates that the integral in the d-dimensional time cone model (1.2) can be completely eliminated by acting $(d+1)/2$ times of the operator $\mathcal{H}_\rho$ to both sides. For instance, taking $m=0,1$ in Theorem 1.1, we obtain a single hyperbolic governing equation

$$\mathcal{H}_\rho u(x,t) = \frac{\partial_t^2 u(x,t)}{\rho^2(t)} - \frac{\rho'(t)\,\partial_t u(x,t)}{\rho^3(t)} - \partial_x^2 u(x,t) = \frac{2\,\Psi(x,t)}{\rho(t)} \quad (x\in\mathbb{R},\ t>0)$$

for $d=1$, and an interesting double hyperbolic governing equation

$$\begin{aligned} \mathcal{H}_\rho^2 u(x,t) = {} & \frac{\partial_t^4 u(x,t)}{\rho^4(t)} - \frac{6\,\rho'(t)\,\partial_t^3 u(x,t)}{\rho^5(t)} - \frac{\{4\,\rho(t)\rho''(t) - 15\,(\rho'(t))^2\}\,\partial_t^2 u(x,t)}{\rho^6(t)} \\ & - \frac{\{\rho^2(t)\rho'''(t) - 10\,\rho(t)\rho'(t)\rho''(t) + 15\,(\rho'(t))^3\}\,\partial_t u(x,t)}{\rho^7(t)} \\ & - \frac{2\,\partial_t^2\triangle u(x,t)}{\rho^2(t)} + \frac{2\,\rho'(t)\,\partial_t\triangle u(x,t)}{\rho^3(t)} + \triangle^2 u(x,t) \\ = {} & \frac{8\pi\,\Psi(x,t)}{\rho(t)} \quad (x\in\mathbb{R}^3,\ t>0) \end{aligned}$$

for $d=3$. Moreover, in these multiple hyperbolic systems, Ψ/ρ appears explicitly as the source term (up to a multiplier), and the initial conditions are always homogeneous. Unfortunately, such concise expressions as (1.5) are unavailable for any even d. In these cases, it can be inferred from Proposition 1.1 that at best $\mathcal{H}_\rho^{d/2}u$ equals $d/2$ terms of integrals concerning Ψ and ρ which cannot be further canceled. As will be witnessed in Section 1.4, this drawback remains certain inconvenience even in the numerical simulation of the two-dimensional forward problem. The apparent difference between odd and even dimensions can be explained by Huygens' principle (see Remark 1.2 in Section 1.3).

1.3 Proof of the main result

In order to deal with the physical model (1.2)–(1.3) in general spatial dimensions, we start from some overall settings. Throughout this section we adopt the smoothness and positivity

assumptions on Ψ and ρ in Theorem 1.1. Denote $x = (x_1, \dots, x_d) \in \mathbb{R}^d$ and let

$$B_d(x,r) := \{y \in \mathbb{R}^d;\, |y-x| < r\}, \quad S_d(x,r) := \partial B_d(x,r)$$

be the open ball and the corresponding sphere centered at x with radius $r > 0$. Then equation (1.2) becomes

$$u(x,t) = \int_0^t \int_{B_d(x,R(t)-R(s))} \Psi(y,s)\,\mathrm{d}y\mathrm{d}s \quad (x \in \mathbb{R}^d,\ t \geq 0). \tag{1.6}$$

Recall that $\rho(t)$ is not a constant in general which generates the irregularity of the domain $\Omega_\rho(x,t)$ of integration. However, this difficulty can be overcome by introducing the change of variable in time

$$\tau = R(t) = \int_0^t \rho(s)\,\mathrm{d}s \quad (t \geq 0), \tag{1.7}$$

which is also adopted in Cannon [18] to treat parabolic equations. Thanks to the strict positivity of ρ, the function $R(t)$ is nonnegative and strictly increasing for $t \geq 0$, allowing a well-defined inverse function $t = R^{-1}(\tau)$ for $\tau \geq 0$. Moreover, it turns out from taking derivative in the identity $R(R^{-1}(\tau)) = \tau$ that $(R^{-1}(\tau))' = 1/\rho(R^{-1}(\tau))$. Therefore, performing the same change of variable in the integral on its right-hand side, we further simplify (1.6) as

$$U_0(x,\tau) := u(x,R^{-1}(\tau)) = \int_0^\tau \int_{B_d(x,\tau-\zeta)} \frac{\Psi(y,R^{-1}(\zeta))}{\rho(R^{-1}(\zeta))}\,\mathrm{d}y\mathrm{d}\zeta \quad (x \in \mathbb{R}^d,\ \tau \geq 0). \tag{1.8}$$

Consequently, it is convenient to consider $U_0(x,\tau)$ instead of $u(x,t)$ hereinafter since now the integration is taken in a regular cone $\Omega_1(x,\tau)$ with vertex (x,τ) and unit slope (see Figure 1.1(b)). In fact, for any smooth function w in $\mathbb{R}^d \times [0,\infty)$, we discover by simple calculations that the same change of variable (1.7) and the definition $W(x,\tau) := w(x,R^{-1}(\tau))$ give

$$\partial_\tau^2 W(x,\tau) = \frac{1}{\rho(t)}\,\partial_t \left(\frac{\partial_t w(x,t)}{\rho(t)} \right)\Big|_{t=R^{-1}(\tau)}, \quad \partial_\tau W(x,0) = \frac{\partial_t w(x,0)}{\rho(0)},$$

or equivalently, by taking $\tau = R(t)$ and recalling the operator $\mathcal{H}_\rho$ in Theorem 1.1,

$$\begin{cases} \mathcal{H}_\rho w(x,t) = \Box W(x,R(t)) & (x \in \mathbb{R}^d,\ t > 0), \\ w(x,0) = W(x,0),\ \partial_t w(x,0) = \rho(0)\,\partial_\tau W(x,0) & (x \in \mathbb{R}^d), \end{cases} \tag{1.9}$$

where $\Box := \partial_\tau^2 - \triangle$ denotes the d'Alembertian with τ as the time variable.

For later convenience, we denote by σ_d the surface area of the d-dimensional unit ball, and write $F(x,\tau) := \Psi(x,R^{-1}(\tau))/\rho(R^{-1}(\tau))$ for simplicity. Then we introduce the following integral brackets for $\ell, j = 0, 1, \dots$, $x \in \mathbb{R}^d$ and $\tau > 0$ that

$$[\ell, S_d, \triangle^j](x,\tau) := \int_0^\tau \int_{S_d(x,\tau-\zeta)} \frac{\triangle^j F(y,\zeta)}{(\tau-\zeta)^\ell}\,\mathrm{d}\sigma\mathrm{d}\zeta \quad (\ell \leq d-1), \tag{1.10}$$

$$[\ell, B_d, \triangle^j](x,\tau) := \int_0^\tau \int_{B_d(x,\tau-\zeta)} \frac{\triangle^j F(y,\zeta)}{(\tau-\zeta)^\ell}\,\mathrm{d}y\mathrm{d}\zeta \quad (\ell \leq d). \tag{1.11}$$

The restriction on ℓ guarantees the well-posedness of the above definitions, that is, there is no singularity near $\tau = 0$. Furthermore, by the smoothness assumption and an averaging argument, we find

$$\lim_{\tau \downarrow 0} [\ell, S_d, \triangle^j](x,\tau) = 0 \ (\ell \leq d-1), \quad \lim_{\tau \downarrow 0} [\ell, B_d, \triangle^j](x,\tau) = 0 \ (\ell \leq d),$$

which allows the redefinition

$$[\ell, S_d, \triangle^j](x,0) = 0 \ (\ell \le d-1), \quad [\ell, B_d, \triangle^j](x,0) = 0 \ (\ell \le d). \tag{1.12}$$

Now we relate the two brackets by differential operations.

Lemma 1.1 *Let the spatial dimensions $d \ge 2$, $\ell = 0, 1, \ldots, d-1$ and $j = 0, 1, \ldots$. Let $[\ell, S_d, \triangle^j](x,\tau)$ and $[\ell, B_d, \triangle^j](x,\tau)$ $(x \in \mathbb{R}^d,\ \tau > 0)$ be defined as in* (1.10) *and* (1.11) *respectively. Then*

$$\triangle[\ell, S_d, \triangle^j] = [\ell, S_d, \triangle^{j+1}], \quad \triangle[\ell, B_d, \triangle^j] = [\ell, B_d, \triangle^{j+1}], \tag{1.13}$$

$$\partial_\tau[\ell, S_d, \triangle^j] = \begin{cases} (d-\ell-1)\,[\ell+1, S_d, \triangle^j] + [\ell, B_d, \triangle^{j+1}] & (\ell < d-1), \\ \sigma_d\, \triangle^j F + [d-1, B_d, \triangle^{j+1}] & (\ell = d-1), \end{cases} \tag{1.14}$$

$$\partial_\tau[\ell, B_d, \triangle^j] = -\ell\,[\ell+1, B_d, \triangle^j] + [\ell, S_d, \triangle^j]. \tag{1.15}$$

The proof involves only elementary calculations and it will be given in Appendix 1.A. Now we are able to state the first conclusion.

Lemma 1.2 (Single hyperbolic systems) *Let $d = 1, 2, \ldots$. Then*
(a) *$U_0(x,\tau)$ defined in* (1.8) *satisfies*

$$\begin{cases} \Box U_0(x,\tau) = \begin{cases} 2\,F(x,\tau) & (d=1), \\ (d-1)\,U_1(x,\tau) & (d \ge 2) \end{cases} & (x \in \mathbb{R}^d,\ t > 0), \\ U_0(x,0) = \partial_\tau U_0(x,0) = 0 & (x \in \mathbb{R}^d), \end{cases} \tag{1.16}$$

where

$$U_1(x,\tau) := [1, S_d, \triangle^0](x,\tau) \quad (d \ge 2). \tag{1.17}$$

(b) *$u(x,t)$ in* (1.6) *satisfies*

$$\begin{cases} \mathcal{H}_\rho u(x,t) = \begin{cases} 2\,\Psi(x,t)/\rho(t) & (d=1), \\ (d-1)\,U_1(x,R(t)) & (d \ge 2) \end{cases} & (x \in \mathbb{R}^d,\ t > 0), \\ u(x,0) = \partial_t u(x,0) = 0 & (x \in \mathbb{R}^d). \end{cases} \tag{1.18}$$

Proof. (a) For $d = 1$, we return to the original definition (1.8) and write

$$U_0(x,\tau) = \int_0^\tau \int_{x-(\tau-\zeta)}^{x+(\tau-\zeta)} F(y,\zeta)\,\mathrm{d}y\mathrm{d}\zeta,$$

following the fundamental differentiations

$$\begin{aligned} \partial_x U_0(x,\tau) &= \int_0^\tau (F(x+(\tau-\zeta),\zeta) - F(x-(\tau-\zeta),\zeta))\,\mathrm{d}\zeta, \\ \partial_x^2 U_0(x,\tau) &= \int_0^\tau (\partial_x F(x+(\tau-\zeta),\zeta) - \partial_x F(x-(\tau-\zeta),\zeta))\,\mathrm{d}\zeta, \\ \partial_\tau U_0(x,\tau) &= \int_0^\tau (F(x+(\tau-\zeta),\zeta) + F(x-(\tau-\zeta),\zeta))\,\mathrm{d}\zeta, \\ \partial_\tau^2 U_0(x,\tau) &= 2\,F(x,\tau) + \int_0^\tau (\partial_x F(x+(\tau-\zeta),\zeta) - \partial_x F(x-(\tau-\zeta),\zeta))\,\mathrm{d}\zeta \\ &= \partial_x^2 U_0(x,\tau) + 2\,F(x,\tau). \end{aligned}$$

On the other hand, the homogeneous initial condition is easily checked for $d = 1$.

Considering dimensions $d \geq 2$, we recognize $U_0(x,\tau) = [0, B_d, \triangle^0](x,\tau)$ and apply Lemma 1.1 with $\ell = j = 0$ to obtain

$$\begin{aligned}\partial_\tau U_0(x,\tau) &= \partial_\tau [0, B_d, \triangle^0](x,\tau) = [0, S_d, \triangle^0](x,\tau),\\ \partial_\tau^2 U_0(x,\tau) &= \partial_t [0, S_d, \triangle^0](x,\tau) = (d-1)\,[1, S_d, \triangle^0](x,\tau) + [0, B_d, \triangle^1](x,\tau)\\ &= \triangle U_0(x,\tau) + (d-1)\,U_1(x,\tau).\end{aligned}$$

Simultaneously, it follows from (1.12) that the initial condition is still homogeneous for $d \geq 2$. This completes the verification of (1.16).

(b) The substitution of $w = u$ and $W = U_0$ in relation (1.9) yields (1.18) immediately from the above result. □

Remark 1.2 The above lemma demonstrates Theorem 1.1 for $d = 1$ and suggests an inductive approach to higher dimensions. Although one may apply a d'Alembertian once more to $U_1(x,\tau)$ for $d \geq 3$ to obtain similar wave equations, another observation provides a straightforward reasoning. Write

$$U_1(x,\tau) = \int_0^\tau V_1(x,\tau;\zeta)\,\mathrm{d}\zeta \quad \text{with} \tag{1.19}$$

$$V_1(x,\tau;\zeta) := \frac{1}{\tau-\zeta}\int_{S_d(x,\tau-\zeta)} F(y,\zeta)\,\mathrm{d}\sigma \quad (d \geq 2). \tag{1.20}$$

In view of Duhamel's principle (see, e.g., Evans [27]), U_1 and V_1 satisfy the same type of equation with corresponding inhomogeneous right-hand term and initial condition.

(a) Especially, we claim for $d = 3$ that $V_1(x,\tau;\zeta)$ is of the form (1.20) if and only if

$$\begin{cases} \Box V_1(x,\tau;\zeta) = 0 & (x \in \mathbb{R}^d,\ \tau > \zeta),\\ V_1(x,\tau;\zeta)|_{\tau=\zeta} = 0,\ \partial_\tau V_1(x,\tau;\zeta)|_{\tau=\zeta} = 4\pi\,F(x,\zeta) & (x \in \mathbb{R}^d). \end{cases} \tag{1.21}$$

Actually, under the translation $\xi = \tau - \zeta$, (1.21) with $d = 3$ is equivalent to

$$\begin{cases} (\partial_\xi^2 - \triangle) V_1(x,\xi+\zeta;\zeta) = 0 & (x \in \mathbb{R}^3,\ \xi > 0),\\ V_1(x,\xi+\zeta;\zeta)|_{\xi=0} = 0,\ \partial_\xi V_1(x,\xi+\zeta;\zeta)|_{\xi=0} = 4\pi\,F(x,\zeta) & (x \in \mathbb{R}^3). \end{cases}$$

Noting that the above system is now independent of ζ, we may apply Poisson's formula for the Cauchy problem of the three-dimensional wave equation to obtain

$$V_1(x,\xi+\zeta;\zeta) = \frac{1}{\xi}\int_{S_3(x,\xi)} F(y,\zeta)\,\mathrm{d}\sigma,$$

which is exactly (1.20) by replacing ξ with $\tau - \zeta$. On the other hand, Duhamel's principle implies that under the relation (1.19), system (1.21) holds for $V_1(x,\tau;\zeta)$ if and only if $U_1(x,\tau)$ satisfies a wave equation for $d = 3$. Consequently, together with Lemma 1.2(a), it turns out that $U_0(x,t)$ satisfies a double wave equation and thus Theorem 1.1 for $d = 3$ follows, stimulating the further discussion in higher spatial dimensions.

(b) However, it follows from [27, §2.4.1] that (1.20) cannot be the solution to (1.21) in even dimensions. Actually, for even d the solution $V_1(\,\cdot\,,\,\cdot\,;\zeta)$ to (1.21) is affected by $F(\,\cdot\,,\zeta)$ inside the cone $\{(y,\tau);\ \tau > \zeta,\ |y - x| < \tau - \zeta\}$, while V_1 in (1.20) only on the lateral. This indeed coincides with Huygens' principle, namely, functions depending only on a sharp wavefront in even dimensions do not satisfy wave equations.

Proposition 1.1 *Let $d \geq 2m+1$ with $m = 0, 1, \ldots$ and $U_0(x,\tau)$ be defined as in (1.8). Then there holds*

$$\begin{cases} \Box U_m = \begin{cases} 2^{m+1}\pi^m F & (d = 2m+1), \\ (d-(2m+1))\, U_{m+1} & (d > 2m+1) \end{cases} & \text{in } \mathbb{R}^d \times \mathbb{R}_+, \\ U_m(\,\cdot\,,0) = \partial_\tau U_m(\,\cdot\,,0) = 0 & \text{in } \mathbb{R}^d, \end{cases} \tag{1.22}$$

where we have for $m \geq 1$ that

$$U_m = \sum_{\ell=1}^{m} c_m^\ell \, P_m^\ell(d)\, [2m-\ell, \partial^{(1-(-1)^\ell)/2} B_d, \triangle^{\lfloor \ell/2 \rfloor}], \quad \text{in particular} \tag{1.23}$$

$$P_m^m(d) = 1, \quad P_m^\ell(d) = (d - 2(m - \lfloor (\ell+1)/2 \rfloor))\, P_{m-1}^\ell(d) \ (1 \leq \ell \leq m-1), \tag{1.24}$$

$$c_m^1 = c_m^m = 1, \quad c_m^\ell = \begin{cases} c_{m-1}^{\ell-1} & (\ell \text{ even}), \\ c_{m-1}^{\ell-1} + c_{m-1}^\ell & (\ell \text{ odd}) \end{cases} \ (2 \leq \ell \leq m-1). \tag{1.25}$$

Here we understand $\partial^1 B_d = S_d$, $\partial^0 B_d = B_d$, $\lfloor \cdot \rfloor$ denotes the integer part of a positive number, and those terms without definitions automatically vanish.

We comment here that the recursion formulas (1.22)–(1.25) result from the conjecture by executing brute-force calculations for the first several m's, which will be presented in Appendix 1.A.

As a direct application of the above conclusion, we immediately obtain the governing equations for U_0 in odd spatial dimensions.

Corollary 1.1 (Multiple wave equations) *Let the spatial dimensions $d = 2m+1$ ($m = 0, 1, \ldots$), $u(x,t)$ satisfy (1.2)–(1.3) and $U_0(x,\tau) := u(x, R^{-1}(\tau))$, where $R(t)$ is defined in (1.6). Assume that $u(x,t)$, $\Psi(x,t)$ and $\rho(t)$ ($x \in \mathbb{R}^d$, $t \geq 0$) are sufficiently smooth functions, and $\rho(t)$ is strictly positive for $t \geq 0$. Then $U_0(x,\tau)$ solves the following initial value problem for the multiple wave equation*

$$\begin{cases} (\partial_\tau^2 - \triangle)^{m+1} U_0(x,\tau) = (2m)!!\, 2^{m+1}\pi^m\, \Psi(x, R^{-1}(\tau))/\rho(R^{-1}(\tau)) & (x \in \mathbb{R}^d, \ \tau > 0), \\ \partial_\tau^\ell U_0(x,0) = 0, \quad \ell = 0, 1, \ldots, d & (x \in \mathbb{R}^d). \end{cases} \tag{1.26}$$

The multiple wave equations for U_0 is equivalent to the multiple hyperbolic equations for u in view of the change of variable (1.6). Nevertheless, Corollary 1.1 will demonstrate its advantage especially in the numerical simulations for the forward problem (see Section 1.4) and the investigation of the inverse source problem (see Chapter 4).

The verification of Proposition 1.1 requires a technical lemma, and the proof is postponed to Appendix 1.A.

Lemma 1.3 *Let the integers c_m^ℓ ($m = 1, 2, \ldots$, $1 \leq \ell \leq m$) be defined as in (1.24) and (1.25). Then*

(a) *For $m \geq 2$ and $2 \leq \ell \leq m$, we have*

$$P_m^{\ell-1}(d) = ((d-m) + (-1)^\ell (m - 2\lfloor \ell/2 \rfloor))\, P_m^\ell(d). \tag{1.27}$$

(b) *For $m \geq 3$ and $2 \leq \ell \leq m-1$, we have*

$$2(m-\ell)\, c_m^\ell = \begin{cases} \ell\, c_m^{\ell+1} & (\ell \text{ even}), \\ (2m-\ell-1)\, c_m^{\ell+1} & (\ell \text{ odd}). \end{cases} \tag{1.28}$$

Proof of Proposition 1.1. It is natural to adopt an inductive argument since the result for $m = 0$ has been proved in Lemma 1.2(a). Thus it suffices to show for some $m \geq 1$ that

(a) U_m in (1.23)–(1.25) satisfies the wave system (1.22), and

(b) for $d > 2m+1$, $\Box U_m/(d-(2m+1))$ preserves expression (1.23)–(1.25) for $m+1$.

To this end, first we unify (1.14)–(1.15) in Lemma 1.1 succinctly and substitute ℓ with $2m-\ell$ to derive

$$\begin{aligned}
&\partial_\tau[2m-\ell, \partial^{(1-(-1)^\ell)/2}B_d, \triangle^{\lfloor \ell/2\rfloor}] \\
&= \left((d-1)\frac{1-(-1)^\ell}{2} - 2m + \ell\right)[2m-\ell+1, \partial^{(1-(-1)^\ell)/2}B_d, \triangle^{\lfloor \ell/2\rfloor}] \\
&\quad + [2m-\ell, \partial^{(1-(-1)^{\ell+1})/2}B_d, \triangle^{\lfloor (\ell+1)/2\rfloor}],
\end{aligned}$$

yielding

$$\begin{aligned}
\partial_\tau U_m &= \sum_{\ell=1}^{m} c_m^\ell\, P_m^\ell(d)\, \partial_\tau[2m-\ell, \partial^{(1-(-1)^\ell)/2}B_d, \triangle^{\lfloor \ell/2\rfloor}] \\
&= \sum_{\ell=1}^{m} c_m^\ell\, P_m^\ell(d) \left\{ \left((d-1)\frac{1-(-1)^\ell}{2} - 2m + \ell\right)[2m-\ell+1, \partial^{(1-(-1)^\ell)/2}B_d, \triangle^{\lfloor \ell/2\rfloor}] \right. \\
&\qquad \left. + [2m-\ell, \partial^{(1-(-1)^{\ell+1})/2}B_d, \triangle^{\lfloor (\ell+1)/2\rfloor}] \right\} \\
&= (d-2m)\, P_m^1(d)\, [2m, S_d, \triangle^0] \\
&\quad + \sum_{\ell=2}^{m} c_m^\ell\, P_m^\ell(d) \left((d-1)\frac{1-(-1)^\ell}{2} - 2m + \ell\right)[2m-\ell+1, \partial^{(1-(-1)^\ell)/2}B_d, \triangle^{\lfloor \ell/2\rfloor}] \\
&\quad + \sum_{\ell=2}^{m} c_m^{\ell-1}\, P_m^{\ell-1}(d)\, [2m-\ell+1, \partial^{(1-(-1)^\ell)/2}B_d, \triangle^{\lfloor \ell/2\rfloor}] \\
&\quad + [m, \partial^{(1-(-1)^{m+1})/2}B_d, \triangle^{\lfloor (m+1)/2\rfloor}] \\
&= P_{m+1}^1(d)\, [2m, S_d, \triangle^0] + \widehat{U}_m,
\end{aligned}$$

where

$$\widehat{U}_m := \sum_{\ell=2}^{m} Q_m^\ell(d)\, [2m-\ell+1, \partial^{(1-(-1)^\ell)/2}B_d, \triangle^{\lfloor \ell/2\rfloor}] + [m, \partial^{(1-(-1)^{m+1})/2}B_d, \triangle^{\lfloor (m+1)/2\rfloor}],$$

in particular

$$Q_m^\ell(d) := c_m^\ell\, P_m^\ell(d) \left((d-1)\frac{1-(-1)^\ell}{2} - 2m + \ell\right) + c_m^{\ell-1}\, P_m^{\ell-1}(d) \quad (\ell = 2, \ldots, m).$$

Here we have applied (1.24) with m replaced by $m+1$ to get $(d-2m)\, P_m^1(d) = P_{m+1}^1(d)$. Meanwhile, using the fact that $d \geq 2m+1$, we may apply (1.12) to argue that each integral bracket in U_m and $\partial_\tau U_m$ vanish at $\tau = 0$ and hence $(1.22)_2$ holds.

Furthermore, we employ a similar argument for $\widehat{U}_m$ to obtain

$$\begin{aligned}
\partial_\tau \widehat{U}_m &= \sum_{\ell=2}^{m} Q_m^\ell(d) \left\{ \left((d-1)\frac{1-(-1)^\ell}{2} - 2m + \ell - 1\right)[2m-\ell+2, \partial^{(1-(-1)^\ell)/2}B_d, \triangle^{\lfloor \ell/2\rfloor}] \right. \\
&\qquad \left. + [2m-\ell+1, \partial^{(1-(-1)^{\ell+1})/2}B_d, \triangle^{\lfloor (\ell+1)/2\rfloor}] \right\} \\
&\quad + \left((d-1)\frac{1-(-1)^{m+1}}{2} - m\right)[m+1, \partial^{(1-(-1)^{m+1})/2}B_d, \triangle^{\lfloor (m+1)/2\rfloor}]
\end{aligned}$$

$$
\begin{aligned}
&+[m,\partial^{(1-(-1)^m)/2}B_d,\triangle^{\lfloor m/2\rfloor+1}]\\
&=-(2m-1)\,P^2_{m+1}(d)\,[2m,B_d,\triangle^1]\\
&\quad+\sum_{\ell=1}^{m-2}\left\{Q^{\ell+2}_m(d)\left((d-1)\frac{1-(-1)^\ell}{2}-2m+\ell+1\right)+Q^{\ell+1}_m(d)\right\}\\
&\qquad\times[2m-\ell,\partial^{(1-(-1)^\ell)/2}B_d,\triangle^{\lfloor \ell/2\rfloor+1}]\\
&\quad+\left\{Q^m_m(d)+\left((d-1)\frac{1-(-1)^{m-1}}{2}-m\right)\right\}[m+1,\partial^{(1-(-1)^{m-1})/2}B_d,\triangle^{\lfloor (m-1)/2\rfloor+1}]\\
&\quad+[m,\partial^{(1-(-1)^m)/2}B_d,\triangle^{\lfloor m/2\rfloor+1}],
\end{aligned}
$$

where we have used (1.25), (1.24) and Lemma 1.3(a) to find

$$
Q^2_m(d)=c^2_m\,P^2_m(d)\,(-2m+2)+c^1_m\,P^1_m(d)=(d-2m)\,P^2_m(d)=P^2_{m+1}(d).
$$

On the other hand, we differentiate $[2m,S_d,\triangle^0]$ with respect to d to proceed

$$
\begin{aligned}
\partial^2_\tau U_m&=P^1_{m+1}(d)\,\partial_\tau[2m,S_d,\triangle^0]+\partial_\tau\widehat{U}_m\\
&=\begin{cases}P^1_{m+1}(d)\left(\sigma_d\,F+[2m,B_d,\triangle^1]\right)+\partial_\tau\widehat{U}_m & (d=2m+1),\\ P^1_{m+1}(d)\left((d-2m-1)\,[2m+1,S_d,\triangle^0]+[2m,B_d,\triangle^1]\right)\\ \quad+\partial_\tau\widehat{U}_m & (d>2m+1),\end{cases}
\end{aligned}
$$

while

$$
\triangle U_m=\sum_{\ell=1}^m c^\ell_m\,P^\ell_m(d)\,[2m-\ell,\partial^{(1-(-1)^\ell)/2}B_d,\triangle^{\lfloor \ell/2\rfloor+1}].
$$

Representing $(1.22)_1$ by the above expressions and comparing the both sides, we claim that it suffices to prove for $d\ge 2m+1$ that

$$
\begin{aligned}
&\sigma_{2m+1}\,P^1_{m+1}(2m+1)=2^{m+1}\pi^m,\\
&P^1_{m+1}(d)-(2m-1)\,P^2_{m+1}(d)=(d-2m-1)\,c^2_{m+1}\,P^2_{m+1}(d)
\end{aligned}
\quad(m\ge 1),\tag{1.29}
$$

and

$$
\begin{aligned}
&Q^m_m(d)+\left((d-1)\frac{1-(-1)^{m-1}}{2}-m\right)-c^{m-1}_m\,P^{m-1}_m(d)\\
&=(d-2m-1)\,c^{m+1}_{m+1}\,P^{m+1}_{m+1}(d)\quad(m\ge 2),
\end{aligned}\tag{1.30}
$$

$$
\begin{aligned}
&Q^{\ell+2}_m(d)\left((d-1)\frac{1-(-1)^\ell}{2}-2m+\ell+1\right)+Q^{\ell+1}_m(d)-c^\ell_m\,P^\ell_m(d)\\
&=(d-2m-1)\,c^{\ell+2}_{m+1}\,P^{\ell+2}_{m+1}(d)\quad(m\ge 3,\ \ell=1,\dots,m-2).
\end{aligned}\tag{1.31}
$$

In fact, as long as (1.29)–(1.31) are valid, requirements (a) and (b) are satisfied simultaneously and the proof is complete.

First, the repeated applications of Lemma 1.3(a) with m replaced by $m+1$ yields

$$
P^1_{m+1}(d)=(d-2)\,P^2_{m+1}(d)=(d-2)(d-2m)\,P^3_{m+1}(d)=\cdots=\prod_{j=1}^m(d-2j),
$$

which, together with the fact $\sigma_{2m+1}=2^{m+1}\pi^m/(2m-1)!!$, leads to

$$
\sigma_{2m+1}\,P^1_{m+1}(2m+1)=\frac{2^{m+1}\pi^m}{(2m-1)!!}\prod_{j=1}^m(2m+1-2j)=2^{m+1}\pi^m
$$

and meanwhile

$$\begin{aligned} P^1_{m+1}(d) - (2m-1)\,P^2_{m+1}(d) &= (d-2)\,P^2_{m+1}(d) - (2m-1)\,P^2_{m+1}(d) \\ &= (d-2m-1)\,c^2_{m+1}\,P^2_{m+1}(d), \end{aligned}$$

that is, (1.29). Next, it follows from the expansion of $Q^m_m(d)$ that

$$\begin{aligned} &Q^m_m(d) + \left((d-1)\frac{1-(-1)^{m-1}}{2} - m\right) - c^{m-1}_m\,P^{m-1}_m(d) \\ &= \left((d-1)\frac{1-(-1)^{m}}{2} - m\right) + c^{m-1}_m\,P^{m-1}_m(d) + \left((d-1)\frac{1-(-1)^{m-1}}{2} - m\right) \\ &\quad - c^{m-1}_m\,P^{m-1}_m(d) \\ &= d-2m-1 = (d-2m-1)\,c^{m+1}_{m+1}\,P^{m+1}_{m+1}(d) \end{aligned}$$

or (1.30). Similarly, we expand $Q^{\ell+1}_m(d)$ and $Q^{\ell+2}_m(d)$ for $\ell = 1,\dots,m-2$ and utilize Lemma 1.3(a) to calculate

$$\begin{aligned} &Q^{\ell+2}_m(d)\left((d-1)\frac{1-(-1)^{\ell}}{2} - 2m + \ell + 1\right) + Q^{\ell+1}_m(d) - c^{\ell}_m\,P^{\ell}_m(d) \\ &= \left\{c^{\ell+2}_m\,P^{\ell+2}_m(d)\left((d-1)\frac{1-(-1)^{\ell}}{2} - 2m + \ell + 2\right) + c^{\ell+1}_m\,P^{\ell+1}_m(d)\right\} \\ &\quad \times \left((d-1)\frac{1-(-1)^{\ell}}{2} - 2m + \ell + 1\right) \\ &\quad + \left\{c^{\ell+1}_m\,P^{\ell+1}_m(d)\left((d-1)\frac{1-(-1)^{\ell+1}}{2} - 2m + \ell + 1\right) + c^{\ell}_m\,P^{\ell}_m(d)\right\} - c^{\ell}_m\,P^{\ell}_m(d) \\ &= \left\{c^{\ell+2}_m\left((d-1)\frac{1-(-1)^{\ell}}{2} - 2m + \ell + 2\right)\left((d-1)\frac{1-(-1)^{\ell}}{2} - 2m + \ell + 1\right)\right. \\ &\quad \left. + c^{\ell+1}_m\,(d-4m+2\ell+1)(d-m+(-1)^{\ell}(m-2\lfloor \ell/2\rfloor - 2))\right\} P^{\ell+2}_m(d) \\ &= \begin{cases} \left\{c^{\ell+2}_m\,(2m-\ell-2)(2m-\ell-1) + c^{\ell+1}_m\,(d-4m+2\ell+1)(d-\ell-2)\right\} P^{\ell+2}_m(d) & (\ell \text{ even}), \\ \left\{(d-2m+\ell+1)\left(c^{\ell+2}_m\,(d-2m+\ell) + c^{\ell+1}_m\,(d-4m+2\ell+1)\right)\right\} P^{\ell+2}_m(d) & (\ell \text{ odd}). \end{cases} \end{aligned}$$

On the other hand, it immediately follows from (1.24) that

$$P^{\ell+2}_{m+1}(d) = (d - 2(m - \lfloor(\ell+1)/2\rfloor))\,P^{\ell+2}_m(d) = \begin{cases} (d-2m+\ell)\,P^{\ell+2}_m(d) & (\ell \text{ even}), \\ (d-2m+\ell+1)\,P^{\ell+2}_m(d) & (\ell \text{ odd}). \end{cases}$$

Therefore, by Lemma 1.3(b) and (1.25), we obtain for even ℓ that

$$\begin{aligned} &c^{\ell+2}_m\,(2m-\ell-2)(2m-\ell-1) + c^{\ell+1}_m\,(d-4m+2\ell+1)(d-\ell-2) \\ &= c^{\ell+1}_m\,\{2(m-\ell-1)(2m-\ell-1) + (d-4m+2\ell+1)(d-\ell-2)\} \\ &= c^{\ell+1}_m\,(d-2m-1)(d-2m+\ell) = c^{\ell+2}_{m+1}\,(d-2m-1)(d-2m+\ell), \end{aligned}$$

and parallelly for odd ℓ that

$$\begin{aligned} &(d-2m+\ell+1)\left(c^{\ell+2}_m\,(d-2m+\ell) + c^{\ell+1}_m\,(d-4m+2\ell+1)\right) \\ &= (d-2m+\ell+1)\left\{\left((\ell+1)c^{\ell+2}_m - 2(m-\ell-1)c^{\ell+1}_m\right) + (c^{\ell+1}_m + c^{\ell+2}_m)(d-2m-1)\right\} \\ &= c^{\ell+2}_{m+1}\,(d-2m-1)(d-2m+\ell+1). \end{aligned}$$

In other words, we balance the both sides of (1.31), which finishes the proof. □

At this stage, the main conclusion of multiple hyperbolic systems degenerates to a straightforward corollary of the above result.

Proof of Theorem 1.1. In view of Proposition 1.1, it suffices to show by induction on m that for $m = 0, 1, \ldots$ and $d \geq 2m+1$, there holds

$$\begin{cases} \mathcal{H}_\rho^{m+1} u = \begin{cases} (2m)!!\, 2^{m+1} \pi^m \, \Psi/\rho & (d = 2m+1), \\ \displaystyle\prod_{\ell=0}^{m} (d-2\ell-1)\, U_{m+1}(\,\cdot\,, R(\,\cdot\,)) & (d > 2m+1) \end{cases} & \text{in } \mathbb{R}^d \times \mathbb{R}_+, \\ \partial_t^\ell u(\,\cdot\,, 0) = 0, \quad \ell = 0, 1, \ldots, 2m+1 & \text{in } \mathbb{R}^d. \end{cases} \tag{1.32}$$

The result for $m = 0$ was obtained in Lemma 1.2(b). In order to verify (1.32) for each $m \geq 1$, we suppose the validity for some $m-1$, especially there holds for $d \geq 2m+1$ that

$$\begin{cases} \mathcal{H}_\rho^m u(x,t) = \displaystyle\prod_{\ell=0}^{m-1} (d-2\ell-1)\, U_m(x, R(t)) & (x \in \mathbb{R}^d,\ t > 0), \\ \partial_t^\ell u(x,0) = 0, \quad \ell = 0, 1, \ldots, 2m-1 & (x \in \mathbb{R}^d). \end{cases}$$

Taking $w := \mathcal{H}_\rho^m u$, then in view of (1.9) we find

$$W(x,\tau) = w(x, R^{-1}(\tau)) = \mathcal{H}_\rho^m u(x,t)\big|_{t=R^{-1}(\tau)} = \prod_{\ell=0}^{m-1} (d-2\ell-1)\, U_m(x,\tau),$$

where U_m satisfies (1.22) by Proposition 1.1. This, together with (1.9), yields immediately

$$\begin{aligned} \mathcal{H}_\rho^{m+1} u(x,t) = \mathcal{H}_\rho w(x,t) = \Box W(x, R(t)) &= \prod_{\ell=0}^{m-1} (d-2\ell-1)\, \Box U_m(x, R(t)) \\ &= \begin{cases} \displaystyle\prod_{\ell=0}^{m-1} (d-2\ell-1)\, 2^{m+1} \pi^m \, F(x, R(t)) & (d = 2m+1) \\ \displaystyle\prod_{\ell=0}^{m-1} (d-2\ell-1)\, (d-2m-1)\, U_{m+1}(x, R(t)) & (d > 2m+1) \end{cases} \\ &= \begin{cases} (2m)!!\, 2^{m+1} \pi^m \, \Psi(x,t)/\rho(t) & (d = 2m+1) \\ \displaystyle\prod_{\ell=0}^{m} (d-2\ell-1)\, U_{m+1}(x, R(t)) & (d > 2m+1) \end{cases} \quad (x \in \mathbb{R}^d,\ t > 0), \end{aligned}$$

while the initial condition for $d \geq 2m+1$ reads

$$\begin{aligned} \mathcal{H}_\rho^m u(x,0) &= \prod_{\ell=0}^{m-1} (d-2\ell-1)\, U_m(x,0) = 0, \\ \partial_t \mathcal{H}_\rho^m u(x,0) &= \rho(0) \prod_{\ell=0}^{m-1} (d-2\ell-1)\, \partial_\tau U_m(x,0) = 0. \end{aligned}$$

Since $\rho(0) \neq 0$ and $\mathcal{H}_\rho^m u(x,0)$ is now a linear combination of $\partial_t^j u(x,0)$ $(j = 0, \ldots, 2m-1, 2m)$, it follows from the inductive assumption on the homogeneous initial condition for lower order time derivatives than $2m$ that $\partial_t^{2m} u(x,0) = 0$ and thus $\partial_t^{2m+1} u(x,0) = 0$ $(x \in \mathbb{R}^d)$. This completes the demonstration of (1.32) for $m \geq 1$ and hence Theorem 1.1. $\square$

1.4 Numerical simulations for forward problems

In this section, we implement numerical computations for forward problems in practical dimensions, namely, solving for the expectation number $u(x,t)$ of transformation events by given (discrete) data of $\Psi(x,t)$ and $\rho(t)$ with $d = 1,2,3$. It will be demonstrated that even finite difference schemes for the derived hyperbolic-type systems can dramatically improve the efficiency of simulations compared with direct approaches based on (1.2)–(1.3).

Throughout this section, we consider the systems in the time interval $[0,T]$ and assume the periodicity of $u(x,t)$ in space. More precisely, it is supposed, e.g. for $d = 3$, that there exist $L_\ell > 0$ $(\ell = 1,2,3)$ such that

$$u(x_1 + i\,L_1, x_2 + j\,L_2, x_3 + k\,L_3, t) = u(x_1,x_2,x_3,t) \quad (\forall\, i,j,k \in \mathbb{Z}),$$

so that it suffices to restrict the systems in $\overline{\Omega}\times[0,T]$, $\Omega := \prod_{\ell=1}^{d}(0,L_\ell)$ $(d = 1,2,3)$ and impose the periodic boundary conditions. Thus the data of Ψ and ρ are assigned only on the knots

$$0 = t_0 < t_1 < \cdots < t_{N_t} = T, \quad 0 = x_\ell^1 < x_\ell^2 < \cdots < x_\ell^{N_\ell} = L_\ell \ (1 \le \ell \le d).$$

Without lose of generality we assume an equidistant lattice in space, that is, $x_\ell^i = (i-1)\,\Delta x$ $(i = 1,\dots,N_\ell)$ with the step size $\Delta x > 0$.

Although one may solve for the unknown u by, e.g., hyperbolic-type systems (1.5) with the periodic boundary condition when $d = 1,3$, it is advantageous to consider the wave-type systems (1.26) for U_0 and utilize the relation $u(\,\cdot\,,t) = U_0(\,\cdot\,,R(t))$ instead. In this manner we can not only circumvent the numerical differentiation problem for ρ, but also simplify the choice of the step length in time. For simplicity, we write $U := U_0$ and introduce $V := \Box U$ for $d = 2,3$. To clarify, we formulate the initial-boundary value problem, e.g., for the three-dimensional case, as

$$\begin{cases} \Box U = V,\ \Box V = 8\pi F & \text{in } \Omega\times(0,T], \\ U = \partial_\tau U = V = \partial_\tau V = 0 & \text{in } \Omega\times\{0\}, \\ U,V : \text{periodic} & \text{on } \partial\Omega\times(0,T], \end{cases} \tag{1.33}$$

where we recall $\Omega = \prod_{\ell=1}^{d}(0,L_\ell)$ and $F(x,\tau) = \Psi(x,R^{-1}(\tau))/\rho(R^{-1}(\tau))$.

Such a consideration of the equivalent systems relies obviously on the knowledge of the change of variable $\tau = R(t) = \int_0^t \rho(s)\,\mathrm{d}s$, whose accurate value is absent due to the discrete data $\{\rho(t_n)\}_{n=0}^{N_t}$. Hence we shall first apply, for instance, a composite trapezoid quadrature to provide a piecewise linear approximation of $R(t)$, say $\widehat{R}(t)$. Now that U satisfies a wave equation with the unit propagation speed, we may partition the alternative time interval $[0,\widehat{R}(T)]$ of τ by a uniform step length $\Delta\tau > 0$, yielding the knots $\tau_n = n\,\Delta\tau$ $(n = 0,1,\dots,N_\tau)$ with $N_\tau\,\Delta\tau = \widehat{R}(T)$. Note that $\Delta\tau$ is required to satisfy the Courant-Friedrichs-Lewy condition $\sqrt{d}\,\Delta\tau \le \Delta x$ when using an explicit scheme of the finite difference method, which can be loosen or removed if some weighted multilevel schemes are employed. For later use we introduce the ratio $\kappa := (\Delta\tau/\Delta x)^2$.

Thanks to the strict positivity of ρ, it is easy to find out an increasing sequence $\{\widehat{t}_n\}_{n=0}^{N_\tau}$ such that $\widehat{R}(\widehat{t}_n) = \tau_n$. Thus, the estimation of $U(\,\cdot\,,\tau_n)$ stands for a reasonable approximation of $u(\,\cdot\,,\widehat{t}_n)$ due to the relation (1.8). Moreover, we recognize that the equidistant partition in τ corresponds with a self-adaptive partition in t, i.e., the knots $\{\widehat{t}_n\}$ accumulate where ρ is large while are sparsely distributed for small ρ (see Figure 1.2).

Interpreting Ψ and ρ as piecewise linear, we may obtain the term

$$F(\,\cdot\,,\tau_n) = \frac{\Psi(\,\cdot\,,R^{-1}(\tau_n))}{\rho(R^{-1}(\tau_n))} \approx \frac{\Psi(\,\cdot\,,\widehat{t}_n)}{\rho(\widehat{t}_n)} \quad (0 \le n \le N_\tau)$$

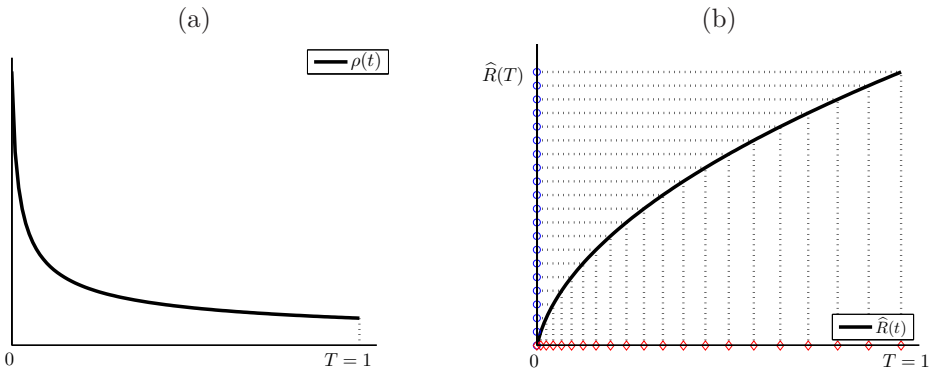

Figure 1.2: An example of the self-adaptiveness. (a) Plot of $\rho(t) = (t+0.01)^{-1/2}$. (b) Plot of $\widehat{R}(t) \approx 2(\sqrt{t+0.01} - 0.1)$, circle $= \tau_n$ and diamond $= \widehat{t}_n$.

by interpolating the discrete data $\{\Psi(\,\cdot\,, t_n), \rho(t_n)\}_{n=0}^{N_t}$. For $d = 3$, we denote

$$F_n^{i,j,k} := \frac{\Psi(x_1^i, x_2^j, x_3^k, \widehat{t}_n)}{\rho(\widehat{t}_n)},$$

let $U_n^{i,j,k}$ be the approximation of $U(x_1^i, x_2^j, x_3^k, \tau_n)$, and define the difference operators

$$\begin{cases} \delta_{x_1}^2 U_n^{i,j,k} := U_n^{i+1,j,k} - 2\,U_n^{i,j,k} + U_n^{i-1,j,k} & (i = 1, \dots, N_1), \\ \delta_{x_2}^2 U_n^{i,j,k} := U_n^{i,j+1,k} - 2\,U_n^{i,j,k} + U_n^{i,j-1,k} & (j = 1, \dots, N_2), \\ \delta_{x_3}^2 U_n^{i,j,k} := U_n^{i,j,k+1} - 2\,U_n^{i,j,k} + U_n^{i,j,k-1} & (k = 1, \dots, N_3), \end{cases}$$

where we understand $U_n^{0,j,k} = U_n^{N_1,j,k}$, $U_n^{N_1+1,j,k} = U_n^{1,j,k}$, etc. due to the periodicity. Similar notations are parallelly shared by the counterparts of U and Ψ for $d = 1, 2$ as well as V for $d = 2, 3$.

Now we are well-prepared to explain the implementation of numerical approaches. Due to the difference between odd and even spatial dimensions, we treat the cases of $d = 1, 3$ and $d = 2$ separately.

1.4.1 One- and three-dimensional cases

We start from the one-dimensional case. Applying a three-leveled finite difference scheme to (1.16) with the periodic boundary condition, we obtain

$$\begin{cases} U_{n+1}^i - 2\,U_n^i + U_{n-1}^i = \kappa\,\delta_{x_1}^2 \left(\eta\,U_{n+1}^i - (1-2\eta)\,U_n^i + \eta\,U_{n-1}^i\right) \\ \qquad\qquad + 2\,\Delta\tau^2\,F_n^i \quad (1 \le i \le N_1, 1 \le n \le N_\tau - 1), \\ U_0^i = U_1^i = 0 \quad (1 \le i \le N_1), \\ U_n^0 = U_n^{N_1},\ U_n^{N_1+1} = U_n^1 \quad (1 \le n \le N_\tau - 1), \end{cases} \tag{1.34}$$

where $\eta \in [0, 1/2]$ is a parameter. (1.34) becomes the von Neumann scheme when $\eta = 1/4$, and it is unconditionally stable as long as $\eta \ge 1/4$. The numerical result with $\eta = 1/4$, $T = 1$, $L_1 = \pi$ and the given

$$\rho(t) = \frac{1}{2\sqrt{t+1}}, \quad \Psi(x,t) = \exp\left(-\frac{(x-\pi/2)^2}{2}\right)(1 - \cos(10\,x))\exp\left(1 - \frac{t}{10}\right) \tag{1.35}$$

is illustrated in Figure 1.3.

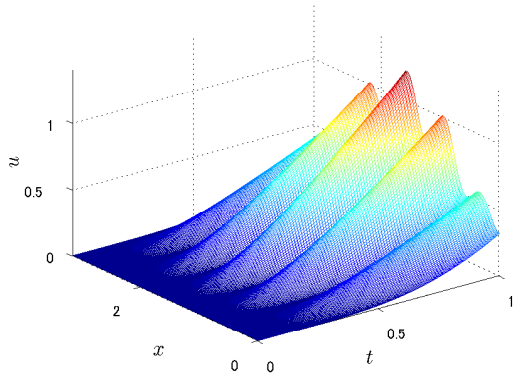

Figure 1.3: Numerical result of the one-dimensional forward problem with Ψ and ρ given by (1.35).

Next, for $d = 3$ it suffices to solve for V by the given data $4\pi F$ first, and then solver for U by the source term V according to (1.33). To avoid massive matrix manipulations while preserve the unconditional stability as the von Neumann scheme for $d = 1$, we apply the alternating direction implicit (ADI) method (see Fairweather and Metchell [28]) to both V and U as follows

$$\begin{cases} V^{i,j,k}_{n+1/3} - 2\,V^{i,j,k}_{n} + V^{i,j,k}_{n-1} = \kappa\,\delta^2_{x_1}\left(\eta\,V^{i,j,k}_{n+1/3} + (1-2\eta)\,V^{i,j,k}_{n} + \eta\,V^{i,j,k}_{n-1}\right) \\ \qquad\qquad + \kappa\,(\delta^2_{x_2} + \delta^2_{x_3})V^{i,j,k}_{n} + 8\pi\,\Delta\tau^2\,F^{i,j,k}_{n}, \\ V^{i,j,k}_{n+2/3} - V^{i,j,k}_{n+1/3} = \kappa\eta\,\delta^2_{x_2}\left(V^{i,j,k}_{n+2/3} - 2\,V^{i,j,k}_{n} + V^{i,j,k}_{n-1}\right), \\ V^{i,j,k}_{n+1} - V^{i,j,k}_{n+2/3} = \kappa\eta\,\delta^2_{x_3}\left(V^{i,j,k}_{n+1} - 2\,V^{i,j,k}_{n} + V^{i,j,k}_{n-1}\right), \end{cases}$$

$$\begin{cases} U^{i,j,k}_{n+1/3} - 2\,U^{i,j,k}_{n} + U^{i,j,k}_{n-1} = \kappa\,\delta^2_{x_1}\left(\eta\,U^{i,j,k}_{n+1/3} + (1-2\eta)\,U^{i,j,k}_{n} + \eta\,U^{i,j,k}_{n-1}\right) \\ \qquad\qquad + \kappa\,(\delta^2_{x_2} + \delta^2_{x_3})U^{i,j,k}_{n} + \Delta\tau^2\,V^{i,j,k}_{n}, \\ U^{i,j,k}_{n+2/3} - U^{i,j,k}_{n+1/3} = \kappa\eta\,\delta^2_{x_2}\left(U^{i,j,k}_{n+2/3} - 2\,U^{i,j,k}_{n} + U^{i,j,k}_{n-1}\right), \\ U^{i,j,k}_{n+1} - U^{i,j,k}_{n+2/3} = \kappa\eta\,\delta^2_{x_3}\left(U^{i,j,k}_{n+1} - 2\,U^{i,j,k}_{n} + U^{i,j,k}_{n-1}\right), \end{cases}$$

where $\eta \in [0, 1/2]$. Such a scheme inherits the unconditional stability property when $\eta \geq 1/4$ as that for $d = 1$. Here the initial and boundary treatments are parallel to that of (1.34), and such notations as $U^{i,j,k}_{n+1/3}$ stand for some intermediate values in pursue of $U^{i,j,k}_{n+1}$. We implement the above scheme with $\eta = 1/4$, $T = 100$, $L_1 = L_2 = L_3 = 1$ and

$$\rho(t) = \frac{1}{5\sqrt{100\,t+1}}, \quad \Psi(x,t) = f(x)\left(1 - \exp\left(-\frac{t}{10}\right)\right). \tag{1.36}$$

Here the spatial component f of Ψ describes a soccer-shaped structure satisfying the periodicity with the addition of a random noise subjected to the Cauchy distribution, producing few outstanding pixels with a low-amplitude background (see Kaipio and Somersalo [41, §3.3.2]). The numerical simulation results at four moments are illustrated in Figure 1.4. At each moments we show several representative sections cut at $x_3 = 0.25$, $x_3 = 0.5$, $x_3 = 0.75$ and $x_3 = 1$.

1.4.2 The two-dimensional case

Now we consider the two-dimensional case. In Remark 1.2 we mentioned the different situations between even and odd spatial dimensions, and such difference results in practical difficulties in the treatment for $d = 2$. After a polar coordinate transform, the source term in

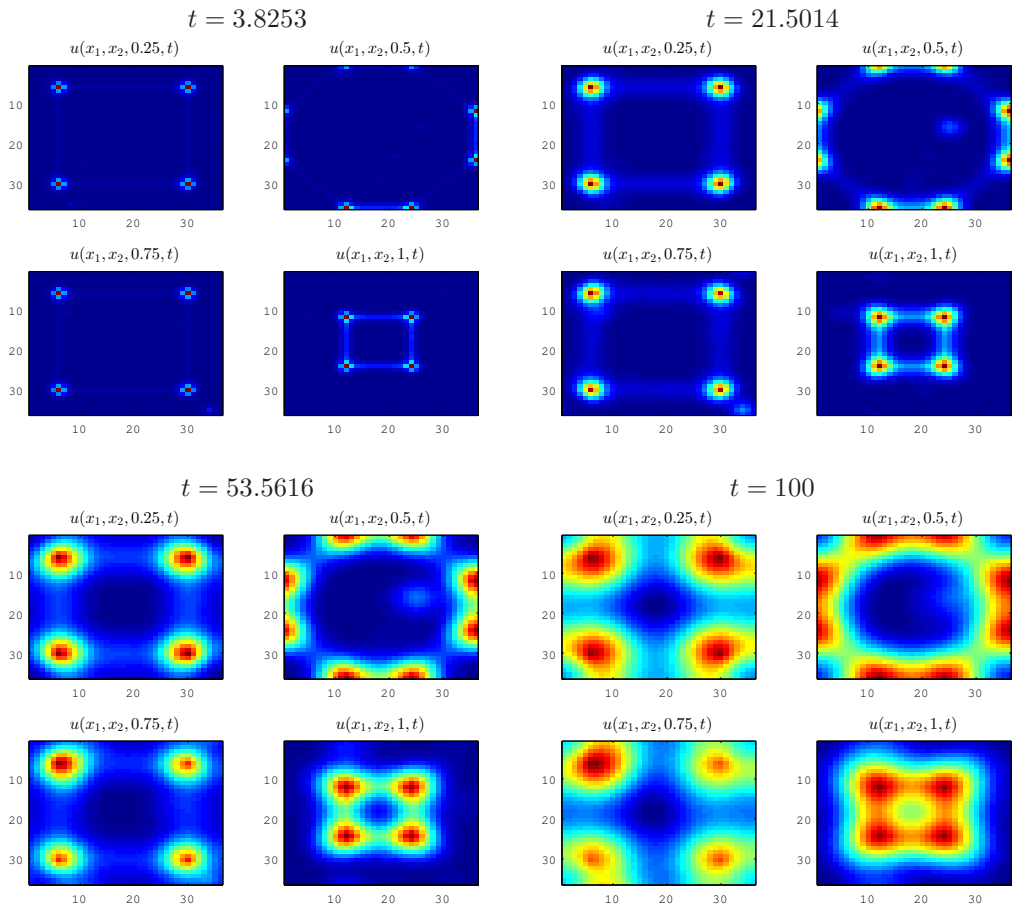

Figure 1.4: Numerical simulation for the three-dimensional forward problem at four moments. Ψ and ρ given by (1.36). At each moment we show several representative sections with $x_3 = 0.25$, $x_3 = 0.5$, $x_3 = 0.75$ and $x_3 = 1$.

the governing equation (1.16) reads

$$V(x,\tau) = [1, S_2, \triangle^0](x_1, x_2, \tau) = \int_0^\tau W(x_1, x_2, \tau, \zeta)\,\mathrm{d}\zeta, \quad \text{where} \tag{1.37}$$

$$W(x_1, x_2, \tau, \zeta) := \int_0^{2\pi} F(x_1 + (\tau-\zeta)\cos\psi, x_2 + (\tau-\zeta)\sin\psi, \zeta)\,\mathrm{d}\psi. \tag{1.38}$$

In other words, we shall numerically treat the integral on the lateral of the cone $\Omega_1(x,\tau)$. At the moment it is necessary to discretize the above integral at all grid points.

Suppose that we are now in a position to approximate $V(x_1^i, x_2^j, \tau_n)$ for some $1 \le i \le N_1$ and $1 \le j \le N_2$. First we discrete (1.37) by a composite trapezoid quadrature as

$$\begin{aligned} V(x_1^i, x_2^j, \tau_n) &\approx \Delta\tau \left(\frac{W(x_1^i, x_2^j, \tau_n, \tau_0)}{2} + \sum_{k=1}^{n-1} W(x_1^i, x_2^j, \tau_n, \tau_k) + \frac{W(x_1^i, x_2^j, \tau_n, \tau_n)}{2} \right) \\ &= \Delta\tau \left(\pi\, F(x_1^i, x_2^j, \tau_n) + \sum_{k=1}^{n-1} W(x_1^i, x_2^j, \tau_n, \tau_{n-k}) + \frac{W(x_1^i, x_2^j, \tau_n, \tau_0)}{2} \right), \end{aligned} \tag{1.39}$$

where $W(x_1^i, x_2^j, \tau_n, \tau_{n-k})$ $(k = 1, \ldots, n)$, by definition, denotes the integral of $F(x_1^i, x_2^j, \tau_{n-k})$ on a ring centered at (x_1^i, x_2^j) with radius $k\,\Delta\tau$. Therefore, it suffices to develop a sampling strategy to collect sufficient knots on the ring so as to employ another numerical integral. Meanwhile, we observe that regardless of the strategy we utilize, the relative positions between the obtained sampling points and the corresponding center is independent of i, j in the same level time. On the other hand, for fixed i and j, the sampling points at $\tau = \tau_n$ can be recycled repeatedly afterwards. In this sense, the information from any reasonable strategy is global, implying the sufficiency of considering the ensemble of concentric rings with radiuses $k\,\Delta\tau$, $k = 1, \ldots, N_\tau$ prior to the computation.

Actually, a naive but pragmatic strategy works, namely, collecting all the intersection points with the spatial lattice on each ring and then approximating (1.38) by a non-equidistant composite trapezoid quadrature with respect to the arguments of these points (see Figure 1.5). Evidently, such strategy is by nature self-adaptive in sense of the observation that it collects $\mathcal{O}(k)$ knots on the ring with radius $k\,\Delta\tau$, which supplies sufficient amount of samplings to result in good approximations of the integral $W(x_1^i, x_2^j, \tau_n, \tau_{n-k})$. On the other hand, since most probably the desired knots do not locate at the lattice, such interpolation as weighted average of the two adjacent grid points are required for the approximation.

To this end, we shall first identify one of the adjacent grids and then record the relative direction (up/down/left/right) of another. Without lose of generality, we specify the first grid point be the one closer to the origin. Thus it is easy to obtain the corresponding weight and argument. Consequently, six pieces of information

$$(\widetilde{i}, \widetilde{j}, \widehat{i}, \widehat{j}, b, \psi) \tag{1.40}$$

are necessary for the identification of a desired point: $(\widetilde{i}, \widetilde{j}) \in \mathbb{Z}^2$ for the relative position of the first reference point from the origin, $(\widehat{i}, \widehat{j}) \in \{(\pm 1, 0), (0, \pm 1)\}$ for the relative direction of the second point from the first, $b \in [0, 1]$ for the relative distance from the first grid, and $\psi \in [0, 2\pi]$ for its argument.

Thanks to the equidistant assumption of the spatial lattice, it suffices to lock on the intersection points in the x_1-direction in the first quadrant (see Figure 1.5(a)). In other words, we search for the desired points on the horizonal lines

$$\Sigma_m := \{(x_1, x_2) \in \mathbb{R}^2 \mid 0 < x_1 \le N_{\max}\,\Delta x,\ x_2 = m\,\Delta x\}, \quad m = 0, 1, \ldots, M_0,$$

where $M_0 := \lceil \widetilde{R}(T)/\Delta x \rceil$ assigns an optimal search range according to the largest radius. Suppose now we are executing the searching process on Σ_m. Since the distance between the original point and Σ_m is greater than $m\,\Delta x$, we may eliminate the shorter radiuses by finding the smallest k such that $k\,\Delta\tau > m\,\Delta x$. On the other hand, it also turns out to be unnecessary to search on the whole line Σ_m especially for large m; only such interval that $0 < x_1^2 \le \widetilde{R}(T)^2 - (m\,\Delta x)^2$ should be under consideration. In conclusion, these tricks greatly trim the unnecessary searchings, and it is not difficult to identify the nearest grid point left to the intersection point and the second one is always on the right. Equipped with the weight b and argument ψ which are easily computed, by this means we are able to collect all the desired information in the horizonal direction in the first quadrant.

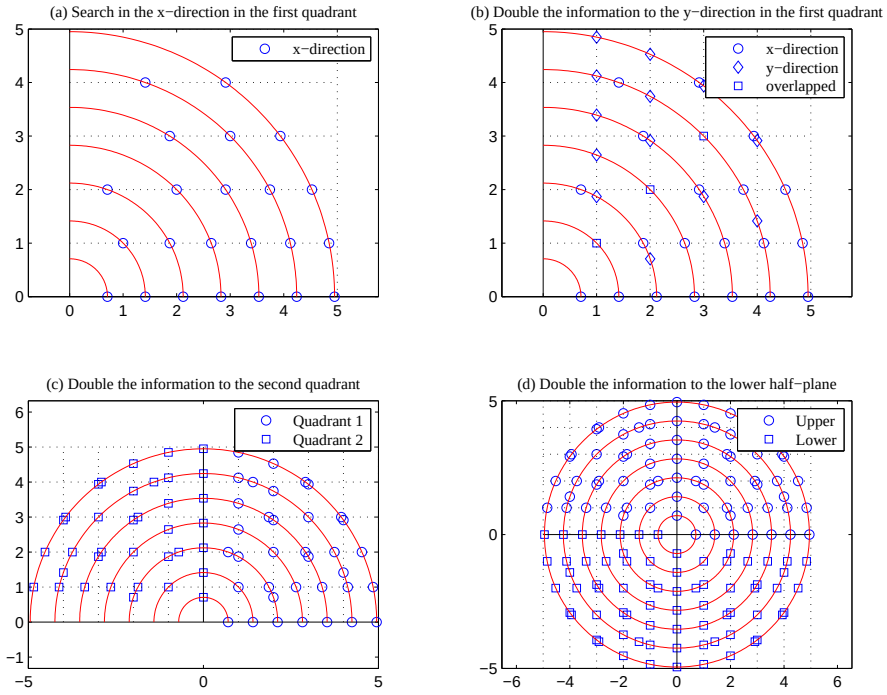

Figure 1.5: Demonstration of the detailed implementation of the searching strategy for intersection points between the equidistant lattice and the concentric rings with $\Delta x = \sqrt{2}\,\Delta t$.

Owing to the uniform mesh size Δx, we may duplicate the above information to the perpendicular direction in the first quadrant. Noting that later we will make a rotation of $\pi/2$ so that the intersection points on the x_1-axis will transfer to the x_2-axis, we do not exert the duplication for Σ_0. More precisely, for a given point identified by (1.40), its reflection with respect to the diagonal reads $(\widetilde{j}, \widetilde{i}, \widehat{j}, \widehat{i}, b, \pi/2 - \psi)$. To fit into the framework of numerical integral (1.41), we shall rearrange the obtained points on each ring so that their arguments are in increasing order. We make rearrangement in this stage because the rotation afterwards will definitely keep such order. Here it is noticeable that occasionally several intersections just locate on the lattice so that the horizonal and perpendicular searching overlap (see Figure 1.5(b)). However, since they share the same argument, the substitution into (1.41) will cancel the extra term automatically so that such special cases are ignorable.

At this step, we may first apply a rotation of $\pi/2$ to double the information from the first quadrant to the second, and then rotate another π to double from the upper half plane to the lower half. These are equivalent to the transformation of the already obtained information (1.40)

to $(-\widetilde{j},\widetilde{i},-\widehat{j},\widehat{i},b,\psi+\pi/2)$ and $(-\widetilde{i},-\widetilde{j},-\widehat{i},-\widehat{j},b,\psi+\pi)$ subsequently (see Figure 1.5(c)–(d)). Until now we have finished the collection of all information

$$(\widetilde{i}_m^k,\widetilde{j}_m^k,\widehat{i}_m^k,\widehat{j}_m^k,b_m^k,\psi_m^k)\quad\text{with } 0=\psi_0^k\le\cdots\le\psi_{N_k}^k=2\pi,\quad k=1,\dots,N_\tau,\ m=0,\dots,N_k,$$

which can be immediately applied into the following composite trapezoid quadrature for $1\le i\le N_1$, $1\le j\le N_2$ that

$$\begin{aligned}W(x_1^i,x_2^j,\tau_n,\tau_{n-k})&\approx\sum_{m=1}^{N_k}\frac{\psi_m^k-\psi_{m-1}^k}{2}\Big\{F(x_1^i+m\,\Delta x\cos\psi_{m-1}^k,x_2^j+m\,\Delta x\sin\psi_{m-1}^k,\tau_{n-k})\\&\qquad+F(x_1^i+m\,\Delta x\cos\psi_m^k,x_2^j+m\,\Delta x\sin\psi_m^k,\tau_{n-k})\Big\}\\&\approx\sum_{m=1}^{N_k-1}\frac{\psi_{m+1}^k-\psi_{m-1}^k}{2}\Big\{(1-b_m^k)\,F^{n-k}_{i+\widetilde{i}_m^k,j+\widetilde{j}_m^k}+b_m^k\,F^{n-k}_{i+\widetilde{i}_m^k+\widehat{i}_m^k,j+\widetilde{j}_m^k+\widehat{j}_m^k}\Big\}\\&\quad+\left(\pi-\frac{\psi_{N_k-1}^k-\psi_1^k}{2}\right)\Big\{(1-b_0^k)\,F^{n-k}_{i+\widetilde{i}_0^k,j}+b_0^k\,F^{n-k}_{i+\widetilde{i}_0^k+1,j}\Big\}\end{aligned}\tag{1.41}$$

for $k=1,\dots,n$. Of course, here we extend $F(\,\cdot\,,\tau)$ periodically so that all the indexes above make sense, which can be equivalently implemented by taking module operations with respect to N_1 or N_2 in either direction. Finally, the combination of (1.39) with (1.41) is expected to return a good approximation $V_n^{i,j}$ to $V(x_1^i,x_2^j,\tau_n)$.

Now we are ready to proceed to the discretization of the system (1.16) with $d=2$. Similarly to that for $d=3$, we take advantage of the two-dimensional version of the ADI method (see Lees [45])

$$\begin{cases}U^{i,j}_{n+1/2}-2\,U^{i,j}_n+U^{i,j}_{n-1}=\kappa\,\delta_{x_1}^2\left(\eta\,U^{i,j}_{n+1/2}+(1-2\eta)\,U^{i,j}_n+\eta\,U^{i,j}_{n-1}\right)\\\qquad\qquad\qquad+\kappa\,\delta_{x_2}^2U^{i,j}_n+\Delta\tau^2\,V^{i,j}_n,\\U^{i,j}_{n+1}-U^{i,j}_{n+1/2}=\kappa\eta\,\delta_{x_2}^2\left(U^{i,j}_{n+1}-2\,U^{i,j}_n+U^{i,j}_{n-1}\right)\end{cases}$$

with $\eta\in[0,1/2]$ ($1\le i\le N_1,1\le j\le N_2,1\le n\le N_\tau-1$). Still the stability properties are identical to that of odd spatial dimensions. We implement the above scheme with $\eta=1/4$, $T=50$, $L_1=L_2=1$ and

$$\rho(t)=\frac{1}{50\sqrt{t+1}},\quad\Psi(x,t)=f(x)\left(1-\exp\left(-\frac{t}{10}\right)\right).\tag{1.42}$$

In Figure 1.6, we capture several cuts at different stages of the phase transformation.

1.5 Conclusion and future works

In summary, it reveals that Cahn's time cone model (1.2)–(1.3) concerning phase transformation kinetics can be equivalently described by a class of multiple hyperbolic equations with the homogeneous initial condition, in which the growth speed $\rho(t)$ mainly plays the role of the propagation speed of wave. Especially, such systems take the simplest forms in odd spatial dimensions, where the nucleation rate $\Psi(x,t)$ accounts for the source term (see Theorem 1.1). Moreover, by the change of variable (1.7) which only involves $\rho(t)$, the governing equation (1.5) is further reduced to a class of multiple wave equations with a unit propagation speed (see Corollary 1.1). To a certain extent, the derivation of hyperbolic-type governing equations provides an appropriate formulation which enables systematic investigations of problems related

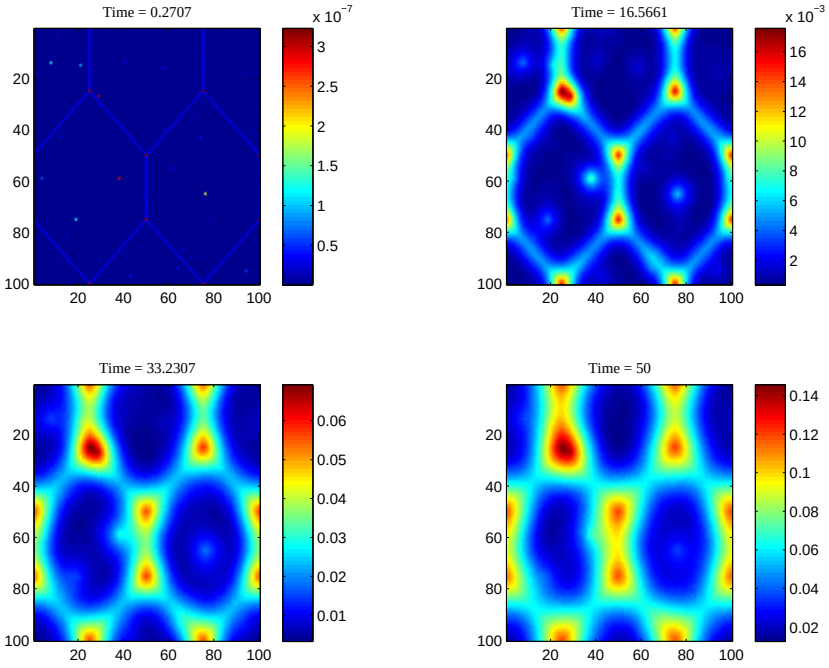

Figure 1.6: Numerical simulation of the two-dimensional forward problem with Ψ and ρ given by (1.42).

to structure transformations in both theoretical and numerical senses. As a tentative application, it was demonstrated in the previous section that efficient forward solvers are readily implemented on the basis of this alternative framework instead of the original model.

More significantly, as can be witnessed in the remaining chapters of Part I, the transform from an integral equation to partial differential equations also initiates smooth discussions on the corresponding inverse problems by using classical results of inverse hyperbolic problems. In Chapter 2, we shall study the numerical identification of the growth speed $\rho(t)$ on the basis of Theorem 1.1 in a framework of the coefficient inverse problem. In Chapter 4, we will investigate the determination of the nucleation rate $\Psi(x,t)$ on the basis of Corollary 1.1, and it turns out that the reasoning can be easily carried out from a viewpoint of inverse source problems of the hyperbolic type. More challenging topics may involve the simultaneous identification of both Ψ and ρ by more informative observations. At the same time, the computational methods for the above mentioned inverse problems are also of great interests.

For a better understanding of the overall scenario, we outline the framework of the above contents as follows.

$$
\begin{array}{ccc}
u = \int_{\Omega_\rho} \Psi & \xrightarrow{U(\cdot,\tau):=u(\cdot,R^{-1}(\tau))} & U = \int_{\Omega_1} F \\
\Big\downarrow & & \Big\downarrow \\
\mathcal{H}_\rho^{m+1} u = c_m\, \Psi/\rho & \xleftarrow{u(\cdot,t)=U(\cdot,R(t))} & (\partial_\tau^2 - \triangle)^{m+1} U = c_m\, F \\
\Big\downarrow \rho\text{: unknown} & & \Big\downarrow \rho\text{: given} \\
\text{Coefficient inverse problem} & & \text{Forward solver, Inverse source problem}
\end{array}
$$

1.A Technical details

Here we provide detailed proofs of the technical lemmata in Section 1.3.

Proof of Lemma 1.1. For the boundary integral $[\ell, S_d, \triangle^j]$, we introduce the polar transform

$$y = x + (\tau - \zeta)\, p(\psi) \quad (\psi = (\psi_1, \dots, \psi_{d-2}, \psi_{d-1}) \in D_d := [0,\pi]^{d-2} \times [0, 2\pi]),$$
$$p(\psi) := (\cos\psi_1, \sin\psi_1 \cos\psi_2, \dots, \sin\psi_1 \cdots \sin\psi_{d-2}\cos\psi_{d-1}, \sin\psi_1 \cdots \sin\psi_{d-2}\sin\psi_{d-1}).$$

Then the Jacobian reads $(\tau-\zeta)^{d-1}\, q(\psi)$, where $q(\psi) := \sin^{d-2}\psi_1 \cdots \sin\psi_{d-2}$. Therefore, we can write expression (1.10) equivalently as

$$[\ell, S_d, \triangle^j](x,\tau) = \int_0^\tau \int_{D_d} (\tau-\zeta)^{d-\ell-1}\, q(\psi)\, \triangle^j F(x + (\tau-\zeta)\, p(\psi), \zeta)\, \mathrm{d}\psi \mathrm{d}\zeta.$$

Parallelly, for the interior integral $[\ell, B_d, \triangle^j]$, we apply a similar polar transform

$$y = x + r\, p(\psi) \quad (0 < r < \tau - \zeta,\ \psi = (\psi_1, \dots, \psi_{d-2}, \psi_{d-1}) \in D_d)$$

with the Jacobian $r^{d-1}\, q(\psi)$, where $p(\psi)$, D_d and $q(\psi)$ are defined as before. Then (1.11) can be rewritten as

$$[\ell, B_d, \triangle^j](x,\tau) = \int_0^\tau \int_0^{\tau-\zeta} \int_{D_d} \frac{r^{d-1}\, q(\psi)\, \triangle^j F(x + r\, p(\psi), \zeta)}{(\tau-\zeta)^\ell}\, \mathrm{d}\psi \mathrm{d}r \mathrm{d}\zeta.$$

With these alternative representations, it is straightforward to verify (1.13) that

$$\begin{aligned}
\triangle[\ell, S_d, \triangle^j](x,\tau) &= \int_0^\tau \int_{D_d} (\tau-\zeta)^{d-\ell-1}\, q(\psi)\, \triangle^{j+1} F(x + (\tau-\zeta)\, p(\psi), \zeta)\, \mathrm{d}\psi \mathrm{d}\zeta \\
&= [\ell, S_d, \triangle^{j+1}](x,\tau), \\
\triangle[\ell, B_d, \triangle^j](x,\tau) &= \int_0^\tau \int_0^{\tau-\zeta} \int_{D_d} \frac{r^{d-1}\, q(\psi)\, \triangle^{j+1} F(x + r\, p(\psi), \zeta)}{(\tau-\zeta)^\ell}\, \mathrm{d}\psi \mathrm{d}r \mathrm{d}\zeta \\
&= [\ell, B_d, \triangle^{j+1}](x,\tau).
\end{aligned}$$

For $[\ell, S_d, \triangle^j]$ with $\ell < d-1$, we apply Green's formula and notice the fact that $p(\psi)$ coincides with the unit outward normal vector $\nu(y)$ at $y = x + (\tau-\zeta)\, p(\psi)$ to proceed

$$\begin{aligned}
\partial_\tau [\ell, S_d, \triangle^j](x,\tau) &= \int_0^\tau \partial_\tau \left(\int_{D_d} (\tau-\zeta)^{d-\ell-1}\, q(\psi)\, \triangle^j F(x + (\tau-\zeta)\, p(\psi), \zeta)\, \mathrm{d}\psi \right) \mathrm{d}\zeta \\
&= (d-\ell-1) \int_0^\tau \int_{D_d} (\tau-\zeta)^{d-\ell-2}\, q(\psi)\, \triangle^j F(x + (\tau-\zeta)\, p(\psi), \zeta)\, \mathrm{d}\psi \mathrm{d}\zeta \\
&\quad + \int_0^\tau \int_{D_d} (\tau-\zeta)^{d-\ell-1}\, q(\psi)\, \nabla \triangle^j F(x + (\tau-\zeta)\, p(\psi), \zeta) \cdot p(\psi)\, \mathrm{d}\psi \mathrm{d}\zeta \\
&= (d-\ell-1)\, [\ell+1, S_d, \triangle^j](x,\tau) + \int_0^\tau \int_{S_d(x,\tau-\zeta)} \frac{\nabla \triangle^j F(y,\zeta) \cdot \nu(y)}{(\tau-\zeta)^\ell}\, \mathrm{d}\sigma \mathrm{d}\zeta \\
&= (d-\ell-1)\, [\ell+1, S_d, \triangle^j](x,\tau) + \int_0^\tau \int_{B_d(x,\tau-\zeta)} \frac{\triangle^{j+1} F(y,\zeta)}{(\tau-\zeta)^\ell}\, \mathrm{d}y \mathrm{d}\zeta \\
&= (d-\ell-1)\, [\ell+1, S_d, \triangle^j](x,\tau) + [\ell, B_d, \triangle^{j+1}](x,\tau).
\end{aligned}$$

For $\ell = d-1$, a similar argument yields immediately

$$\partial_\tau [d-1, S_d, \triangle^j](x,\tau) = \int_{D_d} q(\psi)\, \triangle^j F(x,\tau)\, \mathrm{d}\psi$$

$$
\begin{aligned}
&\quad + \int_0^\tau \int_{D_d} q(\psi)\, \nabla \triangle^j F(x + (\tau-\zeta)\, p(\psi), \zeta) \cdot p(\psi)\, \mathrm{d}\psi \mathrm{d}\zeta \\
&= \sigma_d\, \triangle^j F(x,\tau) + \int_0^\tau \int_{S_d(x,\tau-\zeta)} \frac{\nabla \triangle^j F(y,\zeta) \cdot \nu(y)}{(\tau-\zeta)^{d-1}}\, \mathrm{d}\sigma \mathrm{d}\zeta \\
&= \sigma_d\, \triangle^j F(x,\tau) + \int_0^\tau \int_{B_d(x,\tau-\zeta)} \frac{\triangle^{j+1} F(y,\zeta)}{(\tau-\zeta)^{d-1}}\, \mathrm{d}y \mathrm{d}\zeta \\
&= \sigma_d\, \triangle^j F(x,\tau) + [d-1, B_d, \triangle^{j+1}](x,\tau),
\end{aligned}
$$

which is indeed (1.14). For $[\ell, B_d, \triangle^j]$ with $\ell \le d-1$, we employ a parallel calculation to derive (1.15) as

$$
\begin{aligned}
\partial_\tau [\ell, B_d, \triangle^j](x,\tau) &= \int_0^\tau \partial_\tau \left(\int_0^{\tau-\zeta} \int_{D_d} \frac{r^{d-1} q(\psi)\, \triangle^j F(x + r\, p(\psi), \zeta)}{(\tau-\zeta)^\ell}\, \mathrm{d}\psi \mathrm{d}r \right) \mathrm{d}\zeta \\
&= -\ell \int_0^\tau \int_0^{\tau-\zeta} \int_{D_d} \frac{\triangle^j F(x + r\, p(\psi), \zeta)}{(\tau-\zeta)^{\ell+1}}\, \mathrm{d}\psi \mathrm{d}r \mathrm{d}\zeta \\
&\quad + \int_0^\tau \int_{D_d} (\tau-\zeta)^{d-\ell-1}\, q(\psi)\, \triangle^j F(x + (\tau-\zeta)\, p(\psi), \zeta)\, \mathrm{d}\psi \mathrm{d}\zeta \\
&= -\ell\, [\ell+1, B_d, \triangle^j](x,\tau) + [\ell, S_d, \triangle^j](x,\tau).
\end{aligned}
$$

The proof is completed. □

Proof of Lemma 1.3. We proceed for both assertions by induction on m.

(a) For $m = 2$, (1.24) reads $P_2^1(d) = d-2$ and $P_2^2(d) = 1$, indicating (1.27) immediately by taking $m = \ell = 2$. Supposing (1.27) holds for some $m \ge 2$, we shall show that it still holds for $m+1$, namely

$$
P_{m+1}^{\ell-1}(d) = ((d-m-1) + (-1)^\ell (m+1-2\lfloor \ell/2 \rfloor))\, P_{m+1}^\ell(d) \quad (2 \le \ell \le m+1,\ m \ge 2).
$$

The case $\ell = m+1$ is trivial, otherwise we replace m by $m+1$ in (1.24) and apply the inductive assumption (1.27) for m to find

$$
\begin{aligned}
P_{m+1}^{\ell-1}(d) &= (d - 2(m+1-\lfloor \ell/2 \rfloor))\, P_m^{\ell-1}(d) \\
&= (d - 2(m+1-\lfloor \ell/2 \rfloor))\, (d-m+(-1)^\ell (m-2\lfloor \ell/2 \rfloor))\, P_m^\ell(d), \\
P_{m+1}^\ell(d) &= (d - 2(m+1-\lfloor (\ell+1)/2 \rfloor))\, P_m^\ell(d).
\end{aligned}
$$

As a result, it suffices to show

$$
\begin{aligned}
&(d - 2(m+1-\lfloor \ell/2 \rfloor))\, (d-m+(-1)^\ell (m-2\lfloor \ell/2 \rfloor)) \\
&= (d-m-1+(-1)^\ell (m+1-2\lfloor \ell/2 \rfloor))\, (d - 2(m+1-\lfloor (\ell+1)/2 \rfloor)),
\end{aligned}
$$

which can be easily verified by discussing the parity of ℓ.

(b) For $m = 3$, (1.25) implies $c_3^2 = 1$ and (1.28) follows immediately by taking $m = 3$ and $\ell = 2$. Supposing (1.28) is valid for some $m \ge 3$, we shall show that it still holds for $m+1$, namely

$$
2(m-\ell+1)\, c_{m+1}^\ell = \begin{cases} \ell\, c_{m+1}^{\ell+1} & (\ell \text{ even}), \\ (2m-\ell+1)\, c_{m+1}^{\ell+1} & (\ell \text{ odd}) \end{cases} \quad (2 \le \ell \le m,\ m \ge 4).
$$

For odd ℓ, (1.25) yields $c_{m+1}^\ell = c_m^{\ell-1} + c_m^\ell$ and $c_{m+1}^{\ell+1} = c_m^\ell$, while the inductive assumption (1.28) implies $2(m-\ell+1)\, c_m^{\ell-1} = (\ell-1)\, c_m^\ell$ since $\ell - 1$ is even. Therefore

$$
2(m-\ell+1)\, c_{m+1}^\ell = 2(m-\ell+1)\, (c_m^{\ell-1} + c_m^\ell) = (2m-\ell+1)\, c_m^\ell = (2m-\ell+1)\, c_{m+1}^{\ell+1}.
$$

Parallelly, we obtain for even ℓ that

$$2(m-\ell+1)\,c_{m+1}^{\ell}=2(m-\ell+1)\,c_{m}^{\ell-1}=(2m-\ell)\,c_{m}^{\ell}=\ell\,(c_{m}^{\ell}+c_{m}^{\ell+1})=\ell\,c_{m+1}^{\ell+1}$$

since now $\ell-1$ is odd. This ends the proof. □

Finally, we explain the discovery of the recursion relations (1.22)–(1.25) in Proposition 1.1.

In Lemma 1.2, we have shown the validity of Proposition 1.1 for $m=0$. In the sequel, we start from $U_1(x,\tau)$ defined in (1.17) and proceed to the case of $m=6$. In this way, it is not only possible to confirm that each $U_m(x,\tau)$ satisfies the wave equation (1.22), but also essential to make a conjecture on the recursive expression of $U_m(x,t)$.

To this end, we apply repeatedly Lemma 1.1 and condition (1.12) to obtain (1.22) for $m=1,2,\ldots,5$, where

$$\begin{aligned}
U_2 &= (d-2)\,[3,S_d,\triangle^0]+[2,B_d,\triangle^1],\\
U_3 &= (d-2)(d-4)\,[5,S_d,\triangle^0]+(d-4)\,[4,B_d,\triangle^1]+[3,S_d,\triangle^1],\\
U_4 &= (d-2)(d-4)(d-6)\,[7,S_d,\triangle^0]+(d-4)(d-6)\,[6,B_d,\triangle^1]\\
&\quad+2(d-4)\,[5,S_d,\triangle^1]+[4,B_d,\triangle^2],\\
U_5 &= (d-2)(d-4)(d-6)(d-8)\,[9,S_d,\triangle^0]+(d-4)(d-6)(d-8)\,[8,B_d,\triangle^1]\\
&\quad+3(d-4)(d-6)\,[7,S_d,\triangle^1]+2(d-6)\,[6,B_d,\triangle^2]+[5,S_d,\triangle^2],\\
U_6 &= (d-2)(d-4)(d-6)(d-8)(d-10)\,[11,S_d,\triangle^0]\\
&\quad+(d-4)(d-6)(d-8)(d-10)\,[10,B_d,\triangle^1]+4(d-4)(d-6)(d-8)\,[9,S_d,\triangle^1]\\
&\quad+3(d-6)(d-8)\,[8,B_d,\triangle^2]+3(d-6)\,[7,S_d,\triangle^2]+[6,B_d,\triangle^3].
\end{aligned}$$

According to the above expressions, it is straightforward to conjecture that U_m ($m\geq 1$) is a summation of m terms. Moreover, each term consists of three components, namely an integral bracket, a polynomial with respect to d, and a positive integer parameter. First of all, it is not difficult to infer that the integral bracket in the ℓ-th term of U_m takes the form of $[2m-\ell,\partial^{(1-(-1)^{\ell})/2}B_d,\triangle^{\lfloor \ell/2\rfloor}]$, which is indeed that in (1.23). On the other hand, since the relations of the polynomials and parameters are not too obvious, we collect all the information of $P_m^{\ell}(d)$ and c_m^{ℓ} for $m=1,2,\ldots,6$ and $\ell=1,2,\ldots,m$ in Table 1.1.

	Parameters in $P_m^{\ell}(d)$						c_m^{ℓ}					
ℓ	1	2	3	4	5	6	1	2	3	4	5	6
$m=1$	()						1					
							↓	↘				
$m=2$	(2)	()					1	1				
							↓	↘	↘			
$m=3$	(2,4)	(4)	()				1	1	1			
							↓	↘	↘	↓	↘	
$m=4$	(2,4,6)	(4,6)	(4)	()			1	1	2	1		
							↓	↘	↘	↓	↘	↘
$m=5$	$(2,\ldots,8)$	(4,6,8)	(4,6)	(6)	()		1	1	3	2	1	
							↓	↘	↘	↓	↘	↘ ↓ ↘
$m=6$	$(2,\ldots,10)$	$(4,\ldots,10)$	(4,6,8)	(6,8)	(6)	()	1	1	4	3	3	1

Table 1.1: Recursive relations of the $P_m^{\ell}(d)$ and c_m^{ℓ} for the first several m's.

Then it is obvious that $P_m^m(d)=1$ and $c_m^1=c_m^m=1$. For $\ell\leq m-1$, it is observed that $P_m^{\ell}(d)$ can be obtained by multiplying $(d-2(m-\lfloor(\ell+1)/2\rfloor))$ to $P_{m-1}^{\ell}(d)$, that is, (1.24).

Regarding c_m^ℓ for $2 \leq \ell \leq m-1$, we find out that the dependency of c_m^ℓ on the previous level differs from each other according to the parity of ℓ, and we indicate the dependency in Table 1.1 by arrows. Finally, we conclude (1.25) as the possible iterative relation for c_m^ℓ.

Chapter 2

Growth Speed Identification in the One-Dimensional Time Cone Model

In Chapter 1, a class of hyperbolic-type equations was derived for the time cone model which describes the phase transformation kinetics. Such a derivation provides remarkable convenience for the mathematical treatments and the corresponding numerical analysis especially in odd spatial dimensions.

As one of the applications, in this chapter we investigate an inverse problem of determining the growth speed in the one-dimensional time cone model by the final observation data. On the basis of the hyperbolic equation, the problem turns out to be a coefficient inverse problem which is highly nonlinear with respect to the observation data. A two-step truncated Tikhonov-type regularization method is proposed to reconstruct the growth speed from the noise contaminated data. Numerical prototype examples are presented to illustrate the validity and effectiveness of the proposed scheme.

2.1 Introduction

As was explained in Chapter 1, nucleation and growth mechanisms are important kinetics of phase transformations which arise in various subjects in material sciences. We recall that the nucleation event appears randomly in the untransformed or uncrystallized part of the specimen, and the growth event describes the expansion of each nucleus which is usually radial and ceases at the contact surface when two nucleating regions tie each other (impingement). The mathematical models for these important physical phenomena rest on statistical principles, which are formulated by Kolmogorov [43], Johnson and Mehl [39] and Avrami [2–4] at the earliest stage. Under certain simplifications that the nucleation rate Ψ and the growth speed ρ are constants, those pioneering works results in the well-known JMAK equation (1.4) in the three-dimensional case.

Activities on investigating an alternative variable instead of the expected crystalline volume fraction was started by Jackson [36] in a one-dimensional infinite specimen. Cahn [17] generalized the approach in high-dimensional finite specimens and proposed the time cone model, which avoids the concepts of extended volume fraction appearing in the classical theory. The time cone model was further investigated from different engineering disciplines, for instance,

in [5, Chapter 21]. Exact solutions of the expected nuclei number as well as the degree of crystallization can be obtained for finite specimen geometries with a nucleation rate $\Psi(x,t)$ and a time-dependent growth speed $\rho(t)$.

At the same time, independently of the time cone model, a similar concept of the so-called causal cone (see [13, Figures 1–2] and [24]) is investigated for the polymer crystallization, where results for both heterogeneous nucleation rate $\Psi(x,t)$ and growth speed $\rho(x,t)$ are derived. The non-isothermal polymer crystallization process based on the causal cone approach is investigated by [13] and a series of papers [12,50] later on. From an averaged viewpoint, the non-isothermal nucleation model yields a nonlinear hyperbolic-parabolic coupled system (see [13]), where the hyperbolic equation describes the degree of crystallinity and the parabolic equation describes the heat conduction process of the specimen. In the coupled system in [13], the latent heat released by the growing nucleation region or crystals plays the role of the heat source. For further details concerning the time cone model and the causal cone approach, we refer to Section 1.1 and the references therein.

Though mathematical modeling of the phase transformation process has been well extended from different viewpoints, the literatures on inverse problems of the nucleation process are limited. To the best of the author's knowledge, only [11,14,20] and the dissertation [10] are devoted to the inverse problems appearing in polymer crystallization processes based on the casual cone approach in the one-dimensional case. In [14], the authors investigate the non-isothermal hyperbolic-parabolic coupled system and provide a Landweber iterative regularization scheme for a stable reconstruction of the nucleation rate Ψ which depends on the temperature. Abundant theoretical justification and other iterative regularization schemes in [11] support the accurate and efficient identification of the nucleation rate. In particular, we note that the dissertation [10] well analyzes both the forward and the inverse problems of the polymer crystallization process. The recent work in [20] extends the nucleation rate identification from the deterministic setup to a stochastic one.

The aim of this chapter is to investigate the identification of the time-dependent growth speed $\rho(t)$ in the one-dimensional time cone model by the final observation data. In the original formulation (1.2)–(1.3) of the time cone model, $\rho(t)$ is coupled in the integral and thus is not easy to de-convolute and identify. Nevertheless, on the basis of the hyperbolic governing equation (see Lemma 2.1) derived in the previous chapter, the determination of $\rho(t)$ turns out to be a coefficient inverse problem, and the spectral method along with a two-step truncated Tikhonov-type regularization can be applied for the reconstruction.

The rest of the chapter is organized as follows. In Section 2.2, we first revisit the governing equation in the one-dimensional case and then represent the solution by an eigensystem expansion to formulate the parameter identification problem for the time dependent growth speed $\rho(t)$. A reconstruction algorithm based on the eigenfunction expansion method and the nonlinear Tikhonov regularization is proposed in Section 2.3 to solve the inverse problem. A numerical example in Section 2.4 verifies the accuracy of our proposed method. The final section gives remarks and conclusions.

2.2 Hyperbolic governing equation and spectral method

As the starting point, first we recall the one-dimensional time cone model and the equivalent initial value problem for a hyperbolic equation. Although this is the simplest case of Theorem 1.1, we collect the result here for self-containedness.

Lemma 2.1 *Let $u(x,t)$ satisfy*

$$u(x,t) = \int_{\Omega_\rho(x,t)} \Psi(y,s)\,\mathrm{d}y\mathrm{d}s \quad (x \in \mathbb{R},\ t \geq 0), \quad \textit{where}$$
$$\Omega_\rho(x,t) := \left\{ (y,s);\ 0 < s < t,\ |y-x| < \int_s^t \rho(\tau)\,\mathrm{d}\tau \right\}.$$

Assume that $u(x,t)$, $\Psi(x,t)$ and $\rho(t)$ $(x \in \mathbb{R},\ t \geq 0)$ are sufficiently smooth functions, and $\rho(t)$ is strictly positive for $t \geq 0$. Then $u(x,t)$ solves the following initial value problem for the hyperbolic equation

$$\begin{cases} \dfrac{1}{\rho(t)}\,\partial_t\left(\dfrac{\partial_t u(x,t)}{\rho(t)}\right) = \partial_x^2 u(x,t) + \dfrac{2\,\Psi(x,t)}{\rho(t)} & (x \in \mathbb{R},\ t > 0), \\ u(x,0) = \partial_t u(x,0) = 0 & (x \in \mathbb{R}). \end{cases} \tag{2.1}$$

Following the path in [13], the time cone model can be coupled with the heat conduction process to obtain a similar hyperbolic-parabolic coupled system in the non-isothermal phase transformation process. Namely, in one dimension we have

$$\begin{cases} \partial_t \theta(x,t) = \kappa\,\partial_x^2 \theta(x,t) + \eta\,\mathrm{e}^{-u(x,t)}\partial_t u(x,t), \\ \dfrac{1}{\rho(t)}\,\partial_t\left(\dfrac{\partial_t u(x,t)}{\rho(t)}\right) = \partial_x^2 u(x,t) + \dfrac{2\,\Psi(\theta(x,t))}{\rho(t)}, \end{cases}$$

where θ is the temperature, the constant κ denotes the heat conductivity, and the constant η denotes the latent heat.

In the rest of the chapter, we will mostly investigate a one-dimensional model problem slightly different from the original one. More precisely, with fixed $L > 0$ and $T > 0$, we restrict the problem in a bounded space-time region $(0,L)\times(0,T)$ and impose the homogeneous Dirichlet boundary condition to consider the following initial-boundary value problem

$$\begin{cases} \dfrac{1}{\rho(t)}\,\partial_t\left(\dfrac{\partial_t u(x,t)}{\rho(t)}\right) = \partial_x(D(x)\partial_x u(x,t)) + \dfrac{2\,\Psi(x,t)}{\rho(t)} & (0 < x < L,\ 0 < t \leq T), \\ u(x,0) = \partial_t u(x,0) = 0 & (0 < x < L), \\ u(0,t) = u(L,t) = 0 & (0 < t \leq T) \end{cases} \tag{2.2}$$

where $D \in C^1[0,L]$ and $D > 0$ on $[0,L]$. The basic solvability and the stability of the forward model can be found in the classic literatures, e.g., Lions and Magenes [47]. We note that the boundary condition we consider here is slightly different from the BCE model in [13], but it can be released to the periodic Dirichlet boundary condition. Here we only consider the homogeneous Dirichlet boundary condition for illustration.

We clarify our coefficient inverse problem as follows.

Problem 2.1 *Let $L > 0$, $T > 0$ be given, and u satisfy* (2.2)*. Provided that the nucleation rate $\Psi(x,t)$ is known, determine $\rho(t)$ $(0 < t < T)$ by the final observation data $y^\delta \in L^2(0,L)$ satisfying $\|y^\delta - u(\,\cdot\,,T)\|_{L^2(0,L)} \leq \delta$, where $\delta > 0$ is the noise level.*

To represent the explicit solution to (2.2), we introduce the eigensystem $\{(\lambda_n, \varphi_n)\}_{n=1}^\infty$ to the elliptic operator therein, that is, the pairs (λ_n, φ_n) satisfying

$$\begin{cases} -\partial_x(D(x)\partial_x \varphi_n(x)) = \lambda_n \varphi_n(x) & (0 < x < L), \\ \varphi_n(0) = \varphi_n(L) = 0. \end{cases}$$

After normalizing, the eigenfunctions $\{\varphi_n\}$ form a complete orthonormal system of $L^2(0,L)$. We then seek an explicit solution of the governing equation (2.2) in the form of separated variables

$$u(x,t)=\sum_{n=1}^{\infty}u_n(t)\varphi_n(x). \tag{2.3}$$

Simultaneously, the nucleation rate $\Psi(x,t)$ which plays the role of the source term in (2.2) can also be represented as

$$\Psi(x,t)=\sum_{n=1}^{\infty}\Psi_n(t)\varphi_n(x)\quad\text{with }\Psi_n(t)=\int_0^L\Psi(x,t)\varphi_n(x)\,\mathrm{d}x.$$

Substituting the eigenfunction expansion (2.3) into problem (2.2), we obtain the following initial value problems for ordinary differential equations with respect to u_n:

$$\begin{cases}\dfrac{1}{\rho(t)}\dfrac{\mathrm{d}}{\mathrm{d}t}\left(\dfrac{u_n'(t)}{\rho(t)}\right)+\lambda_n u_n(t)=\dfrac{2\,\Psi_n(t)}{\rho(t)},\\ u_n(0)=u_n'(0)=0.\end{cases}$$

A series of calculation gives

$$\begin{aligned}u_n(t)=\frac{2}{\sqrt{\lambda_n}}\Bigg\{&\sin\left(\sqrt{\lambda_n}\,R(t)\right)\int_0^t\Psi_n(s)\cos\left(\sqrt{\lambda_n}\,R(s)\right)\mathrm{d}s\\&-\cos\left(\sqrt{\lambda_n}\,R(t)\right)\int_0^t\Psi_n(s)\sin\left(\sqrt{\lambda_n}\,R(s)\right)\mathrm{d}s\Bigg\},\end{aligned} \tag{2.4}$$

where (see also (1.7))

$$R(t)=\int_0^t\rho(s)\mathrm{d}s. \tag{2.5}$$

Together with the expansion (2.3), the solution $u(x,t)$ to problem (2.2) is

$$\begin{aligned}u(x,t)=\sum_{n=1}^{\infty}\frac{2}{\sqrt{\lambda_n}}\Bigg\{&\sin\left(\sqrt{\lambda_n}\,R(t)\right)\int_0^t\Psi_n(s)\cos\left(\sqrt{\lambda_n}\,R(s)\right)\mathrm{d}s\\&-\cos\left(\sqrt{\lambda_n}\,R(t)\right)\int_0^t\Psi_n(s)\,\sin\left(\sqrt{\lambda_n}\,R(s)\right)\mathrm{d}s\Bigg\}\varphi_n(x).\end{aligned} \tag{2.6}$$

In the simplest case, i.e. $D(x)\equiv 1$, the particular eigenvalues λ_n and eigenfunctions φ_n of the elliptic differential operator are

$$\lambda_n=\left(\frac{\pi n}{L}\right)^2,\quad \varphi_n(x)=\sqrt{\frac{2}{L}}\sin\left(\sqrt{\lambda_n}\,x\right). \tag{2.7}$$

To show the accuracy of the eigenfunction expansion method, the numerical comparison between the eigenfunction expansion (2.6) and the standard finite difference method for the forward model (2.2) will be provided in the Section 2.4.

2.3 Identification of the growth speed

Coefficient inverse problems are of interest to many theoretical studies and practical applications such as [33,51,52]. Generally speaking, these results are investigated under the assumption that lateral boundary data was given. In this chapter, such kind of additional data is of absence, instead we have a finite time observation. Recall the governing hyperbolic equation (2.2), the

kinetics of the phase transformation process are determined by the nucleation rate $\Psi(x,t)$ as well as the growth speed $\rho(t)$ (see also (2.1)). These two functions become interesting when one want to identify the unknown properties of a specimen. As mentioned in the introduction, existing literatures on the identification problems arising in the phase transformation process are mostly lying in the reconstruction of the nucleation rate [10, 11, 14] where these results are obtained for the parabolic-hyperbolic coupled system in the one dimensional sample. In the remaining of this chapter, we will investigate, at a first stage, the identification of the spatially homogeneous growth speed $\rho(t)$ in the isothermal case.

In view of the formulation in Problem 2.1, the observation data is polluted by the measuring error or the numerical discretization error of the forward model. Due to its nature of the ill-posedness, we employ the Tikhonov regularization method to solve it. In order to reach the final goal $\rho(t)$, we shall first reconstruct an intermediate variable $R(t)$ defined in (2.5) because only $R(t)$ appears explicitly in the representation (2.6) of the solution.

Suppose that we have the noisy final observation data $y^\delta(x)$ satisfying $\|y^\delta - u(\,\cdot\,,T)\|_{L^2(0,L)} \leq \delta$. Denote by y_n^δ the Fourier coefficient of $y^\delta(x)$ with respect to $\varphi_n(x)$, i.e.

$$y^\delta(x) = \sum_{n=1}^{\infty} y_n^\delta \varphi_n(x), \quad y_n^\delta = \int_0^L y^\delta(x)\varphi_n(x)\,\mathrm{d}x.$$

Taking $t = T$ in the expansion (2.3) and applying Parseval's identity, we have

$$\sum_{n=1}^{\infty} \big(y_n^\delta - u_n(T)\big)^2 = \|y^\delta - u(\,\cdot\,,T)\|_{L^2(0,L)}^2 \leq \delta^2. \tag{2.8}$$

According to (2.4), we see

$$\begin{aligned} u_n(T) = \frac{2}{\sqrt{\lambda_n}} \Bigg\{ &\sin\Big(\sqrt{\lambda_n}\,R(T)\Big) \int_0^T \Psi_n(s) \cos\Big(\sqrt{\lambda_n}\,R(s)\Big)\,\mathrm{d}s \\ &- \cos\Big(\sqrt{\lambda_n}\,R(T)\Big) \int_0^T \Psi_n(s) \sin\Big(\sqrt{\lambda_n}\,R(s)\Big)\,\mathrm{d}s \Bigg\}, \end{aligned} \tag{2.9}$$

where the unknown variable $R(t)$ needs to be reconstructed.

To seek a regularized solution of (2.8), we restrict $R \in \mathcal{P}_M$, where $\mathcal{P}_M$ collects all polynomials with orders no higher than M. To treat the infinite summation in (2.8), we simply make a truncation until $n = N$. In such a manner, we propose the following truncated Tikhonov-type regularization

$$R_\alpha^{M,N} := \operatorname*{arg\,min}_{R \in \mathcal{P}_M} \sum_{n=1}^{N} \big(y_n^\delta - u_n(T)\big)^2 + \alpha \|R\|_{L^2(0,T)}^2, \tag{2.10}$$

where $\alpha > 0$ is the regularization parameter. Substituting (2.9) into (2.10) and taking Fréchet derivative with respect to R, we obtain the following Euler-Lagrange equation for the minimizer:

$$\begin{aligned} 2\alpha\, R(t) = 4 \sum_{n=1}^{N} \Bigg[y_n^\delta - \frac{2}{\sqrt{\lambda_n}} \Bigg\{ &\sin\Big(\sqrt{\lambda_n}\,R(T)\Big) \int_0^T \Psi_n(s) \cos\Big(\sqrt{\lambda_n}\,R(s)\Big)\,\mathrm{d}s \\ &- \cos\Big(\sqrt{\lambda_n}\,R(T)\Big) \int_0^T \Psi_n(s) \sin\Big(\sqrt{\lambda_n}\,R(s)\Big)\,\mathrm{d}s \Bigg\} \Bigg] \\ \times \Bigg\{ &- \cos\Big(\sqrt{\lambda_n}\,R(T)\Big) \int_0^T \Psi_n(s) \cos\Big(\sqrt{\lambda_n}\,R(s)\Big)\,\mathrm{d}s \end{aligned}$$

$$
\begin{aligned}
&+\sin\left(\sqrt{\lambda_n}\,R(T)\right)\Psi_n(t)\sin\left(\sqrt{\lambda_n}\,R(t)\right)\\
&-\cos\left(\sqrt{\lambda_n}\,R(T)\right)\Psi_n(t)\cos\left(\sqrt{\lambda_n}\,R(t)\right)\\
&+\sin\left(\sqrt{\lambda_n}\,R(T)\right)\int_0^T\Psi_n(s)\sin\left(\sqrt{\lambda_n}\,R(s)\right)\mathrm{d}s\Bigg\}. \qquad (2.11)
\end{aligned}
$$

Generally speaking, Euler-Lagrange equations are nonlinear Fredholm type integral equations of the second kind with respect to the unknown functions. Notice that we are seeking for a solution in the polynomial function space and the Euler-Lagrange equation involves heavy computational costs on the numerical integration. Therefore, it is reasonable to utilize the pseudo-spectral method to solve it.

Denote by $\{\vartheta_j,\sigma_j\}_{j=0}^M$ the $(M+1)$th-order Gauss-Legendre-Labbato points and their corresponding weights respectively. Define $R(t)=\sum_{j=0}^M R_j\,p_j(t)$, where $p_j(t)$ denotes the j-th Lagrange interpolation polynomial for $t_j=T(1+\vartheta_j)/2$ $(j=0,1,\ldots,M)$. We substitute such an $R(t)$ into the Euler-Lagrange equation (2.11) and evaluate it at each t_k $(k=0,1,\ldots,M)$ to deduce

$$
\begin{aligned}
2\alpha\,R_k=4\sum_{n=1}^N\Bigg[y_n^\delta-\frac{T}{\sqrt{\lambda_n}}\Bigg\{&\sin\left(\sqrt{\lambda_n}\,R_M\right)\sum_{j=0}^M\Psi_n(t_j)\cos\left(\sqrt{\lambda_n}\,R_j\right)\sigma_j\\
&-\cos\left(\sqrt{\lambda_n}\,R_M\right)\sum_{j=0}^M\Psi_n(t_j)\sin\left(\sqrt{\lambda_n}\,R_j\right)\sigma_j\Bigg\}\Bigg]\\
\times\Bigg\{&-\frac{T}{2}\cos\left(\sqrt{\lambda_n}\,R_M\right)\sum_{j=0}^M\Psi_n(t_j)\cos\left(\sqrt{\lambda_n}\,R_j\right)\sigma_j\\
&+\sin\left(\sqrt{\lambda_n}\,R_M\right)\Psi_n(t_k)\sin\left(\sqrt{\lambda_n}\,R_k\right)\\
&-\cos\left(\sqrt{\lambda_n}\,R_M\right)\Psi_n(t_k)\cos\left(\sqrt{\lambda_n}\,R_k\right)\\
&+\frac{T}{2}\sin\left(\sqrt{\lambda_n}\,R_M\right)\sum_{j=0}^M\Psi_n(t_j)\sin\left(\sqrt{\lambda_n}\,R_j\right)\sigma_j\Bigg\}. \qquad (2.12)
\end{aligned}
$$

To solve this nonlinear algebraic system, we turn to MatLab routine which employs several standard iterative solvers, for instance, Levenberg-Marquardt method or Gauss-Newton method.

Provided that by (2.12) we have obtained $R_\alpha^{M,N}$ with the appropriately chosen regularization parameter α by the discrepancy principle, we can now proceed to the final destination to reconstruct $\rho(t)$. At a first glance, it seems that one can immediately find a good approximation of $\rho(t)$ as $\rho_\alpha^{M,N}(t)=(R_\alpha^{M,N}(t))'=D_M R_\alpha^{M,N}(t)$, where D_M is the discrete difference matrix related to the Gauss-Legendre-Labbato points. However, the numerical differentiation is known to be another ill-posed problem which may cause tremendous error. We refer to [55] where a natural spline based Tikhonov regularization method is proposed to solve this problem. The regularization parameter here can be chosen in some heuristic or noisy-dependent rules, but we omit the details here.

2.4 Numerical example

In this section, we implement a numerical example to illustrate the validity and efficiency of the proposed schemes in the previous two sections. Notice that in the reconstruction al-

gorithm of the growth speed, namely, (2.12), an analytical form of the exact solution $u(x,T)$ is considered. For creating the final observation data, we employ two methods to solve the forward problem. One is a stochastic simulation based upon the definition of time-cone and the other is a finite difference scheme on the deterministic equations (2.2). Both methods produce reasonable results (see Figure 2.1), which confirms that the deterministic equations (2.2) well describe the average status of the crystallization of polymers. For the stochastic case, there are several algorithms for simulation of a Poisson process and we utilize the standard approach, i.e., thinning method which is a random sampling method (see [10, §2.6.2]). For the finite difference scheme, the standard three-points stencil method is adopted to solve the deterministic differential equation (2.2), which verifies the validity and effectiveness of modeling and eigenfunction expansion method.

For testing our numerical schemes, set

$$D(x) \equiv 1, \quad \rho(t) = \frac{1}{2\sqrt{1+t}}, \quad \Psi(x,t) = 10\,\mathrm{e}^{-t}\,x^2(L-x)^2.$$

Then the eigensystem $\{(\lambda_n, \varphi_n)\}$ is given by (2.7), and a simple calculation yields

$$\begin{aligned}\Psi_n(t) &= \int_0^L \Psi(x,t)\varphi_n(x)\,\mathrm{d}x = \sqrt{\frac{2}{L}}\,10\,\mathrm{e}^{-t}\int_0^L x^2(L-x)^2\sin\Big(\frac{\pi n\,x}{L}\Big)\,\mathrm{d}x \\ &= \sqrt{\frac{2}{L}}\,\frac{40\,\mathrm{e}^{-t}L^4}{\pi^5 n^5}(1-(-1)^n)(12-\pi^2 n^2).\end{aligned}$$

For the sake of completeness, we discuss the procedure of stochastic simulation in a reasonable detail. Generating equally separated sub-cells $\Omega_{i\ell}$ in the domain $[0,T]\times[0,R]$, we calculate the value $\Psi_{i\ell} = \int_{\Omega_{i\ell}} \Psi(x,t)\,\mathrm{d}x\mathrm{d}t$. Here the nucleation rate $\Psi(x,t)$ is assumed to be separable, i.e., $\Psi(x,t) = f(x)g(t)$, where $f(x)$ represents the spatial probability density function. Utilizing such a value Ψ_{ij} as a parameter, we can generate a positive integer by a Poisson distribution generator, e.g. MatLab function `poissrnd`. We then label each sub-cell with this positive integer which represents the random number of nucleation events in this sub-cell. Finally we calculate u at discrete points (x_i, T) and collect the positive integers in the time cone which overlaps the sub-cells $\Omega_{i\ell}$. The overlapping portion of the time-cone with respect to each sub-cell $\Omega_{i\ell}$ determines the ratio to the positive integers labeled in specific sub-cells. For the standard three-points stencil finite difference scheme, we omit the details here.

The computational results are shown in Figure 2.1, where (a) represents one stochastic simulation, (b) and (c) are average values of nucleation events of two thousand and twenty thousand stochastic simulations, respectively. In this particular example, we choose $T = 1$ and the discretization levels for time and space are $(50, 160)$ respectively such that 8000 sub-cells are generated in the whole domain. From Figure 2.1, we can observe that the expectation of stochastic simulations is close to the performance of the deterministic governing equations (2.2). In real situations, this expectation can be obtained by measuring one-dimensional observation data, for instance, at different places of a high-dimensional specimen.

Finally, we are ready to proceed to the reconstruction of the growth speed $\rho(t)$. As mentioned above, to treat the instability of the inversion, we consider the finite difference solution as the exact solution. The noisy observation data y^δ then are generated by two ways: one is from the expectation of stochastic simulations, e.g., Figure 2.1(b)–(c), and the other is from the following form

$$y^\delta = u(\,\cdot\,,T) \times (1 + \delta\,\mathrm{rand}(-1,1)),$$

where $\mathrm{rand}(-1,1)$ denotes the uniformly distributed random number in $[-1,1]$ and δ is the relative noisy level. Note that the computation of the Fourier coefficients y_n^δ in the Euler-Lagrange

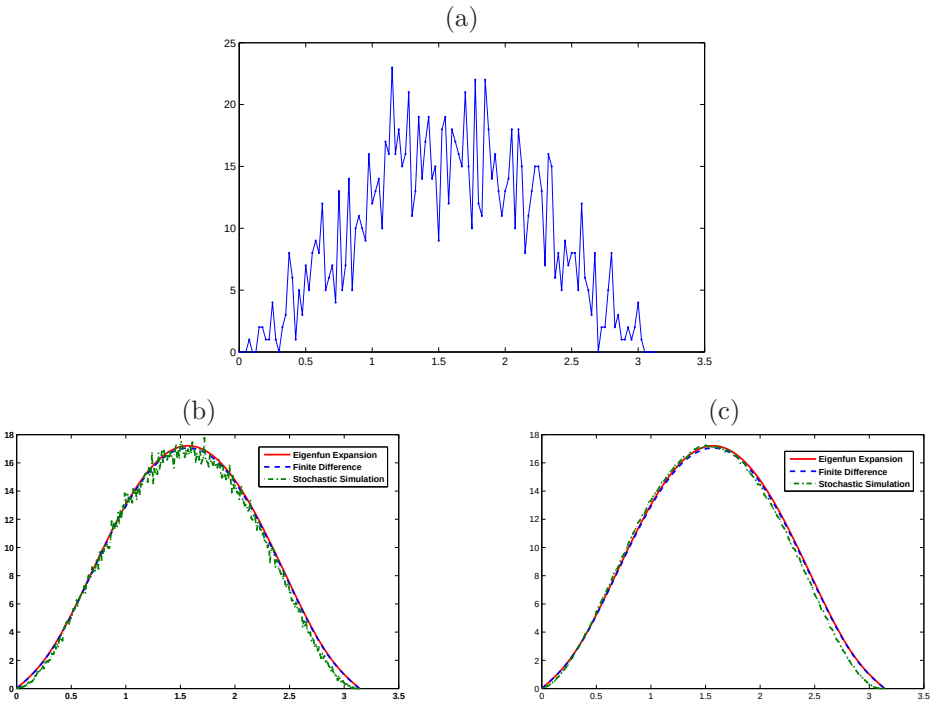

Figure 2.1: (a) Plot of $u(\cdot\,, T)$ by one stochastic simulation. (b) Average of 2000 simulations and finite difference/eigenfunction expansion solutions of (2.2). (c) Average of 20000 simulations.

equation (2.12) involves numerical integration as well, we adopt the Gauss quadrature again which is associated to the Gauss-Legendre-Labbato points and weights $\{\vartheta_j, \sigma_j\}_{j=0}^{M}$ mentioned in the previous section. More precisely, we obtain the approximated y_n^δ by a linear interpolation with respect to the pointwise values $y^\delta(R(1+\vartheta_j)/2)$. Substituting y_n^δ into (2.12) and employing the standard solver for the nonlinear system, we obtain the regularized reconstruction of $R_\alpha^{M,N}$ where the regularization parameter α is chosen in an a posteriori manner by the discrepancy principle. The value of the regularization parameter α for different examples can be found in the captions of Figures 2.2–2.3 respectively.

To reconstruct the growth speed $\rho(t)$, we need to extract further information from the intermediate result $R_\alpha^{M,N}$ which involves another ill-posed problem, i.e., the numerical differentiation. It is known that a direct inverse of the discrete matrix for the Gauss-Legendre polynomials is ill-posed in the sense that its conditional number is 10^{17} when M is chosen to be 8. To obtain a stable and appropriate reconstruction of $\rho(t)$, a natural spline based Tikhonov regularization method in [55] is utilized. The intermediate reconstructed $R_\alpha^{M,N}$ as well as the reconstructed growth speed $\rho(t)$ are shown in Figures 2.2–2.3 respectively under different noise levels.

The performance of our proposed method essentially depends on the choices of the regularization parameters M and α. The parameter M plays the role of the discretization level for Gauss-Lobatto rules where the numerical integration can be calculated in an accurate manner. The larger the M, the more accurate approximation of the integral equation, but it yields a large ill-posed linear system. In our numerical test, we fix $M = 8$ which provides reasonable reconstruction of the growth speed. One can adjusts the choice of M under the a priori smooth assumption, i.e. on the known $\Psi_n(t)$ which might provide better results. At the same time, the regularization parameter α is more important compared with the discretization level M and

we refer to the monograph [25, Chapter 4] where detailed discussion on parameter choice rules are presented. In our proposed method, a classic discrepancy principle is implemented to the first-step Tikhonov regularization such that the choice of α satisfies

$$\sum_{n=1}^{N} \left(y_n^\delta - u_n(T)\right)^2 \approx (c_1\delta)^2,$$

where $c_1 \approx 3$, $M = 8$ and $N = 20$. As for the second-step Tikhonov regularization on numerical differentiation, we simply choose $\alpha \approx (8\delta)^2$ where we expect that the noise level in the second-step is enhanced from the previous step. Discussion on the error estimation for such a parameter choice can be found in [55].

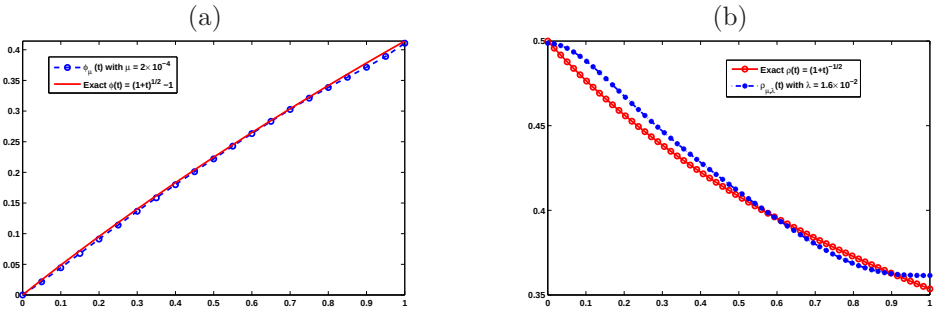

Figure 2.2: The numerical performance for the growth speed identification with the noisy observation data y^δ from averaged stochastic simulations. (a) The intermediate reconstructed $R_\alpha^{M,N}(t)$ with $M = 8$ and $\alpha = 2 \times 10^{-4}$. (b) The reconstructed $\rho_\alpha^{M,N}(t)$ from $R_\alpha^{M,N}(t)$ by implementing the regularization method in [55] with a regularization parameter $\alpha = 1.6 \times 10^{-2}$.

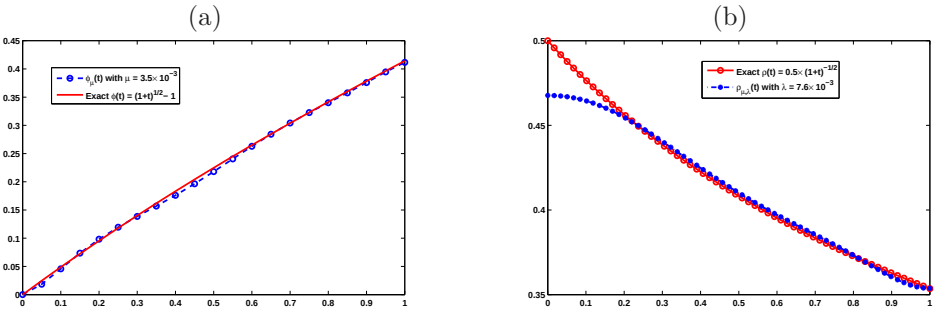

Figure 2.3: The numerical performance for the growth speed identification with the noisy level $\delta = 1\%$ of finite difference solution. (a) The intermediate reconstructed $R_\alpha^{M,N}(t)$ with $M = 8$ and $\alpha = 3.5 \times 10^{-3}$. (b) The reconstructed $\rho_\alpha^{M,N}(t)$ from $R_\alpha^{M,N}(t)$ by implementing the regularization method in [55] with a regularization parameter $\alpha = 7.6 \times 10^{-3}$.

2.5 Conclusion

In the phase transformation kinetics, both the nucleation and the growth mechanics are crucial in describing the properties of the specimens. Mathematically, the crystallization process obeys a governing equation of the hyperbolic type with the homogeneous initial condition and an appropriate boundary condition, where the nucleation rate $\Psi(x,t)$ and the growth speed $\rho(t)$ determine the specified kinetics. As for the inverse problems, the identification of

the nucleation rate can be formulated to an inverse source problem where a series of papers [11, 14, 20] are devoted to the non-isothermal hyperbolic-parabolic coupled system. In this chapter, we restrict to the one-dimensional case and follow the derivation in Chapter 1, where the consistence between the BCE model in [13] is also provided. In particular, an analytic solution of the hyperbolic governing equation is considered by a spectral method. A two-step truncated Tikhonov-type regularization scheme is proposed to identify the growth speed $\rho(t)$ in the form of a coefficient inverse problem for the hyperbolic equation. We note that a similar idea is recently considered to reconstruct a random source in the Helmholtz equation [6, 46]. Numerical examples show that the proposed scheme reconstructs the growth speed in an accurate manner.

We close the chapter by some general remarks for the future work mainly on inverse problems. Notice that in existing literatures, only one-dimensional inverse problems are considered for identifying the nucleation rate or the growth speed. How to extend the current work to higher dimensional cases would be important for both academical and industrial researchers. Simultaneously, concerning the identification of the nucleation rate $\Psi(x, t)$, a degenerate form, for instance, $\Psi(x, t) = f(x)\, g(x, t)$ where $g(x, t)$ is known, might be interesting since in a practical sense a priori spatial information would be available. This will be the main concentration of the next two chapters.

Chapter 3

Iterative Thresholding Algorithm for Inverse Source Problems for Hyperbolic Equations

In the previous chapter, the derivation of the hyperbolic-type equations from Cahn's time cone model demonstrated its significance in treating a corresponding coefficient inverse problem. In view of the hyperbolic equation, the identification of the nucleation rate turns out to be an inverse source problem, which is also important in practices especially in the three spatial dimensions. However, existing works on the related numerical reconstruction methods are absent. As a preparation, in this chapter we derive an efficient iterative thresholding algorithm for identifying the source term in a hyperbolic equation from partial interior measurements. We adopt the classical Tikhonov regularization to transform the ill-posed inverse source problem into an output least squares nonlinear minimization, which will be solved by the proposed iterative algorithm. It reveals that the iteration is computationally very easy and efficient: the minimizer at each step possess an explicit solution. Abundant amounts of numerical experiments are presented to demonstrate the accuracy and efficiency of the algorithm.

3.1 Introduction

Let $T > 0$ and Ω be an open bounded domain in $\mathbb{R}^d$ $(d = 1, 2, 3)$ whose boundary is of C^2 class. Consider the initial-boundary value problem for a hyperbolic equation with the homogeneous Neumann boundary condition

$$u(f)\begin{cases} \partial_t^2 u(x,t) - \triangle u(x,t) = f(x)\, h(x,t) & (x \in \Omega,\ 0 < t \le T), \\ u(x,0) = \partial_t u(x,0) = 0 & (x \in \Omega), \\ \partial_\nu u(x,t) = 0 & (x \in \partial\Omega,\ 0 < t \le T), \end{cases} \tag{3.1}$$

where $\nu = \nu(x)$ is the unit outward normal vector at $x \in \partial\Omega$ and $\partial_\nu u := \nabla u \cdot \nu$ denotes the normal derivative. Here we write the solution as $u(f)$ to emphasize its dependency upon the time-independent function f. Various conditions in (3.1) will be specified later, and the corresponding well-posedness result will be provided in Lemma 3.1.

The main focus of this chapter is the numerical treatment for the following inverse source problem.

Problem 3.1 *Let $\omega \subset \Omega$ and $T > 0$ be suitably given, and $u(f)$ solve* (3.1). *Determine $f(x)$ $(x \in \Omega)$ by the partial interior observation data $u(f)$ in $\omega \times (0, T)$.*

The investigation of the above problem from numerical aspects not only originates from the interest on mathematics, but also roots in its significance in practice. In our formulation (3.1), the source term $f(x)\,h(x,t)$ is incompletely separated into its spatial and temporal components, and the purposed inverse problem means the determination of the spatial component. Especially, if the source term is in form of complete separation of variables, i.e. h is space-independent, (3.1) becomes an approximation to a model for elastic waves, and the term $f(x)\,h(t)$ acts as the external force modeling vibrations (see Yamamoto [56]). Recently, it reveals in Liu and Yamamoto [49] that the one-dimensional time cone model for phase transformation kinetics (see Cahn [17]) is equivalent to (3.1), where $f(x)$ stands for the spatial distribution of the nucleation rate.

Although inverse hyperbolic problems have attracted considerable attentions during the last two decades, there are not many specific works on Problem 3.1 in our setting, that is, inverse source hyperbolic problems with the Neumann boundary condition. In [31, 32, 35, 57], Problem 3.1 was discussed as a linearization of the related inverse coefficient problem. Meanwhile, in spite of the physically more natural realization of the Neumann boundary condition, the majority of existing works dealt with the Dirichlet counterpart which is technically easier (see, e.g., [53, 56, 57] and the references therein). With the establishment of Carleman estimates for Neumann problems (e.g., [30, 44]), the global Lipschitz stability for the reconstruction was proved for the boundary measurement case in Imanuvilov and Yamamoto [32] and the interior measurement case in [31] under the probably optimal geometrical condition on observable regions. The present chapter is mainly motivated by [31, Corollary 3.1] which dominates the unknown function f by the data $u(f)|_{\omega\times(0,T)}$ in system (3.1). For comprehensive discussions on inverse hyperbolic problems by Carleman estimates, see Bellassoued and Yamamoto [8].

Correspondingly, works on numerical reconstructions of source terms in hyperbolic equations are quite limited compared with those of coefficients. Regarding the numerical approaches to coefficient inverse hyperbolic problems and related topics, we refer to the two monographs [40, 42]. In [48], the authors developed a spectral method for the inverse coefficient problem for the hyperbolic equation derived in [49]. On the other hand, a class of iterative thresholding algorithms was purposed for linear inverse problems in early 2000s, whose convergence was first rigorously analyzed in Daubechies et al. [22]. As an extension of classical gradient algorithms with regularization, the iterative thresholding algorithm and its updated versions have proved to be feasible mainly in the abundant applications to image processing due to their simplicity (see [7, 9, 23, 29]). However, the flavor of this method is not familiar among the school of inverse problems for partial differential equations. Very recently, the iterative thresholding algorithm was utilized in Jiang et al. [38] to treat inverse problems for elliptic and parabolic equations.

In this chapter, we interpret the numerical solution to the ill-posed Problem 3.1 as the minimizer of an object functional with the Tikhonov regularization. By calculating the Frechét derivative and introducing the adjoint system of (3.1), we find the Euler equation that the minimizer should satisfy. This leads to the desired iteration method, which only requires to solve one forward and one backward problems at each step. It turns out that the derived iteration coincides with the iteration thresholding algorithm, and the convergence automatically follows. On the basis of dramatically fast forward solvers, a lot of numerical experiments up to three spatial dimensions are implemented to test the performance of our method from various aspects. To the best of the author's knowledge, the present chapter is the first attempt to apply

the iterative thresholding algorithm to inverse hyperbolic problems.

The remainder of this chapter is organized as follows. In Section 3.2, we briefly introduce the well-posedness of the forward problem (3.1) and the stability result for Problem 3.1. In Section 3.3, we reformulate our inverse source problem for numerical treatments, and purpose the iteration thresholding algorithm. Abundant amounts of numerical tests along with discussions on the performance are carried out in Section 3.4. Finally, concluding remarks and future works will be mentioned in Section 3.5.

3.2 Preliminary

We start from introducing some notations and relevant works on forward and inverse problems for hyperbolic equations. Let $H^1(\Omega)$, $H^1(\Omega \times (0,T))$, etc. denote usual Sobolev spaces. For later use, first we give a definition of the generalized solution to the initial-boundary value problem (3.1).

Definition 3.1 (see Isakov [34]) *Let $f \in L^2(\Omega)$ and $h \in L^2(0,T;L^\infty(\Omega))$. We say that $u(f) \in H^1(\Omega \times (0,T))$ is a generalized solution to problem* (3.1) *if it satisfies*

$$\int_0^T \int_\Omega (\nabla u(f) \cdot \nabla z - (\partial_t u(f))\, \partial_t z)\, \mathrm{d}x\mathrm{d}t = \int_0^T \int_\Omega f\, h\, z\, \mathrm{d}x\mathrm{d}t$$

for any test function $z \in H^1(\Omega \times (0,T))$ with $z|_{t=T} = 0$, and the initial condition $u(f)|_{t=0} = 0$.

The above definition of the generalized solution is easily understood by applying integration by parts to sufficiently smooth solutions. Concerning the solvability and stability issues for (3.1), we refer to the following well-known result.

Lemma 3.1 (see Lions and Magenes [47]) *Let $f \in L^2(\Omega)$, $h \in L^2(0,T;L^\infty(\Omega))$ and $\partial\Omega$ be of C^2 class. Then there exists a unique generalized solution $u(f) \in \mathcal{D}$ to the initial-boundary value problem* (3.1)*, where*

$$\mathcal{D} := \left\{ w \in C([0,T];H^1(\Omega));\ \partial_t w \in C([0,T];L^2(\Omega)) \right\}. \tag{3.2}$$

Moreover, there exists a constant $C = C(\Omega,T,h) > 0$ such that

$$\|u(f)(\,\cdot\,,t)\|_{H^1(\Omega)} + \|\partial_t u(f)(\,\cdot\,,t)\|_{L^2(\Omega)} \le C\|f\|_{L^2(\Omega)}.$$

Regarding the uniqueness and stability of Problem 3.1, we state without proof the following result which is a special case of [31, Corollary 3.1].

Lemma 3.2 *Let ω be a subdomain of Ω such that*

$$\{x \in \partial\Omega;\ (x-x_0)\cdot\nu(x) \ge 0\} \subset \partial\omega \text{ for some } x_0 \notin \overline{\Omega \setminus \omega},\ \text{and } T > \sup_{x\in\Omega} |x - x_0|. \tag{3.3}$$

Further assume that for any $x \in \partial\Omega \setminus \partial\omega$, there exists an open ball U_x centered at x such that $U_x \cap \Omega$ is convex. Let $u(f)$ be the solution to the initial-boundary vale problem (3.1)*, where $f \in L^2(\Omega)$, $h \in H^1(0,T;L^\infty(\Omega))$ and $|h(\,\cdot\,,0)| \ge h_0$ a.e. in Ω for some constant $h_0 > 0$. Then there exists a constant $C = C(\omega,\Omega,T,h) > 0$ such that*

$$\|f\|_{L^2(\Omega)} \le C\left(\|\partial_t u(f)\|_{L^2(\omega\times(0,T))} + \|\partial_t^2 u(f)\|_{L^2(\omega\times(0,T))}\right).$$

Lemma 3.2 is the starting point for developing a feasible numerical reconstruction of the source term, because the theoretical stability is guaranteed under condition (3.3) on the observable subdomain ω and duration T. Although such a condition mainly originates from its necessity in the proof of Lemma 3.2 by Carleman estimates, it also follows naturally from the essence of wave propagation. On the one hand, ω cannot be too localized to capture waves in all directions. On the other hand, due to the finite propagation speed, adequate observation time should be given for the distant wave to reach ω. We illustrate a typical choice of x_0, ω and T in Figure 3.1 for readers' better understanding.

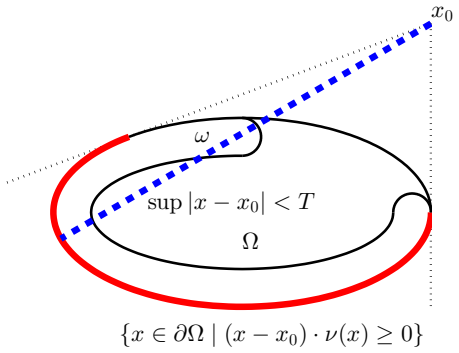

Figure 3.1: A typical example for the spatial and temporal assumption guaranteeing the stability of Problem 3.1.

3.3 Iterative thresholding algorithm

In this section, we specify $f_{\text{true}} \in L^2(\Omega)$ as the true solution to Problem 3.1 and investigate its numerical reconstruction by the noise contaminated observation data u^δ in $\omega \times (0, T)$, which satisfies $\|u^\delta - u(f_{\text{true}})\|_{L^2(\omega\times(0,T))} \leq \delta$ and δ stands for the noise level. For avoiding ambiguity, we interpret $u^\delta \equiv 0$ out of $\omega \times (0, T)$ so that it is well-defined in $\Omega \times (0, T)$.

With the a priori knowledge on the boundedness of f_{true} and appropriate observation data, the reconstruction can be carried out through a classical Tikhonov regularization technique. We formulate the reconstruction as the following output least square formulation with the Tikhonov regularization

$$\min_{f\in L^2(\Omega)} J(f), \quad J(f) := \|u(f) - u^\delta\|^2_{L^2(\omega\times(0,T))} + \alpha\|f\|^2_{L^2(\Omega)}, \tag{3.4}$$

where $\alpha > 0$ is the regularization parameter.

Nearly all effective iterative methods for solving nonlinear optimizations need the information of the derivatives of the concerned objective functional. It follows from a direct computation that the Fréchet derivative $J'(f)\widetilde{f}$ of $J(f)$ for any direction $\widetilde{f} \in L^2(\Omega)$ reads

$$\begin{aligned} J'(f)\widetilde{f} &= 2\int_0^T\int_\omega \big(u(f) - u^\delta\big)\,\big(u'(f)\widetilde{f}\,\big)\,\mathrm{d}x\mathrm{d}t + 2\alpha\int_\Omega f\,\widetilde{f}\,\mathrm{d}x \\ &= 2\int_0^T\int_\omega \big(u(f) - u^\delta\big)\,u(\widetilde{f}\,)\,\mathrm{d}x\mathrm{d}t + 2\alpha\int_\Omega f\,\widetilde{f}\,\mathrm{d}x. \end{aligned} \tag{3.5}$$

Here $u'(f)\widetilde{f}$ denotes the Fréchet derivative of $u(f)$ in the direction $\widetilde{f}$, and the linearity of (3.1) immediately yields

$$u'(f)\widetilde{f} = \lim_{\epsilon\to 0}\frac{u(f + \epsilon\,\widetilde{f}\,) - u(f)}{\epsilon} = u(\widetilde{f}\,).$$

Obviously, it is extremely expensive to use this formula to evaluate $J'(f)\widetilde{f}$ for all $\widetilde{f} \in L^2(\Omega)$, since one should solve system (3.1) for $u(\widetilde{f})$ with $\widetilde{f}$ varying in $L^2(\Omega)$ in the computation for a fixed f.

In order to reduce the computational costs for computing the Fréchet derivatives, we introduce the adjoint system of (3.1), that is, the following system for a backward hyperbolic equation

$$z(f)\begin{cases}\partial_t^2 z - \triangle z = \chi_\omega \left(u(f) - u^\delta\right) & \text{in } \Omega \times [0,T),\\ z = \partial_t z = 0 & \text{in } \Omega \times \{T\},\\ \partial_\nu z = 0 & \text{on } \partial\Omega \times [0,T),\end{cases} \tag{3.6}$$

where χ_ω denotes the characterization function of ω. The generalized solution to (3.6) can be defined in the same way as that in Definition 3.1. On the other hand, since Lemma 3.1 and $f \in L^2(\Omega)$ indicate $u(f) \in \mathcal{D}$ (see (3.2) for the definition of $\mathcal{D}$), we have $\chi_\omega \left(u(f) - u^\delta\right) \in L^2(\Omega \times (0,T))$ and thus $z(f) \in \mathcal{D}$ again by Lemma 3.1. Therefore, by the definition of the generalized solutions, the first term in (3.5) is further treated as

$$\begin{aligned}\int_0^T\!\!\int_\omega \left(u(f) - u^\delta\right) u(\widetilde{f})\,\mathrm{d}x\mathrm{d}t &= \int_0^T\!\!\int_\Omega \chi_\omega \left(u(f) - u^\delta\right) u(\widetilde{f})\,\mathrm{d}x\mathrm{d}t\\ &= \int_0^T\!\!\int_\Omega \Big(\nabla u(\widetilde{f}) \cdot \nabla z(f) - (\partial_t u(\widetilde{f}))\,\partial_t z(f)\Big)\,\mathrm{d}x\mathrm{d}t\\ &= \int_0^T\!\!\int_\Omega \widetilde{f}\,h\,z(f)\,\mathrm{d}x\mathrm{d}t,\end{aligned} \tag{3.7}$$

implying

$$J'(f)\widetilde{f} = 2\int_\Omega \left(\int_0^T h\,z(f)\,\mathrm{d}t + \alpha\,f\right)\widetilde{f}\,\mathrm{d}x, \quad \widetilde{f} \in L^2(\Omega).$$

This suggests a characterization of the solution to the minimization problem (3.4).

Proposition 3.1 *$f^* \in L^2(\Omega)$ is the minimizer of the functional $J(f)$ in (3.4) only if it satisfies the Euler equation*

$$\int_0^T h\,z(f^*)\,\mathrm{d}t + \alpha\,f^* = 0, \tag{3.8}$$

where $z(f^*)$ solves the backward system (3.6) with the coefficient f^*.

To solve the nonlinear equation (3.8) for f^*, one may employ the iteration

$$f_{m+1} = \frac{K}{K+\alpha} f_m - \frac{1}{K+\alpha}\int_0^T h\,z(f_m)\,\mathrm{d}t, \tag{3.9}$$

where $K > 0$ is a tuning parameter acting as a weight between the previous step and the iterative update.

To discuss the choice of K to guarantee the convergence, we take advantage of the fact that the iteration (3.9) in principle coincides with the iterative thresholding algorithm, which can be derived from the minimization problem of a surrogate functional (see, e.g., [22]). Actually, fixing $\widetilde{f} \in L^2(\Omega)$, we introduce a surrogate functional $J^s(f, \widetilde{f})$ of $J(f)$ as

$$J^s(f,\widetilde{f}) := J(f) + K\|f - \widetilde{f}\,\|^2_{L^2(\Omega)} - \|u(f) - u(\widetilde{f})\|^2_{L^2(\omega\times(0,T))}.$$

For the positivity of J^s, there should hold $K\|f\|^2_{L^2(\Omega)} \geq \|u(f)\|^2_{L^2(\omega\times(0,T))}$ for all $f \in L^2(\Omega)$. This is achieved by choosing

$$K \geq \|A\|^2, \tag{3.10}$$

where A is a linear operator defined as

$$A : L^2(\Omega) \to L^2(\omega \times (0,T)),$$
$$f \mapsto u(f)|_{\omega\times(0,T)},$$

and the boundedness of A is readily seen from Lemma 3.1. Therefore, there holds

$$J(f) = J^s(f,f) \le J^s(f,\widetilde{f}),$$

and thus $J^s(f,\widetilde{f})$ can be regarded as a small perturbation of $J(f)$ when $\widetilde{f}$ is close to f. On the other hand, it follows from (3.7) that

$$\begin{aligned}
J^s(f,\widetilde{f}) &= 2\int_0^T\!\!\int_\omega u(f)\left(u(\widetilde{f}) - u^\delta\right)\mathrm{d}x\mathrm{d}t + \|u^\delta\|^2_{L^2(\omega\times(0,T))} - \|u(\widetilde{f})\|^2_{L^2(\omega\times(0,T))} \\
&\quad + \alpha\|f\|^2_{L^2(\Omega)} + K\|f-\widetilde{f}\,\|^2_{L^2(\Omega)} \\
&= K\|f-\widetilde{f}\,\|^2_{L^2(\Omega)} + \alpha\|f\|^2_{L^2(\Omega)} + 2\int_0^T\!\!\int_\Omega f\,h\,z(\widetilde{f})\,\mathrm{d}x\mathrm{d}t \\
&\quad - \|u(\widetilde{f})\|^2_{L^2(\omega\times(0,T))} + \|u^\delta\|^2_{L^2(\omega\times(0,T))} \\
&= (K+\alpha)\|f\|^2_{L^2(\Omega)} - 2\int_\Omega f\left(K\widetilde{f} - \int_0^T h\,z(\widetilde{f})\,\mathrm{d}t\right)\mathrm{d}x \\
&\quad + K\|\widetilde{f}\,\|^2_{L^2(\Omega)} - \|u(\widetilde{f})\|^2_{L^2(\omega\times(0,T))} + \|u^\delta\|^2_{L^2(\omega\times(0,T))}.
\end{aligned}$$

Since this is a quadratic form with respect to f when u^δ and $\widetilde{f}$ are fixed, we see

$$\operatorname*{arg\,min}_{f\in L^2(\Omega)} J^s(f,\widetilde{f}) = \frac{K}{K+\alpha}\widetilde{f} - \frac{1}{K+\alpha}\int_0^T h\,z(\widetilde{f})\,\mathrm{d}t.$$

Consequently, the iterative update (3.9) is equivalent to solving the minimization problem $\min_{f\in L^2(\Omega)} J^s(f,\widetilde{f})$ with $\widetilde{f} = f_m$. Moreover, the convergence of this iteration was proved in [22] for any bounded linear operator A, provided that the constant $K > 0$ is chosen according to condition (3.10).

Now we are well prepared to state the main algorithm for the numerical reconstruction.

Algorithm 3.1 *Choose a tolerance $\varepsilon > 0$, a regularization parameter $\alpha > 0$ and a tuning constant $K > 0$ according to* (3.10)*. Give an initial guess f_0, and set $m = 0$.*

1. *Compute f_{m+1} by the iterative update* (3.9)*.*
2. *If $\|f_{m+1} - f_m\|_{L^2(\Omega)}/\|f_m\|_{L^2(\Omega)} \le \varepsilon$, then stop the iteration. Otherwise, update $m \leftarrow m+1$ and return to Step* 1*.*

It turns out that at each iteration step, we only need to solve the forward system (3.1) once for $u(f_m)$ and the backward system (3.6) once for $z(f_m)$ subsequently. Therefore, it is very easy and cheap to implement Algorithm 3.1. As will be shown from many numerical experiments in the next section, we see that our proposed Algorithm 3.1 is also considerably efficient and accurate even for three spatial dimensions.

We conclude this section by stating the convergence result of Algorithm 3.1, which is a direct application of [22, Theorem 3.1].

Lemma 3.3 *Let $K > 0$ be a constant satisfying condition* (3.10)*. Then for any $f_0 \in L^2(\Omega)$, the sequence $\{f_m\}_{m=1}^\infty$ produced by the iteration* (3.9) *converges strongly to the solution to the minimization problem* (3.4)*.*

3.4 Numerical experiments

In this section, we will apply the established Algorithm 3.1 to the numerical identification of the spatial component f of the source term in system (3.1). The general settings of the numerical reconstruction are assigned as follows. For simplicity, we take $\Omega = (0,1)^d$ $(d = 1, 2, 3)$. The duration T may change with respect to the choices of ω according to condition (3.3) which guarantees a reasonable reconstruction. Actually, since an observable subdomain ω has certain thickness in practice, the condition on T can be relaxed to $T > \operatorname{diam}(\Omega \setminus \overline{\omega})$ in numerical tests. Although in Section 3.3 the difference between the noiseless data $u(f_{\text{true}})$ and the actually observed data u^δ was evaluated in the $L^2(\omega \times (0,T))$-norm, here for simplicity we produce u^δ by adding uniform random noises to the noiseless data, i.e.

$$u^\delta(x,t) = u(f_{\text{true}})(x,t) + \delta \operatorname{rand}(-1,1), \quad \forall\, x \in \omega,\ \forall\, t \in (0,T),$$

where $\operatorname{rand}(-1,1)$ denotes the uniformly distributed random number in $[-1,1]$ and $\delta \geq 0$ is the noise level. Here we choose δ as a certain portion of the amplitude of the exact solution, i.e.

$$\delta := \delta_0 \max_{\overline{\Omega} \times [0,T]} |u(f_{\text{true}})|, \quad 0 < \delta_0 < 1.$$

As for the various parameters involved in Algorithm 3.1, we take $\varepsilon = 1\%\, \delta_0$ as the tolerance, and choose the regularization parameter as $\alpha = 0.1\%\, \delta$. The initial guess f_0 is always taken as a constant, which is usually rather inaccurate in the test problems. Finally, the tuning parameter $K > 0$ will be chosen according to the size of the subdomain ω, the duration T, and the known component $h(x,t)$ of the source term.

At each step of the iteration (3.9) in all of the numerical experiments, the forward system (3.1) and the backward system (3.6) are solved by some absolutely stable schemes of the finite difference method. In our implementations, we apply the von Neumann scheme for one-dimensional case and the alternating direction implicit (ADI) method for two- and three-dimensional cases (see [28, 45]). For instance, in case of $d = 3$, we work on the equidistant grids

$$x_1^i = x_2^i = x_3^i = i\,\Delta x \ (i = 0, 1, \ldots, N_x), \quad t_n = n\,\Delta t \ (n = 0, 1, \ldots, N_t)$$

with $N_x\,\Delta x = 1$ and $N_t\,\Delta t = T$, where h and τ are the step lengths in space and time respectively. By introducing the ratio $\kappa := (\Delta t/\Delta x)^2$ and the difference operators

$$\begin{aligned}
\delta_{x_1}^2 u_n^{i,j,k} &:= u_n^{i+1,j,k} - 2\,u_n^{i,j,k} + u_n^{i-1,j,k},\\
\delta_{x_2}^2 u_n^{i,j,k} &:= u_n^{i,j+1,k} - 2\,u_n^{i,j,k} + u_n^{i,j-1,k},\\
\delta_{x_3}^2 u_n^{i,j,k} &:= u_n^{i,j,k+1} - 2\,u_n^{i,j,k} + u_n^{i,j,k-1},
\end{aligned}$$

we discretize the time evolution of the governing equation in (3.1) as

$$\begin{aligned}
u_{n+1/3}^{i,j,k} - 2\,u_n^{i,j,k} + u_{n-1}^{i,j,k} &= \frac{\kappa}{4}\,\delta_{x_1}^2 \left(u_{n+1/3}^{i,j,k} + 2\,u_n^{i,j,k} + u_{n-1}^{i,j,k}\right) + \kappa\left(\delta_{x_2}^2 + \delta_{x_3}^2\right) u_n^{i,j,k}\\
&\quad + \Delta t^2 f(x_1^i, x_2^j, x_3^k)\, h(x_1^i, x_2^j, x_3^k, t_n),\\
u_{n+2/3}^{i,j,k} - u_{n+1/3}^{i,j,k} &= \frac{\kappa}{4}\,\delta_{x_2}^2 \left(u_{n+2/3}^{i,j,k} - 2\,u_n^{i,j,k} + u_{n-1}^{i,j,k}\right),\\
u_{n+1}^{i,j,k} - u_{n+2/3}^{i,j,k} &= \frac{\kappa}{4}\,\delta_{x_3}^2 \left(u_{n+1}^{i,j,k} - 2\,u_n^{i,j,k} + u_{n-1}^{i,j,k}\right),
\end{aligned}$$

where $u_n^{i,j,k}$ stands for an approximation of $u(x_1^i, x_2^j, x_3^k, t_n)$, and $u_{n+1/3}^{i,j,k}$, $u_{n+2/3}^{i,j,k}$ denote some intermediate values. The backward system (3.6) is discretized in the same manner. It turns out

that the ADI method performs efficiently even in three-dimensional case. In fact, it only takes about 5 seconds for a problem of $50^3 \times 100$ scale. On the other hand, the involved integrals in time are simply approximated by the composite trapezoidal rule.

In what follows, we shall demonstrate the reconstruction method by abundant test examples in one, two and three spatial dimensions. Other than the illustrative figures, we mainly evaluate the numerical performance by the number M of iterations, the relative L^2 error

$$\mathrm{err} := \frac{\|f_M - f_{\mathrm{true}}\|_{L^2(\Omega)}}{\|f_{\mathrm{true}}\|_{L^2(\Omega)}}$$

and the elapsed time, where f_M is recognized as the result of the numerical reconstruction.

3.4.1 One-dimensional examples

In case of $d = 1$, we always take $T = 1$ and divide the space-time region $\overline{\Omega} \times [0, T] = [0, 1] \times [0, 1]$ as a 101×101 equidistant mesh and test the performance of Algorithm 3.1 from various aspects. The choice $T = 1$ is sufficient because there always holds $\mathrm{diam}(\Omega \setminus \overline{\omega}) < 1$ whatever ω we set.

Example 3.1 In this example, we carry out numerical tests with different combinations of the noise level δ and the observable subdomain ω to see their influences upon the reconstructions. Take the known component of the source term as $h(x, t) = x + t + 1$, let $f_{\mathrm{true}}(x) = \cos(\pi x) + 1$ and set the initial guess as $f_0 \equiv 1$. First we fix $\omega = \Omega \setminus [1/10, 9/10]$ and change the noise levels as 1%, 2%, 4% and 8% of the amplitude of $u(f_{\mathrm{true}})$. Then we fix an 1% noise and reduce the size of ω from $\omega = \Omega \setminus [1/5, 4/5]$ to $\omega = \Omega \setminus [1/20, 19/20]$. The choices of parameters in the tests and corresponding numerical performances are listed in Table 3.1. For a better understanding of reconstructions, we visualize several representative examples in Table 3.1 to compare the exact and recovered solutions in Figure 3.2.

Table 3.1: Parameters and corresponding numerical performances in Example 3.1 under various combinations of noise levels and the observable subdomains.

δ_0	ω	K	M	err	elapsed time (s)	illustration
1%	$\Omega \setminus [1/10, 9/10]$	0.02	113	1.86%	2.71	Figure 3.2(a)
2%	$\Omega \setminus [1/10, 9/10]$	0.02	84	2.91%	2.04	
4%	$\Omega \setminus [1/10, 9/10]$	0.02	73	3.32%	1.65	
8%	$\Omega \setminus [1/10, 9/10]$	0.02	65	3.79%	1.63	Figure 3.2(b)
1%	$\Omega \setminus [1/5, 4/5]$	0.04	118	1.15%	2.78	Figure 3.2(c)
1%	$\Omega \setminus [1/20, 19/20]$	0.015	122	2.77%	2.81	Figure 3.2(d)

Example 3.2 Now we compare the numerical performances by selecting various exact solutions f_{true} with different monotonicity and smoothness. More precisely, we fix $h(x, t) = 2 + \pi^2 t^2$ and choose (a) $f^{\mathrm{a}}_{\mathrm{true}}(x) = x$, (b) $f^{\mathrm{b}}_{\mathrm{true}}(x) = \sin(\pi x) + x$, (c) $f^{\mathrm{c}}_{\mathrm{true}}(x) = \frac{1}{2}\cos(2\pi x) + 1$ or (d) $f^{\mathrm{d}}_{\mathrm{true}}(x) = 1 - |2x - 1|$. In all cases, we set the noise level as 5% of the amplitude of $u(f_{\mathrm{true}})$, and take $\omega = \Omega \setminus [1/10, 9/10]$. Correspondingly, the tuning parameter is chosen as $K = 0.1$. The comparisons of exact and reconstructed solutions are shown in Figure 3.3. The numbers M of iterations and relative errors are listed in Table 3.2.

In the above examples, it is readily seen that even with quite coarse initial guesses f_0, the numerical reconstructions appear to be satisfactory in view of the ill-posedness of the inverse

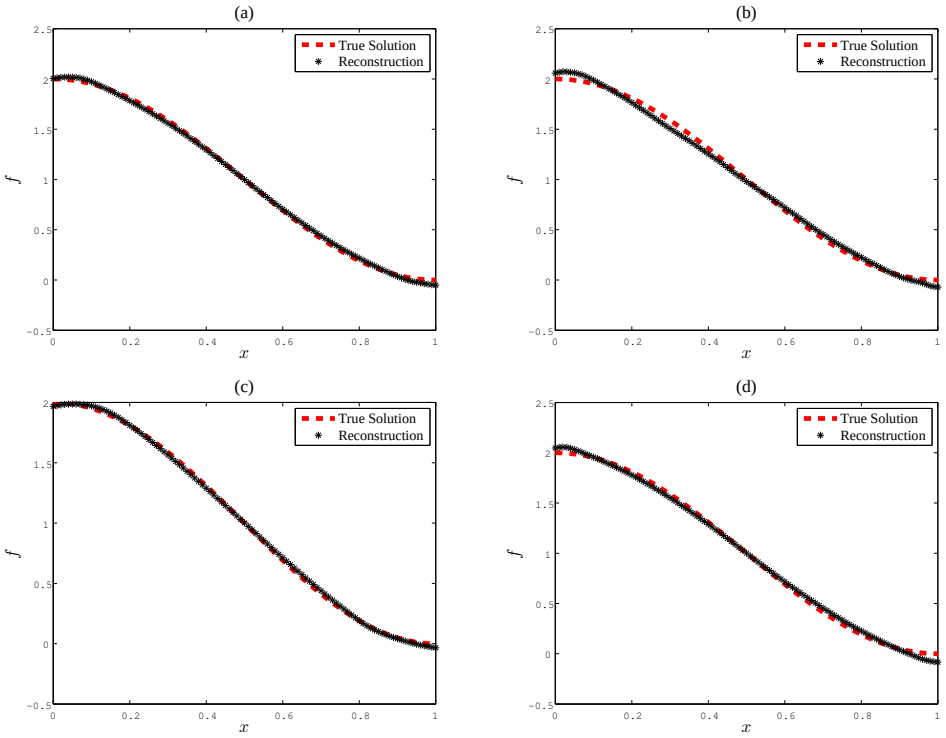

Figure 3.2: Illustrations of the exact and reconstructed solutions in Example 3.1 with several combinations of the noise level and subdomain. (a) $\delta_0 = 1\%$, $\omega = \Omega \setminus [1/10, 9/10]$. (b) $\delta_0 = 8\%$, $\omega = \Omega \setminus [1/10, 9/10]$. (c) $\delta_0 = 1\%$, $\omega = \Omega \setminus [1/5, 4/5]$. (d) $\delta_0 = 1\%$, $\omega = \Omega \setminus [1/20, 19/20]$.

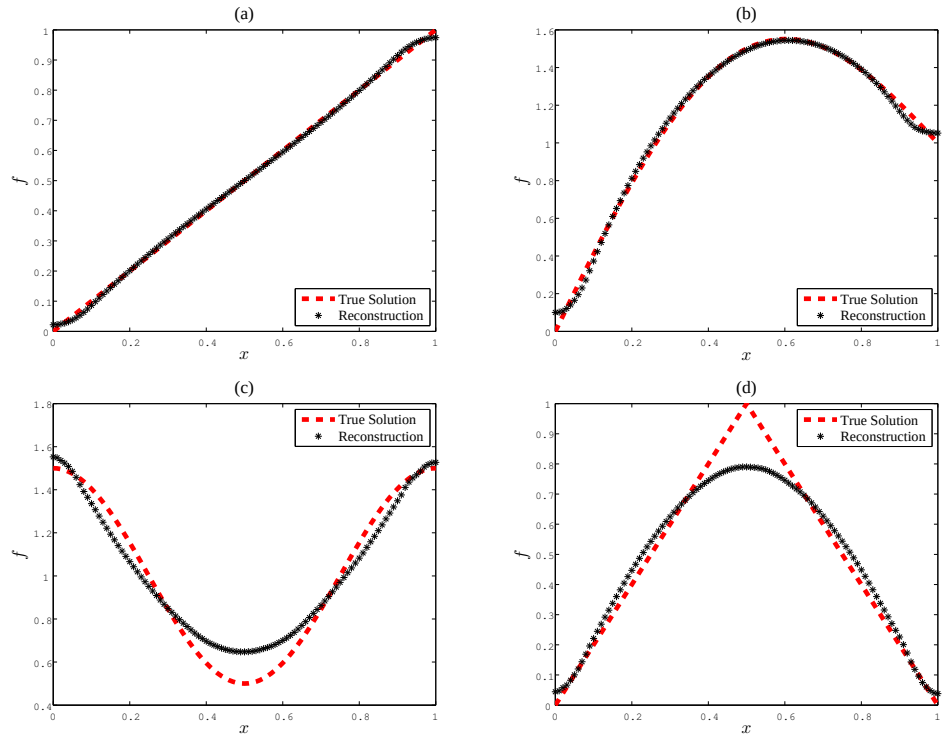

Figure 3.3: Illustrations of the exact and reconstructed solutions for Example 3.2. (a) $f^{\mathrm{a}}_{\mathrm{true}}(x) = x$. (b) $f^{\mathrm{b}}_{\mathrm{true}}(x) = \sin(\pi x) + x$. (c) $f^{\mathrm{c}}_{\mathrm{true}}(x) = \frac{1}{2}\cos(2\pi x) + 1$. (d) $f^{\mathrm{d}}_{\mathrm{true}}(x) = 1 - |2x - 1|$.

Table 3.2: Numerical performances of the reconstructions in Example 3.2 for various choices of exact solutions with different smoothness.

$f_{\text{true}}(x)$	initial guess	M	err	illustration
x	0.5	6	1.41%	Figure 3.3(a)
$\sin(\pi x)+x$	2.5	43	2.03%	Figure 3.3(b)
$\frac{1}{2}\cos(2\pi x)+1$	1	179	7.55%	Figure 3.3(c)
$1-\lvert 2x-1\rvert$	0.5	223	11.41%	Figure 3.3(d)

source problem. We evaluate the performance of our algorithm by analyzing the numerical results from the following aspects.

First, it is readily seen from Figures 3.2 and 3.3 that both of the above examples yield quite smooth reconstructions. In fact, according to the regularity result in Lemma 3.1, one can expect an $H^1(\Omega)$-regularity throughout the iteration (3.9), as long as the initial guess f_0 and the known component $h(x,t)$ of the source term are sufficiently smooth. Such a smoothness, however, prevents us from proper identifications of non-smooth true solutions (see case (d) of Example 3.2).

Second, the reconstructed solutions appear more sensitive to the size of the observable domain ω than to the data noise, but the non-monotonicity outside ω is difficult to reconstruct. The influence of the smallness of ω is witnessed from the second part of Table 3.1, which obviously comes from the limited information captured in ω. On the other hand, cases (a)–(c) in Example 3.2 imply a tendency that the better the monotonicity of f_{true} is, the more accurate the identification will be, and the convergence will also be faster. In conclusion, although the conditional stability of the reconstruction is guaranteed by Lemma 3.2, in practice the signal strength from $\Omega\setminus\overline{\omega}$ is overwhelmed by that inside ω, so that the behavior of f outside ω cannot remarkably influence the observation data in $\omega\times(0,T)$.

Third, Example 3.1 suggests a considerably strong robustness of our algorithm against the measurement error. Actually, one can see from the first part of Table 3.1 that the relative errors of the reconstructions only increase temperately as the observation noises are doubled. This phenomenon can be explained as follows. Suppose that the m-th iteration f_m is of certain regularity, say $f_m\in L^2(\Omega)$. According to Lemma 3.1, the solution $u(f_m)$ to (3.1) should be sufficiently smooth, namely $u(f_m)\in\mathcal{D}$ (see (3.2) for the definition of $\mathcal{D}$). Since the iteration (3.9) in principle aims at minimizing the surrogate functional $J^s(\,\cdot\,,f_m)$, it turns out that $u(f_m)|_{\omega\times(0,T)}$ tends to take an averaged state of u^δ in a sense that the error can be minimized. Therefore, provided that the observation data keep oscillating around the accurate ones, the reconstruction performs stably and insensitively in spite of the noise amplitude to a certain extent.

3.4.2 Two-dimensional examples

Now we turn to the case of $d=2$. Without lose of generality, we always generate the subdomain ω by removing a closed rectangle in $\Omega=(0,1)^2$ whose edges are parallel to the coordinate axes. Due to the geometry condition for the reconstruction, $\overline{\omega}$ should include at least two adjacent edges of $\overline{\Omega}$. Simultaneously, the condition $T>\operatorname{diam}(\Omega\setminus\overline{\omega})$ implies that the time duration T should be longer than the diagonal of the removed rectangle. In the sequel, the largest size of such rectangles will be taken as 0.9^2, and hence we will set $T=1.3>0.9\times\sqrt{2}$ in all tests for consistency. As before, we set the step size as 0.01 and divide the space-time region

as a $101^2 \times 131$ mesh in computation. Since the one-dimensional examples suggest that the reconstruction is insensitive to the noise, the noise level is always set as 5% of the amplitude of $u(f_{\text{true}})$.

Example 3.3 In the first two-dimensional example, we fix $h(x,t) = 5 + \pi^2 t^2$ and

$$f_{\text{true}}(x) = f_{\text{true}}(x_1, x_2) = \frac{1}{2}\cos(\pi x_1)\cos(\pi x_2) + 1. \tag{3.11}$$

We test the algorithm by changing the subdomain ω as follows. First, we keep the coverage $\partial\Omega \subset \overline{\omega}$ and reduce its thickness from 1/5, 1/10 to 1/20, that is, we take $\omega = \Omega\setminus[1/5, 4/5]^2$, $\omega = \Omega\setminus[1/10, 9/10]^2$ and $\omega = \Omega\setminus[1/20, 19/20]^2$ subsequently. Next, we fix the thickness as 1/10 and reduce the coverage of $\partial\Omega$ from 3 edges to 2, for instance, we choose $\omega = \Omega\setminus[1/10, 1]\times[1/10, 9/10]$ and $\omega = \Omega \setminus [1/10, 1]^2$. The choices of ω and various parameters as well as the corresponding numerical performances are listed in Table 3.3. The surface plots of the exact solution f_{true} and several representative reconstructions f_M are illustrated in Figure 3.4.

Table 3.3: Parameters and corresponding numerical performances in Example 3.3 under various choices of observable subdomains.

ω	K	f_0	M	err	elapsed time (s)	illustration
$\Omega \setminus [1/5, 4/5]^2$	3	1	31	0.98%	30.28	
$\Omega \setminus [1/10, 9/10]^2$	1.7	1	27	2.27%	26.79	Figure 3.4(b)
$\Omega \setminus [1/20, 19/20]^2$	1	1	27	2.96%	26.35	
$\Omega \setminus [1/10, 1] \times [1/10, 9/10]$	1.3	1	27	3.46%	26.40	Figure 3.4(c)
$\Omega \setminus [1/10, 1]^2$	1	1.5	73	7.51%	71.72	Figure 3.4(d)

Example 3.4 Parallelly to Example 3.2 for the one-dimensional case, we investigate the influence of the monotonicity of f_{true} upon the numerical performance. To this end, we fix $h(x,t) = h(x_1, x_2, t) = x_1 - x_2 + 3t + 2$ and select three true solutions

$$f^{\text{a}}_{\text{true}}(x) = f^{\text{a}}_{\text{true}}(x_1, x_2) = \frac{1}{2}\cos(\pi x_1) + 1, \tag{3.12}$$

$$f^{\text{b}}_{\text{true}}(x) = f^{\text{b}}_{\text{true}}(x_1, x_2) = 3 - \exp\left(1 - \frac{x_1 + x_2}{2}\right), \tag{3.13}$$

$$f^{\text{c}}_{\text{true}}(x) = f^{\text{c}}_{\text{true}}(x_1, x_2) = \frac{1}{2}\cos(\pi x_1)\cos(2\pi x_2) + 1. \tag{3.14}$$

Here we take $\omega = \Omega \setminus [1/10, 9/10] \times [0, 9/10]$ as an intermediate choice, and set $K = 0.27$, $f_0 \equiv 1$. We compare the exact and reconstructed solutions in Figure 3.5. The numbers M of iterations and relative errors are shown in Table 3.4.

Table 3.4: Numerical performances of the reconstructions in Example 3.4 for various choices of exact solutions.

f_{true}	M	err	illustration
$f^{\text{a}}_{\text{true}}$ (see (3.12))	33	2.70%	Figure 3.5(a1)–(a2)
$f^{\text{b}}_{\text{true}}$ (see (3.13))	41	2.97%	Figure 3.5(b1)–(b2)
$f^{\text{c}}_{\text{true}}$ (see (3.14))	119	7.22%	Figure 3.5(c1)–(c2)

As expected, the above two-dimensional examples inherit mostly those phenomena observed in their one-dimensional counterparts and here we will not repeat the discussion again. Nevertheless we shall mention that, other than the thickness of ω, the iteration steps and relative

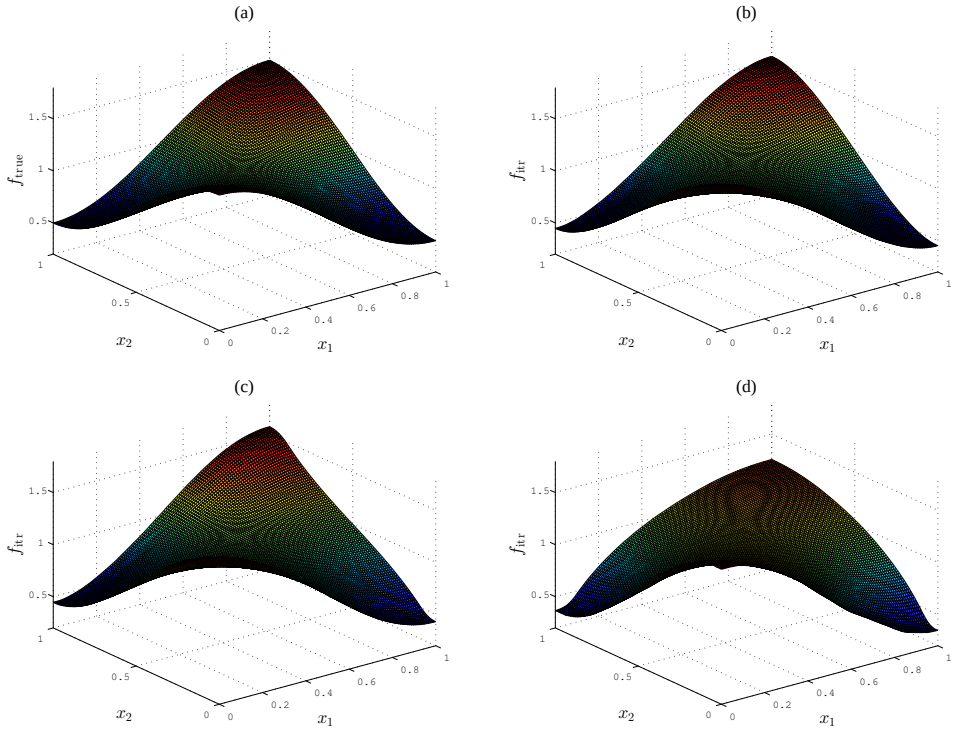

Figure 3.4: Comparison of the true solution to some reconstructed solutions in Example 3.3 with different subdomains of observation. (a) The true solution f_{true} defined in (3.11). (b) Reconstruction with $\omega = \Omega \setminus [1/10, 9/10]^2$. (c) Reconstruction with $\omega = \Omega \setminus [1/10, 1] \times [1/10, 9/10]$. (d) Reconstruction with $\omega = \Omega \setminus [1/10, 1]^2$.

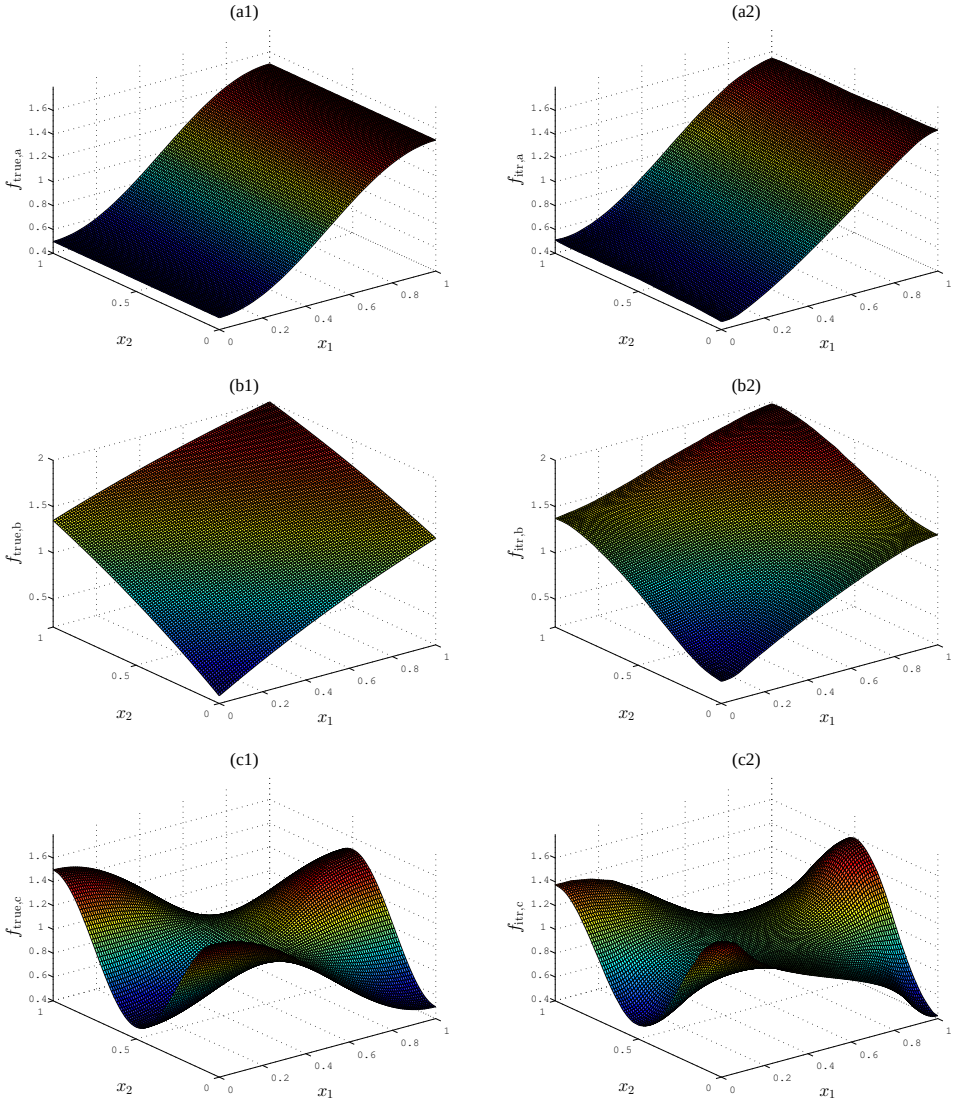

Figure 3.5: Illustrations of the exact and reconstructed solutions in Example 3.4 with the same settings and choices of parameters. (a1) $f^{\mathrm{a}}_{\mathrm{true}}$ defined in (3.12). (a2) Reconstruction of $f^{\mathrm{a}}_{\mathrm{true}}$. (b1) $f^{\mathrm{b}}_{\mathrm{true}}$ defined in (3.13). (b2) Reconstruction of $f^{\mathrm{b}}_{\mathrm{true}}$. (c1) $f^{\mathrm{c}}_{\mathrm{true}}$ defined in (3.14). (c2) Reconstruction of $f^{\mathrm{c}}_{\mathrm{true}}$.

errors of the numerical reconstructions also depend heavily on how much $\overline{\omega}$ can cover $\partial\Omega$. Although in all tests the algorithm performs quite well when $\partial\Omega$ is included in $\overline{\omega}$, it performs worse when $\overline{\omega}$ only covers 3 or 2 edges of $\partial\Omega$ in the sense of larger relative errors and more iteration steps. We can see clearly from Figures 3.4(c) and 3.5(c2) that the numerical solutions f_M fail to match with $f_{\rm true}$ especially on the uncovered edge, though $f_{\rm true}$ are well-reconstructed inside ω. In particular, Figure 3.4(d) indicates a dramatic difference at the uncovered corner $x = (1, 1)$ when $\omega = \Omega \setminus [1/10, 1]^2$. These demonstrate again the numerical ill-posedness regardless of the fact that the theoretical stability (Lemma 3.2) is valid under condition (3.3).

3.4.3 Three-dimensional examples

Finally, we proceed to the three-dimensional reconstruction of the source term $f_{\rm true}$. Similarly to the previous subsection, the subdomain ω is generated by removing a closed cube in $\Omega = (0, 1)^3$ whose edges are parallel to the coordinate axes. According to the geometry condition for the reconstruction, $\overline{\omega}$ should include at least three mutually adjacent faces of $\overline{\Omega}$. Since the largest size of the removed cubes will be 0.96^3, we set $T = 1.7 > 0.96 \times \sqrt{3}$ in all numerical tests in order to guarantee the condition $T > \mathrm{diam}(\Omega \setminus \overline{\omega})$. Considering the computational complexity for $d = 3$, we enlarge the mesh size in space and time as 0.02 to produce a $51^3 \times 86$ mesh for $\overline{\Omega} \times [0, T]$. As before, we still set the noise level as 5% of the amplitude of $u(f_{\rm true})$.

Example 3.5 Fix $h(x, t) = 2 + 3\pi^2 t^2$ and

$$f_{\rm true}(x) = f_{\rm true}(x_1, x_2, x_3) = \frac{1}{2}\cos(\pi x_1)\cos(\pi x_2)\cos(\pi x_3) + 1. \tag{3.15}$$

Similarly to the previous subsections, we study the influence of the choice of ω upon the numerical performance. First we keep the coverage $\partial\Omega \subset \overline{\omega}$ and use the thicknesses 2/25 and 1/25 to generate $\omega = \Omega \setminus [2/25, 23/25]^3$ and $\omega = \Omega \setminus [1/25, 24/25]^3$. Next we fix a thickness of 1/25 and reduce the faces of $\partial\Omega$ that $\overline{\omega}$ covers from 5 till 3 which is the minimum possible, that is, e.g. $\omega = \Omega \setminus [1/25, 24/25]^2 \times [1/25, 1]$, $\omega = \Omega \setminus [1/25, 24/25] \times [1/25, 1]^2$ and $\omega = \Omega \setminus [1/25, 1]^3$. The choices of ω and various parameters as well as the corresponding numerical performances are listed in Table 3.5. To visualize three-variate functions $f_{\rm true}$ and several of its representative reconstructions f_M, we show 4 sections for each of these functions at $x_3 = 0.2, 0.4, 0.6, 0.8$ in Figure 3.6.

Table 3.5: Parameters and corresponding numerical performances in Example 3.5 under various choices of observable subdomains.

ω	K	f_0	M	err	elapsed time (s)	illustration
$\Omega \setminus [2/25, 23/25]^3$	22	1	40	1.83%	608.68	
$\Omega \setminus [1/25, 24/25]^3$	12	1	38	2.49%	496.60	Figure 3.6(b)
$\Omega \setminus [1/25, 24/25]^2 \times [1/25, 1]$	10	1	38	3.07%	546.37	Figure 3.6(c)
$\Omega \setminus [1/25, 24/25] \times [1/25, 1]^2$	7.5	1	40	3.87%	520.20	Figure 3.6(d)
$\Omega \setminus [1/25, 1]^3$	6	0.5	39	8.84%	515.18	

Example 3.6 Finally, as before we test our algorithm by selecting true solutions with different degrees of monotonicity. We fix $h(x, t) = 5 + \pi^2 t^2$, and choose

$$f^{\rm a}_{\rm true}(x) = f^{\rm a}_{\rm true}(x_1, x_2, x_3) = \left(x_1 - \frac{1}{5}\right)\left(x_2 - \frac{1}{2}\right)^2 - \frac{1}{2}\cos(\pi x_1)\, x_3 + \frac{1}{2} x_2\, \mathrm{e}^{-x_3}, \tag{3.16}$$

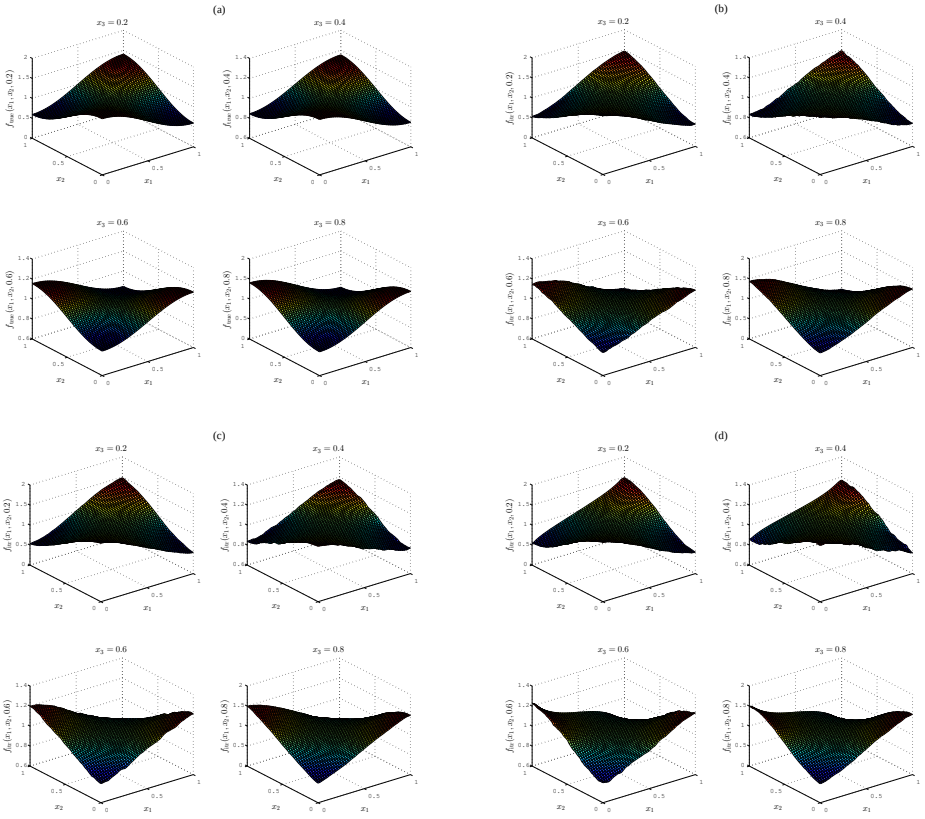

Figure 3.6: Comparison of the true solution to some reconstructed solutions in Example 3.5 with different subdomains of observation. (a) The true solution f_{true} defined in (3.15). (b) Reconstruction with $\omega = \Omega \setminus [1/25, 24/25]^3$. (c) Reconstruction with $\omega = \Omega \setminus [1/25, 24/25]^2 \times [1/25, 1]$. (d) Solution with $\omega = \Omega \setminus [1/25, 24/25] \times [1/25, 1]^2$.

$$f^{\mathrm{b}}_{\mathrm{true}}(x) = f^{\mathrm{b}}_{\mathrm{true}}(x_1, x_2, x_3) = \frac{1}{2}\cos(\pi x_1)\cos(2\pi x_2)\cos(\pi x_3) + 1, \tag{3.17}$$

$$f^{\mathrm{c}}_{\mathrm{true}}(x) = f^{\mathrm{c}}_{\mathrm{true}}(x_1, x_2, x_3) = \frac{1}{2}\cos(\pi x_1)\cos(2\pi x_2)\cos(2\pi x_3) + 1. \tag{3.18}$$

Here we set $\omega = \Omega \setminus [1/25, 24/25] \times [1/25, 1]^2$, $K = 3.5$ and $f_0 \equiv 1$. Comparisons of the corresponding sections of exact and reconstructed solutions are shown in Figure 3.7, and the numerical performances are listed Table 3.6.

Table 3.6: Numerical performances of the reconstructions in Example 3.6 for various choices of exact solutions.

f_{true}	M	err	illustration
$f^{\mathrm{a}}_{\mathrm{true}}$ (see (3.16))	64	3.45%	Figure 3.7(a1)–(a2)
$f^{\mathrm{b}}_{\mathrm{true}}$ (see (3.17))	120	7.85%	Figure 3.7(b1)–(b2)
$f^{\mathrm{c}}_{\mathrm{true}}$ (see (3.18))	101	11.98%	Figure 3.7(c1)–(c2)

Again, the three-dimensional examples show almost identical behaviors to that in lower dimensional cases. In summary, thinner observable subdomains ω result in worse reconstructions, and their coverage of $\partial\Omega$ also dominates the numerical performance to a great extent. On the other hand, the oscillation of f_{true} in $\Omega \setminus \overline{\omega}$ is extremely difficult to recover.

3.5 Concluding remarks

We have proposed in this work an efficient iterative thresholding algorithm for the inverse source problem in a hyperbolic system from partial interior measurements. By introducing the adjoint system (3.6) and the surrogate functional J^s, the stable nonlinear minimization formulated by the Tikhonov regularization can be solved by the iterative thresholding algorithm, which leads to get the explicit minimizer at each iteration. We have observed from many numerical tests that the proposed algorithm is very accurate and efficient. In particular, our algorithm is considerably robust against the measurement error, but is sensitive to the size of the observable domain.

In the next chapter, we will investigate the reconstruction of the nucleation rate $\Psi(x, t)$ in the three-dimensional time cone model (1.2)–(1.3). Since the derivation in Chapter 1 provides a convenience to consider an inverse source problem for the equivalent double wave equation

$$(\partial_t^2 - \triangle)^2 u(x, t) = F(x, t),$$

we can discuss the theoretical and numerical topics on the determination of the spatial component of $F(x, t)$ similarly to that in this chapter. We will establish the global Lipschitz stability and develop the corresponding iteration thresholding algorithm for this inverse problem in the next chapter.

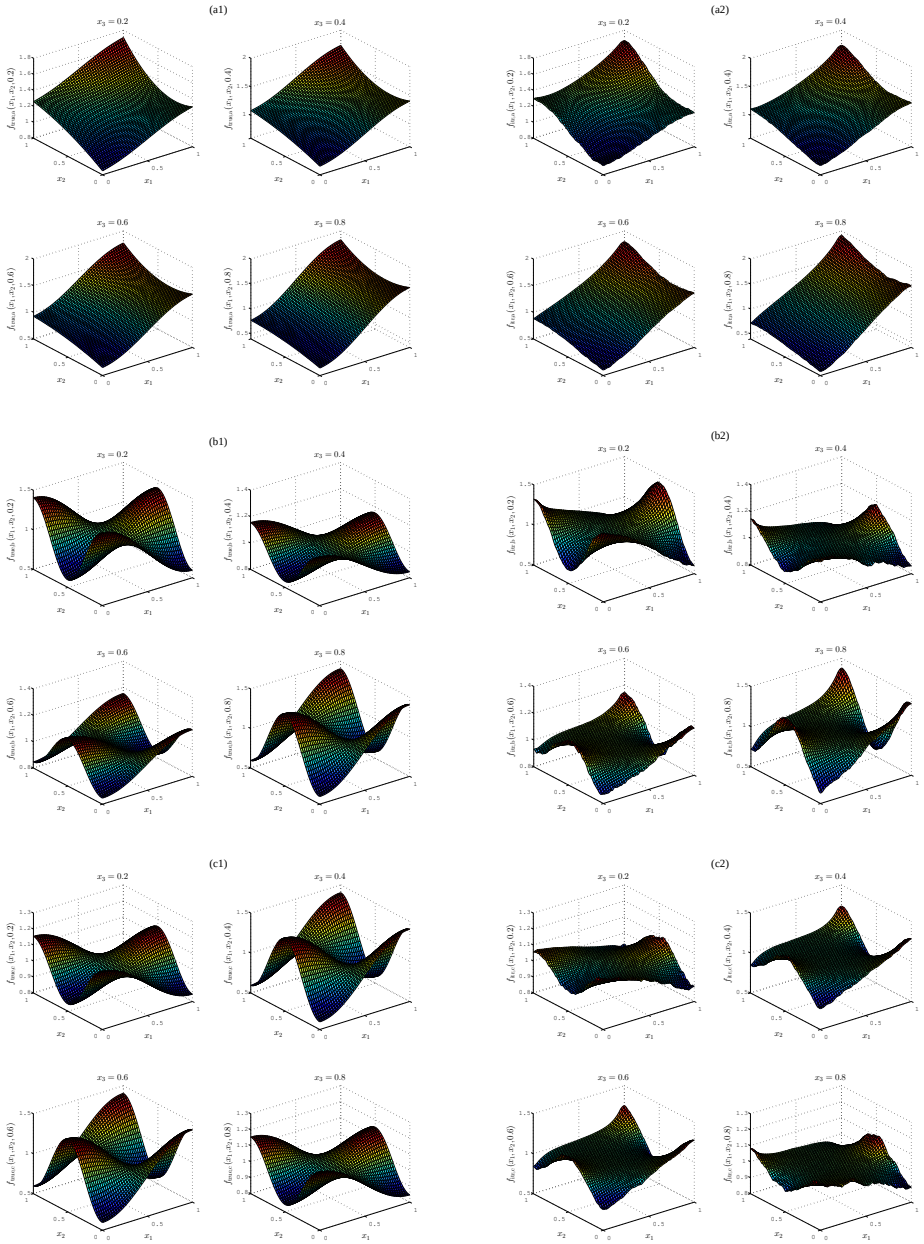

Figure 3.7: Illustrations of the exact and reconstructed solutions in Example 3.6 with the same settings and choices of parameters. (a1) $f^{\mathrm{a}}_{\mathrm{true}}$ defined in (3.16). (a2) Reconstruction of $f^{\mathrm{a}}_{\mathrm{true}}$. (b1) $f^{\mathrm{b}}_{\mathrm{true}}$ defined in (3.17). (b2) Reconstruction of $f^{\mathrm{b}}_{\mathrm{true}}$. (c1) $f^{\mathrm{c}}_{\mathrm{true}}$ defined in (3.18). (c2) Reconstruction of $f^{\mathrm{c}}_{\mathrm{true}}$.

Chapter 4

Nucleation Rate Reconstruction in the Three-Dimensional Time Cone Model

In this chapter, we consider the reconstruction of the nucleation rate in the three-dimensional time cone model, which turns out to be an inverse source problem for a double hyperbolic equation. More precisely, we attempt to recover a spatial component of the nucleation rate by the partial interior observation data. After a direct derivation of the hyperbolic-type governing equation from the original model, we establish the well-posedness result for the forward problem by the classical hyperbolic theory. To guarantee the validity of the reconstruction, we prove the global Lipschitz stability for the inverse problem based on a Carleman estimate. Motivated by the iterative thresholding algorithm for the same problem for the hyperbolic equation proposed in the previous chapter, we develop a similar iterative approach to the identification in a parallel framework. Extensive numerical experiments up to three spatial dimensions demonstrate the efficiency and accuracy of the algorithm, and detailed analysis of the computational performance are also provided.

4.1 Introduction and main results

As was introduced in Chapter 1, the time cone model (see Cahn [17]) describes the phase transformation kinetics which is essential in many natural phenomena and industrial processes. Other than the simulation of the phase transformation on the basis of the forward model, it is also important to identify the involved physical quantities (that is, the nucleation rate $\Psi(x,t)$ and the growth speed $\rho(t)$) from some observation data of the expectation $u(x,t)$ of transformation events. The investigations of these related inverse problem are significant in the system control and monitoring in many practical applications, for instance, to achieve certain mechanical properties of the materials as well as to improve the manufacturing efficiency.

Since the time cone model in its original formulation is inconvenient for mathematical analysis, in Chapter 1 we derived a class of multiple hyperbolic equations that are equivalent to the original model in any odd spatial dimensions. From the viewpoint of the partial differential equations, the problem on reconstructing the growth speed $\rho(t)$ reduces to a coefficient inverse problem and that on reconstructing the nucleation rate $\Psi(x,t)$ reduces to an inverse source problem. As a first attempt, in Chapter 2 we discussed the determination of $\rho(t)$ in one spatial

dimension.

The main concentration of this chapter is the inverse source problem for Cahn's time cone model with the partial interior observation data in three spatial dimensions, which is especially of practical importance. We recall that the original three-dimensional model takes the form

$$u(x,t) = \int_0^t \int_{B_3(x,R(t)-R(s))} \Psi(y,s)\,\mathrm{d}y\mathrm{d}s \quad (x \in \mathbb{R}^3,\ t \geq 0), \tag{4.1}$$

where $B_3(x,r)$ denotes the three-dimensional ball centered at $x \in \mathbb{R}^3$ with radius $r > 0$.

Although the equivalence of (4.1) and a double hyperbolic equation was a special case of Theorem 1.1 with $m = 1$, for the sake of self-containedness we still state the conclusion here.

Proposition 4.1 *Let $u(x,t)$ satisfy (4.1), where $u(x,t)$, $\Psi(x,t)$ and $\rho(t)$ ($x \in \mathbb{R}^3$, $t \geq 0$) are sufficiently smooth and $\rho(t)$ is strictly positive for $t \geq 0$. Introduce the hyperbolic operator*

$$\mathcal{H}_\rho w(x,t) := \frac{1}{\rho(t)}\,\partial_t \left(\frac{\partial_t w(x,t)}{\rho(t)} \right) - \triangle w(x,t).$$

Then $u(x,t)$ satisfies the following double hyperbolic system

$$\begin{cases} \mathcal{H}_\rho^2 u(x,t) = 8\pi\,\Psi(x,t)/\rho(t) & (x \in \mathbb{R}^3,\ t > 0), \\ \partial_t^\ell u(x,0) = 0 & (x \in \mathbb{R}^3,\ \ell = 0,1,2,3). \end{cases} \tag{4.2}$$

The above proposition reveals that, in the terminology of differential equations, the term $\Psi(x,t)/\rho(t)$ acts as the source term in a hyperbolic equation. On the other hand, the nucleation rate usually takes the following form of incomplete separation of variables $\Psi(x,t) = f(x)\,g(x,t)$, and we are interested in the determination of the spatial component f. To this end, we restrict the system (4.2) in a finite space-time region $\Omega \times (0,T)$, where $\Omega \subset \mathbb{R}^3$ is an open bounded domain and $T > 0$. Consider the corresponding initial-boundary value problem

$$\begin{cases} \mathcal{H}_\rho^2 u(x,t) = f(x)\,h(x,t) & (x \in \Omega,\ 0 < t \leq T), \\ \partial_t^\ell u(x,0) = 0 & (x \in \Omega,\ \ell = 0,1,2,3), \\ \partial_\nu u(x,t) = \partial_\nu \triangle u(x,t) = 0 & (x \in \partial\Omega,\ 0 < t \leq T), \end{cases} \quad \text{where } h(x,t) := \frac{8\pi\,g(x,t)}{\rho(t)}. \tag{4.3}$$

Here $\nu = \nu(x)$ is the unit outward normal vector at $x \in \partial\Omega$, and $\partial_\nu u := \nabla u \cdot \nu$ denotes the normal derivative. Although we impose the boundary conditions $\partial_\nu u = \partial_\nu \triangle u = 0$ on $\partial\Omega \times (0,T)$ which seems artificial, it is necessary for the formulation of such a fourth order equation, and the Neumann-type boundary conditions are natural in reality.

Now we are well prepared to purpose the following inverse source problem.

Problem 4.1 *Let $\omega \subset \Omega$ and $T > 0$ be suitably given, and u satisfy (4.3). Provided that g and ρ are known, determine $f(x)$ ($x \in \Omega$) by the partial interior observation data u in $\omega \times (0,T)$.*

To state the main results concerning the above problem, we briefly introduce the basic notations. For $k = 1,2,\ldots$, let $H^k(\Omega)$, $H^k(\Omega \times (0,T))$, etc. denote usual Sobolev spaces (see, e.g., Adams [1]). For $m = 0,1,\ldots$ and a Banach space X, define

$$C^m([0,T];X) := \{w \in C([0,T];X);\ \partial_t^j w \in C([0,T];X),\ j = 1,\ldots,m\},$$
$$H^m(0,T;X) := \{w \in L^2(0,T;X);\ \partial_t^j w \in L^2(0,T;X),\ j = 1,\ldots,m\}$$

and introduce the norms

$$\|w\|_{C^m([0,T];X)} := \sum_{j=0}^m \|\partial_t^j w\|_{C([0,T];X)}, \quad \|w\|_{H^m(0,T;X)} := \sum_{j=0}^m \|\partial_t^j w\|_{L^2(0,T;X)}.$$

Regarding the known functions g and ρ, we assume that

$$\begin{aligned} &g \in H^1(0,T;L^\infty(\Omega)) \text{ and } \exists\, g_0 > 0 \text{ such that } |g(\,\cdot\,,0)| \geq g_0 \text{ a.e. in } \Omega, \\ &\rho \in C^3[0,T] \text{ and } \exists\, \rho_0 > 0 \text{ such that } \rho \geq \rho_0 \text{ in } [0,T]. \end{aligned} \tag{4.4}$$

On the well-posedness of the forward problem for (4.3), we summarize as follows.

Proposition 4.2 *Let $\partial\Omega$ be of C^3 class, $f \in L^2(\Omega)$, and g, ρ satisfy (4.4). Then there is a unique solution u to the system (4.3) such that $u \in \bigcap_{k=1}^3 C^k([0,T];H^{3-k}(\Omega))$. Moreover, there exists a constant $C = C(\Omega,T,\rho) > 0$ such that*

$$\sum_{k=1}^3 \|u\|_{C^k(0,T;H^{3-k}(\Omega))} \leq C\|f\|_{L^2(\Omega)}\|g\|_{H^1(0,T;L^\infty(\Omega))}. \tag{4.5}$$

Now we state the stability result for Problem 4.1 under certain spatial and temporal conditions on the observable subdomain ω and the duration T.

Theorem 4.1 *Let $\partial\Omega$ be of C^3 class and u be the solution to (4.3), where $f \in L^2(\Omega)$ and g, ρ satisfy (4.4). Suppose that ω is a subdomain of Ω such that*

$$\begin{aligned} &\{x \in \partial\Omega;\, (x-x_0)\cdot\nu(x) \geq 0\} \subset \partial\omega \text{ for some } x_0 \notin \overline{\Omega \setminus \omega}\,, \\ &R(T) = \int_0^T \rho(t)\,\mathrm{d}t > \sup_{x\in\Omega} |x - x_0|, \quad \text{and} \\ &\forall\, x \in \partial\Omega \setminus \partial\omega,\ \exists\, U_x : \text{open ball centered at } x \text{ such that } U_x \cap \Omega \text{ is convex.} \end{aligned} \tag{4.6}$$

Then there exists a constant $C = C(\Omega,\omega,T,g,\rho) > 0$ such that

$$C^{-1}D \leq \|f\|_{L^2(\Omega)} \leq C\,D, \quad \text{where} \tag{4.7}$$

$$D := \|\partial_t^4 u - \rho^2\partial_t^2\triangle u\|_{L^2(\omega\times(0,T))} + \|\partial_t u\|_{L^2(0,T;H^2(\omega))} + \sum_{k=2}^3 \|\partial_t^k u\|_{L^2(\omega\times(0,T))}. \tag{4.8}$$

In the above theorem, although the conditions on ω and T mainly come from the proof by Carleman estimates, in principle they originate from the nature of the finite propagation speed of wave. We emphasize that the estimate (4.7) gives an equivalent relation between $\|f\|_{L^2(\Omega)}$ and D, where the first inequality almost follows directly from Proposition 4.2, and the second one guarantees a global Lipschitz stability for the inverse source problem. On the other hand, the term $\|\partial_t^4 u - \rho^2\partial_t^2\triangle u\|_{L^2(\omega\times(0,T))}$ in (4.8) seems incompletely decomposed. However, it can be seen from the proof of Proposition 4.2 that neither $\partial_t^4 u$ nor $\partial_t^2\triangle u$ makes sense in $L^2(\Omega\times(0,T))$, whereas one can show $\partial_t^4 u - \rho^2\partial_t^2\triangle u \in C([0,T];L^2(\Omega))$. In other words, inequality (4.5) in Proposition 4.2 is a sharp estimate in our setting.

Theorem 4.1 is the main theoretical result of this chapter, which also motivates the development of corresponding numerical reconstructions by a similar iterative thresholding algorithm introduced in the previous chapter. By use of the adjoint system of (4.3) in correspondence with Problem 4.1, it turns out that a parallel deduction of the iterative update is also valid for the double hyperbolic equation, followed by a similar guarantee for the convergence on the choice of the involved parameter.

As was mentioned before, the literatures on inverse problems for the phase transformation kinetics are quite limited, and most of those works are concerned with the one-dimensional prototype problem (see [10, 11, 14, 20]). The present chapter is the first work on identifying the nucleation rate in the three-dimensional model from both theoretical and numerical aspects.

The remainder of this chapter is organized as follows. In Section 4.2, we give proofs for Propositions 4.1 and 4.2 concerning the forward problem. Theorem 4.1, which asserts the global Lipschitz stability for Problem 4.1, is proved in Section 4.3 by the Carleman estimate. In Section 4.4, we reformulate our inverse source problem for numerical treatments, and purpose the iteration thresholding algorithm. Numerical tests up to three spatial dimensions along with discussions on the performance are carried out in Section 4.5. Finally, as an appendix, in Section 4.A we consider the inverse source problem with the same unknown function f but by the final observation in a slightly different setting. In this case, tt turns out that the reconstruction is only available in small domains.

4.2 Proofs of Propositions 4.1 and 4.2

We start from the derivation of the double hyperbolic equation (4.2) from the original model (4.1), and then validate the well-posedness of the corresponding initial-boundary value problem (4.3). Although a generalization of Proposition 4.1 was already proved for all odd spatial dimensions in Chapter 1, here we still provide a proof only in the three-dimensional case, which is a concrete realization of Remark 1.2.

Proof of Proposition 4.1. Introduce the change of variable in time

$$\tau = R(t) = \int_0^t \rho(s)\,\mathrm{d}s \quad (t \geq 0). \tag{4.9}$$

Thanks to the strict positivity of ρ, the function $R(t)$ is nonnegative and strictly increasing for $t \geq 0$, allowing a well-defined inverse function $t = R^{-1}(\tau)$ for $\tau \geq 0$. Moreover, it turns out from taking derivative in the identity $R(R^{-1}(\tau)) = \tau$ that $(R^{-1}(\tau))' = 1/\rho(R^{-1}(\tau))$. Therefore, we perform the same change of variable $\zeta = R(s)$ for $0 < s < t$ in the integral on the right-hand side of (4.1), and introduce an auxiliary function

$$U(x,\tau) := u(x, R^{-1}(\tau)) \tag{4.10}$$

to deduce

$$U(x,\tau) = \int_0^\tau \int_{B_3(x,\tau-\zeta)} F(y,\zeta)\,\mathrm{d}y\mathrm{d}\zeta \quad (x \in \mathbb{R}^3,\ \tau \geq 0), \quad F(x,\tau) := \frac{\Psi(x, R^{-1}(\tau))}{\rho(R^{-1}(\tau))}. \tag{4.11}$$

Now that the integral in (4.11) is taken in a regular cone $\Omega_1(x,\tau)$ with peak (x,τ) and unit slope, it is convenient to study $U(x,\tau)$ instead of $u(x,t)$ hereinafter. In fact, for any smooth function w defined in $\mathbb{R}^3 \times [0,\infty)$, it turns out that the same change of variable (4.9) and the definition $W(x,\tau) := w(x, R^{-1}(\tau))$ yield

$$\partial_\tau^2 W(x,\tau) = \frac{1}{\rho(t)}\,\partial_t \left(\frac{\partial_t w(x,t)}{\rho(t)} \right) \Big|_{t=R^{-1}(\tau)}, \quad \partial_\tau W(x,0) = \frac{\partial_t w(x,0)}{\rho(0)},$$

or, by taking $\tau = R(t)$ and recalling the operator $\mathcal{H}_\rho$,

$$\begin{cases} \mathcal{H}_\rho w(x,t) = \Box W(x,\tau)|_{\tau=R(t)} & (x \in \mathbb{R}^3,\ t > 0), \\ w(x,0) = W(x,0),\ \partial_t w(x,0) = \rho(0)\,\partial_\tau W(x,0) & (x \in \mathbb{R}^3), \end{cases} \tag{4.12}$$

where $\Box := \partial_\tau^2 - \triangle$ denotes the d'Alembertian with τ as the time variable.

Now we proceed to the derivation. First, it is readily seen that $U(x,0)=0$ by (4.11). To proceed, we adopt the polar coordinate transformation

$$y = x + r\,p(\psi_1,\psi_2) \quad (0<r<\tau-\zeta,\ 0<\psi_1<\pi,\ 0<\psi_2<2\pi), \quad \text{where}$$
$$p(\psi_1,\psi_2) := (\cos\psi_1, \sin\psi_1\cos\psi_2, \sin\psi_1\sin\psi_2).$$

Since the corresponding Jacobian is $r^2\sin\psi_1$, (4.11) is then equivalently represented as

$$U(x,\tau) = \int_0^\tau\!\!\int_0^{\tau-\zeta} r^2 \int_0^\pi \sin\psi_1 \int_0^{2\pi} F(x+r\,p(\psi_1,\psi_2),\zeta)\,\mathrm{d}\psi_2\mathrm{d}\psi_1\mathrm{d}r\mathrm{d}\zeta.$$

Now we can directly verify

$$\begin{aligned}\triangle U(x,\tau) &= \int_0^\tau\!\!\int_0^{\tau-\zeta} r^2 \int_0^\pi \sin\psi_1 \int_0^{2\pi} \triangle F(x+r\,p(\psi_1,\psi_2),\zeta)\,\mathrm{d}\psi_2\mathrm{d}\psi_1\mathrm{d}r\mathrm{d}\zeta \\ &= \int_0^\tau\!\!\int_{B_3(x,\tau-\zeta)} \triangle F(y,\zeta)\,\mathrm{d}y\mathrm{d}\zeta\end{aligned}$$

and, as a byproduct, we have $\triangle U(x,0)=0$. On the other hand, we calculate

$$\begin{aligned}\partial_\tau U(x,\tau) &= \int_0^\tau \partial_\tau \left\{ \int_0^{\tau-\zeta} r^2 \int_0^\pi \sin\psi_1 \int_0^{2\pi} F(x+r\,p(\psi_1,\psi_2),\zeta)\,\mathrm{d}\psi_2\mathrm{d}\psi_1\mathrm{d}r \right\} \mathrm{d}\zeta \\ &= \int_0^\tau (\tau-\zeta)^2 \int_0^\pi \sin\psi_1 \int_0^{2\pi} F(x+(\tau-\zeta)\,p(\psi_1,\psi_2),\zeta)\,\mathrm{d}\psi_2\mathrm{d}\psi_1\mathrm{d}\zeta\end{aligned}$$

and hence $\partial_\tau U(x,0)=0$. To deal with $\partial_\tau^2 U$, we notice the fact that $p(\psi_1,\psi_2)$ coincides with the unit outward normal vector $\nu(y)$ at $y=x+(\tau-\zeta)\,p(\psi_1,\psi_2)$ to obtain

$$\begin{aligned}\partial_\tau^2 U(x,\tau) &= \int_0^\tau \partial_\tau \left\{ (\tau-\zeta)^2 \int_0^\pi \sin\psi_1 \int_0^{2\pi} F(x+(\tau-\zeta)\,p(\psi_1,\psi_2),\zeta)\,\mathrm{d}\psi_2\mathrm{d}\psi_1 \right\} \mathrm{d}\zeta \\ &= 2\int_0^\tau (\tau-\zeta) \int_0^\pi \sin\psi_1 \int_0^{2\pi} F(x+(\tau-\zeta)\,p(\psi_1,\psi_2),\zeta)\,\mathrm{d}\psi_2\mathrm{d}\psi_1\mathrm{d}\zeta \\ &\quad + \int_0^\tau (\tau-\zeta)^2 \int_0^\pi \sin\psi_1 \int_0^{2\pi} \nabla F(x+(\tau-\zeta)\,p(\psi_1,\psi_2),\zeta)\cdot p(\psi_1,\psi_2)\,\mathrm{d}\psi_2\mathrm{d}\psi_1\mathrm{d}\zeta \\ &= 2\int_0^\tau \frac{1}{\tau-\zeta} \int_{\partial B_3(x,\tau-\zeta)} F(y,\zeta)\,\mathrm{d}\sigma\mathrm{d}\zeta + \int_0^\tau\!\!\int_{\partial B_3(x,\tau-\zeta)} \nabla F(y,\zeta)\cdot\nu(y)\,\mathrm{d}\sigma\mathrm{d}\zeta \\ &= V(x,\tau) + \int_0^\tau\!\!\int_{B_3(x,\tau-\zeta)} \triangle F(y,\zeta)\,\mathrm{d}y\mathrm{d}\zeta = V(x,\tau) + \triangle U(x,\tau)\end{aligned}$$

or equivalently

$$\Box U(x,\tau) = V(x,\tau), \tag{4.13}$$

where we utilize the polar coordinate transformation $y=x+(\tau-\zeta)\,p(\psi_1,\psi_2)$ for $y\in\partial B_3(x,\tau-\zeta)$ in the third equality and apply Green's formula in the fourth equality. Here $\mathrm{d}\sigma$ stands for the surface infinitesimal, and we write

$$V(x,\tau) := 2\int_0^\tau \widehat{V}(x,\tau;\zeta)\,\mathrm{d}\zeta, \quad \widehat{V}(x,\tau;\zeta) := \frac{1}{\tau-\zeta}\int_{\partial B_3(x,\tau-\zeta)} F(x,\zeta)\,\mathrm{d}y. \tag{4.14}$$

Regarding $\zeta>0$ as a fixed parameter, we observe that $\widehat{V}(\,\cdot\,,\,\cdot\,;\zeta)$ takes the form of Poisson's formula for the Cauchy problem of the three-dimensional wave equation (see [27]), that is, $\widehat{V}(\,\cdot\,,\,\cdot\,;\zeta)$ satisfies

$$\begin{cases} \Box\widehat{V}(x,\tau;\zeta) = 0 & (x\in\mathbb{R}^3,\ \tau>\zeta), \\ \widehat{V}(x,\tau;\zeta)|_{\tau=\zeta} = 0,\ \partial_\tau\widehat{V}(x,\tau;\zeta)|_{\tau=\zeta} = 4\pi\,F(x,\zeta) & (x\in\mathbb{R}^3). \end{cases}$$

Consequently, it follows from Duhamel's principle that V still satisfies a wave equation

$$\begin{cases} \Box V(x,\tau) = 8\pi\, F(x,\tau) & (x \in \mathbb{R}^3,\ \tau > 0), \\ V(x,0) = \partial_\tau V(x,0) = 0 & (x \in \mathbb{R}^3). \end{cases} \tag{4.15}$$

Together with (4.13), we obtain

$$\partial_\tau^2 U(x,0) = \triangle U(x,0) + V(x,0) = 0.$$

Similar calculations indicate $\partial_\tau \triangle U(x,0) = 0$ and thus

$$\partial_\tau^3 U(x,0) = \partial_\tau \triangle U(x,0) + \partial_\tau V(x,0) = 0.$$

Therefore, the combination of (4.13), (4.15) and the above initial conditions implies

$$\begin{cases} \Box^2 U(x,\tau) = 8\pi\, F(x,\tau) & (x \in \mathbb{R}^3,\ \tau > 0), \\ \partial_\tau^\ell U(x,0) = 0, & (x \in \mathbb{R}^3,\ \ell = 0,1,2,3), \end{cases} \quad \text{where } F(x,\tau) = \frac{\Psi(x, R^{-1}(\tau))}{\rho(R^{-1}(\tau))}. \tag{4.16}$$

Finally, the double hyperbolic system (4.2) for u immediately follows from (4.16) and repeated uses of the relation (4.12). □

In the above proof, it is readily seen that arguments based on the auxiliary functions U defined in (4.11) and V introduced in (4.14) are more convenient than that based on the original u in (4.1). Correspondingly, instead of the system (4.3) for u, it suffices to investigate the following two initial-boundary value problems

$$\begin{cases} \Box U(x,\tau) = V(x,\tau) & (x \in \Omega,\ 0 < \tau \le R(T)), \\ U(x,0) = \partial_\tau U(x,0) = 0 & (x \in \Omega), \\ \partial_\nu U(x,\tau) = 0 & (x \in \partial\Omega,\ 0 < \tau \le R(T)) \end{cases} \tag{4.17}$$

and

$$\begin{cases} \Box V(x,\tau) = f(x)\, H(x,\tau) & (x \in \Omega,\ 0 < \tau \le R(T)), \\ V(x,0) = \partial_\tau V(x,0) = 0 & (x \in \Omega), \\ \partial_\nu V(x,\tau) = 0 & (x \in \partial\Omega,\ 0 < \tau \le R(T)), \end{cases} \tag{4.18}$$

where

$$H(x,\tau) := \frac{8\pi\, g(x, R^{-1}(\tau))}{\rho(R^{-1}(\tau))}.$$

Actually, provided that the growth speed ρ is sufficiently smooth (e.g., ρ satisfies (4.4)), all the properties of u and U can be mutually converted according to the relation (4.10). It will soon be witnessed that the arguments can be greatly simplified by using (4.17)–(4.18).

To investigate the solvability and stability of (4.3), we first recall the classical well-posedness result for the following initial-boundary value problem

$$\begin{cases} \partial_t^2 w - \triangle w = G & \text{in } \Omega \times (0,T], \\ w = a,\ \partial_t w = b & \text{in } \Omega \times \{0\}, \\ \partial_\nu w = 0 & \text{on } \partial\Omega \times (0,T]. \end{cases} \tag{4.19}$$

Lemma 4.1 (see Lions and Magenes [47]) *Let $k = 1, 2, \ldots$. Assume that $\partial\Omega$ is of C^{k+1} class, $G \in H^{k-1}(\Omega \times (0,T))$, $a \in H^k(\Omega)$, $b \in H^{k-1}(\Omega)$, and the k-th order compatibility condition is satisfied on $\partial\Omega \times \{0\}$. Then there is a unique solution w to the system (4.19) such that $w \in C([0,T]; H^k(\Omega)) \cap C^1([0,T]; H^{k-1}(\Omega))$. Moreover, there exists a constant $C = C(\Omega, T) > 0$ such that*

$$\|w\|_{C([0,T];H^k(\Omega))} + \|\partial_t w\|_{C([0,T];H^{k-1}(\Omega))} \le C\left(\|G\|_{H^{k-1}(\Omega\times(0,T))} + \|a\|_{H^k(\Omega)} + \|b\|_{H^{k-1}(\Omega)}\right).$$

Based on the above lemma, it is straightforward to establish the well-posedness result for the initial-boundary value problem (4.3).

Proof of Proposition 4.2. In this proof, $C > 0$ denotes a generic constant dependent at most on Ω, T and ρ, which may change line by line. As was mentioned before, instead of the system (4.3) for u, it suffices to study systems (4.17)–(4.18) to deduce

$$\sum_{k=1}^{3} \|U\|_{C^k([0,R(T)];H^{3-k}(\Omega))} \le C\|f\|_{L^2(\Omega)}\|H\|_{H^1(0,R(T);L^\infty(\Omega))}. \tag{4.20}$$

In fact, by the relation (4.10), we formally calculate

$$\begin{aligned}
&\partial_x^\gamma \partial_t^k u(x,t) = \rho^k(t)\,\partial_x^\gamma \partial_\tau^k U(x,R(t)), \quad k = 0,1,\ |\gamma| \le 2,\\
&\partial_x^\gamma \partial_t^2 u(x,t) = \rho^2(t)\,\partial_x^\gamma \partial_\tau^2 U(x,R(t)) + \rho'(t)\,\partial_x^\gamma \partial_\tau U(x,R(t)), \quad |\gamma| \le 1,\\
&\partial_t^3 u(x,t) = \rho^3(t)\,\partial_\tau^3 U(x,R(t)) + 3\rho(t)\rho'(t)\,\partial_\tau^2 U(x,R(t)) + \rho''(t)\,\partial_\tau U(x,R(t)).
\end{aligned} \tag{4.21}$$

As long as the estimate (4.20) is verified, it follows from the above relations that for $0 \le t \le T$,

$$\begin{aligned}
&\|\partial_t^k u(\,\cdot\,,t)\|_{H^2(\Omega)} \le C\|\partial_\tau^k U(\,\cdot\,,R(t))\|_{H^2(\Omega)}, \quad k = 0,1,\\
&\|\partial_t^k u(\,\cdot\,,t)\|_{H^{3-k}(\Omega)} \le C\sum_{j=1}^{k} \|\partial_\tau^j U(\,\cdot\,,R(t))\|_{H^{3-k}(\Omega)}, \quad k = 2,3.
\end{aligned} \tag{4.22}$$

On the other hand, since ρ is sufficiently smooth and strictly positive, by definition we have $H \in H^1(0,R(T);L^\infty(\Omega))$ and

$$\|H\|_{H^1(0,R(T);L^\infty(\Omega))} \le C\|g\|_{H^1(0,T;L^\infty(\Omega))}. \tag{4.23}$$

Therefore, the combination of (4.20)–(4.23) yields (4.5) immediately.

Now we turn to systems (4.18) and (4.17) subsequently. Since $f\,H \in L^2(\Omega\times(0,R(T)))$, by taking $k = 1$ in Lemma 4.1 we see $V \in C([0,R(T)];H^1(\Omega)) \cap C^1([0,R(T)];L^2(\Omega)) \subset H^1(\Omega\times(0,R(T)))$, and

$$\begin{aligned}
\|V\|_{H^1(\Omega\times(0,R(T)))} &\le C\left(\|V\|_{C([0,R(T)];H^1(\Omega))} + \|V\|_{C^1([0,R(T)];L^2(\Omega))}\right)\\
&\le C\|f\,H\|_{L^2(\Omega\times(0,R(T)))} \le C\|f\|_{L^2(\Omega)}\|H\|_{L^2(0,R(T);L^\infty(\Omega))}.
\end{aligned} \tag{4.24}$$

Next we consider $\widetilde{V} := \partial_\tau V$, whose governing system is easily derived from (4.18) that

$$\begin{cases}
\Box\widetilde{V} = f\,\partial_\tau H & \text{in } \Omega\times(0,R(T)],\\
\widetilde{V} = 0,\ \partial_\tau\widetilde{V} = f\,H(\,\cdot\,,0) & \text{in } \Omega\times\{0\},\\
\partial_\nu\widetilde{V} = 0 & \text{on } \partial\Omega\times(0,R(T)].
\end{cases}$$

As $f\,\partial_\tau H \in L^2(\Omega\times(0,R(T)))$ and $f\,H(\,\cdot\,,0) \in L^2(\Omega)$, we apply Lemma 4.1 again with $k = 1$ to conclude $\widetilde{V} \in C([0,R(T)];H^1(\Omega)) \cap C^1([0,R(T)];L^2(\Omega)) \subset H^1(\Omega\times(0,R(T)))$ and

$$\begin{aligned}
\|\partial_\tau V\|_{H^1(\Omega\times(0,R(T)))} = \|\widetilde{V}\|_{H^1(\Omega\times(0,R(T)))} &\le C\left(\|f\,\partial_\tau H\|_{L^2(\Omega\times(0,R(T)))} + \|f\,H(\,\cdot\,,0)\|_{L^2(\Omega)}\right)\\
&\le C\|f\|_{L^2(\Omega)}\|H\|_{H^1(0,R(T);L^\infty(\Omega))}.
\end{aligned} \tag{4.25}$$

Especially, we obtain

$$\|\partial_\tau^2 V\|_{C([0,R(T)];L^2(\Omega))} \le C\|f\|_{L^2(\Omega)}\|H\|_{H^1(0,R(T);L^\infty(\Omega))}. \tag{4.26}$$

In view of the system (4.17), $V \in H^1(\Omega \times (0, R(T)))$ acts as the source term. Therefore, now the application of Lemma 4.1 with $k = 2$ indicates $U \in C([0, R(T)]; H^2(\Omega))$ and, along with (4.24),

$$\|U\|_{C([0,R(T)];H^2(\Omega))} \le C\|V\|_{H^1(\Omega\times(0,R(T)))} \le C\|f\|_{L^2(\Omega)}\|H\|_{L^2(0,R(T);L^\infty(\Omega))}. \tag{4.27}$$

Further, we introduce $\widetilde{U} := \partial_\tau U$ and consider its governing system

$$\begin{cases} \Box\widetilde{U} = \partial_\tau V = \widetilde{V} & \text{in } \Omega \times (0, R(T)], \\ \widetilde{U} = \partial_\tau \widetilde{U} = 0 & \text{in } \Omega \times \{0\}, \\ \partial_\nu \widetilde{U} = 0 & \text{on } \partial\Omega \times (0, R(T)]. \end{cases}$$

Similarly, by applying Lemma 4.1 again with $k = 2$ and using (4.25), we obtain $\partial_\tau U = \widetilde{U} \in C([0, R(T)]; H^2(\Omega))$ and

$$\|\partial_\tau U\|_{C([0,R(T)];H^2(\Omega))} \le C\|\widetilde{V}\|_{H^1(\Omega\times(0,R(T)))} \le C\|f\|_{L^2(\Omega)}\|H\|_{H^1(0,R(T);L^\infty(\Omega))}. \tag{4.28}$$

Finally, we take higher time derivative $\widehat{U} := \partial_\tau \widetilde{U}$ and consider

$$\begin{cases} \Box\widehat{U} = \partial_\tau \widetilde{V} & \text{in } \partial\Omega \times (0, R(T)], \\ \widehat{U} = \partial_\tau \widehat{U} = 0 & \text{in } \Omega \times \{0\}, \\ \partial_\nu \widehat{U} = 0 & \text{on } \partial\Omega \times (0, R(T)], \end{cases}$$

where $\partial_\tau \widetilde{V} \in L^2(\Omega \times (0, R(T)))$ by (4.25). Consequently, Lemma 4.1 with $k = 1$ implies $\partial_\tau^2 U = \widehat{U} \in C([0, R(T)]; H^1(\Omega)) \cap C^1([0, R(T)]; L^2(\Omega))$ and

$$\begin{aligned} \|\partial_\tau^2 U\|_{C([0,R(T)];H^1(\Omega))} + \|\partial_\tau^2 U\|_{C^1([0,R(T)];L^2(\Omega))} &\le C\|\partial_\tau \widetilde{V}\|_{L^2(\Omega\times(0,R(T)))} \\ &\le C\|f\|_{L^2(\Omega)}\|H\|_{H^1(0,R(T);L^\infty(\Omega))}. \end{aligned} \tag{4.29}$$

Collecting the estimates (4.27)–(4.29), we obtain (4.20) and the proof is finished. □

4.3 Proof of Theorem 4.1

This section is devoted to the proof of Theorem 4.1 which is the key focus of this chapter. The main ingredient for the global Lipschitz stability (i.e. the second inequality in (4.7)) is the following Carleman estimate, which is a simplified version of [31, Proposition 2.1] (see also [30]).

Lemma 4.2 *Let $\partial\Omega$ be of C^2 class and assumption (4.6) be satisfied with fixed x_0, ω and T. Define the weight function $\varphi(x,t)$ with a parameter $\lambda > 0$ as*

$$\varphi(x,t) := \exp\left\{\lambda\left(|x - x_0|^2 - \beta\, t^2\right)\right\}, \quad \text{where } 0 < \beta < 1. \tag{4.30}$$

Then there exists $\lambda_0 > 0$ such that for all $\lambda > \lambda_0$, there exist $\xi_0 = \xi_0(\lambda)$ and a constant $C = C(\xi_0, \lambda_0, \Omega, x_0, \omega, T, g, \rho) > 0$ such that

$$\begin{aligned} \int_{-T}^{T}\int_\Omega \xi\left(|\partial_t w|^2 + |\nabla w|^2 + \xi^2 w^2\right) \mathrm{e}^{2\xi\varphi}\,\mathrm{d}x\mathrm{d}t \le C\int_{-T}^{T}\int_\Omega |\partial_t^2 w - \triangle w|^2\, \mathrm{e}^{2\xi\varphi}\,\mathrm{d}x\mathrm{d}t \\ + C\int_{-T}^{T}\int_\omega \xi\left(|\partial_t w|^2 + \xi^2 w^2\right)\mathrm{e}^{2\xi\varphi}\,\mathrm{d}x\mathrm{d}t \end{aligned} \tag{4.31}$$

for all $\xi > \xi_0$, where w satisfies

$$\begin{cases} \partial_t^2 w - \triangle w \in L^2(\Omega \times (-T, T)), & w \in H^1(\Omega \times (-T, T)), \\ w = \partial_t w = 0 & \text{in } \Omega \times \{\pm T\}, \\ \partial_\nu w = 0 & \text{on } \partial\Omega \times (-T, T). \end{cases} \tag{4.32}$$

Applying the above lemma with another a priori estimate to some suitably chosen auxiliary functions, we are able to prove Theorem 4.1 in a similar methodology to the proof of [31, Theorem 3.1].

Proof of Theorem 4.1. We divide the proof into five steps.

Step 1. We first show the first inequality of (4.7), that is,

$$D = \|\partial_t^4 u - \rho^2 \partial_t^2 \triangle u\|_{L^2(\omega\times(0,T))} + \|\partial_t u\|_{L^2(0,T;H^2(\omega))} + \sum_{k=2}^{3} \|\partial_t^k u\|_{L^2(\omega\times(0,T))} \le C\|f\|_{L^2(\Omega)}.$$

In this step, $C > 0$ denotes a generic constant dependent at most on Ω, T, g and ρ. Except of the term $\partial_t^4 u - \rho^2 \partial_t^2 \triangle u$, a direct application of Proposition 4.2 indicates

$$\|\partial_t u\|_{L^2(0,T;H^2(\omega))} + \sum_{k=2}^{3} \|\partial_t^k u\|_{L^2(\omega\times(0,T))} \le C \sum_{k=1}^{3} \|u\|_{C^k([0,T];H^{3-k}(\Omega))} \le C\|f\|_{L^2(\Omega)}.$$

To treat $\partial_t^4 u - \rho^2 \partial_t^2 \triangle u$, we perform a further formal calculation on the basis of (4.21) to find

$$\begin{aligned}\partial_t^4 u(x,t) = {} & \rho^4(t)\, \partial_\tau^4 U(x, R(t)) + 6\rho^2(t)\rho'(t)\, \partial_\tau^3 U(x, R(t)) \\ & + \left\{3(\rho'(t))^2 + 4\rho(t)\rho''(t)\right\} \partial_\tau^2 U(x, R(t)) + \rho'''(t)\, \partial_\tau U(x, R(t)),\end{aligned}$$

Together with the expression of $\partial_t^2 \triangle u$, we estimate

$$\begin{aligned}\|\partial_t^4 u - \rho^2 \partial_t^2 \triangle u\|_{L^2(\omega\times(0,T))} &\le C\|\partial_t^4 u - \rho^2 \partial_t^2 \triangle u\|_{C([0,T];L^2(\Omega))} \\ &\le C\left(\|\partial_\tau^2 V\|_{C([0,R(T)];L^2(\Omega))} + \sum_{k=1}^{3} \|U\|_{C^k([0,R(T)];H^{3-k}(\Omega))}\right) \\ &\le C\|f\|_{L^2(\Omega)},\end{aligned}$$

where the last inequality follows from (4.26) and (4.20).

Step 2. For the second inequality in (4.7), from the viewpoint of the equivalent systems (4.17)–(4.18) for U and V, it suffices to show

$$\|f\|_{L^2(\Omega)} \le C\,\widetilde{D}, \quad \text{where } \widetilde{D}^2 := \|\partial_\tau^2 V\|^2_{L^2(\omega\times(0,R(T)))} + \|\partial_\tau V\|^2_{L^2(\omega\times(0,R(T)))}. \tag{4.33}$$

In fact, similarly to (4.21), we can represent $\partial_\tau^2 V$ and $\partial_\tau V$ in terms of ρ, u and their higher order derivatives, enabling the dominance of $\widetilde{D}$ by D.

In order to utilize the Carleman estimate (4.31) to verify (4.33), several preparations are required to fit into the framework of Lemma 4.2. Since the negative time is involved in Lemma 4.2 and the initial value of V vanishes up to its first derivative in τ, we perform even extensions to V and H so that the governing system (4.18) still holds in $\Omega\times(-R(T), R(T))$. For convenience, we still denote the extended functions as V and H respectively. Simultaneously, the observation data in $\omega\times(0, R(T))$ are also duplicated into $\omega\times(-R(T), R(T))$.

On the other hand, noting that the initial/terminate condition in (4.32) is not satisfied in general, it is necessary to introduce a cutoff function in τ, and we proceed as follows. According to assumption (4.6), $R(T)$ is strictly larger than $\sup_{x\in\Omega}|x - x_0|$, which allows a delicate choice of $\beta \in (0,1)$ such that $\sqrt{\beta}\, R(T) > \sup_{x\in\Omega}|x - x_0|$. By definition (4.30) of the weight function, this indicates

$$\varphi(x, \pm R(T)) = \exp\left\{\lambda\left(|x - x_0|^2 - \beta\, R^2(T)\right)\right\} < 1, \quad \forall\, x \in \overline{\Omega}\,.$$

Due to the continuity of φ, the above fact implies that for any $\varepsilon > 0$ satisfying $\varepsilon < 1 - \sup_{x\in\Omega} \varphi(x, \pm R(T))$, there exists $\delta = \delta(\varepsilon) > 0$ such that

$$\varphi(x,\tau) < 1-\varepsilon, \quad \forall\, (x,|\tau|) \in \overline{\Omega} \times [R(T)-2\delta, R(T)]. \tag{4.34}$$

Fixing the above ε and δ, we define a cutoff function $\eta \in C_0^\infty([-R(T), R(T)])$ such that

$$0 \le \eta \le 1, \quad \eta(\tau) = \begin{cases} 1, & |\tau| \le R(T) - 2\delta, \\ 0, & R(T) - \delta \le |\tau| \le R(T). \end{cases} \tag{4.35}$$

Since the choice of δ depends only on $\Omega, x_0, \omega, T, g$ and ρ, we can suitably specify η such that η' and η'' are bounded by a constant depending only on the above factors. Figure 4.1 provides an intuitional graph of the relation of $\varphi(\,\cdot\,,\tau)$ and $\eta(\tau)$.

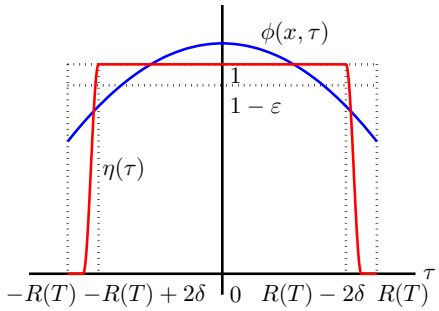

Figure 4.1: The profile of $\varphi(x,\tau)$ for some $x \in \Omega$ and the choice of a cutoff function $\eta(\tau)$ with a suitable β.

Step 3. Henceforth, $C > 0$ denotes a generic constant dependent at most on $\lambda_0, \Omega, x_0, \omega, T, g$ and ρ but independent of ξ, which may change line by line. For simplicity, we abbreviate $Q := \Omega \times (-R(T), R(T))$.

Now we have collected all the necessities to apply Lemma 4.2 to $\widetilde{W} := \eta\, \partial_\tau V$, which satisfies

$$\begin{cases} \Box \widetilde{W} = \widetilde{F} := \eta\, f\, \partial_\tau H + 2\,\eta'\, \partial_\tau^2 V + \eta''\, \partial_\tau V & \text{in } Q, \\ \widetilde{W} = \partial_\tau \widetilde{W} = 0 & \text{in } \Omega \times \{\pm R(T)\}, \\ \widetilde{W} = 0,\ \partial_\tau \widetilde{W} = f\, H(\,\cdot\,,0) & \text{in } \Omega \times \{0\}, \\ \partial_\nu \widetilde{W} = 0 & \text{on } \partial\Omega \times (-R(T), R(T)). \end{cases} \tag{4.36}$$

Since $\partial_\tau V \in H^1(Q)$ by the a priori estimate (4.25), we see $\widetilde{F} \in L^2(Q)$ and thus $\widetilde{W} \in H^1(Q)$ again by applying Lemma 4.1. Now that all the conditions in (4.32) are fulfilled, the application of Lemma 4.2 asserts that there exists $\lambda_0 > 0$ such that for all $\lambda > \lambda_0$, there exists $\xi_0 = \xi_0(\lambda)$ and $C > 0$ such that

$$I_1 := \int_Q \xi \left(|\partial_\tau \widetilde{W}|^2 + |\nabla \widetilde{W}|^2 + \xi^2\, \widetilde{W}^2 \right) \mathrm{e}^{2\xi\varphi}\, \mathrm{d}x\mathrm{d}\tau \le C\,(I_2 + I_3) \quad \text{for all } \xi > \xi_0, \text{ where} \tag{4.37}$$

$$I_2 := \int_Q |\Box \widetilde{W}|^2\, \mathrm{e}^{2\xi\varphi}\, \mathrm{d}x\mathrm{d}\tau = \int_Q |\widetilde{F}|^2\, \mathrm{e}^{2\xi\varphi}\, \mathrm{d}x\mathrm{d}\tau,$$

$$I_3 := \int_{-R(T)}^{R(T)} \int_\omega \xi \left(|\partial_\tau \widetilde{W}|^2 + \xi^2\, \widetilde{W}^2 \right) \mathrm{e}^{2\xi\varphi}\, \mathrm{d}x\mathrm{d}\tau.$$

To deal with I_2, we take advantage of the definition (4.35) of η and the property (4.34) of φ to estimate

$$I_2 \le C \int_Q |\eta\, f\, \partial_\tau H|^2\, \mathrm{e}^{2\xi\varphi}\, \mathrm{d}x\mathrm{d}\tau + C \int_{R(T)-2\delta}^{R(T)-\delta} \int_\Omega \left(|\eta'\, \partial_\tau^2 V|^2 + |\eta''\, \partial_\tau V|^2 \right) \mathrm{e}^{2\xi\varphi}\, \mathrm{d}x\mathrm{d}\tau$$

$$
\begin{aligned}
&\le C\int_Q |f\,\partial_\tau H|^2\,\mathrm{e}^{2\xi\varphi}\,\mathrm{d}x\mathrm{d}\tau + C\int_{R(T)-2\delta}^{R(T)-\delta}\int_\Omega \left(|\partial_\tau^2 V|^2 + |\partial_\tau V|^2\right)\mathrm{e}^{2\xi\varphi}\,\mathrm{d}x\mathrm{d}\tau\\
&\le C\|f\,\partial_\tau H\,\mathrm{e}^{\xi\varphi}\|^2_{L^2(Q)} + C\,\mathrm{e}^{2\xi(1-\varepsilon)}\int_{R(T)-2\delta}^{R(T)-\delta}\int_\Omega \left(|\partial_\tau^2 V| + |\partial_\tau V|^2\right)\mathrm{d}x\mathrm{d}\tau\\
&\le C\|f\,\partial_\tau H\,\mathrm{e}^{\xi\varphi}\|^2_{L^2(Q)} + C\,\mathrm{e}^{2\xi(1-\varepsilon)}\|\partial_\tau V\|^2_{H^1(Q)}\\
&\le C\|f\,\partial_\tau H\,\mathrm{e}^{\xi\varphi}\|^2_{L^2(\Omega\times(-R(T),R(R)))} + C\,\mathrm{e}^{2\xi(1-\varepsilon)}\|f\|^2_{L^2(\Omega)} \quad \text{for all } \xi>\xi_0, \qquad (4.38)
\end{aligned}
$$

where the last inequality follows from the a priori estimate (4.25) for $\partial_\tau V$. Similarly, we bound I_3 by using the definitions of φ and η that

$$
\begin{aligned}
I_3 &\le \xi^3 \exp\left\{2\xi\sup_{x\in\Omega}\varphi(x,0)\right\}\int_{-R(T)}^{R(T)}\int_\omega \left(|\partial_\tau\widetilde{W}|^2 + \widetilde{W}^2\right)\mathrm{d}x\mathrm{d}\tau\\
&\le C\,\mathrm{e}^{C\xi}\int_0^{R(T)}\int_\omega \left(|\partial_\tau^2 V|^2 + |\partial_\tau V|^2\right)\mathrm{d}x\mathrm{d}\tau = C\,\mathrm{e}^{C\xi}\widetilde{D}^2 \quad \text{for all } \xi>\xi_0. \qquad (4.39)
\end{aligned}
$$

Therefore, we collect the estimates (4.37)–(4.39) to conclude

$$
I_1 \le C\left(\|f\,\partial_\tau H\,\mathrm{e}^{\xi\varphi}\|^2_{L^2(Q)} + \mathrm{e}^{2\xi(1-\varepsilon)}\|f\|^2_{L^2(\Omega)} + \mathrm{e}^{C\xi}\widetilde{D}^2\right) \quad \text{for all } \xi>\xi_0. \qquad (4.40)
$$

Step 4. Next, we further introduce an auxiliary function $\widehat{W} := \widetilde{W}\,\mathrm{e}^{\xi\varphi} = \eta\,\partial_\tau V\,\mathrm{e}^{\xi\varphi}$, and formally calculate

$$
\begin{aligned}
&\partial_\tau\widehat{W} = \left\{\partial_\tau\widetilde{W} + \xi\,(\partial_\tau\varphi)\,\widetilde{W}\right\}\mathrm{e}^{\xi\varphi},\ \nabla\widehat{W} = \left\{\nabla\widetilde{W} + \xi\,\widetilde{W}\,\nabla\varphi\right\}\mathrm{e}^{\xi\varphi},\\
&\partial_\tau^2\widehat{W} = \left\{\partial_\tau^2\widetilde{W} + 2\xi\,(\partial_\tau\varphi)\,\partial_\tau\widetilde{W} + \xi\left(\partial_\tau^2\varphi + \xi\,|\partial_\tau\varphi|^2\right)\widetilde{W}\right\}\mathrm{e}^{\xi\varphi}, && \text{in } Q,\\
&\triangle\widehat{W} = \left\{\triangle\widetilde{W} + 2\xi\,\nabla\varphi\cdot\nabla\widetilde{W} + \xi\left(\triangle\varphi + \xi\,|\nabla\varphi|^2\right)\widetilde{W}\right\}\mathrm{e}^{\xi\varphi}\\
&\partial_\nu\widehat{W} = (\partial_\nu\widetilde{W})\,\mathrm{e}^{\xi\varphi} + \xi\,(\partial_\nu\varphi)\,\widetilde{W}\,\mathrm{e}^{\xi\varphi} && \text{on } \partial\Omega\times(-R(T),R(T)).
\end{aligned}
$$

Along with the system (4.36) that $\widetilde{W}$ satisfies, we derive

$$
\begin{cases}
\Box\widehat{W} = \widehat{F}\,\mathrm{e}^{\xi\varphi} & \text{in } Q,\\
\widehat{W} = \partial_\tau\widehat{W} = 0 & \text{in } \Omega\times\{\pm R(T)\},\\
\widehat{W} = 0,\ \partial_\tau\widehat{W} = f\,H(\,\cdot\,,0)\,\mathrm{e}^{\xi\varphi(\,\cdot\,,0)} & \text{in } \Omega\times\{0\},\\
\partial_\nu\widehat{W} = \xi\,(\partial_\nu\varphi)\widehat{W} & \text{on } \partial\Omega\times(-R(T),R(T)),
\end{cases}
\quad \text{where}
$$

$$
\widehat{F} := \widetilde{F} + 2\xi\left\{(\partial_\tau\varphi)\,\partial_\tau\widetilde{W} - \nabla\varphi\cdot\nabla\widetilde{W}\right\} + \xi\left\{\Box\varphi + \xi\left(|\partial_\tau\varphi|^2 - |\nabla\varphi|^2\right)\right\}\widetilde{W}.
$$

Note that for a fixed λ, such functions as $\varphi, \partial_\tau\varphi, \nabla\varphi$ and $\Box\varphi$ are all bounded by a constant independent of ξ. With this observation and inequalities (4.38) and (4.40), we multiply $\partial_\tau\widehat{W}$ to $\Box\widehat{W}$ and integrate in $\Omega\times(-R(T),0)$ to deduce

$$
\begin{aligned}
I_4 &:= 2\int_{-R(T)}^0\int_\Omega (\Box\widehat{W})\,\partial_\tau\widehat{W}\,\mathrm{d}x\mathrm{d}\tau \le \int_Q |\widehat{F}||\partial_\tau\widehat{W}|\,\mathrm{e}^{2\xi\varphi}\,\mathrm{d}x\mathrm{d}\tau\\
&\le \int_Q \left\{|\widetilde{F}| + C\xi\left(|\partial_\tau\widetilde{W}| + |\nabla\widetilde{W}| + \xi\,|\widetilde{W}|\right)\right\}\left(|\partial_\tau\widetilde{W}| + C\xi\,|\widetilde{W}|\right)\mathrm{e}^{2\xi\varphi}\,\mathrm{d}x\mathrm{d}\tau\\
&\le \int_Q |\widetilde{F}|^2\,\mathrm{e}^{2\xi\varphi}\,\mathrm{d}x\mathrm{d}\tau + C\int_Q \xi\left(|\partial_\tau\widetilde{W}|^2 + |\nabla\widetilde{W}|^2 + \xi^2\,\widetilde{W}^2\right)\mathrm{e}^{2\xi\varphi}\,\mathrm{d}x\mathrm{d}\tau = I_2 + C\,I_1, \qquad (4.41)
\end{aligned}
$$

where the third inequality is obtained by, for example,

$$
2\,|\partial_\tau\widetilde{W}||\nabla\widetilde{W}| \le |\partial_\tau\widetilde{W}|^2 + |\nabla\widetilde{W}|^2, \quad 2\xi\,|\partial_\tau\widetilde{W}||\widetilde{W}| \le |\partial_\tau\widetilde{W}|^2 + \xi^2\,\widetilde{W}^2.
$$

On the other hand, by an integration by parts and the condition (4.4), we can also estimate I_4 from below as

$$\begin{aligned}
I_4 &= 2\int_{-R(T)}^{0}\int_{\Omega}\left(\partial_\tau^2\widehat{W}-\triangle\widehat{W}\right)\partial_\tau\widehat{W}\,\mathrm{d}x\mathrm{d}\tau\\
&= \int_{-R(T)}^{0}\partial_\tau\left(\int_{\Omega}|\partial_\tau\widehat{W}|^2\,\mathrm{d}x\right)\mathrm{d}\tau+2\int_{-R(T)}^{0}\int_{\Omega}\nabla\widehat{W}\cdot\nabla(\partial_\tau\widehat{W})\,\mathrm{d}x\mathrm{d}\tau-I_5\\
&= \|\partial_\tau\widehat{W}(\,\cdot\,,\tau)\|_{L^2(\Omega)}^2\Big|_{\tau=-R(T)}^{\tau=0}+\int_{-R(T)}^{0}\partial_\tau\left(\int_{\Omega}|\nabla\widehat{W}|^2\,\mathrm{d}x\right)\mathrm{d}\tau-I_5\\
&= \|f\,H(\,\cdot\,,0)\,\mathrm{e}^{\xi\varphi(\,\cdot\,,0)}\|_{L^2(\Omega)}^2+\|\nabla\widehat{W}(\,\cdot\,,\tau)\|_{L^2(\Omega)}^2\Big|_{\tau=-R(T)}^{\tau=0}-I_5\\
&\geq \frac{8\pi\,g_0}{\rho(0)}\|f\,\mathrm{e}^{\xi\varphi(\,\cdot\,,0)}\|_{L^2(\Omega)}^2-I_5,\quad\text{where } I_5:=2\int_{-R(T)}^{0}\int_{\partial\Omega}(\partial_\nu\widehat{W})\,\partial_\tau\widehat{W}\,\mathrm{d}\sigma\mathrm{d}\tau.
\end{aligned}\tag{4.42}$$

To deal with I_5, we recall $\partial_\nu\widehat{W}=\xi\,(\partial_\nu\varphi)\,\widehat{W}$ on $\partial\Omega\times(-R(T),0)$ and apply again integral by parts and the trace theorem to obtain

$$\begin{aligned}
I_5 &= 2\xi\int_{-R(T)}^{0}\int_{\partial\Omega}(\partial_\nu\varphi)\,\widehat{W}\,(\partial_\tau\widehat{W})\,\mathrm{d}\sigma\mathrm{d}\tau=\xi\int_{\partial\Omega}\int_{-R(T)}^{0}(\partial_\nu\varphi)\,\partial_\tau(\widehat{W}^2)\,\mathrm{d}\tau\mathrm{d}\sigma\\
&= \xi\left(\int_{\partial\Omega}(\partial_\nu\varphi)\,\widehat{W}^2\,\mathrm{d}\sigma\right)\Big|_{\tau=-R(T)}^{\tau=0}-\xi\int_{-R(T)}^{0}\int_{\partial\Omega}(\partial_\tau\partial_\nu\varphi)\,\widehat{W}^2\,\mathrm{d}\sigma\mathrm{d}\tau\\
&\leq C\xi\int_{-R(T)}^{0}\|\widehat{W}(\,\cdot\,,\tau)\|_{L^2(\partial\Omega)}^2\,\mathrm{d}\tau\leq C\xi\int_{-R(T)}^{0}\int_{\Omega}\left(|\nabla\widehat{W}|^2+\widehat{W}^2\right)\mathrm{d}x\mathrm{d}\tau\\
&\leq C\xi\int_{-R(T)}^{0}\int_{\Omega}\left\{2\left(|\nabla\widetilde{W}|^2+\xi^2\,|\nabla\varphi|^2\,\widetilde{W}^2\right)+\widetilde{W}^2\right\}\mathrm{e}^{2\xi\varphi}\,\mathrm{d}x\mathrm{d}\tau\\
&\leq C\xi\int_{-R(T)}^{0}\int_{\Omega}\left(|\nabla\widetilde{W}|^2+\xi^2\,\widetilde{W}^2\right)\mathrm{e}^{2\xi\varphi}\,\mathrm{d}x\mathrm{d}\tau\leq C\,I_1.
\end{aligned}\tag{4.43}$$

Hence, collecting the estimates (4.41)–(4.43) and applying (4.38) and (4.40), we immediately get

$$\|f\,\mathrm{e}^{\xi\varphi(\,\cdot\,,0)}\|_{L^2(\Omega)}^2\leq C\left(\|f\,\partial_\tau H\,\mathrm{e}^{\xi\varphi}\|_{L^2(Q)}^2+\mathrm{e}^{2\xi(1-\varepsilon)}\|f\|_{L^2(\Omega)}^2+\mathrm{e}^{C\xi}\widetilde{D}^2\right)\tag{4.44}$$

for all $\xi>\xi_0$.

Step 5. The final step aims at absorbing both terms including f on the right-hand side of (4.44) into the left-hand side by choosing sufficiently large $\xi>\xi_0$. By definition (4.30), we see $\varphi(x,0)=\exp\left(\lambda|x-x_0|^2\right)\geq 1$ for all $x\in\overline{\Omega}$, indicating that $\mathrm{e}^{2\xi(1-\varepsilon)}\|f\|_{L^2(\Omega)}^2$ is absorbable in the sense that

$$\lim_{\xi\to\infty}\frac{\mathrm{e}^{2\xi(1-\varepsilon)}\|f\|_{L^2(\Omega)}^2}{\|f\,\mathrm{e}^{\xi\varphi(\,\cdot\,,0)}\|_{L^2(\Omega)}^2}\leq\lim_{\xi\to\infty}\frac{\mathrm{e}^{2\xi(1-\varepsilon)}\|f\|_{L^2(\Omega)}^2}{\mathrm{e}^{2\xi}\|f\|_{L^2(\Omega)}^2}=0.\tag{4.45}$$

Similarly, we treat $\|f\,\partial_\tau H\,\mathrm{e}^{\xi\varphi}\|_{L^2(Q)}^2$ as

$$\begin{aligned}
\|f\,\partial_\tau H\,\mathrm{e}^{\xi\varphi}\|_{L^2(Q)}^2 &= \int_{\Omega}|f(x)|^2\,\mathrm{e}^{2\xi\varphi(x,0)}\left(\int_{-R(T)}^{R(T)}|\partial_\tau H(x,\tau)|^2\,\mathrm{e}^{2\xi(\varphi(x,\tau)-\varphi(x,0))}\,\mathrm{d}\tau\right)\mathrm{d}x\\
&\leq \int_{\Omega}|f(x)|^2\,\mathrm{e}^{2\xi\varphi(x,0)}\\
&\quad\times\left[\int_{-R(T)}^{R(T)}\|\partial_\tau H(\,\cdot\,,\tau)\|_{L^\infty(\Omega)}^2\exp\left\{2\xi\,\mathrm{e}^{\lambda|x-x_0|^2}\left(\mathrm{e}^{-\lambda\beta\,\tau^2}-1\right)\right\}\mathrm{d}\tau\right]\mathrm{d}x
\end{aligned}$$

$$\leq \|f\,\mathrm{e}^{\xi\varphi(\,\cdot\,,0)}\|^2_{L^2(\Omega)} \int_{-R(T)}^{R(T)} \mu_\xi(\tau)\,\mathrm{d}\tau, \quad \text{where}$$
$$\mu_\xi(\tau) := \|\partial_\tau H(\,\cdot\,,\tau)\|^2_{L^\infty(\Omega)} \exp\left\{C\xi\left(\mathrm{e}^{-\lambda\beta\,\tau^2}-1\right)\right\}, \quad \xi>\xi_0.$$

It follows from $\partial_\tau H \in L^2(-R(T),R(T);L^\infty(\Omega))$ that the sequence $\{\mu_\xi\}_{\xi>\xi_0}$ is dominated by an integrable function $\|\partial_\tau H(\,\cdot\,,\tau)\|^2_{L^\infty(\Omega)}$. Meanwhile, it is readily seen that $\{\mu_\xi\}$ vanishes pointwisely except for $\tau=0$ as $\xi\to\infty$. These allow the usage of Lebesgue's dominated convergence theorem to absorb

$$\lim_{\xi\to\infty} \frac{\|f\,\partial_\tau H\,\mathrm{e}^{\xi\varphi}\|^2_{L^2(Q)}}{\|f\,\mathrm{e}^{\xi\varphi(\,\cdot\,,0)}\|^2_{L^2(\Omega)}} \leq \lim_{\xi\to\infty}\int_{-R(T)}^{R(T)} \mu_\xi(\tau)\,\mathrm{d}\tau = 0. \tag{4.46}$$

Since $C>0$ in the estimate (4.44) is independent of ξ, (4.45)–(4.46) guarantee a constant $\xi_1>\xi_0$ such that

$$C\left(\|f\,\partial_\tau H\,\mathrm{e}^{\xi\varphi}\|^2_{L^2(Q)} + \mathrm{e}^{2\xi(1-\varepsilon)}\|f\|^2_{L^2(\Omega)}\right) \leq \frac{1}{2}\|f\,\mathrm{e}^{\xi\varphi(\,\cdot\,,0)}\|^2_{L^2(\Omega)}$$

for all $\xi>\xi_1$, and consequently

$$\|f\|^2_{L^2(\Omega)} \leq \|f\,\mathrm{e}^{\xi\varphi(\,\cdot\,,0)}\|^2_{L^2(\Omega)} \leq C\,\mathrm{e}^{C\xi}\widetilde{D}^2 \quad \text{for all } \xi>\xi_1.$$

The verification of inequality (4.33) is completed by fixing any $\xi>\xi_1$ in the above estimate, which ends the proof. □

4.4 Iteration thresholding algorithm

In this section, we concentrate on the development of an efficient iterative thresholding algorithm for the numerical treatment of Problem 4.1 by using an appropriate backward system of (4.3). The derivation of the main algorithm essentially proceeds parallelly as that in Section 3.3. For simplicity, we only handle the case of a unit growth speed $\rho(t)\equiv 1$ because the discussion on ρ is not the main concentration of this chapter, and such a simplification will not affect the generality. For clarification, we formulate

$$u(f)\begin{cases}(\partial_t^2-\triangle)^2 u(x,t)=f(x)\,h(x,t) & (x\in\Omega,\ 0<t\leq T),\\ \partial_t^\ell u(x,0)=0 & (x\in\Omega,\ \ell=0,1,2,3),\\ \partial_\nu u(x,t)=\partial_\nu\triangle u(x,t)=0 & (x\in\partial\Omega,\ 0<t\leq T),\end{cases} \tag{4.47}$$

where $f\in L^2(\Omega)$ and $h\in H^1(0,T;L^\infty(\Omega))$ by assumption (4.4). Here we write the solution as $u(f)$ to emphasize its dependency upon f. For later use, first we give a definition of the generalized solution to (4.47).

Definition 4.1 *Let $f\in L^2(\Omega)$ and $h\in L^2(0,T;L^\infty(\Omega))$. We say that $u(f)\in H^2(\Omega\times(0,T))$ is a generalized solution to problem (4.47) it $u(f)=\partial_t u(f)=0$ in $\Omega\times\{0\}$, $\partial_\nu u(f)=0$ on $\partial\Omega\times(0,T)$, and it satisfies*

$$\int_0^T\!\!\int_\Omega \left(\partial_t^2 u(f)-\triangle u(f)\right)\left(\partial_t^2 z-\triangle z\right)\mathrm{d}x\mathrm{d}t = \int_0^T\!\!\int_\Omega f\,h\,z\,\mathrm{d}x\mathrm{d}t$$

for any test function $z\in H^2(\Omega\times(0,T))$ with $z=\partial_t z=0$ in $\Omega\times\{T\}$ and $\partial_\nu z=0$ on $\partial\Omega\times(0,T)$.

The above definition of the generalized solution is easily understood by applying integration by parts to sufficiently smooth solutions, and it is also in accordance with the classical well-posedness result (see Lemma 4.1). Actually, by a similar reasoning as that for Proposition 4.2, one can show that $u(f) \in H^2(\Omega \times (0,T))$ automatically holds, and the unspecified initial and boundary conditions are also satisfied in the sense of distributions. On the other hand, since we require $h \in H^1(0,T;L^\infty(\Omega))$ for the theoretical stability, Definition 4.1 is definitely valid in our setting.

Henceforth, we specify $f_{\rm true} \in L^2(\Omega)$ as the true solution to Problem 4.1. By u^δ we denote the noise contaminated observation data in $\omega \times (0,T)$ satisfying $\|u^\delta - u(f_{\rm true})\|_{L^2(\omega\times(0,T))} \le \delta$, where δ stands for the noise level. To avoid ambiguity, we interpret $u^\delta \equiv 0$ out of $\omega \times (0,T)$ so that u^δ is well-defined throughout $\Omega \times (0,T)$.

As many of the numerical treatments for ill-posed problems with measurement errors, now we reformulate Problem 4.1 as the following minimization problem with a Tikhonov regularization

$$\min_{f\in L^2(\Omega)} J(f), \quad J(f) := \|u(f) - u^\delta\|^2_{L^2(\omega\times(0,T))} + \alpha\|f\|^2_{L^2(\Omega)}, \tag{4.48}$$

where $\alpha > 0$ is the regularization parameter. As usual, first we investigate the Fréchet derivative $J'(f)$ of $J(f)$ at the direction $\widetilde{f} \in L^2(\Omega)$ to find

$$\begin{aligned} J'(f)\widetilde{f} &= 2\int_0^T\!\!\int_\omega \big(u(f) - u^\delta\big)\,(u'(f)\widetilde{f}\,)\,\mathrm{d}x\mathrm{d}t + 2\alpha\int_\Omega f\,\widetilde{f}\,\mathrm{d}x \\ &= \int_0^T\!\!\int_\omega \big(u(f) - u^\delta\big)\,u(\widetilde{f}\,)\,\mathrm{d}x\mathrm{d}t + 2\alpha\int_\Omega f\,\widetilde{f}\,\mathrm{d}x. \end{aligned} \tag{4.49}$$

Here $u'(f)\widetilde{f}$ denotes the Fréchet derivative of $u(f)$ in the direction $\widetilde{f}$, and the linearity of (4.47) with respect to the source term immediately yields

$$u'(f)\widetilde{f} = \lim_{\epsilon\to 0}\frac{u(f+\epsilon\,\widetilde{f}\,) - u(f)}{\epsilon} = u(\widetilde{f}\,).$$

Obviously, it is extremely expensive to use (4.49) directly to evaluate $J'(f)\widetilde{f}$ for all $\widetilde{f} \in L^2(\Omega)$, since one should solve the system (4.47) for $u(\widetilde{f}\,)$ with $\widetilde{f}$ varying in $L^2(\Omega)$ in the computation for a single fixed f.

In order to reduce the computational costs in evaluating the Fréchet derivatives, we introduce the adjoint system of (4.47) for Problem 4.1, that is, the following backward terminate-boundary value problem

$$z(f)\begin{cases} (\partial_t^2 - \triangle)^2 z = \chi_\omega\big(u(f) - u^\delta\big) & \text{in } \Omega\times[0,T), \\ \partial_t^\ell z = 0 \quad (\ell = 0,1,2,3) & \text{in } \Omega\times\{T\}, \\ \partial_\nu z = \partial_\nu\triangle z = 0 & \text{on } \partial\Omega\times[0,T), \end{cases} \tag{4.50}$$

where χ_ω denotes the characterization function of ω. The generalized solution to (4.50) is similarly defined as that in Definition 4.1. In fact, since $\chi_\omega\big(u(f) - u^\delta\big) \in L^2(\Omega\times(0,T))$, it is readily seen that $z(f) \in H^2(\Omega\times(0,T))$. Therefore, for $f, \widetilde{f} \in L^2(\Omega)$, we use $z(f)$ and $u(\widetilde{f}\,)$ as mutual test functions for each other to further treat the first term in (4.49) as

$$\begin{aligned} \int_0^T\!\!\int_\omega \big(u(f) - u^\delta\big)\,u(\widetilde{f}\,)\,\mathrm{d}x\mathrm{d}t &= \int_0^T\!\!\int_\Omega \chi_\omega\big(u(f) - u^\delta\big)\,u(\widetilde{f}\,)\,\mathrm{d}x\mathrm{d}t \\ &= \int_0^T\!\!\int_\Omega \big(\partial_t^2 z(f) - \triangle z(f)\big)\Big(\partial_t^2 u(\widetilde{f}\,) - \triangle u(\widetilde{f}\,)\Big)\,\mathrm{d}x\mathrm{d}t \\ &= \int_0^T\!\!\int_\Omega \widetilde{f}\,h\,z(f)\,\mathrm{d}x\mathrm{d}t, \end{aligned} \tag{4.51}$$

indicating

$$J'(f)\widetilde{f} = 2\int_\Omega \left(\int_0^T h\, z(f)\,\mathrm{d}t + \alpha\, f\right)\widetilde{f}\,\mathrm{d}x.$$

Since $\widetilde{f}$ is arbitrarily chosen in $L^2(\Omega)$, the above observation suggests a characterization of the solution to the minimization problem (4.48).

Lemma 4.3 *$f^* \in L^2(\Omega)$ is the minimizer of the functional $J(f)$ in (4.48) only if it satisfies the Euler equation*

$$\int_0^T h\, z(f^*)\,\mathrm{d}t + \alpha\, f^* = 0, \tag{4.52}$$

where $z(f^*)$ solves the backward system (4.50) with the coefficient f^*.

To solve the nonlinear equation (4.52), one may employ the iteration

$$f_{m+1} = \frac{K}{K+\alpha} f_m - \frac{1}{K+\alpha}\int_0^T h\, z(f_m)\,\mathrm{d}t, \tag{4.53}$$

where $K > 0$ is a tuning parameter acting as a weight between the previous and current steps.

It turns out that the convergence of the above iteration relies on the choice of K. To this end, we notice the fact that (4.53) in principle coincides with the iterative thresholding algorithm, which can be deduced from the minimization problem of a surrogate functional (see, e.g., [22]). Actually, fixing $\widetilde{f} \in L^2(\Omega)$, we introduce a surrogate functional $J^s(f, \widetilde{f}\,)$ of $J(f)$ as

$$J^s(f, \widetilde{f}\,) := J(f) + K\|f - \widetilde{f}\,\|^2_{L^2(\Omega)} - \|u(f) - u(\widetilde{f}\,)\|^2_{L^2(\omega\times(0,T))}.$$

For the positivity of J^s, there should hold $K\|f\|^2_{L^2(\Omega)} \geq \|u(f)\|^2_{L^2(\omega\times(0,T))}$ for all $f \in L^2(\Omega)$. This is achieved by taking any

$$K \geq \|A\|^2, \quad \text{where} \quad \begin{aligned} &A : L^2(\Omega) \to L^2(\omega\times(0,T)),\\ &f \mapsto u(f)|_{\omega\times(0,T)}. \end{aligned} \tag{4.54}$$

The boundedness of the linear operator A immediately follows from Proposition 4.2. Hence, there holds

$$J(f) = J^s(f,f) \leq J^s(f,\widetilde{f}), \quad \forall\, \widetilde{f} \in L^2(\Omega),$$

and thus $J^s(f, \widetilde{f}\,)$ can be regarded as a small perturbation of $J(f)$ when $\widetilde{f}$ is chose to f. On the other hand, we see from (4.51) that

$$\begin{aligned} J^s(f,\widetilde{f}\,) &= 2\int_0^T\!\!\int_\omega u(f)\left(u(\widetilde{f}\,) - u^\delta\right)\mathrm{d}x\mathrm{d}t + \|u^\delta\|^2_{L^2(\omega\times(0,T))} - \|u(\widetilde{f}\,)\|^2_{L^2(\omega\times(0,T))}\\ &\quad + \alpha\|f\|^2_{L^2(\Omega)} + K\|f - \widetilde{f}\,\|^2_{L^2(\Omega)}\\ &= K\|f - \widetilde{f}\,\|^2_{L^2(\Omega)} + \alpha\|f\|^2_{L^2(\Omega)} + 2\int_0^T\!\!\int_\Omega f\, h\, z(\widetilde{f}\,)\,\mathrm{d}x\mathrm{d}t\\ &\quad - \|u(\widetilde{f}\,)\|^2_{L^2(\omega\times(0,T))} + \|u^\delta\|^2_{L^2(\omega\times(0,T))}\\ &= (K+\alpha)\|f\|^2_{L^2(\Omega)} - 2\int_\Omega f\left(K\,\widetilde{f} - \int_0^T h\, z(\widetilde{f}\,)\,\mathrm{d}t\right)\mathrm{d}x\\ &\quad + K\|\widetilde{f}\,\|^2_{L^2(\Omega)} - \|u(\widetilde{f}\,)\|^2_{L^2(\omega\times(0,T))} + \|u^\delta\|^2_{L^2(\omega\times(0,T))}. \end{aligned}$$

Since this is a quadratic form with respect to f when u^δ and $\widetilde{f}$ are fixed, we conclude

$$\arg\min_{f\in L^2(\Omega)} J^s(f,\widetilde{f}\,) = \frac{K}{K+\alpha}\widetilde{f} - \frac{1}{K+\alpha}\int_0^T h\, z(\widetilde{f}\,)\mathrm{d}t.$$

Consequently, the iterative update (4.53) is equivalent to solving the minimization problem $\min_{f\in L^2(\Omega)} J^s(f,\widetilde{f}\,)$ with $\widetilde{f}=f_m$. Moreover, the convergence of this iteration was proven in [22] for any bounded linear operator A, provided that the constant $K>0$ is chosen according to condition (4.54).

Now we are ready to state the main algorithm for the numerical reconstruction.

Algorithm 4.1 *Choose a tolerance $\varepsilon>0$, a regularization parameter $\alpha>0$ and a tuning parameter $K>0$ according to* (4.54)*. Give an initial guess f_0, and set $m=0$.*

1. *Compute f_{m+1} by the iterative update* (4.53)*.*
2. *If $\|f_{m+1}-f_m\|_{L^2(\Omega)}/\|f_m\|_{L^2(\Omega)}\le\varepsilon$, stop the iteration. Otherwise, update $m\leftarrow m+1$ and return to Step* 1*.*

It reveals that at each step in the iteration, it suffices to solve the forward system (4.47) once for $u(f_m)$ and the backward system (4.50) once for $z(f_m)$ subsequently, which only involves the computational costs for solving four wave equations. Therefore, the implementation of Algorithm 4.1 is easy and time-saving. As will be shown in many numerical experiments in the next section, the purposed algorithm is also considerably efficient and accurate even for three spatial dimensions.

We summarize this section by stating the convergence result concerning Algorithm 4.1, which is a direct application of [22, Theorem 3.1].

Lemma 4.4 *Let $K>0$ be a constant satisfying condition* (4.54)*, and $\alpha>0$ be a suitably chosen regularization parameter. Then for any $f_0\in L^2(\Omega)$, the sequence $\{f_m\}_{m=1}^{\infty}$ generated by the iteration* (4.53) *converges strongly to the solution of the minimization problem* (4.48)*.*

4.5 Numerical experiments

Now we are well prepared to apply the iterative thresholding algorithm developed in the previous section to the numerical treatment for Problem 4.1. Although the double hyperbolic equation was derived from the three-dimensional time cone model, we are also interested in implementing several examples in lower spatial dimensions in order to observe the numerical performances, because Algorithm 4.1 itself is independent of dimensions.

On the basis of the governing equation (4.47), we assign the general settings of the reconstruction as follows. Without lose of generality, we set $\Omega=(0,1)^d$ $(d=1,2,3)$, and the duration is basically taken as $T=1$. Nevertheless, considering assumption (4.6) for the theoretical stability, sometimes we may enlarge T with respect to the choices of ω to guarantee a reasonable reconstruction. Although the difference between the noiseless data $u(f_{\rm true})$ and the actually observed data u^δ was evaluated in the $L^2(\omega\times(0,T))$-norm in Section 4.4, here for simplicity we produce u^δ by adding uniform random noises to $u(f_{\rm true})$, i.e.

$$u^\delta(x,t)=u(f_{\rm true})(x,t)+\delta\,\mathrm{rand}(-1,1),\quad \forall\, x\in\omega,\ \forall\, t\in(0,T),$$

where $\mathrm{rand}(-1,1)$ denotes the uniformly distributed random number in $[-1,1]$, and $\delta\ge0$ is the noise level. Here we choose δ as a certain portion of the amplitude of the true solution, namely

$$\delta:=\delta_0\max_{\overline{\Omega}\times[0,T]}|u(f_{\rm true})|,\quad 0\le\delta_0<1.$$

Regarding the parameters involved in Algorithm 4.1, we take $\varepsilon=1\%\,\delta_0$ as the stopping criteria, and $\alpha=\delta^3$ as the regularization parameter. The choice of α is based on repeated experiments,

which mostly leads to accurate results. We will always take constant initial guesses f_0, which are usually rather inaccurate in our numerical tests. Finally, the tuning parameter $K > 0$ will be selected according to the size of ω, the duration T, and the known component $h(x,t)$ of the source term.

We briefly mention the numerical discretization for solving the forward system (4.3) and the backward system (4.50) at each step of the iteration (4.53). Similarly to (4.17)–(4.18), we define $v := \partial_t^2 u - \triangle u$ and deal with two wave equations with respect to u and v instead of (4.47). In our implementations, we employ the von Neumann scheme for the one-dimensional case, and the alternating direction implicit (ADI) method for two- and three-dimensional cases (see [28, 45]). For instance, in case of $d = 3$, we work on the equidistant grids

$$x_1^i = x_2^i = x_3^i = i\,\Delta x \ (i = 0, 1, \dots, N_x), \quad t_n = n\,\Delta t \ (n = 0, 1, \dots, N_t)$$

with $N_x\,\Delta x = 1$ and $N_t\,\Delta t = T$, where Δx and Δt are the step lengths in space and time respectively. Introducing the ratio $\kappa := (\Delta t/\Delta x)^2$ and the difference operators

$$\begin{aligned}
\delta_{x_1}^2 w_n^{i,j,k} &:= w_n^{i+1,j,k} - 2\,w_n^{i,j,k} + w_n^{i-1,j,k},\\
\delta_{x_2}^2 w_n^{i,j,k} &:= w_n^{i,j+1,k} - 2\,w_n^{i,j,k} + w_n^{i,j-1,k},\\
\delta_{x_3}^2 w_n^{i,j,k} &:= w_n^{i,j,k+1} - 2\,w_n^{i,j,k} + w_n^{i,j,k-1},
\end{aligned}$$

we discretize the time evolution of the governing equation in (4.47) as

$$\begin{cases}
v_{n+1/3}^{i,j,k} - 2\,v_n^{i,j,k} + v_{n-1}^{i,j,k} = \dfrac{\kappa}{4}\,\delta_{x_1}^2\left(v_{n+1/3}^{i,j,k} + 2\,v_n^{i,j,k} + v_{n-1}^{i,j,k}\right) + \kappa\left(\delta_{x_2}^2 + \delta_{x_3}^2\right) v_n^{i,j,k}\\
\qquad\qquad + \Delta t^2\, f(x_1^i, x_2^j, x_3^k)\, h(x_1^i, x_2^j, x_3^k, t_n),\\
v_{n+2/3}^{i,j,k} - v_{n+1/3}^{i,j,k} = \dfrac{\kappa}{4}\,\delta_{x_2}^2\left(v_{n+2/3}^{i,j,k} - 2\,v_n^{i,j,k} + v_{n-1}^{i,j,k}\right),\\
v_{n+1}^{i,j,k} - v_{n+2/3}^{i,j,k} = \dfrac{\kappa}{4}\,\delta_{x_3}^2\left(v_{n+1}^{i,j,k} - 2\,v_n^{i,j,k} + v_{n-1}^{i,j,k}\right),
\end{cases}$$

$$\begin{cases}
u_{n+1/3}^{i,j,k} - 2\,u_n^{i,j,k} + u_{n-1}^{i,j,k} = \dfrac{\kappa}{4}\,\delta_{x_1}^2\left(u_{n+1/3}^{i,j,k} + 2\,u_n^{i,j,k} + u_{n-1}^{i,j,k}\right) + \kappa\left(\delta_{x_2}^2 + \delta_{x_3}^2\right) u_n^{i,j,k}\\
\qquad\qquad + \Delta t^2\, v_n^{i,j,k},\\
u_{n+2/3}^{i,j,k} - u_{n+1/3}^{i,j,k} = \dfrac{\kappa}{4}\,\delta_{x_2}^2\left(u_{n+2/3}^{i,j,k} - 2\,u_n^{i,j,k} + u_{n-1}^{i,j,k}\right),\\
u_{n+1}^{i,j,k} - u_{n+2/3}^{i,j,k} = \dfrac{\kappa}{4}\,\delta_{x_3}^2\left(u_{n+1}^{i,j,k} - 2\,u_n^{i,j,k} + u_{n-1}^{i,j,k}\right),
\end{cases}$$

where $u_n^{i,j,k}$ and $v_n^{i,j,k}$ stand for approximations of $u(x_1^i, x_2^j, x_3^k, t_n)$ and $v(x_1^i, x_2^j, x_3^k, t_n)$ respectively, and $u_{n+1/3}^{i,j,k}$, $u_{n+2/3}^{i,j,k}$, etc. denote some intermediate values. The backward system (4.50) is discretized in the same manner. It turns out that the ADI method performs efficiently even in the three-dimensional case: it takes less than 3 seconds for a problem of $40^3 \times 40$ scale. On the other hand, the involved integrals in (4.53) are simply approximated by the composite trapezoid rule.

In the following, we shall test the reconstruction method by a lot of test examples in one, two and three spatial dimensions. Other than the illustrative figures, we mainly evaluate the numerical performances by the number M of iterations, the relative L^2 error

$$\mathrm{err} := \frac{\|f_M - f_{\mathrm{true}}\|_{L^2(\Omega)}}{\|f_{\mathrm{true}}\|_{L^2(\Omega)}}$$

and the elapsed time, where f_M is understood as the numerical solution to Problem 4.1.

4.5.1 One- and two-dimensional examples

We start from the one-dimensional case, where we set a step length of 1/100 for both space and time. We will choose such observable subdomains ω that cover the boundary of the whole domain, namely $\partial\omega \supset \partial\Omega = \{0, 1\}$. In this case, it is readily seen that taking $T = 1$ is enough to validate assumption (4.6). On the other hand, we always take $h(x, t) = 2+t$, which is strictly isolated from zero at $t = 0$ and hence satisfies assumption (4.4).

Example 4.1 In this example, we fix $f_{\text{true}}(x) = 1 - \cos(\pi x)$ and the initial guess $f_0 \equiv 1$. We carry out numerical tests with different combinations of the noise level δ and the thickness of ω to see their influences on the stability of reconstructions. First, we fix $\omega = \Omega \setminus [0.1, 0.9]$ and enlarge the noise levels from 1%, 2%, 4% to 8% of the amplitude of $u(f_{\text{true}})$. Next, we fix $\delta_0 = 8\%$ and shrink the size of ω from $\Omega \setminus [0.2, 0.8]$ to $\Omega \setminus [0.05, 0.95]$. The choices of parameters in the tests and corresponding numerical performances are listed in Table 4.1. For a better understanding of the reconstructions, we visualize several representative examples in Table 4.1 to compare the true solution with the recovered ones in Figure 4.2.

Table 4.1: Parameter settings and the corresponding numerical performances in Example 4.1 under various combinations of noise levels and observable subdomains.

δ_0	ω	K	M	err	elapsed time	illustration
1%	$\Omega \setminus [0.1, 0.9]$	1.5×10^{-4}	9	0.22%	0.56 s	Figure 4.2(a)
2%	$\Omega \setminus [0.1, 0.9]$	1.5×10^{-4}	8	0.25%	0.49 s	
4%	$\Omega \setminus [0.1, 0.9]$	1.5×10^{-4}	8	0.36%	0.47 s	
8%	$\Omega \setminus [0.1, 0.9]$	1.5×10^{-4}	7	0.87%	0.43 s	
8%	$\Omega \setminus [0.2, 0.8]$	4×10^{-4}	11	0.48%	0.59 s	
8%	$\Omega \setminus [0.05, 0.95]$	10^{-4}	11	2.01%	0.62 s	Figure 4.2(b)

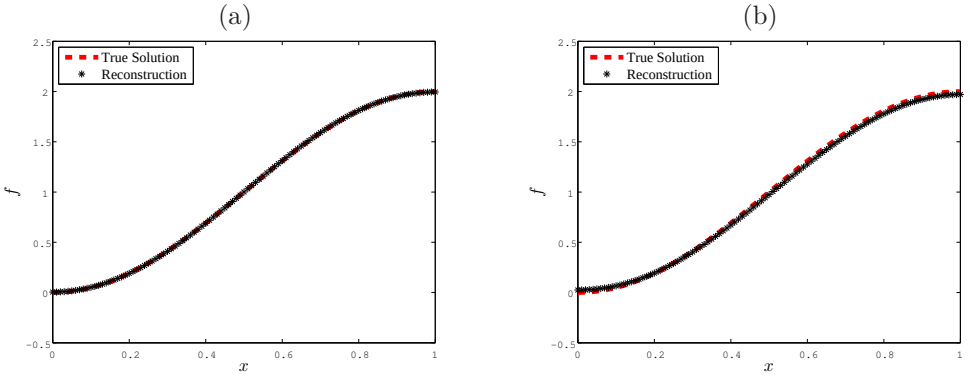

Figure 4.2: Illustrations of the true solution and several representative reconstructed solutions in Example 4.1 with various combinations of noise levels and observable subdomains. (a) $\delta_0 = 1\%$, $\omega = \Omega \setminus [0.1, 0.9]$. (b) $\delta_0 = 8\%$, $\omega = \Omega \setminus [0.05, 0.95]$.

Remarkably, Example 4.1 suggests a strong robustness of Algorithm 4.1 against the measurement error. In fact, one can easily observe from the first part of Table 4.1 that the relative errors of the numerical solutions only increase moderately as the noise levels are doubled. Considering the appearance of approximation errors at various procedures in the algorithm, relative errors less than 1% in numerical reconstructions are more than satisfactory in view of the ill-posedness of Problem 4.1. As was explained in Subsection 3.4.1 where a similar algorithm

for single hyperbolic equations was studied, this phenomenon results from the tendency that $u(f)|_{\omega\times(0,T)}$ takes an averaged state of u^δ in a sense that the difference can be minimized. Consequently, as long as the observation data keep oscillating around $u(f_{\text{true}})$, the algorithm is insensitive to the noise level to a certain extent.

In contrast, the reconstructions appear more sensitive to the smallness of the observable subdomains ω than to the measurement error. This can be witnessed from the second part of Table 4.1, which obviously comes from the limited information captured in ω.

Here we emphasize that a delicate choice of the tuning parameter K is crucial to the convergence speed. Although Lemma 4.4 ensures the convergence by taking sufficiently large $K > 0$, a critical choice of K according to (4.54) can considerably accelerate the iteration (4.53). However, to this end one should give a sharp estimate for the operator norm of A defined in (4.54), which is impossible in general. Throughout this section, K are adjusted by repeated experiments to achieve fast convergence and accurate results.

Thanks to the robustness of Algorithm 4.1 against the measurement error, henceforth the noise level will be taken as 5% of the amplitude of $u(f_{\text{true}})$ in all examples.

Example 4.2 Now we investigate the influence of the properties of the true solution f_{true} upon the numerical performance of Algorithm 4.1. More precisely, we fix $\omega = \Omega \setminus [0.1, 0.9]$, and select (a) $f^{\text{a}}_{\text{true}}(x) = x$, (b) $f^{\text{b}}_{\text{true}}(x) = \sin(\pi x) + x$, (c) $f^{\text{c}}_{\text{true}}(x) = 1 - \cos(2\pi x)/2$ or (d) $f^{\text{d}}_{\text{true}}(x) = |2x - 1|$. Correspondingly, we set $K = 10^{-4}$. Comparisons of the true solutions with the reconstructed ones are shown in Figure 4.3. The numbers M of iterations and relative errors are collected in Table 4.2.

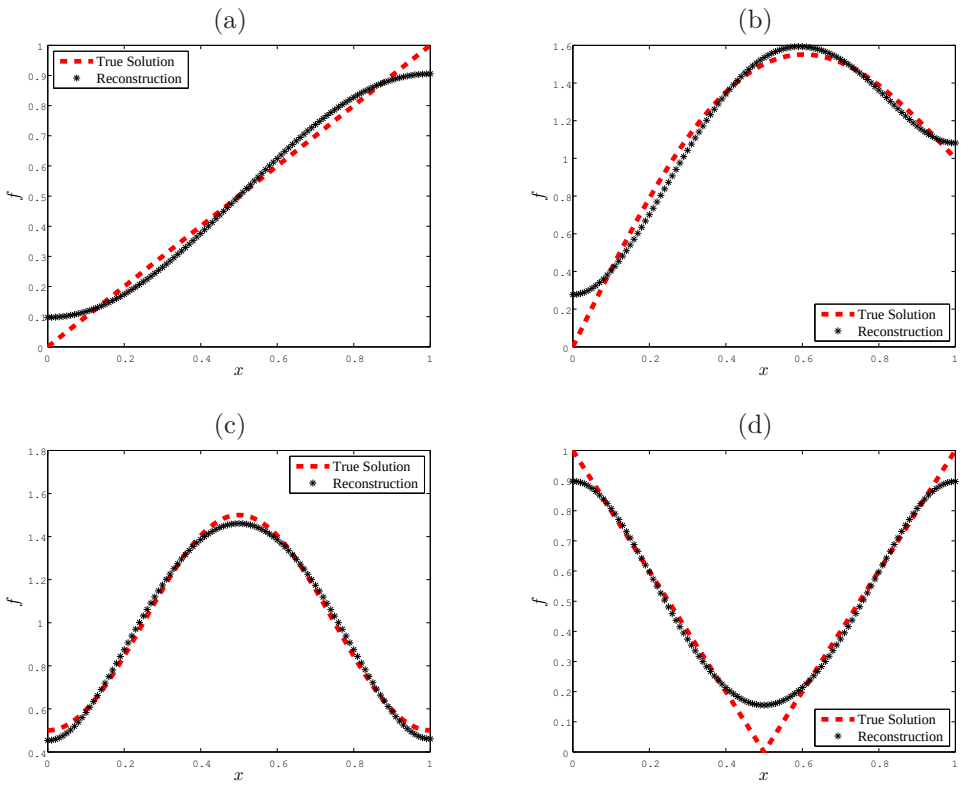

Figure 4.3: Illustrations of the true solutions and the corresponding reconstructions in Example 4.2. (a) $f^{\text{a}}_{\text{true}}(x) = x$. (b) $f^{\text{b}}_{\text{true}}(x) = \sin(\pi x) + x$. (c) $f^{\text{c}}_{\text{true}}(x) = 1 - \cos(2\pi x)/2$. (d) $f^{\text{d}}_{\text{true}}(x) = |2x - 1|$.

Table 4.2: Numerical performances of the reconstructions in Example 4.2 with various choices of true solutions.

$f_{\text{true}}(x)$	f_0	M	err	illustration
x	$1/2$	20	6.16%	Figure 4.3(a)
$\sin(\pi x)+x$	5	54	5.38%	Figure 4.3(b)
$1-\cos(2\pi x)/2$	5	34	2.51%	Figure 4.3(c)
$\lvert 2x-1\rvert$	-2	69	7.91%	Figure 4.3(d)

The last three lines of Table 4.2 suggest the delicacy in selecting the initial guess f_0. Actually, for the reconstructions of $f^{\text{b}}_{\text{true}}$, $f^{\text{c}}_{\text{true}}$ and $f^{\text{d}}_{\text{true}}$, we adopt such initial guesses that are quite separated from the true solutions. As is shown in Figure 4.3(b)–(d), these true solutions achieve maximum (minimum) inside Ω, and repeated experiments indicate that only an initial guess strictly larger than the maximum (smaller than the minimum) can yield reasonable result. This reveals the possible existence of local minimizers to which the iteration may converge with different initial guesses.

Next, it appears in Figures 4.2 and 4.3 that the normal derivatives of the reconstructed solutions vanish on the boundary. In fact, since f_0 is always taken as constant, by induction we see from (4.53) that

$$\partial_\nu f_{m+1}=\frac{K}{K+\alpha}\partial_\nu f_m-\frac{1}{K+\alpha}\int_0^T h\,\partial_\nu z(f_m)\,\mathrm{d}t=0\quad\text{on }\partial\Omega$$

because $\partial_\nu z(f_m)|_{\partial\Omega\times(0,T)}=0$ and h is chosen as x-independent. This may lead to certain divergence of the reconstruction from the true solution near the boundary, which is extremely obvious in Figure 4.3(a)–(b).

Finally, we also find a strong smoothing property of Algorithm 4.1. According to the regularity result in Proposition 4.2, one can expect an $H^3(\Omega)$-regularity throughout the iteration (4.53) provided that the initial guess f_0 and the known component h of the source term are sufficiently smooth. Such an increased smoothness, however, prevents us from proper identifications of non-smooth true solutions (see Figure 4.3(d)).

Now we turn to the two-dimensional case, where we set the mesh size in time and space as $1/80$. Without lose of generality, we always generate the subdomain ω by removing a closed rectangle in $\Omega=(0,1)^2$ whose edges are parallel to the coordinate axes. Due to the geometry condition for the reconstruction, $\partial\omega$ should include at least two adjacent edges of $\partial\Omega$. Meanwhile, although assumption (4.6) asserts that $T>\operatorname{diam}(\Omega\setminus\overline{\omega})$ is necessary, numerical experiments demonstrates that taking $T=1$ works in most instances.

Example 4.3 In this example, we fix $h(x,t)=1+t$ and consider the reconstruction of

$$f_{\text{true}}(x)=f_{\text{true}}(x_1,x_2)=1-\cos(\pi x_1)\cos(\pi x_2).$$

First, we fix the initial guess as $f_0\equiv 1$ and test the algorithm with the subdomains

$$\omega=\Omega\setminus[0.2,0.8]^2,\quad \omega=\Omega\setminus[0.1,0.9]^2,\quad \omega=\Omega\setminus[0.05,0.95]^2,\quad \omega=\Omega\setminus[0.1,0.9]\times[0,0.9].$$

In the first three choices, we keep the coverage $\partial\omega\supset\partial\Omega$ and reduce the thickness of ω from 0.2, 0.1 to 0.05. The last choice of ω, however, only covers 3 edges of $\partial\Omega$. The settings of ω and K as well as the corresponding numerical performances are listed in Table 4.3. As a representative, the surface plot of the reconstructed solution with $\omega=\Omega\setminus[0.05,0.95]^2$ is illustrated in Figure 4.4(a).

Table 4.3: Several pairs of parameter settings and the corresponding numerical performances in Example 4.3 under various choices of observable subdomains. Here we fix $T = 1$ and $f_0 \equiv 1$.

ω	K	M	err	elapsed time	illustration
$\Omega \setminus [0.2, 0.8]^2$	8.5×10^{-5}	18	0.19%	9.77 s	
$\Omega \setminus [0.1, 0.9]^2$	5×10^{-5}	16	0.26%	9.01 s	
$\Omega \setminus [0.05, 0.95]^2$	3×10^{-5}	17	0.40%	9.99 s	Figure 4.4(a)
$\Omega \setminus [0.1, 0.9] \times [0, 0.9]$	4.5×10^{-5}	18	1.14%	9.85 s	

Next, we further reduce the coverage of $\partial\Omega$ and fix $\omega = \Omega \setminus [0, 0.9]^2$ to see the influence of the observing duration T and the initial guess f_0. More precisely, we consider the following three pairs

$$T = 1,\ f_0 \equiv 1; \quad T = 1.3,\ f_0 \equiv 1 \quad \text{and} \quad T = 1,\ f_0 \equiv 0.$$

The choices of K and the corresponding numerical performances are collected in Table 4.4. Especially, we display the reconstructed values at the corner $x = (0, 0)$ for further comparisons. The surface plots of the reconstructed solutions are illustrated in Figure 4.4(b)–(d).

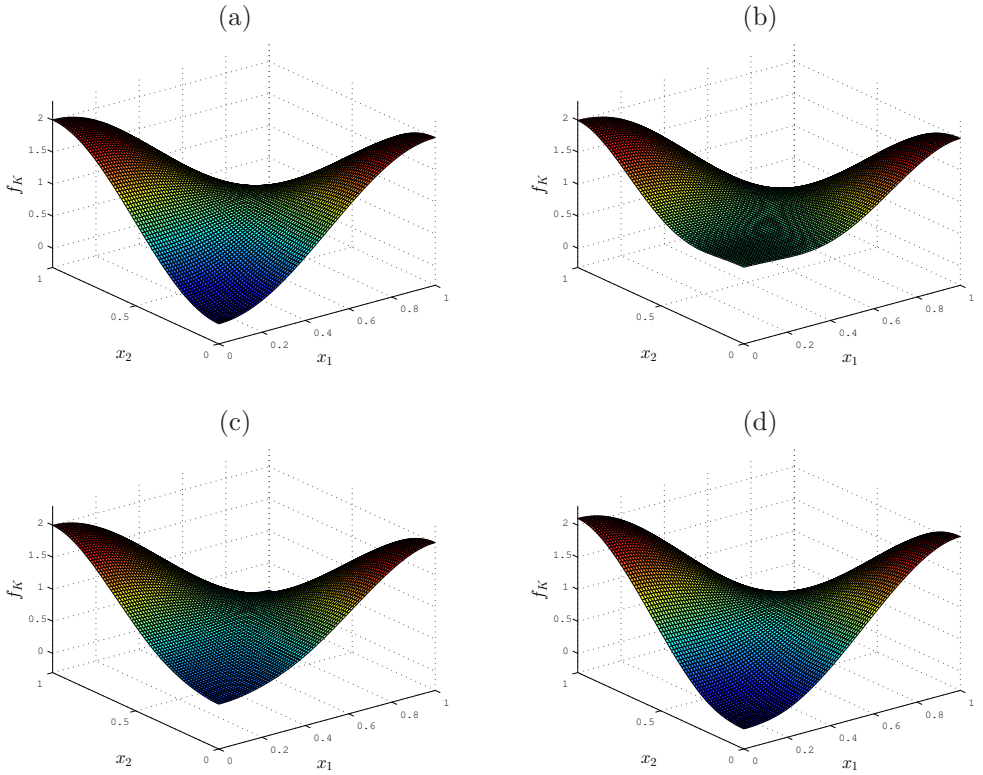

Figure 4.4: Illustrations of several representative reconstructed solutions in Example 4.3 with different settings. (a) $\omega = \Omega \setminus [0.05, 0.95]^2$, $T = 1$, $f_0 \equiv 1$. (b) $\omega = \Omega \setminus [0, 0.9]^2$, $T = 1$, $f_0 \equiv 1$. (c) $\omega = \Omega \setminus [0, 0.9]^2$, $T = 1.3$, $f_0 \equiv 1$. (d) $\omega = \Omega \setminus [0, 0.9]^2$, $T = 1$, $f_0 \equiv 0$.

As expected, it is readily seen from Example 4.3 (especially Table 4.3) that in the two-dimensional case, our algorithm mostly inherits the robustness, accuracy and efficiency observed in its one-dimensional counterpart. Nevertheless, we discover the difference on the length T. As was mentioned before, assumption (4.6) requires $T > \mathrm{diam}(\Omega \setminus \overline{\omega})$ for the theoretical stability,

Table 4.4: Several pairs of parameter settings and the corresponding numerical performances in Example 4.3 with the observable subdomain $\omega = \Omega \setminus [0, 0.9]^2$.

T	f_0	K	M	err	$f_M(0,0)$	illustration
1	1	4×10^{-5}	145	18.33%	0.89	Figure 4.4(b)
1.3	1	3.4×10^{-4}	202	8.92%	0.40	Figure 4.4(c)
1	0	4×10^{-5}	71	5.77%	0.01	Figure 4.4(d)

which is not satisfied in most of our tests. However, all test examples in Table 4.3 show surprisingly high accuracy of reconstructions, indicating a possibility that assumption (4.6) on T is more than necessary.

Other than those similarities to the one-dimensional case, here we should emphasize that the numerical performance depends more heavily on how much $\overline{\omega}$ can cover $\partial\Omega$ than its thickness. Typically, we compare the relative errors and iteration steps for $\omega = \Omega \setminus [0.05, 0.95]^2$ and $\omega = \Omega \setminus [0, 0.9]^2$. Although the areas of ω are identical in both cases, that ω covering only 2 edges of $\partial\Omega$ yields much larger error and requires more steps until convergence. In detail, we pay special attention on the uncovered corner $x = (0, 0)$, and it turns out that $f_M(0, 0) \approx 0.89$. One can also see clearly from Figure 4.4(b) that the numerical solution f_M fails to match with f_{true} near $x = (0, 0)$, though it seems much better elsewhere.

To treat the case of $\omega = \Omega \setminus [0, 0.9]^2$, we enlarge the observing duration according to assumption (4.6) and set $T = 1.3 > \text{diam}(\Omega \setminus \overline{\omega})$. After performing the same reconstruction, we find a great improvement in the numerical result, namely, the relatively error is remarkably reduced, and especially $f_M(0, 0) \approx 0.40$ (see also Figure 4.4(c)). This supports the feasibility of assumption (4.6) in some sense, that is, an adequate observing duration is required for the distant information to reach ω due to the finite propagation speed of wave.

In addition, we adjust the initial guess to see the importance of a priori information. We take again $T = 1$ and set $f_0 \equiv 0$, which matches well with f_{true} near the uncovered corner $x = (0, 0)$. We conclude from Figure 4.4(d) and Table 4.4 that the corresponding numerical performance is even better than that with $T = 1.3$ and $f_0 \equiv 1$, and the iteration converges faster. As one can imagine, the reconstructed value at $x = (0, 0)$ becomes extremely close to the true value $f_{\text{true}}(0, 0) = 0$.

4.5.2 Three-dimensional examples

Finally, we proceed to the reconstruction of the source term f_{true} in three spatial dimensions. To reduce the computational complexity, we enlarge the mesh size to 1/40 in time and space. Similarly to the two-dimensional case, we generate the observable subdomain ω by removing a closed cube in $\Omega = (0, 1)^3$ whose edges are parallel to the coordinate axes, and require $\partial\omega$ to include at least three mutually adjacent faces of $\partial\Omega$ according to the geometry condition. For simplicity, we fix $T = 1$ and $h(x, t) = 1 + t$. To visualize the three-variate functions $f_M(x_1, x_2, x_3)$, we will show 4 representative sections for each of them at $x_3 = 1/8$, $3/8$, $5/8$ and $7/8$.

Example 4.4 Consider the reconstruction of

$$f_{\text{true}}(x) = f_{\text{true}}(x_1, x_2, x_3) = 1 - \cos(\pi x_1)\cos(\pi x_2)\cos(\pi x_3).$$

As before, we test Algorithm 4.1 by choosing various ω with different thicknesses and coverage

of $\partial\Omega$ as follows

$$\omega = \Omega \setminus [0.1, 0.9]^3, \quad \omega = \Omega \setminus [0.05, 0.95]^3, \quad \omega = \Omega \setminus [0, 0.95] \times [0.05, 0.95]^2,$$
$$\omega = \Omega \setminus [0, 0.95]^2 \times [0.05, 0.95], \quad \omega = \Omega \setminus [0, 0.95]^3.$$

Except for the choice of $\omega = \Omega \setminus [0, 0.9]^3$, we keep $f_0 \equiv 1$ as the initial guess, whereas choose $f_0 \equiv 1$ or $f_0 \equiv 0$ to test the influence of the initial guess in this critical case. The settings of parameters and the corresponding numerical performances are listed in Table 4.5, and several representative reconstructed solutions are illustrated in Figure 4.5. Especially, we note that for $\omega = \Omega \setminus [0, 0.9]^3$, the reconstructed value at the uncovered corner $x = (0, 0, 0)$ with $f_0 \equiv 1$ is approximately 0.94 and, in contrast, that with $f_0 \equiv 0$ yields $f_M(0, 0, 0) \approx 0.02$.

Table 4.5: Parameter settings and the corresponding numerical performances in Example 4.4 under various choices of observable subdomains and initial guesses.

ω	f_0	K	M	err	elapsed time	illustration
$\Omega \setminus [0.1, 0.9]^3$	1	6×10^{-5}	39	0.61%	237.31 s	
$\Omega \setminus [0.05, 0.95]^3$	1	4×10^{-5}	41	0.76%	265.43 s	
$\Omega \setminus [0, 0.95] \times [0.05, 0.95]^2$	1	3×10^{-5}	37	0.91%	236.40 s	Figure 4.5(a)
$\Omega \setminus [0, 0.95]^2 \times [0.05, 0.95]$	1	2.8×10^{-5}	42	1.50%	264.75 s	Figure 4.5(b)
$\Omega \setminus [0, 0.95]^3$	1	2.7×10^{-5}	86	12.31%	551.36 s	Figure 4.5(c)
$\Omega \setminus [0, 0.95]^3$	0	2.7×10^{-5}	60	6.23%	387.91 s	Figure 4.5(d)

Example 4.5 Finally, we test our algorithm by selecting true solutions with different degrees of monotonicity as before. We choose

$$f^{\mathrm{a}}_{\mathrm{true}}(x) = f^{\mathrm{a}}_{\mathrm{true}}(x_1, x_2, x_3) = 1 - \sin x_1 \cos(\pi x_2)\, x_3, \tag{4.55}$$
$$f^{\mathrm{b}}_{\mathrm{true}}(x) = f^{\mathrm{b}}_{\mathrm{true}}(x_1, x_2, x_3) = 1 + \exp\left(\frac{x_1 + x_2}{2}\right) \sin x_3, \tag{4.56}$$
$$f^{\mathrm{c}}_{\mathrm{true}}(x) = f^{\mathrm{c}}_{\mathrm{true}}(x_1, x_2, x_3) = 1 - \cos(\pi x_1)\, x_2 \cos(2x_3) \tag{4.57}$$

and set $\omega = \Omega \setminus [0, 0.95]^2 \times [0.05, 0.95]$, $K = 3 \times 10^{-5}$. Comparisons of the corresponding sections of true solutions and the reconstructed ones are shown in Figure 4.6, and the numerical performances are listed in Table 4.6.

Table 4.6: Numerical performances of the reconstructions in Example 4.5 for various choices of true solutions.

f_{true}	f_0	M	err	illustration
$f^{\mathrm{a}}_{\mathrm{true}}$ (see (4.55))	1	26	2.18%	Figure 4.6(a1)–(a2)
$f^{\mathrm{b}}_{\mathrm{true}}$ (see (4.56))	2	28	3.31%	Figure 4.6(b1)–(b2)
$f^{\mathrm{c}}_{\mathrm{true}}$ (see (4.57))	1	29	3.62%	Figure 4.6(c1)–(c2)

Again, the iterative thresholding algorithm behaves almost identically in the above three-dimensional examples as that in lower dimensional ones. Collecting the phenomena observed in all the above examples, we evaluate the performance of Algorithm 4.1 as follows.

- Algorithm 4.1 processes strong robustness against the oscillating measurement errors.
- The convergence speed of Algorithm 4.1 depends heavily on a delicate choice of the tuning parameter K.

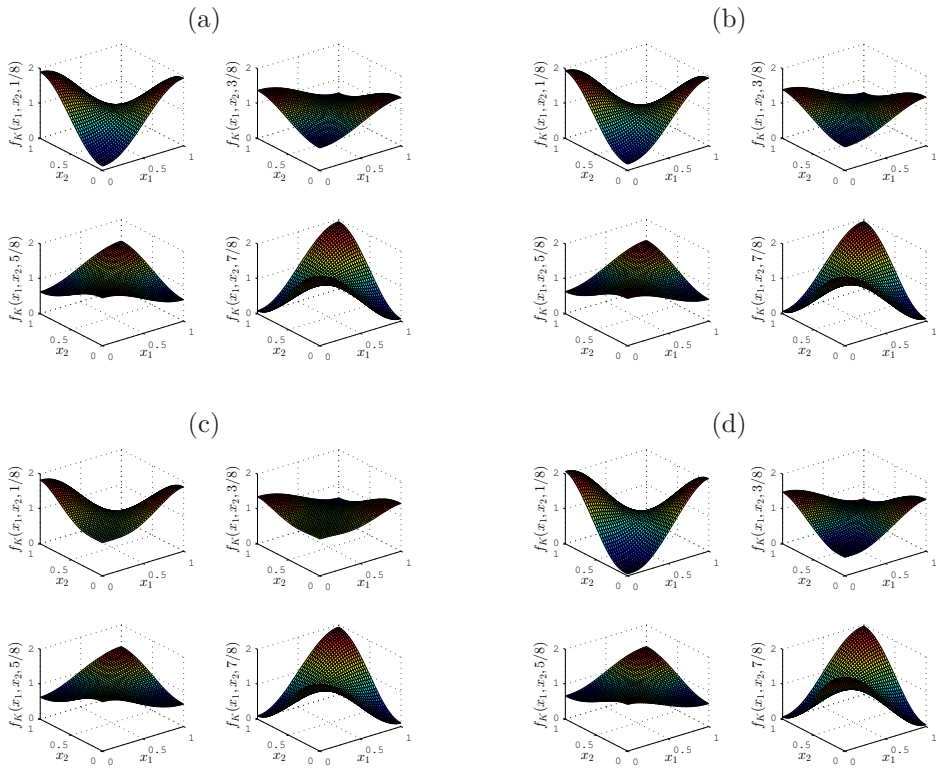

Figure 4.5: Illustrations of several representative reconstructed solutions in Example 4.4 with various observable subdomains and initial guesses. (a) $\omega = \Omega \setminus [0, 0.95] \times [0.05, 0.95]^2$, $f_0 \equiv 1$. (b) $\omega = \Omega \setminus [0, 0.95]^2 \times [0.05, 0.95]$, $f_0 \equiv 1$. (c) $\omega = \Omega \setminus [0, 0.95]^3$, $f_0 \equiv 1$. (d) $\omega = \Omega \setminus [0, 0.95]^3$, $f_0 \equiv 0$.

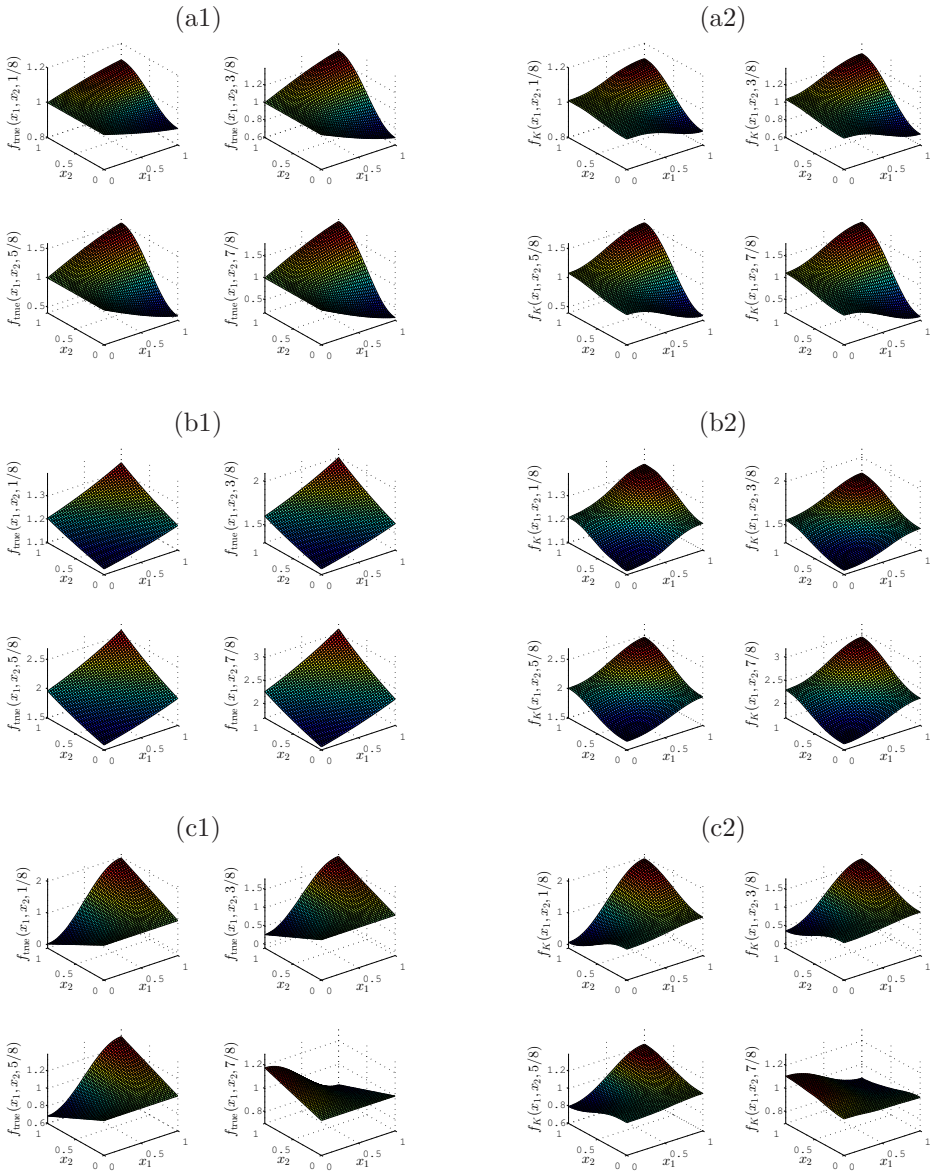

Figure 4.6: Illustrations of the true solutions and the corresponding reconstructions in Example 4.5. (a1) $f^{\mathrm{a}}_{\mathrm{true}}$ defined in (4.55). (a2) Reconstruction of $f^{\mathrm{a}}_{\mathrm{true}}$. (b1) $f^{\mathrm{b}}_{\mathrm{true}}$ defined in (4.56). (b2) Reconstruction of $f^{\mathrm{b}}_{\mathrm{true}}$. (c1) $f^{\mathrm{c}}_{\mathrm{true}}$ defined in (4.57). (c2) Reconstruction of $f^{\mathrm{c}}_{\mathrm{true}}$.

- The thickness of the observable subdomain ω influences moderately on the numerical performance.
- The boundary behavior of the reconstruction relies on that of the initial guess f_0 and the known component $h(x,t)$ of the source term, which may cause local inaccuracy.
- The extent to which $\partial\omega$ can cover $\partial\Omega$ greatly dominates the numerical performance.
- When $\partial\omega$ fails to cover the majority of $\partial\Omega$, the numerical performance can be improved by increasing the observing duration T or adjusting the initial guess f_0.

4.A Reconstruction by final observation data

Independent of the previous sections, in this appendix we consider the determination of f from the final observation data $u(\,\cdot\,,T)$. More precisely, we impose the homogeneous Dirichlet boundary condition to the three-dimensional time cone model and formulate the inverse source problem as follows.

Problem 4.2 *Let $\Omega \subset \mathbb{R}^3$ and $T > 0$ be given, and u satisfy*

$$\begin{cases} \mathcal{H}_\rho u = f\,h & \text{in } \Omega \times (0,T], \\ \partial_t^\ell u = 0 \quad (\ell = 0,1,2,3) & \text{in } \Omega \times \{0\}, \\ u = \triangle u = 0 & \text{on } \partial\Omega \times (0,T], \end{cases} \tag{4.58}$$

where h was defined in (4.3)*. Provided that ρ and g are known, determine $f(x)$ $(x \in \Omega)$ by the final observation data u in $\Omega \times \{T\}$.*

To discuss the stability for the above problem, we need the follow lemma, which is a Dirichlet counterpart of Lemma 4.1.

Lemma 4.5 *Assume that $\partial\Omega$ is of C^2 class, $G \in L^2(\Omega \times (0,T))$, $a \in H_0^1(\Omega)$ and $b \in L^2(\Omega)$. Then there is a unique solution to*

$$\begin{cases} \partial_t^2 w - \triangle w = G & \text{in } \Omega \times (0,T], \\ w = a,\ \partial_t w = b & \text{in } \Omega \times \{0\}, \\ w = 0 & \text{on } \partial\Omega \times (0,T]. \end{cases} \tag{4.59}$$

such that $w \in C([0,T]; H_0^1(\Omega)) \cap C^1([0,T]; L^2(\Omega))$, and there holds the energy estimate

$$\begin{aligned} E(t) &:= \left(\|\partial_t w(\,\cdot\,,t)\|_{L^2(\Omega)} + \|\nabla w(\,\cdot\,,t)\|_{L^2(\Omega)}\right)^{1/2} \\ &\le \left(\|b\|_{L^2(\Omega)} + \|\nabla a\|_{L^2(\Omega)}\right)^{1/2} + \|G\|_{L^1(0,t;L^2(\Omega))} \quad (0 \le t \le T). \end{aligned} \tag{4.60}$$

Moreover, there exists $C_\Omega > 0$ depending only on the diameter $\mathrm{diam}(\Omega)$ *of Ω such that*

$$\|w(\,\cdot\,,t)\|_{L^2(\Omega)} \le C_\Omega \left\{ \left(\|b\|_{L^2(\Omega)} + \|\nabla a\|_{L^2(\Omega)}\right)^{1/2} + \|G\|_{L^1(0,t;L^2(\Omega))} \right\} \quad (0 \le t \le T). \tag{4.61}$$

Proof. The basic solvability of (4.59) is the classical result (see, e.g., Lions and Magenes [47]). To show the energy estimate (4.60), we multiply $\partial_t w$ to both sides of (4.59) and take formal integral in Ω for any $t \in [0,T]$ to obtain

$$E(t)\,E'(t) = \frac{1}{2}\frac{\mathrm{d}}{\mathrm{d}t}\left(E(t)^2\right) = \frac{1}{2}\frac{\mathrm{d}}{\mathrm{d}t}\left(\int_\Omega \left(|\partial_t w(x,t)|^2 + |\nabla w(x,t)|^2\right)\mathrm{d}x\right)$$

$$
\begin{aligned}
&= \frac{1}{2}\frac{\mathrm{d}}{\mathrm{d}t}\left(\int_\Omega |\partial_t w(x,t)|^2\,\mathrm{d}x\right) + \int_\Omega \nabla\partial_t w(x,t)\cdot\nabla w(x,t)\,\mathrm{d}x \\
&\quad - \int_{\partial\Omega} \partial_t w(x,t)\,\partial_\nu w(x,t)\,\mathrm{d}\sigma \\
&= \int_\Omega \partial_t w(x,t)\,(\partial_t^2 w(x,t) - \triangle w(x,t))\,\mathrm{d}x = \int_\Omega \partial_t w(x,t)\,G(x,t)\,\mathrm{d}x \\
&\le \|\partial_t w(\,\cdot\,,t)\|_{L^2(\Omega)}\,\|G(\,\cdot\,,t)\|_{L^2(\Omega)} \le E(t)\,\|G(\,\cdot\,,t)\|_{L^2(\Omega)}
\end{aligned}
$$

or equivalently $E'(t) \le \|G(\,\cdot\,,t)\|_{L^2(\Omega)}$ except for the trivial case, where we have applied Green's formula and Hölder's inequality. Hence, taking integral in $(0,t)$ and noting the fact $L^1(0,t;L^2(\Omega)) \subset L^2(0,t;L^2(\Omega))$, we have

$$
E(t) - E(0) = \int_0^t E'(s)\,\mathrm{d}s \le \int_0^t \|G(\,\cdot\,,s)\|_{L^2(\Omega)}\,\mathrm{d}s \le \|G\|_{L^1(0,t;L^2(\Omega))} \quad (0 \le t \le T),
$$

which is indeed (4.60). Moreover, we further apply Poincaré's inequality to deduce

$$
\|w(\,\cdot\,,t)\|_{L^2(\Omega)} \le C_\Omega\,\|\nabla w(\,\cdot\,,t)\|_{L^2(\Omega)} \le C_\Omega\,E(t),
$$

where C_Ω is a positive constant only dependent on $\mathrm{diam}(\Omega)$. By (4.60), we obtain (4.61) immediately. □

Based on the repeated uses of Lemma 4.5, we can give a stability estimate for Problem 4.2 under the smallness assumption on Ω.

Proposition 4.3 *Let $\partial\Omega$ be of C^2 class and u be the solution to* (4.58)*, where $f \in L^2(\Omega)$ and g, ρ satisfy*

$$
\begin{aligned}
&g \in H^3(0,T;L^\infty), \quad g(\,\cdot\,,0) = \partial_t g(\,\cdot\,,0) = 0 \text{ a.e. in } \Omega, \\
&\exists\, g_0 > 0 \text{ such that } |g(\,\cdot\,,T)| \ge g_0 \text{ a.e. in } \Omega, \\
&\rho \in C^3[0,T], \quad \exists\, \rho_0 > 0 \text{ such that } \rho \ge \rho_0 \text{ in } [0,T].
\end{aligned}
$$

If $\mathrm{diam}(\Omega)$ *is sufficiently small, then there exists a constant $C = C(\Omega,T,\rho,g) > 0$ such that*

$$
\|f\|_{L^2(\Omega)} \le C\,\|\triangle^2 u(\,\cdot\,,T)\|_{L^2(\Omega)}. \tag{4.62}
$$

Proof. Similarly to the treatments in Section 4.2, it suffices to investigate the following two initial-boundary value problem

$$
\begin{cases} \Box U = V & \text{in } \Omega\times(0,R(T)], \\ U = \partial_\tau U = 0 & \text{in } \Omega\times\{0\}, \\ U = 0 & \text{on } \partial\Omega\times(0,R(T)], \end{cases}
\quad
\begin{cases} \Box V = f\,H & \text{in } \Omega\times(0,R(T)], \\ V = \partial_\tau V = 0 & \text{in } \Omega\times\{0\}, \\ V = 0 & \text{on } \partial\Omega\times(0,R(T)], \end{cases} \tag{4.63}
$$

where $H(\,\cdot\,,\tau) := \dfrac{8\pi\,g(\,\cdot\,,R^{-1}(\tau))}{\rho(R^{-1}(\tau))}$.

First we introduce an auxiliary function $\widetilde{V} := \partial_\tau^2 V$. Since the assumption $g(\,\cdot\,,0) = \partial_t g(\,\cdot\,,0) = 0$ a.e. in Ω implies $H(\,\cdot\,,0) = \partial_t H(\,\cdot\,,0) = 0$ a.e. in Ω, it is easily verified that $\widetilde{V}$ satisfies

$$
\begin{cases} \Box\widetilde{V} = f\,\partial_\tau^2 H & \text{in } \Omega\times(0,R(T)], \\ \widetilde{V} = \partial_\tau\widetilde{V} = 0 & \text{in } \Omega\times\{0\}, \\ \widetilde{V} = 0 & \text{on } \partial\Omega\times(0,R(T)]. \end{cases}
$$

According to (4.61), we have the estimate

$$\begin{aligned}\|\partial_\tau^2 V(\,\cdot\,,\tau)\|_{L^2(\Omega)} = \|\widetilde{V}(\,\cdot\,,\tau)\|_{L^2(\Omega)} &\le C_\Omega \,\|f\,\partial_\tau^2 H\|_{L^1(0,\tau;L^2(\Omega))}\\ &\le C_\Omega \,\|\partial_\tau^2 H\|_{L^1(0,\tau;L^\infty(\Omega))}\,\|f\|_{L^2(\Omega)} \quad (0\le t\le T),\end{aligned}$$

where $C_\Omega>0$ is a constant only dependent on $\mathrm{diam}(\Omega)$. Therefore, by the assumption $|g(\,\cdot\,,t)|\ge g_0$ a.e. in Ω and taking $\tau=R(T)$ in (4.58), the above inequality immediately yields

$$\begin{aligned}\frac{8\pi\, g_0}{\rho(T)}\,\|f\|_{L^2(\Omega)} &\le \|\partial_\tau^2 V(\,\cdot\,,R(T))\|_{L^2(\Omega)} + \|\triangle V(\,\cdot\,,R(T))\|_{L^2(\Omega)}\\ &\le C_\Omega\,\|\partial_\tau^2 H\|_{L^1(0,R(T);L^\infty(\Omega))}\,\|f\|_{L^2(\Omega)}\\ &\quad + \|\partial_\tau^2\triangle U(\,\cdot\,,R(T))\|_{L^2(\Omega)} + \|\triangle^2 u(\,\cdot\,,T)\|_{L^2(\Omega)}.\end{aligned}\tag{4.64}$$

Here we have to further decompose V by the relation $V=\Box U$ since $V(\,\cdot\,,R(T))$ involves the time derivative of $U(\,\cdot\,,R(T))$ which is not observable.

Next, we shall give an estimate for the term $\|\partial_\tau^2\triangle U(\,\cdot\,,R(T))\|_{L^2(\Omega)}$ in (4.64). Since $f\,\partial_\tau^3 H\in L^2(\Omega\times(0,T))$, we further introduce an auxiliary function $\widehat{V}:=\partial_\tau\widetilde{V}=\partial_\tau^3 V$, which satisfies

$$\begin{cases}\Box\widehat{V}=f\,\partial_\tau^3 H & \text{in } \Omega\times(0,R(T)],\\ \widehat{V}=0,\ \partial_\tau\widehat{V}=f\,\partial_\tau^2 H(\,\cdot\,,0) & \text{in } \Omega\times\{0\},\\ \widehat{V}=0 & \text{on } \partial\Omega\times(0,R(T)].\end{cases}$$

Then the application of Lemma 4.5 with respect to $\widehat{V}$ yields the regularity $\partial_\tau^2\widetilde{V}=\partial_\tau\widehat{V}\in C([0,R(T)];L^2)\subset L^2(\Omega\times(0,R(T)))$. Furthermore, it follows from the energy estimate (4.60) that

$$\begin{aligned}\|\partial_\tau^2\widetilde{V}(\,\cdot\,,\tau)\|_{L^2(\Omega)} = \|\partial_\tau\widehat{V}(\,\cdot\,,\tau)\|_{L^2(\Omega)} &\le \|f\,\partial_\tau^2 H(\,\cdot\,,0)\|_{L^2(\Omega)} + \|f\,\partial_\tau^3 H\|_{L^1(0,\tau;L^2(\Omega))}\\ &\le \big(\|\partial_\tau^2 H(\,\cdot\,,0)\|_{L^\infty(\Omega)} + \|\partial_\tau^3 H\|_{L^1(0,R(T);L^\infty(\Omega))}\big)\,\|f\|_{L^2(\Omega)}\end{aligned}\tag{4.65}$$

for $0\le\tau\le R(T)$.

Finally, we introduce $\widetilde{U}:=\partial_\tau^2\triangle U$. Simple calculations give

$$\begin{cases}\Box\widetilde{U}=\triangle\widetilde{V}=\partial_\tau^2\widetilde{V}-f\,\partial_\tau^2 H & \text{in } \Omega\times(0,R(T)],\\ \widetilde{U}=\partial_\tau\widetilde{U}=0 & \text{in } \Omega\times\{0\},\\ \widetilde{U}=0 & \text{on } \partial\Omega\times(0,R(T)],\end{cases}$$

where the inhomogeneous term has already been proved to be in $L^2(\Omega\times(0,R(T)))$. Therefore, it follows from estimates (4.61) and (4.65) that

$$\begin{aligned}\|\partial_\tau^2\triangle U(\,\cdot\,,R(T))\|_{L^2(\Omega)} &= \|\widetilde{U}(\,\cdot\,,R(T))\|_{L^2(\Omega)}\\ &\le C_\Omega\left(\|\partial_\tau^2\widetilde{V}\|_{L^1(0,R(T);L^2(\Omega))} + \|f\,\partial_\tau^2 H\|_{L^1(0,R(T);L^2(\Omega))}\right)\\ &\le C_\Omega\big\{R(T)\left(\|\partial_\tau^2 H(\,\cdot\,,0)\|_{L^\infty(\Omega)} + \|\partial_\tau^3 H\|_{L^1(0,R(T);L^\infty(\Omega))}\right)\\ &\qquad +\|\partial_\tau^2 H\|_{L^1(0,R(T);L^\infty(\Omega))}\big\}\,\|f\|_{L^2(\Omega)},\end{aligned}$$

which, together with (4.64), indicates

$$\begin{aligned}\frac{8\pi\, g_0}{\rho(T)}\,\|f\|_{L^2(\Omega)} \le C_\Omega\big\{&R(T)\left(\|\partial_\tau^2 H(\,\cdot\,,0)\|_{L^\infty(\Omega)} + \|\partial_\tau^3 H\|_{L^1(0,R(T);L^\infty(\Omega))}\right)\\ &+2\,\|\partial_\tau^2 H\|_{L^1(0,R(T);L^\infty(\Omega))}\big\}\,\|f\|_{L^2(\Omega)} + \|\triangle^2 u(\,\cdot\,,T)\|_{L^2(\Omega)}.\end{aligned}$$

The coefficient of $\|f\|_{L^2(\Omega)}$ on the right-hand side can be absorbed into that on the left-hand side provided that $\operatorname{diam}(\Omega)$ is sufficiently small. In fact, if C_Ω is sufficiently small such that, for example,

$$\frac{4\pi\, g_0}{\rho(T)} \geq C_\Omega \left\{ R(T) \left(\|\partial_\tau^2 H(\,\cdot\,,0)\|_{L^\infty(\Omega)} + \|\partial_\tau^3 H\|_{L^1(0,R(T);L^\infty(\Omega))} \right) + 2\, \|\partial_\tau^2 H\|_{L^1(0,R(T);L^\infty(\Omega))} \right\},$$

then there is a constant $C = C(\Omega, R(T), H) = C(\Omega, T, \rho, h) > 0$ such that (4.62) holds. The proof is completed. □

It is natural to consider the removal of the smallness restriction on the domain Ω as well as various assumptions on g. However, it turns out that non-uniqueness of the reconstruction may occur in a relaxed setting. Actually, a conditional uniqueness can be expected from the following simplified one-dimensional example.

Example 4.6 Consider

$$\begin{cases} \mathcal{H}_\rho u(x,t) = f(x)\, g(t)/\rho(t) & (0 < x < L,\ 0 < t \leq T), \\ u(x,0) = \partial_t u(x,0) = 0 & (0 < x < L), \\ u(0,t) = u(L,t) = 0 & (0 < t \leq T), \end{cases} \tag{4.66}$$

that is, g is further assumed to be space-independent. In this case, $f \in L^2(0,L)$ is uniquely determined by $u(\,\cdot\,,T)$ if and only if there holds

$$\int_0^{R(T)} \sin\left(\frac{\pi n\, (R(T) - \tau)}{L} \right) \frac{g(R^{-1}(\tau))}{\rho(R^{-1}(\tau))}\, \mathrm{d}\tau \neq 0 \quad (n = 1, 2, \ldots). \tag{4.67}$$

In other words, (4.67) holds if and only if $u(\,\cdot\,,T) = 0$ implies $f = 0$.

In fact, as usually we investigate the equivalent problem

$$\begin{cases} \Box U(x,t) = 2\, f(x)\, g(R^{-1}(\tau))/\rho(R^{-1}(\tau)) & (0 < x < L,\ 0 < \tau \leq R(T)), \\ U(x,0) = \partial_\tau U(x,0) = 0 & (0 < x < L), \\ U(0,\tau) = u(L,\tau) = 0 & (0 < \tau \leq R(T)) \end{cases}$$

instead of (4.66). By the combination of Duhamel's principle and the separation of variables, it is straightforward to write

$$U(\,\cdot\,,\tau) = \sum_{n=1}^\infty \sqrt{\frac{L}{2\lambda_n}}\, (f, \varphi_n) \left(\int_0^\tau \varphi_n(\tau - \zeta)\, \frac{g(R^{-1}(\zeta))}{\rho(R^{-1}(\zeta))}\, \mathrm{d}\zeta \right) \varphi_n, \tag{4.68}$$

where $(\,\cdot\,,\,\cdot\,)$ denotes the inner product in $L^2(0,L)$, and

$$\lambda_n = \left(\frac{\pi n}{L} \right)^2, \quad \varphi_n(x) = \sqrt{\frac{2}{L}}\, \sin\left(\sqrt{\lambda_n}\, x \right) \quad (n = 1, 2, \ldots)$$

form the eigensystem of $-\partial_x^2$ with the homogeneous Dirichlet boundary condition.

Now we suppose that $u(\,\cdot\,,T) = U(\,\cdot\,,R(T)) = 0$. Since $\{\varphi_n\}_{n=1}^\infty$ is a complete orthonormal system of $L^2(0,L)$, there should holds

$$\sqrt{\frac{L}{2\lambda_n}}\, (f, \varphi_n) \left(\int_0^\tau \varphi_n(\tau - \zeta)\, \frac{g(R^{-1}(\zeta))}{\rho(R^{-1}(\zeta))}\, \mathrm{d}\zeta \right) = 0 \quad (n = 1, 2, \ldots).$$

However, condition (4.67) eliminates other possibilities than $(f, \varphi_n) = 0$ for all $n = 1, 2, \ldots$, indicating $f = 0$ immediately.

On the opposite side, we argue by contradiction. Supposing that there exists a natural number n_0 such that (4.67) is invalid, then it follows from (4.68) that $(f, \varphi_{n_0}) \neq 0$ is possible even if $U(\,\cdot\,, R(T)) = 0$, indicating that f does not necessarily vanishes.

Consequently, the identification of f by $u(\,\cdot\,, T)$ is not unique once the condition (4.67) is dissatisfied by any $n \in \mathbb{N}$.

References for Part I

[1] Adams R A 1975 *Sobolev Spaces* (New York: Academic Press)

[2] Avrami M 1939 Kinetics of phase change. I General theory *J. Chem. Phys.* **7** 1103–12

[3] Avrami M 1940 Kinetics of phase change. II Transformation time relations for random distribution of nuclei *J. Chem. Phys.* **8** 212–24

[4] Avrami M 1941 Granulation, phase change, and microstructure Kinetics of phase change. III *J. Chem. Phys.* **9** 177–84

[5] Balluffi R W, Allen S M and Carter W C 2005 *Kinetics of Materials* (New York: Wiley)

[6] Bao G, Chow S N, Li P and Zhou H 2014 An inverse random source problem for the Helmholtz equation *Math. Comput.* **83** 215–33

[7] Beck A and Teboulle M 2009 A fast iterative shrinkage-thresholding algorithm for linear inverse problems *SIAM J. Imaging Sci.* **2** 183–202

[8] Bellassoued M and Yamamoto M 2014 *Carleman Estimates and Applications to Inverse Problems for Hyperbolic Systems* (Tokyo: Springer) at press

[9] Bioucas-Dias J M and Figueiredo M A 2007 A new TwIST: two-step iterative shrinkage/thresholding algorithms for image restoration *IEEE Trans. Image Process.* **16** 2992–3004

[10] Burger M 2000 Direct and inverse problems in polymer crystallization processes *PhD Dissertation* University of Linz, Austria

[11] Burger M 2001 Iterative regularization of a parameter identification problem occuring in polymer crystallization *SIAM J. Numer. Anal.* **39** 1029–55

[12] Burger M and Capasso V 2001 Mathematical modelling and simulation of non-isothermal crystallization of polymers *Math. Models Methods Appl. Sci.* **11** 1029–53

[13] Burger M, Capasso V and Eder G 2002 Modelling of polymer crystallization in temperature fields *Z. Angew. Math. Mech.* **82** 51–63

[14] Burger M, Capasso V and Engl H W 1999 Inverse problems related to crystallization of polymers *Inverse Problems* **15** 155–73

[15] Burger M, Capasso V and Salani C 2002 Modelling multi-dimensional crystallization of polymers in interaction with heat transfer *Nonlinear Anal. Real World Appl.* **3** 131–60

[16] Cahn J W 1956 Transformation kinetics during continuous cooling *Acta Met.* **4** 572–5

[17] Cahn J W 1995 The time cone method for nucleation and growth kinetics on a finite domain *Mater. Res. Soc. Symp. Proc.* **398** 425–37

[18] Cannon J R 1984 *The One-Dimensional Heat Equation* (New York: Cambridge University Press)

[19] Capasso V (ed.) 2003 *Mathematical Modelling for Polymer Processing. Polymerization, Crystallization, Manufacturing (Mathematics in Industry vol 2)* (Heidelberg: Springer-Verlag)

[20] Capasso V, Engl H W and Kindermann S 2008 Parameter identification in a random environment exemplified by a multiscale model for crystal growth *Multiscale Model. Simul.* **7** 814–41

[21] Capasso V and Salani C 2000 Stochastic birth-and-growth processes modelling crystallization of polymers with spatially heterogeneous parameters *Nonlinear Anal. Real World Appl.* **1** 485–98

[22] Daubechies I, Defrise M and De Mol C 2004 An iterative thresholding algorithm for linear inverse problems with a sparsity constraint *Commun. Pur. Appl. Math.* **57** 1413–57

[23] Daubechies I, Teschke G and Vese L 2007 Iteratively solving linear inverse problems under general convex constraints *Inverse Problems Imaging* **1** 29–46

[24] Eder G 1996 Crystallization kinetic equations incorporating surface and bulk nucleation *Z. Angew. Math. Mech.* **76** 489–92

[25] Engl H W, Hanke M and Neubauer A 2000 *Regularization of Inverse Problems* (Dordrecht: Kluwer)

[26] Escobedo R and Capasso V 2005 Moving bands and moving boundaries with decreasing speed in polymer crystallization *Math. Models Methods Appl. Sci.* **15** 325–41

[27] Evans L C 2010 *Partial Differential Equations 2nd ed* (Providence, RI: American Mathematical Society)

[28] Fairweather G and Mitchell A R 1965 A high accuracy alternating direction method for the wave equation *IMA J. Appl. Math.* **1** 309–16

[29] Fornasier M and Rauhut H 2008 Iterative thresholding algorithms *Appl. Comput. Harmon. Anal.* **25** 187–208

[30] Imanuvilov O Y 2002 On Carleman estimates for hyperbolic equations *Asymptotic Anal.* **32** 185–220

[31] Imanuvilov O Y and Yamamoto M 2001 Global Lipschitz stability in an inverse hyperbolic problem by interior observation *Inverse Problems* **17** 717–28

[32] Imanuvilov O Y and Yamamoto M 2001 Global uniqueness and stability in determining coefficients of wave equations *Commun. Part. Diff. Eq.* **26** 1409–25

[33] Isakov V 1997 On reconstruction of the diffusion and of the principal coefficient of a hyperbolic equation *Inverse Problems in Wave Propagation: Proc. of the IMA Workshop* vol 90 (Berlin: Springer) pp 259–77

[34] Isakov V 2006 *Inverse Problems for Partial Differential Equations* (Berlin: Springer)

[35] Isakov V and Yamamoto M 2000 Carleman estimate with the Neumann boundary condition and its applications to the observability inequality and inverse hyperbolic problems *Contemp. Math.* **268** 191–226

[36] Jackson J J 1974 Dynamics of expanding inhibitory fields *Science* **183** 445–7

[37] Jena A K and Chaturvedi M C 1992 *Phase Transformation in Materials* (New Jersey: Prentice Hall)

[38] Jiang D, Feng H and Zou J 2014 Overlapping domain decomposition methods for linear inverse problems *Inverse Problems Imaging* in press

[39] Johnson W and Mehl R 1939 Reaction kinetics in processes of nucleation and growth *Trans. AIME* **135** 416–42

[40] Kabanikhin S I, Satybaev A D and Shishlenin M A 2004 *Direct Methods of Solving Multidimensional Inverse Hyperbolic Problems* (Utrecht: VSP)

[41] Kaipio J and Somersalo E 2005 *Statistical and Computational Inverse Problems* (New York: Springer)

[42] Klibanov M V and Timonov A 2004 *Carleman Estimates for Coefficient Inverse Problems and Numerical Applications* (Utrecht: VSP)

[43] Kolmogorov A N 1937 On the statistical theory of the crystallization of metals *Bull. Acad. Sci. USSR* **1** 355–9

See also in Kolmogorov A N 1992 *Selected Works of A N Kolmogorov (Probability Theory and Mathematical Statistics 22)* vol 2 (Dordrecht: Kluwer) pp 188–92

[44] Lasiecka I, Triggiani R and Zhang X 2000 Nonconservative wave equations with unobserved Neumann BC: Global uniqueness and observability in one shot *Contemp. Math.* **268** 227–325

[45] Lees M 1962 Alternating direction methods for hyperbolic differential equations *J. Soc. Indust. Appl. Math.* **10** 610–6

[46] Li P J 2011 An inverse random source scattering problem in inhomogeneous media *Inverse Problems* **27** 035004

[47] Lions J-L and Magenes E 1972 *Non-Homogeneous Boundary Value Problems and Applications* (Berlin: Springer)

[48] Liu Y, Xu X and Yamamoto M 2012 Growth rate modeling and identification in the crystallization of polymers *Inverse Problems* **28** 095008

[49] Liu Y and Yamamoto M 2014 On the multiple hyperbolic systems modelling phase transformation kinetics *Appl. Anal.* **93** 1297–1318

[50] Micheletti A and Burger M 2001 Stochastic and deterministic simulation of nonisothermal crystallization of polymers *J. Math. Chem.* **30** 169–93

[51] Nakamura G, Watanabe M and Kaltenbacher B 2009 On the identification of a coefficient function in a nonlinear wave equation *Inverse Problems* **25** 035007

[52] Pilant M and Rundell M 1991 Determining a coefficient in a first-order hyperbolic equation *SIAM J. Appl. Math.* **51** 494–506

[53] Puel J-P and Yamamoto M 1996 On a global estimate in a linear inverse hyperbolic problem *Inverse Problems* **12** 995–1002

[54] Rios P R and Villa E 2009 Transformation kinetics for inhomogeneous nucleation *Acta Mater.* **57** 1199–208

[55] Wang Y B, Jia X Z and Cheng J 2002 A numerical differentiation method and its application to reconstruction of discontinuity *Inverse Problems* **18** 1461–76

[56] Yamamoto M 1995 Stability, reconstruction formula and regularization for an inverse source hyperbolic problem by a control method *Inverse Problems* **11** 481–96

[57] Yamamoto M 1999 Uniqueness and stability in multidimensional hyperbolic inverse problems *J. Math. Pures Appl.* **78** 65–98

Part II

Fractional Diffusion Equations for Anomalous Diffusion

Chapter 5

Strong Maximum Principle for Fractional Diffusion Equations and an Application to an Inverse Source Problem

The strong maximum principle is one of the remarkable characterizations of parabolic equations, which is expected to be partly inherited by fractional diffusion equations. Based on the corresponding weak maximum principle, in this chapter we establish a strong maximum principle for single-term time-fractional diffusion equations, which is slightly weaker than that for the parabolic case. As a direct application, we give a uniqueness result for a related inverse source problem on the determination of the temporal component of the inhomogeneous term which is assumed to be in form of separation of variables.

5.1 Introduction and main results

Let Ω be an open bounded domain in $\mathbb{R}^d$ $(d = 1, 2, 3)$ with a smooth boundary (for example, of C^∞ class), and $0 < \alpha < 1$. Consider

$$\begin{cases} \partial_t^\alpha u(x,t) + \mathcal{A}u(x,t) = F(x,t) & (x \in \Omega,\ 0 < t \le T), \quad (5.1) \\ u(x,0) = a(x) & (x \in \Omega), \quad (5.2) \\ u(x,t) = 0 & (x \in \partial\Omega,\ 0 < t \le T), \quad (5.3) \end{cases}$$

where ∂_t^α denotes the Caputo derivative defined by

$$\partial_t^\alpha f(t) := \frac{1}{\Gamma(1-\alpha)} \int_0^t \frac{f'(s)}{(t-s)^\alpha}\, \mathrm{d}s,$$

and $\Gamma(\,\cdot\,)$ denotes the usual Gamma function. Here $\mathcal{A}$ is an elliptic operator defined for $f \in \mathcal{D}(\mathcal{A}) := H^2(\Omega) \cap H_0^1(\Omega)$ as

$$\mathcal{A}f(x) = -\sum_{i,j=1}^{d} \partial_j(a_{ij}(x)\partial_i f(x)) + c(x)f(x) \quad (x \in \Omega),$$

where $a_{ij} = a_{ji}$ $(1 \le i, j \le d)$ and $c \ge 0$ in $\overline{\Omega}$. Moreover, it is assumed that $a_{ij} \in C^1(\overline{\Omega})$, $c \in C(\overline{\Omega})$ and there exists a constant $\delta > 0$ such that

$$\delta \sum_{i=1}^{d} \xi_i^2 \le \sum_{i,j=1}^{d} a_{ij}(x)\xi_i\xi_j \quad (\forall\, x \in \overline{\Omega},\ \forall\, (\xi_1, \ldots, \xi_d) \in \mathbb{R}^d).$$

The assumptions on the initial value a and the source term F will be specified later. For various properties of the Caputo derivative, we refer to Diethelm [67], Kilbas, Srivastava and Trujillo [86], Podlubny [116] and Zhou [134]. See also [75,123] for further contents on fractional calculus.

The governing equation (5.1) is called a fractional diffusion equation and is a model equation for describing the anomalous diffusion phenomena in highly heterogeneous aquifer and complex viscoelastic material (see Metzler and Klafter [109] and the references therein). Indeed, although the single-term time-fractional diffusion equation inherits certain properties from the classical diffusion equation (i.e., $\alpha = 1$), it differs considerably from the traditional one especially in the senses of its limited smoothing effect in space and slow decay in time. In Luchko [101], a maximum principle for (5.1)–(5.3) was established, and the uniqueness of a classical solution was proved. Luchko [102] represented the generalized solution to (5.1)–(5.3) with $F = 0$ by means of the Mittag-Leffler function and gave the unique existence result. Sakamoto and Yamamoto [121] carried out a comprehensive investigation including the well-posedness of (5.1)–(5.3) as well as the long-time asymptotic behavior of the solution. It turns out that the spatial regularity of the solution is only moderately improved from that of the initial value, and the solution decays with order $t^{-\alpha}$ as $t \to \infty$. Recently, the Lipschitz stability of the solution to (5.1) with respect to α and the diffusion coefficient was proved as a byproduct of an inverse coefficient problem in Li et al. [96]. Very recently, Gorenflo et al. [73] redefined the Caputo derivative in the fractional Sobolev spaces and investigated (5.1) from the viewpoint of the operator theory. Regarding numerical treatments, we refer to [99,108] for the finite difference method and [79–81] for the finite element method. Meanwhile, equation (5.1) has also gained population among inverse problem researchers; recent literatures include [65, 83, 105, 111, 118, 122, 129, 132]. On the controllability theory, we refer to [70, 71]. For other discussions concerning equation (5.1), see, e.g., Gorenflo et al. [74], Luchko [100] and Prüss [117]. As a further generalized model for the anomalous diffusion, Li et al. [89] discussed the time-fractional diffusion equations with distributed orders and gave long time and short time asymptotic estimates.

In this chapter, we are interested in the strong maximum principle for fractional diffusion equations. As one of the remarkable characterizations of parabolic equations, the classical strong maximum principle asserts that the solution u to (5.1)–(5.3) with $\alpha = 1$ and $F = 0$ is strictly positive in $\Omega \times (0, \infty)$ if the initial value a satisfies $a \ge 0$ and $a \not\equiv 0$. Since (5.1) with $0 < \alpha < 1$ keeps some characters of diffusion, it is natural to expect the parallel generalization. Based on the weak maximum principle obtained in [101] (see Lemma 5.3), first we establish a strong maximum principle for the initial-boundary value problem (5.1)–(5.3) with $F = 0$, which is slightly weaker than that for the parabolic case.

Theorem 5.1 *Let $a \in L^2(\Omega)$ satisfy $a \ge 0$ and $a \not\equiv 0$, $F = 0$, and u be the solution to (5.1)–(5.3). Then for any $x \in \Omega$, the set $E_x := \{t > 0;\, u(x,t) \le 0\}$ is at most a countable set which admits only ∞ as its possible accumulation point.*

According to the weak maximum principle (see [101]), it reveals that actually $E_x = \{t > 0;\, u(x,t) = 0\}$, and the above theorem asserts the strict positivity of $u(x,t)$ for all $x \in \Omega$ and

almost all $t > 0$ except for the zero measure set E_x. So far, we do not know if $E_x = \emptyset$ although it can be conjectured.

Next, we consider an inverse source problem for (5.1)–(5.3) under the assumption that the inhomogeneous term F is in form of separation of variables.

Problem 5.1 *Let $x_0 \in \Omega$ and $T > 0$ be arbitrarily given, and u be the solution to (5.1)–(5.3) with $a = 0$ and $F(x,t) = \rho(t)\, g(x)$, where $\rho \in C^1[0,T]$ and $g \in C_0^\infty(\Omega)$. Provided that g is known, determine $\rho(t)$ $(0 \le t \le T)$ by the single point observation data $u(x_0,t)$ $(0 \le t \le T)$.*

The above problem is concerned with the determination of the temporal component ρ in the inhomogeneous term $F(x,t) = \rho(t)\, g(x)$ in (5.1). The spatial component g simulates e.g. a source of contaminants which may be dangerous. Although g is usually limited to a small region given by $\operatorname{supp} g (\subset\subset \Omega)$, its influence may expand wider because $\rho(t)$ is large. We are requested to determine the time-dependent magnitude by the pointwise data $u(x_0,t)$ $(0 \le t \le T)$, where x_0 is understood as a monitoring point.

For the case of $x_0 \in \operatorname{supp} g$, we know the both-sided stability estimate as well as the uniqueness for Problem 5.1 (see Sakamoto and Yamamoto [121]). For the case of $x_0 \notin \operatorname{supp} g$, there were no published results even on the uniqueness. From the practical viewpoints mentioned above, it is very desirable that x_0 should be spatially far from the location of the source, that is, the case $x_0 \notin \operatorname{supp} g$ should be discussed for the inverse problem.

As a direct application of Theorem 5.1, we can give an affirmative answer for the uniqueness regarding Problem 5.1.

Theorem 5.2 *Under the same settings in Problem 5.1, we further assume that $g \ge 0$ and $g \not\equiv 0$. Then $u(x_0,t) = 0$ $(0 \le t \le T)$ implies $\rho(t) = 0$ $(0 \le t \le T)$.*

For the same kind of inverse source problems for parabolic equations, we refer to Cannon and Esteva [63], Saitoh, Tuan and Yamamoto [119, 120].

The rest of this chapter is organized as follows. Section 5.2 introduces the notations and collects the existing results on problem (5.1)–(5.3), and Sections 5.3–5.4 are devoted to the proofs of Theorems 5.1–5.2, respectively.

5.2 Preliminaries

To start with, we fix some general settings and notations. Let $L^2(\Omega)$ be a usual L^2-space with the inner product $(\,\cdot\,,\,\cdot\,)$ and $H_0^1(\Omega)$, $H^2(\Omega)$ denote the Sobolev spaces (see, e.g., Adams [1]). Let $\{(\lambda_n, \varphi_n)\}_{n=1}^\infty$ be the eigensystem of the symmetric uniformly elliptic operator $\mathcal{A}$ in (5.1) such that $0 < \lambda_1 < \lambda_2 \le \cdots$, $\lambda_n \to \infty$ as $n \to \infty$ and $\{\varphi_n\} \subset H^2(\Omega) \cap H_0^1(\Omega)$ forms an orthonormal basis of $L^2(\Omega)$. Then the fractional power $\mathcal{A}^\gamma$ is well-defined for $\gamma \ge 0$ (see, e.g., Pazy [115]) with

$$\mathcal{D}(\mathcal{A}^\gamma) = \left\{ f \in L^2(\Omega);\ \sum_{n=1}^\infty |\lambda_n^\gamma (f, \varphi_n)|^2 < \infty \right\}, \quad \mathcal{A}^\gamma f := \sum_{n=1}^\infty \lambda_n^\gamma (f, \varphi_n)\varphi_n,$$

and $\mathcal{D}(\mathcal{A}^\gamma)$ is a Hilbert space with the norm

$$\|f\|_{\mathcal{D}(\mathcal{A}^\gamma)} = \left(\sum_{n=1}^\infty |\lambda_n^\gamma (f, \varphi_n)|^2 \right)^{1/2}.$$

Also we note that $\mathcal{D}(\mathcal{A}^\gamma) \subset H^{2\gamma}(\Omega)$ for $\gamma > 0$ and especially $\mathcal{D}(\mathcal{A}^{1/2}) = H_0^1(\Omega)$.

For $1 \le p \le \infty$, we say that $f \in L^p(0,T;\mathcal{D}(\mathcal{A}^\gamma))$ provided

$$\|f\|_{L^p(0,T;\mathcal{D}(\mathcal{A}^\gamma))} := \left\{ \begin{array}{ll} \displaystyle\left(\int_0^T \|f(\,\cdot\,,t)\|^p_{\mathcal{D}(\mathcal{A}^\gamma)}\,\mathrm{d}t \right)^{1/p} & \text{if } 1 \le p < \infty \\ \displaystyle\operatorname*{ess\,sup}_{0<t<T} \|f(\,\cdot\,,t)\|_{\mathcal{D}(\mathcal{A}^\gamma)} & \text{if } p = \infty \end{array} \right\} < \infty.$$

Similarly, for $0 \le t_0 < T$, we say that $f \in C([t_0,T];\mathcal{D}(\mathcal{A}^\gamma))$ provided

$$\|f\|_{C([t_0,T];\mathcal{D}(\mathcal{A}^\gamma))} := \max_{t_0 \le t \le T} \|f(\,\cdot\,,t)\|_{\mathcal{D}(\mathcal{A}^\gamma)} < \infty.$$

In addition, we define $C((0,T];\mathcal{D}(\mathcal{A}^\gamma)) := \bigcap_{0<t_0<T} C([t_0,T];\mathcal{D}(\mathcal{A}^\gamma))$.

To represent the explicit solution of (5.1)–(5.3), we first recall the Mittag-Leffler function (see, e.g., Podlubny [116])

$$E_{\alpha,\beta}(z) := \sum_{k=0}^{\infty} \frac{z^k}{\Gamma(\alpha k + \beta)} \quad (z \in \mathbb{C},\ \alpha > 0,\ \beta \in \mathbb{R}), \tag{5.4}$$

which possesses the following properties.

Lemma 5.1 (a) *Let $0 < \alpha < 2$ and $\beta \in \mathbb{R}$ be arbitrary. Then there exists a constant $C = C(\alpha,\beta) > 0$ such that*

$$|E_{\alpha,\beta}(-\eta)| \le \frac{C}{1+\eta} \quad (\eta \ge 0).$$

(b) *For $\lambda > 0$ and $\alpha > 0$, we have*

$$\frac{\mathrm{d}}{\mathrm{d}t} E_{\alpha,1}(-\lambda\, t^\alpha) = -\lambda\, t^{\alpha-1} E_{\alpha,\alpha}(-\lambda\, t^\alpha) \quad (t > 0).$$

Concerning some important existing results of the solution to (5.1)–(5.3) with $0 \le \alpha \le 1$, we state the following two lemmata for later use.

Lemma 5.2 (see [121]) *Fix $T > 0$ arbitrarily. Concerning the solution u to (5.1)–(5.3) with $0 \le t \le T$, the followings hold true.*

(a) *Let $a \in L^2(\Omega)$ and $F = 0$. Then there exists a unique weak solution $u \in C([0,T];L^2(\Omega)) \cap C((0,T];H^2(\Omega) \cap H_0^1(\Omega))$, which is explicitly written as*

$$u(\,\cdot\,,t) = \sum_{n=1}^{\infty} E_{\alpha,1}(-\lambda_n t^\alpha)\,(a,\varphi_n)\,\varphi_n \tag{5.5}$$

in $C([0,T];L^2(\Omega)) \cap C((0,T];H^2(\Omega) \cap H_0^1(\Omega))$. Moreover, $u : (0,T] \to L^2(\Omega)$ is analytically extended to a sector $\{z \in \mathbb{C};\ z \ne 0,\ |\arg z| < \pi/2\}$.

(b) *Let $a \in H^2(\Omega) \cap H_0^1(\Omega)$ and $F = 0$. Then there exists a unique weak solution $u \in C([0,T];H^2(\Omega) \cap H_0^1(\Omega))$, and the representation (5.5) holds in $C([0,T];H^2(\Omega) \cap H_0^1(\Omega))$.*

(c) *Let $a = 0$ and $F \in L^\infty(0,T;L^2(\Omega))$. Then there exists a unique weak solution $u \in L^2(0,T;H^2(\Omega) \cap H_0^1(\Omega))$ such that $\lim_{t\to 0} \|u(\,\cdot\,,t)\|_{L^2(\Omega)} = 0$.*

Lemma 5.3 (Weak maximum principle) *Let $a \in L^2(\Omega)$ be nonnegative, $F = 0$, and u be the solution to (5.1)–(5.3). Then there holds $u \ge 0$ a.e. in $\Omega \times (0,\infty)$.*

We note that the above lemma is a special case of [101, Theorem 2], but the settings on the initial value and the elliptic operator are more general. In fact, the same argument as that in [101] also works in our settings, which indicates Lemma 5.3 immediately. Here we omit the details.

5.3 Proof of Theorem 5.1

Throughout this section, we take $F = 0$ in (5.1). We divide the proof of Theorem 5.1 into three steps.

Step 1. Using the Mittag-Leffler functions and the eigensystem $\{(\lambda_n, \varphi_n)\}_{n=1}^{\infty}$, for $N \in \mathbb{N}$ we set

$$G_N(x, y, t) := \sum_{n=1}^{N} E_{\alpha,1}(-\lambda_n t^\alpha)\, \varphi_n(x)\, \varphi_n(y) \quad (x, y \in \Omega,\ t > 0).$$

According to Lemma 5.2(a), there holds

$$u(x, t) = \lim_{N\to\infty} \int_\Omega G_N(x, y, t)\, a(y)\, \mathrm{d}y$$

in $C([0, \infty); L^2(\Omega)) \cap C([t_0, \infty); H^2(\Omega) \cap H_0^1(\Omega))$ for any $a \in L^2(\Omega)$ and any $t_0 > 0$. Since the spatial dimensions $d \le 3$, the Sobolev embedding implies $H^2(\Omega) \subset C(\overline{\Omega})$. Therefore, for any fixed $x \in \Omega$ and $t > 0$, we see that $G_N(x, \cdot, t)$ is weakly convergent to

$$G(x, y, t) := \sum_{n=1}^{\infty} E_{\alpha,1}(-\lambda_n t^\alpha)\, \varphi_n(x)\, \varphi_n(y) \tag{5.6}$$

as a series with respect to y. In particular, we obtain $G(x, \cdot, t) \in L^2(\Omega)$ for all $x \in \Omega$ and all $t > 0$. Moreover, the solution to (5.1)–(5.3) can be represented as

$$u(x, t) = \int_\Omega G(x, y, t)\, a(y)\, \mathrm{d}y \quad (x \in \Omega,\ t > 0). \tag{5.7}$$

Next we show that for arbitrarily fixed $x \in \Omega$ and $t > 0$, $G(x, y, t) \ge 0$ for almost all $y \in \Omega$. Actually, assume that on the contrary there exist $x_1 \in \Omega$ and $t_1 > 0$ such that

$$|\omega_1| > 0, \quad \omega_1 := \{y \in \Omega;\, G(x_1, y, t_1) < 0\},$$

where $|\cdot|$ denotes the Lebesgue measure. Then it is readily seen that

$$\int_\Omega G(x_1, y, t_1)\, \chi_{\omega_1}(y)\, \mathrm{d}y < 0, \tag{5.8}$$

where χ_{ω_1} is the characteristic function of ω_1 satisfying $\chi_{\omega_1} \in L^2(\Omega)$ and $\chi_{\omega_1} \ge 0$. On the other hand, Lemma 5.3 and (5.7) imply that for all $x \in \Omega$ and $t > 0$, there holds

$$\int_\Omega G(x, y, t)\, a(y)\, \mathrm{d}y \ge 0 \quad (\forall\, a \in L^2(\Omega),\ a \ge 0),$$

which contradicts with (5.8) by taking $a = \chi_{\omega_1}$.

Step 2. Now we fix an initial value $a \in L^2(\Omega)$ such that $a \ge 0$ and $a \not\equiv 0$. Again by Lemma 5.3, we have $u \ge 0$ in $\Omega \times (0, \infty)$. Meanwhile, by Lemma 5.2(a) and the Sobolev embedding, we see $u \in C(\overline{\Omega} \times [0, \infty))$.

Assume contrarily that there exists $x_0 \in \Omega$ such that the set $E_{x_0} = \{t > 0;\, u(x_0, t) \le 0\} = \{t > 0;\, u(x_0, t) = 0\}$ contains an accumulation point which is not ∞. Since $u(x_0, t)$ is analytic with respect to $t > 0$ (see Lemma 5.2(a)), we conclude $u(x_0, t) = 0$ for $t > 0$, that is,

$$u(x_0, t) = \int_\Omega G(x_0, y, t)\, a(y)\, \mathrm{d}y = 0 \quad (t > 0).$$

Since both $G(x_0,\,\cdot\,,t)$ and a are nonnegative in Ω, we deduce $G(x_0,y,t)\,a(y)=0$ for almost all $y\in\Omega$ and $t>0$. Since $a\not\equiv 0$, $G(x_0,\,\cdot\,,\,\cdot\,)$ should vanish in the cylinder $\omega\times(0,\infty)$, where $\omega:=\{x\in\Omega;\,a(x)>0\}$ and $|\omega|>0$. By the representation (5.6), this indicates

$$\sum_{n=1}^{\infty} E_{\alpha,1}(-\lambda_n t^\alpha)\,\varphi_n(x_0)\,\varphi_n(x)=0\quad(t>0,\ x\in\omega). \tag{5.9}$$

Henceforth $C>0$ denotes generic constants independent of n and $t\ge 0$, which may change line by line. Let $\psi\in C_0^\infty(\omega)$ be arbitrarily chosen. Then it follows from (5.9) that

$$\sum_{n=1}^{\infty} E_{\alpha,1}(-\lambda_n t^\alpha)\,\varphi_n(x_0)(\varphi_n,\psi)=0\quad(t>0). \tag{5.10}$$

We shall show that the series is convergent in $C[0,\infty)$. In fact, by the Sobolev embedding $H^2(\Omega)\subset C(\overline{\Omega})$ for $d\le 3$, first we estimate

$$|\varphi_n(x_0)|\le\|\varphi_n\|_{C(\overline{\Omega})}\le C\|\varphi_n\|_{H^2(\Omega)}\le C\|\mathcal{A}\varphi_n\|_{L^2(\Omega)}\le C\lambda_n.$$

Next, since $\psi\in C_0^\infty(\omega)\subset\mathcal{D}(\mathcal{A}^\ell)$ for any $\ell\in\mathbb{N}$, we have

$$|(\varphi_n,\psi)|=\frac{|(\varphi_n,\mathcal{A}^\ell\psi)|}{\lambda_n^\ell}\le\frac{C\|\varphi_n\|_{L^2(\Omega)}\|\psi\|_{C^{2\ell}(\overline{\Omega})}}{\lambda_n^\ell}\le C\lambda_n^{-\ell}.$$

On the other hand, we know $\lambda_n\sim n^{2/d}$ as $n\to\infty$ (see, e.g., Courant and Hilbert [66]). Therefore, the combination of the above estimates yields

$$|E_{\alpha,1}(-\lambda_n t^\alpha)\,\varphi_n(x_0)(\varphi_n,\psi)|\le C\lambda_n^{-(\ell-1)}\le C\,n^{-2(\ell-1)/d}\quad\text{as } n\to\infty,$$

where $E_{\alpha,1}(-\lambda_n t^\alpha)$ is bounded by applying Lemma 5.1(a). Since we restrict $d\le 3$, it suffices to choose $\ell=3$ so that the order $2(\ell-1)/d>1$, which guarantees

$$\sum_{n=1}^{\infty}|E_{\alpha,1}(-\lambda_n t^\alpha)\,\varphi_n(x_0)(\varphi_n,\psi)|<\infty\quad(\forall\,t\ge 0,\ \forall\,\psi\in C_0^\infty(\omega)).$$

Step 3. Recall that the Laplace transform of $E_{\alpha,1}(-\lambda_n t^\alpha)$ reads (see, e.g., Podlubny [116, p.21])

$$\int_0^\infty \mathrm{e}^{-zt}E_{\alpha,1}(-\lambda_n t^\alpha)\,\mathrm{d}t=\frac{z^{\alpha-1}}{z^\alpha+\lambda_n}\quad(\mathrm{Re}\,z>\lambda_n^{1/\alpha}),$$

which is analytically extended to $\mathrm{Re}\,z>0$. Since the series in (5.10) is convergent in $C[0,\infty)$, we can take the Laplace transform with respect to t in (5.10) to derive

$$\sum_{n=1}^{\infty}\frac{z^{\alpha-1}}{z^\alpha+\lambda_n}\,\varphi_n(x_0)(\varphi_n,\psi)=0\quad(\mathrm{Re}\,z>0,\ \forall\,\psi\in C_0^\infty(\Omega)),$$

that is,

$$\sum_{n=1}^{\infty}\frac{1}{\zeta+\lambda_n}\,\varphi_n(x_0)(\varphi_n,\psi)=0\quad(\mathrm{Re}\,\zeta>0,\ \forall\,\psi\in C_0^\infty(\Omega)). \tag{5.11}$$

By a similar argument for the convergence of (5.10), we see that the above series is convergent in any compact set in $\mathbb{C}\setminus\{-\lambda_n\}_{n=1}^\infty$, and the analytic continuation in ζ yields that (5.11) holds for $\zeta\in\mathbb{C}\setminus\{-\lambda_n\}_{n=1}^\infty$. Especially, since the first eigenvalue λ_1 is single, we can choose a small circle around $-\lambda_1$ which does not contain $-\lambda_n$ $(n\ge 2)$. Integrating (5.11) on this circle, we have

$$\varphi_1(x_0)(\varphi_1,\psi)=0\quad(\forall\,\psi\in C_0^\infty(\omega)).$$

Since $\psi \in C_0^\infty(\omega)$ is arbitrarily chosen, there holds $\varphi_1(x_0)\,\varphi_1(x) = 0$ for almost all $x \in \omega$. This contradicts with the strict positivity of the first eigenfunction φ_1 (see, e.g., Evans [27]).

Consequently, for any $x \in \Omega$, the set $E_x = \{t > 0;\, u(x,t) \le 0\}$ contains at most ∞ as an accumulation point. The proof of Theorem 5.1 is completed.

5.4 Proof of Theorem 5.2

Now we turn to the proof of the uniqueness for Problem 5.1. Recall that the governing equation reads

$$\begin{cases} \partial_t^\alpha u(x,t) + \mathcal{A}u(x,t) = \rho(t)\, g(x) & (x \in \Omega,\ 0 < t \le T), \\ u(x,0) = 0 & (x \in \Omega), \\ u(x,t) = 0 & (x \in \partial\Omega,\ 0 < t \le T), \end{cases} \tag{5.12}$$

where $\rho \in C^1[0,T]$ and $g \in C_0^\infty(\Omega)$. First we verify the following Duhamel's principle for the fractional diffusion equation.

Lemma 5.4 *Let u be the solution to (5.12) with $\rho \in C^1[0,T]$ and $g \in C_0^\infty(\Omega)$. Then u allows the representation*

$$u(\,\cdot\,,t) = \int_0^t \mu(t-s)\, v(\,\cdot\,,s)\,\mathrm{d}s \quad (0 < t < T),$$

where

$$\mu(t) := \frac{1}{\Gamma(\alpha)} \frac{\mathrm{d}}{\mathrm{d}t} \int_0^t \frac{\rho(s)}{(t-s)^{1-\alpha}}\,\mathrm{d}s \quad (0 < t < T) \tag{5.13}$$

and v satisfies

$$\begin{cases} \partial_t^\alpha v + \mathcal{A}v = 0 & \text{in } \Omega \times (0,T], \\ v = g & \text{in } \Omega \times \{0\}, \\ v = 0 & \text{on } \partial\Omega \times (0,T]. \end{cases} \tag{5.14}$$

We note that a similar Duhamel's principle was provided in [93, Lemma 3.3], which considers the case of multi-term time-fractional derivatives. Nevertheless, we give an independent proof for the sake of self-containedness.

Proof. First, since $\rho\, g \in L^\infty(0,T;L^2(\Omega))$, Lemma 5.2(c) indicates that $u \in L^2(0,T;H^2(\Omega) \cap H_0^1(\Omega))$ and $\lim_{t\to 0} \|u(\,\cdot\,,t)\|_{L^2(\Omega)} = 0$. By setting

$$\widetilde{u}(\,\cdot\,,t) := \int_0^t \mu(t-s)\, v(\,\cdot\,,s)\,\mathrm{d}s, \tag{5.15}$$

we shall demonstrate

$$u = \widetilde{u} \text{ in } L^2(0,T;H^2(\Omega) \cap H_0^1(\Omega)), \quad \widetilde{u} = 0 \text{ on } \partial\Omega \times (0,T], \quad \lim_{t\to 0} \|\widetilde{u}(\,\cdot\,,t)\|_{L^2(\Omega)} = 0.$$

Since $\rho \in C^1[0,T]$, simple calculations for (5.13) yield

$$\begin{aligned} \mu(t) &= \frac{1}{\Gamma(\alpha)} \frac{\mathrm{d}}{\mathrm{d}t} \left(- \frac{\rho(s)\,(t-s)^\alpha}{\alpha} \bigg|_{s=0}^{s=t} + \frac{1}{\alpha} \int_0^t (t-s)^\alpha \rho'(s)\,\mathrm{d}s \right) \\ &= \frac{1}{\Gamma(\alpha)} \frac{\mathrm{d}}{\mathrm{d}t} \left(\frac{\rho(t)}{\alpha}\, t^\alpha + \frac{1}{\alpha} \int_0^t (t-s)^\alpha \rho'(s)\,\mathrm{d}s \right) \end{aligned}$$

$$= \frac{1}{\Gamma(\alpha)} \left(\frac{\rho(0)}{t^{1-\alpha}} + \int_0^t \frac{\rho'(s)}{(t-s)^{1-\alpha}} \, \mathrm{d}s \right) \tag{5.16}$$

and hence $\mu \in C(0,T]$. Concerning the solution v to (5.14), since $g \in C_0^\infty(\Omega) \subset H^2(\Omega) \cap H_0^1(\Omega)$, it follows from Lemma 5.2(b) that $v \in C([0,T]; H^2(\Omega) \cap H_0^1(\Omega))$. Together with the fact that $\mu \in L^1(0,T)$ by applying Young's inequality to (5.16), we deduce $\widetilde{u} \in C([0,T]; H^2(\Omega) \cap H_0^1(\Omega))$, $\widetilde{u} = 0$ on $\partial\Omega \times (0,T]$ and $\widetilde{u}(\cdot\,,0) = 0$ by definition (5.15). On the other hand, according to the explicit representation (5.5) and Lemma 5.1(b), we see

$$\begin{aligned}
&\partial_t v(\cdot\,,t) = -t^{\alpha-1} w(\cdot\,,t), \quad \text{where} \\
&w(\cdot\,,t) := \sum_{n=1}^\infty \lambda_n \, E_{\alpha,\alpha}(-\lambda_n t^\alpha) \, (g, \varphi_n) \, \varphi_n = \sum_{n=1}^\infty E_{\alpha,\alpha}(-\lambda_n t^\alpha) \, (\mathcal{A} g, \varphi_n) \, \varphi_n.
\end{aligned}$$

A similar argument as that in [121] and Lemma 5.2(a) immediately yield $w \in C([0,T]; L^2(\Omega))$.

In order to show $u = \widetilde{u}$, it suffices to verify that $\widetilde{u}$ also satisfies the governing equation (5.12), which possesses a unique solution (see Lemma 5.2(c)). To calculate $\partial_t^\alpha \widetilde{u}$, first we formally calculate

$$\begin{aligned}
\partial_t \widetilde{u}(\cdot\,,t) &= \partial_t \int_0^t \mu(s) \, v(\cdot\,,t-s) \, \mathrm{d}s = \int_0^t \mu(s) \, \partial_t v(\cdot\,,t-s) \, \mathrm{d}s + \mu(t) \, v(\cdot\,,0) \\
&= - \int_0^t \mu(s) \, (t-s)^{\alpha-1} w(\cdot\,,t-s) \, \mathrm{d}s + \mu(t) \, g.
\end{aligned}$$

Since $\int_0^t |\mu(s) \, (t-s)^{\alpha-1}| \, \mathrm{d}s < \infty$ for $0 < t \le T$ and $w \in C([0,T]; L^2(\Omega))$, we can easily justify that the above differentiation makes sense in $L^2(\Omega)$ for $0 < t \le T$. By definition, we have

$$\begin{aligned}
&\partial_t^\alpha \widetilde{u}(\cdot\,,t) = \frac{1}{\Gamma(1-\alpha)} \int_0^t \frac{\partial_s \widetilde{u}(\cdot\,,s)}{(t-s)^\alpha} \, \mathrm{d}s = I_1 + I_2 \, g, \quad \text{where} \\
&I_1 := \frac{1}{\Gamma(1-\alpha)} \int_0^t \frac{1}{(t-s)^\alpha} \int_0^s \mu(\tau) \, \partial_s v(\cdot\,,s-\tau) \, \mathrm{d}\tau \mathrm{d}s, \\
&I_2 := \frac{1}{\Gamma(1-\alpha)} \int_0^t \frac{\mu(s)}{(t-s)^\alpha} \, \mathrm{d}s.
\end{aligned}$$

The governing equation (5.14) for v and formula (5.16) for μ imply respectively

$$\begin{aligned}
I_1 &= \frac{1}{\Gamma(1-\alpha)} \int_0^t \mu(\tau) \int_\tau^t \frac{\partial_s v(\cdot\,,s-\tau)}{(t-s)^\alpha} \, \mathrm{d}s \mathrm{d}\tau \\
&= \int_0^t \mu(\tau) \left(\frac{1}{\Gamma(-\alpha)} \int_0^{t-\tau} \frac{\partial_s v(\cdot\,,,s)}{(t-\tau-s)^\alpha} \, \mathrm{d}s \right) \mathrm{d}\tau = \int_0^t \mu(\tau) \, \partial_\tau^\alpha v(\cdot\,,t-\tau) \, \mathrm{d}\tau \\
&= - \int_0^t \mu(\tau) \, \mathcal{A} v(\cdot\,,t-\tau) \, \mathrm{d}\tau = -\mathcal{A} \int_0^t \mu(\tau) \, v(\cdot\,,t-\tau) \, \mathrm{d}\tau = -\mathcal{A} \widetilde{u}(\cdot\,,t), \\
I_2 &= \frac{1}{\Gamma(1-\alpha)\,\Gamma(\alpha)} \int_0^t \frac{1}{(t-s)^\alpha} \left(\frac{\rho(0)}{s^{1-\alpha}} + \int_0^s \frac{\rho'(\tau)}{(s-\tau)^{1-\alpha}} \, \mathrm{d}\tau \right) \mathrm{d}s \\
&= \frac{1}{\Gamma(1-\alpha)\,\Gamma(\alpha)} \left(\rho(0) \int_0^t \frac{\mathrm{d}s}{(t-s)^\alpha \, s^{1-\alpha}} + \int_0^t \rho'(\tau) \int_\tau^t \frac{\mathrm{d}s}{(t-s)^\alpha (s-\tau)^{1-\alpha}} \, \mathrm{d}\tau \right) \\
&= \rho(0) + \int_0^t \rho'(\tau) \, \mathrm{d}\tau = \rho(t).
\end{aligned} \tag{5.17}$$

Therefore, we conclude $\partial_t^\alpha \widetilde{u} + \mathcal{A} \widetilde{u} = \rho \, g$ and the proof is completed. □

At this stage, we can proceed to show Theorem 5.2 by applying the established strong maximum principle.

Completion of Proof of Theorem 5.2. Let the conditions in the statement of Theorem 5.2 be valid, namely, it is assumed that $\rho \in C^1[0,T]$, $g \in C_0^\infty(\Omega)$, $g \geq 0$, $g \not\equiv 0$, and the solution u to (5.12) vanishes in $\{x_0\} \times [0,T]$ for some $x_0 \in \Omega$. According to Duhamel's principle proved above, we have

$$u(x_0,t) = \int_0^t \mu(t-s)\, v(x_0,s)\, \mathrm{d}s = 0 \quad (0 \leq t \leq T),$$

where μ was defined in (5.13) and v solves (5.14). It reveals in the proof of Lemma 5.4 that $\mu \in L^1(0,T)$. Meanwhile, Lemma 5.2(b) and the Sobolev embedding indicate $v \in C([0,T]; H^2(\Omega) \cap H_0^1(\Omega)) \subset C(\overline{\Omega} \times [0,T])$, yielding $v(x_0, \cdot\,) \in C[0,T] \subset L^1(0,T)$. Therefore, the Titchmarsh convolution theorem (see [128]) implies the existence of $T_1, T_2 \geq 0$ satisfying $T_1 + T_2 \geq T$ such that $\mu(t) = 0$ for almost all $t \in (0, T_1)$ and $v(x_0,t) = 0$ for all $t \in [0, T_2]$. However, since the initial value g of (5.14) satisfies $g \geq 0$ and $g \not\equiv 0$, Theorem 5.1 asserts that $v(x_0, \cdot\,,)$ only admits at most a finite number of zero points. As a result, the only possibility is $T_2 = 0$ and thus $T_1 = T$. Together with the fact that $\mu \in C(0,T]$, we have proved

$$\mu(t) = 0 \quad (t \in (0,T]). \tag{5.18}$$

Next, we claim that $\rho(0) = 0$. In fact, if we assume contrarily that $\rho(0) \neq 0$, then by $\rho \in C^1[0,T]$ and the representation (5.16) for μ, we estimate

$$|\mu(t)| \geq \frac{1}{\Gamma(\alpha)} \left(\frac{|\rho(0)|}{t^{1-\alpha}} - \int_0^t \frac{|\rho'(s)|}{(t-s)^{1-\alpha}}\, \mathrm{d}s \right) \geq \frac{1}{\Gamma(\alpha)} \left(\frac{|\rho(0)|}{t^{1-\alpha}} - \frac{\|\rho'\|_{C[0,T]}}{\alpha}\, t^\alpha \right) \quad (0 < t \leq T).$$

Therefore, for sufficiently small $t > 0$ such that $t < \alpha\, |\rho(0)| / \|\rho'\|_{C[0,T]}$, the above inequality indicates $\mu(t) \neq 0$, which contradicts with (5.18). Moreover, there holds $\lim_{t \to 0} \mu(t) = 0$.

Finally, it suffices to utilize the following reverse formula

$$\rho(t) = \frac{1}{\Gamma(1-\alpha)} \int_0^t \frac{\mu(s)}{(t-s)^\alpha}\, \mathrm{d}s,$$

which was already obtained as a byproduct in (5.17). The above formula, together with (5.18) and $\lim_{t \to 0} \mu(t) = 0$, imply $\rho \equiv 0$ in $[0,T]$ immediately, which completes the proof. □

Chapter 6

Initial-Boundary Value Problems for Multi-Term Time-Fractional Diffusion Equations with Positive Constant Coefficients

In this chapter, we investigate the well-posedness and the long-time asymptotic behavior for initial-boundary value problems for multi-term time-fractional diffusion equations. The governing equation under consideration includes a linear combination of Caputo derivatives in time with decreasing orders in $(0, 1)$ and positive constant coefficients. By exploiting several important properties of multinomial Mittag-Leffler functions, various estimates follow from the explicit solutions in form of these special functions. Then we prove the uniqueness and continuous dependency of the solutions on initial values and source terms. As a direct application, we further verify the Lipschitz continuous dependency of solutions with respect to coefficients and orders of fractional orders, which is fundamental for the optimization approach to the related coefficient inverse problem. Finally, by a Laplace transform argument, it turns out that the decay rate of the solution as $t \to \infty$ is given by the minimum order of the time-fractional derivatives.

6.1 Introduction

Let Ω be an open bounded domain in $\mathbb{R}^d$ with a smooth boundary (for example, of C^∞ class) and $T > 0$ be fixed arbitrarily. For a fixed positive integer m, let α_j and q_j $(j = 1, \dots, m)$ be positive constants such that $1 > \alpha_1 > \cdots > \alpha_m > 0$. Consider the following initial-boundary value problem for the multi-term time-fractional diffusion equation

$$\begin{cases} \displaystyle\sum_{j=1}^{m} q_j \partial_t^{\alpha_j} u(x,t) + \mathcal{A}u(x,t) = F(x,t) & (x \in \Omega,\ 0 < t \le T), \quad (6.1) \\ u(x,0) = a(x) & (x \in \Omega), \quad (6.2) \\ u(x,t) = 0 & (x \in \partial\Omega,\ 0 < t \le T), \quad (6.3) \end{cases}$$

where the elliptic operator $\mathcal{A}$ and the Caputo derivative $\partial_t^{\alpha_j}$ are defined as that in Chapter 5, and we can assume $q_1 = 1$ without lose of generality. The regularities of the initial value

a and the source term F will be specified later, and we abbreviate $\boldsymbol{\alpha} := (\alpha_1, \dots, \alpha_m)$ and $\boldsymbol{q} := (q_1, \dots, q_m)$ for later convenience.

In the case of $m = 1$, equation (6.1) is reduced to its single-term counterpart (5.1). As was mentioned in the previous chapter, the above formulation has been studied extensively from different aspects due to its vast capability of modeling the diffusion in heterogeneous media (see Adams and Gelhar [58], Ginoa et al. [72], Hatano and Hatano [76], Nigmatullin [114] and the references therein). As a natural extension, equation (6.1) is expected to improve the modeling accuracy in depicting the anomalous diffusion due to its potential feasibility. However, to the authors' best knowledge, published works on this extension are quite limited in spite of rich literatures on its single-term version. Luchko [103] developed the maximum principle for problem (6.1)–(6.3) and constructed a generalized solution when $F = 0$ by means of the multinomial Mittag-Leffler functions. Jiang et al. [77] considered fractional derivatives in both time and space and derived analytical solutions. As for the asymptotic behavior, for $m = 2$ it reveals in Mainardi et al. [106] that the dominated decay rate of the solution is related to the minimum order of time fractional derivative. On the other hand, Beckers and Yamamoto [60] investigated (6.1)–(6.3) with $m = 2$ and $q_2 = q_2(x)$ and obtained a weaker regularity result than that in [121]. Following the same line, Li and Yamamoto [94] further generalized the formulation to $m \geq 2$ and $q_j = q_j(x)$ $(j = 2, \dots, m)$ and obtained the analyticity and the weak unique continuation. On the inverse problems, we refer to [95] for the determination of m, $\boldsymbol{\alpha}$ and constant $\boldsymbol{q}$, and [87] for that of m, $\boldsymbol{\alpha}$, x-dependent $\boldsymbol{q}$ and a zeroth order coefficient in $\mathcal{A}$. Very recently, Jin et al. [78] developed semidiscrete and fully discrete Galerkin finite element methods for (6.1)–(6.3).

In this chapter, we are concerned with the well-posedness and the long-time asymptotic behavior of the solution to the initial-boundary value problem (6.1)–(6.3), and we attempt to establish results parallel to that for the single-term case. On the basis of the explicit representation of the solution, by exploiting several properties of the multinomial Mittag-Leffler function, we give estimates for the solution, which imply the continuous dependency of solutions on initial values and source terms. Next we will deduce the Lipschitz stability of the solution to (6.1)–(6.3) with respect to α_j, q_j $(j = 1, \dots, m)$ and diffusion coefficients. As a direct corollary, we can establish an existence result for the optimization approach to the simultaneous reconstruction of various coefficients. Finally, for the long-time asymptotic behavior, we employ the Laplace transform in time to show that the decay rate as $t \to \infty$ is exactly $t^{-\alpha_m}$, where α_m is the minimum order of Caputo derivatives in time.

The rest of this chapter is organized as follows. The main results concerning problem (6.1)–(6.3) are collected in Section 6.2: Theorems 6.1–6.3 and Corollary 6.1 are concerned with the well-posedness, and Theorem 6.4 gives the long-time asymptotic estimate of the solution. The proofs of the well-posedness results are given in Section 6.3 on the basis of several properties of the multinomial Mittag-Leffler functions. Due to the difference of techniques, the asymptotic behavior is proved in Section 6.4. Next, the proofs of technical lemmata on the multinomial Mittag-Leffler functions are postponed to Section 6.5. Finally, concluding remarks are given in Section 6.6.

6.2 Main results

In this section, we state the main results obtained in this chapter. More precisely, we give a priori estimates for the solution u to (6.1)–(6.3) with respect to the initial value (Theorem 6.1), the source term (Theorem 6.2), and Lipschitz continuous dependency of the solutions on

coefficients and orders (Theorem 6.3) so that stability and uniqueness follow, and we describe the asymptotic behavior of the solution in Theorem 6.4.

To this end, first we recall the settings and notations introduced in Section 5.2, especially the eigensystem $\{(\lambda_n, \varphi_n)\}_{n=1}^{\infty}$ of the operator $\mathcal{A}$ as well as the fractional power $\mathcal{A}^\gamma$ and the induced function spaces $\mathcal{D}(\mathcal{A}^\gamma)$ with $\gamma \geq 0$. On the other hand, the orders $\boldsymbol{\alpha} = (\alpha_1, \ldots, \alpha_m)$ and the coefficients $\boldsymbol{q} = (q_1, \ldots, q_m)$ are restricted in the admissible sets

$$\begin{aligned} \mathcal{U} &:= \{(\alpha_1, \ldots, \alpha_m) \in \mathbb{R}^m;\, \overline{\alpha} \geq \alpha_1 \geq \alpha_2 \geq \cdots \geq \alpha_m \geq \underline{\alpha}\}, \\ \mathcal{V} &:= \{(q_1, \ldots, q_m) \in \mathbb{R}^m;\, q_1 = 1,\ q_j \in [\underline{q}, \overline{q}]\ (j = 2, \ldots, m)\}, \end{aligned} \tag{6.4}$$

where we fix $1 > \overline{\alpha} > \underline{\alpha} > 0$ and $\overline{q} > \underline{q} > 0$. Without lose of generality, here we allow the coincidence of some adjacent orders in $\boldsymbol{\alpha}$. Actually, if it happens that $\alpha_j = \alpha_{j+1}$, then the governing equation (6.1) just degenerates to its lower order version.

Now we are well-prepared to consider the dependency of the solution u to the initial-boundary value problem (6.1)–(6.3) upon the initial value a and the source term F. In view of the superposition principle, it suffices to deal with the cases $F = 0$, $a \neq 0$ and $a = 0$, $F \neq 0$ separately.

Theorem 6.1 *Let $F = 0$. Fix $\boldsymbol{\alpha} \in \mathcal{U}$, $\boldsymbol{q} \in \mathcal{V}$ and $a \in \mathcal{D}(\mathcal{A}^\gamma)$ with some $\gamma \in [0, 1]$, where we interpret $\frac{1}{1-\gamma} = \infty$ if $\gamma = 1$. Concerning the solution u to the initial-boundary value problem (6.1)–(6.3), the followings hold true.*

(a) *There is a unique solution $u \in C([0, T]; L^2(\Omega)) \cap C((0, T]; H^2(\Omega) \cap H_0^1(\Omega))$ to (6.1)–(6.3). Actually, $u \in L^{\frac{1}{1-\gamma}}(0, T; H^2(\Omega) \cap H_0^1(\Omega))$ and there exists a constant $C = C(\Omega, T, \boldsymbol{\alpha}, \boldsymbol{q}, \mathcal{A}) > 0$ such that*

$$\|u\|_{C([0,T];L^2(\Omega))} \leq C\|a\|_{L^2(\Omega)}, \tag{6.5}$$

$$\|u(\cdot, t)\|_{H^2(\Omega)} \leq C\|a\|_{\mathcal{D}(\mathcal{A}^\gamma)} t^{\alpha_1(\gamma-1)} \quad (0 < t \leq T). \tag{6.6}$$

(b) *We have*

$$\lim_{t \to 0} \|u(\cdot, t) - a\|_{\mathcal{D}(\mathcal{A}^\gamma)} = 0. \tag{6.7}$$

(c) *There holds $\partial_t u \in C((0, T]; L^2(\Omega))$. Moreover, there is a constant $C = C(\Omega, T, \boldsymbol{\alpha}, \boldsymbol{q}, \mathcal{A}) > 0$ such that*

$$\|\partial_t u(\cdot, t)\|_{L^2(\Omega)} \leq C\|a\|_{\mathcal{D}(\mathcal{A}^\gamma)} t^{\alpha_1\gamma - 1} \quad (0 < t \leq T). \tag{6.8}$$

(d) *If $\gamma > 0$, then $\partial_t^\beta u \in L^{\frac{1}{1-\gamma}}(0, T; L^2(\Omega))$ for $0 < \beta \leq \alpha_1$. Moreover, for $0 < \beta < 1$, there exists a constant $C = C(\Omega, T, \boldsymbol{\alpha}, \boldsymbol{q}, \mathcal{A}) > 0$ such that*

$$\|\partial_t^\beta u(\cdot, t)\|_{L^2(\Omega)} \leq C\|a\|_{\mathcal{D}(\mathcal{A}^\gamma)} t^{\alpha_1\gamma - \beta} \quad (0 < t \leq T). \tag{6.9}$$

We note that for larger $\gamma \in (0, 1]$, the assumption $a \in \mathcal{D}(\mathcal{A}^\gamma)$ on an initial value is stronger, and estimates (6.6)–(6.9) are improved, that is, the singularities of the right-hand side at $t = 0$ in (6.6), (6.8) and (6.9) are weaker and the norm on the left-hand side of (6.7) is stronger.

Theorem 6.2 *Let $a = 0$. Fix $\boldsymbol{\alpha} \in \mathcal{U}$, $\boldsymbol{q} \in \mathcal{V}$ and $F \in L^p(0, T; \mathcal{D}(\mathcal{A}^\gamma))$ with some $p \in [1, \infty]$ and $\gamma \in [0, 1]$, where we interpret $1/p = 0$ if $p = \infty$. Concerning the solution u to the initial-boundary value problem (6.1)–(6.3), the followings hold true.*

(a) *If $p = 2$, then there is a unique solution $u \in L^2(0, T; \mathcal{D}(\mathcal{A}^{\gamma+1}))$ to (6.1)–(6.3). Moreover, there exists a constant $C = C(\Omega, T, \boldsymbol{\alpha}, \boldsymbol{q}, \mathcal{A}) > 0$ such that*

$$\|u\|_{L^2(0,T;\mathcal{D}(\mathcal{A}^{\gamma+1}))} \leq C\|F\|_{L^2(0,T;\mathcal{D}(\mathcal{A}^\gamma))}.$$

(b) *If $p \neq 2$, then there is a unique solution $u \in \bigcap_{0<\epsilon\leq 1} L^p(0,T;\mathcal{D}(\mathcal{A}^{\gamma+1-\epsilon}))$ to* (6.1)–(6.3). *Moreover, there exists a constant $C = C(\Omega, T, \boldsymbol{\alpha}, \boldsymbol{q}, \mathcal{A}) > 0$ such that*

$$\|u\|_{L^p(0,T;\mathcal{D}(\mathcal{A}^{\gamma+1-\epsilon}))} \leq \frac{C}{\epsilon}\|F\|_{L^p(0,T;\mathcal{D}(\mathcal{A}^{\gamma}))} \quad \text{for each } \epsilon \in (0,1]. \tag{6.10}$$

(c) *If $\alpha_1 p > 1$, then*

$$\lim_{t\to 0}\|u(\,\cdot\,,t)\|_{\mathcal{D}(\mathcal{A}^{\kappa})} = 0 \tag{6.11}$$

for $0 < \kappa < \gamma + 1 - \frac{1}{\alpha_1 p}$.

For larger γ, the conclusions of Theorem 6.2(a) is improved, and in (6.10) if we would like to estimate the left-hand side by a stronger norm in $\mathcal{D}(\mathcal{A}^{\gamma+1-\epsilon})$, then $\epsilon > 0$ should be smaller at the expense that the factor $\frac{C}{\epsilon}$ of the right-hand side should be larger. The role of ϵ is the same for estimate (6.15) later.

Remark 6.1 We compare the conclusions in Theorems 6.1–6.2 with those of single-term cases obtained in [121]. In case of the homogeneous source term, i.e. $F = 0$ in (6.1), it turns out that Theorem 6.1 is a parallel extension of its single-term counterpart. For instance, in Theorem 6.1 the regularity results for initial values $a \in L^2(\Omega)$, $a \in H_0^1(\Omega)$ and $a \in H^2(\Omega) \cap H_0^1(\Omega)$ agree with those in [121, Theorem 2.1]. Especially, it will be readily seen from the proof of Theorem 6.1 that the regularity of the solution u at any positive time can be improved from the initial regularity by 2 orders in space, namely, $u(\,\cdot\,,t) \in \mathcal{D}(\mathcal{A}^{\gamma+1})$ if $a \in \mathcal{D}(\mathcal{A}^{\gamma})$ for $0 < t \leq T$.

On the other hand, if the source term F does not vanish, the improvement of regularity in space is strictly less than 2 orders except for the special case that F is L^2 in time. For example, if $F \in L^2(\Omega \times (0,T))$, then it follows from Theorem 6.2(a) that $u \in L^2(0,T;H^2(\Omega) \cap H_0^1(\Omega))$, which coincides with [121, Theorem 2.2]. However, if $F \in L^p(0,T;L^2(\Omega))$ with $p \neq 2$, then Theorem 6.2(b) asserts $u \in L^p(0,T;\mathcal{D}(\mathcal{A}^{1-\epsilon}))$, where $\epsilon \in (0,1]$ can be arbitrarily small but is never zero. The technical reason is that only in case of $p = 2$ one can take advantage of a newly established property in Bazhlekova [59] (see Lemma 6.4).

Now as the elliptic operator $\mathcal{A}$, we consider a special but physically important form

$$\mathcal{A}_D u(x,t) := -\mathrm{div}(D(x)\nabla u(x,t)),$$

where $D = D(x)$ denotes a diffusion coefficient. On the basis of these established results, we can consider the dependency of the solution on D and the orders of Caputo derivatives. More precisely, we evaluate the difference between the solutions u and $\widetilde{u}$ to

$$\begin{cases} \displaystyle\sum_{j=1}^{m} q_j \partial_t^{\alpha_j} u + \mathcal{A}_D u = 0 & \text{in } \Omega \times (0,T], \\ u = a & \text{in } \Omega \times \{0\}, \\ u = 0 & \text{on } \partial\Omega \times (0,T] \end{cases} \tag{6.12}$$

and

$$\begin{cases} \displaystyle\sum_{j=1}^{m} \widetilde{q}_j \partial_t^{\widetilde{\alpha}_j} \widetilde{u} + \mathcal{A}_{\widetilde{D}} \widetilde{u} = 0 & \text{in } \Omega \times (0,T], \\ \widetilde{u} = a & \text{in } \Omega \times \{0\}, \\ \widetilde{u} = 0 & \text{on } \partial\Omega \times (0,T] \end{cases} \tag{6.13}$$

respectively.

Theorem 6.3 *Fix $a \in \mathcal{D}(\mathcal{A}^\gamma)$ with some $\gamma \in (0,1]$. Let u and $\widetilde{u}$ be the solutions to* (6.12) *and* (6.13) *respectively, where $\boldsymbol{\alpha}, \widetilde{\boldsymbol{\alpha}} \in \mathcal{U}$, $\boldsymbol{q}, \widetilde{\boldsymbol{q}} \in \mathcal{V}$ (see definition* (6.4) *for $\mathcal{U}, \mathcal{V}$) and*

$$D, \widetilde{D} \in \mathcal{W} := \{D \in C^1(\overline{\Omega});\ D \geq \delta \text{ in } \overline{\Omega},\ \|D\|_{C^1(\overline{\Omega})} \leq M\} \tag{6.14}$$

with fixed $\delta > 0$ and $M > 0$. Then there exists a constant $C = C(\Omega, T, \|a\|_{\mathcal{D}(\mathcal{A}^\gamma)}, \mathcal{U}, \mathcal{V}, \mathcal{W}) > 0$ such that

$$\|u - \widetilde{u}\|_{L^{\frac{1}{1-\gamma}}(0,T;\mathcal{D}(\mathcal{A}^{1-\epsilon}))} \leq \frac{C}{\epsilon}\left(\sum_{j=1}^m |\alpha_j - \widetilde{\alpha}_j| + \sum_{j=2}^m |q_j - \widetilde{q}_j| + \|D - \widetilde{D}\|_{C^1(\overline{\Omega})}\right) \tag{6.15}$$

for each $\epsilon \in (0,1]$ if $0 < \gamma < \frac{1}{2}$, and

$$\|u - \widetilde{u}\|_{L^2(0,T;H^2(\Omega))} \leq C\left(\sum_{j=1}^m |\alpha_j - \widetilde{\alpha}_j| + \sum_{j=2}^m |q_j - \widetilde{q}_j| + \|D - \widetilde{D}\|_{C^1(\overline{\Omega})}\right) \tag{6.16}$$

if $\gamma \geq \frac{1}{2}$.

The above theorem extends a similar Lipschitz stability result in [96] for the single-term case. It is also fundamental for the optimization approach to the related coefficient inverse problem by extra measurements. As a typical example, we apply Theorem 6.3 to establish an existence result for the simultaneous reconstruction of $\boldsymbol{\alpha}, \boldsymbol{q}, D(x)$ by the partial boundary observation of the normal derivative of the solution.

Corollary 6.1 *Fix $p > d$ and a subboundary $\Sigma \subset \partial\Omega$ arbitrarily. Denote by $u(\boldsymbol{\alpha}, \boldsymbol{q}, D)$ the unique solution to* (6.12) *with $a \in L^2(\Omega), \boldsymbol{\alpha} \in \mathcal{U}, \boldsymbol{q} \in \mathcal{V}$ and*

$$D \in \widetilde{\mathcal{W}} := \left\{D \in W^{2,p}(\Omega); D \geq \delta \text{ in } \overline{\Omega},\ \|D\|_{W^{2,p}(\Omega)} \leq \widetilde{M}\right\} \tag{6.17}$$

with fixed $\delta > 0$ and $\widetilde{M} > 0$, where $\mathcal{U}, \mathcal{V}$ was defined in (6.4). *Then for any given $w \in L^1(0,T;L^2(\Sigma))$, there exists a minimizer to the minimization problem*

$$\min_{(\boldsymbol{\alpha},\boldsymbol{q},D)\in\mathcal{U}\times\mathcal{V}\times\widetilde{\mathcal{W}}} \|\partial_\nu u(\boldsymbol{\alpha}, \boldsymbol{q}, D) - w\|_{L^1(0,T;L^2(\Sigma))}.$$

In [96], a similar result for the single-term case was established under the homogeneous Neumann boundary condition with the observation data $u(\alpha, D)$ on $\Sigma \times (0,T)$, which is physically more natural than the setting in Corollary 6.1. In fact, one can give parallel proofs for Theorems 6.1–6.3 with the boundary condition $\partial_\nu u = 0$ on $\partial\Omega \times (0,T]$ instead of (6.3), but here we omit this part for consistency.

In Sakamoto and Yamamoto [121], the decay rate of the solution to the single-term time-fractional diffusion equation (5.1) was shown to be $t^{-\alpha}$ as $t \to \infty$. Here we give a generalization for the multi-term case where we specify the principal term of the solution as $t \to \infty$.

Theorem 6.4 *Let $F = 0$. Fix $\boldsymbol{\alpha} \in \mathcal{U}$, $\boldsymbol{q} \in \mathcal{V}$ and $a \in L^2(\Omega)$. Then there is a unique solution $u \in C([0,\infty); L^2(\Omega)) \cap C((0,\infty); H^2(\Omega) \cap H_0^1(\Omega))$ to* (6.1)–(6.3). *Moreover, there exists a constant $C = C(\Omega, T, \boldsymbol{\alpha}, \boldsymbol{q}, \mathcal{A}) > 0$ such that*

$$\left\|u(\cdot\,,t) - \frac{q_m}{\Gamma(1-\alpha_m)}\frac{\mathcal{A}^{-1}a}{t^{\alpha_m}}\right\|_{H^2(\Omega)} \leq \frac{C\|a\|_{L^2(\Omega)}}{t^{\min\{\alpha_{m-1}, 2\alpha_m\}}} \quad \text{as } t \to \infty. \tag{6.18}$$

Remark 6.2 We explain the significance of the Theorem 6.4. It reveals that the decay rate of $u(\cdot\,,t)$ in sense of $H^2(\Omega)$ is exactly $t^{-\alpha_m}$ as $t \to \infty$. In fact, inequality (6.18) implies that there exist constants $C_2 > C_1 > 0$ such that

$$C_1\|a\|_{L^2(\Omega)}t^{-\alpha_m} \le \|u(\cdot\,,t)\|_{H^2(\Omega)} \le C_2\|a\|_{L^2(\Omega)}t^{-\alpha_m} \quad \text{as } t \to \infty. \tag{6.19}$$

Consequently, it turns out that the decay rate $t^{-\alpha_m}$ is the best possible. In other words, if

$$\|u(\cdot\,,t)\|_{H^2(\Omega)} \le C\,t^{-\beta} \quad \text{as } t \to \infty$$

for some order $\beta > \alpha_m$ and some constant $C > 0$, then $u(x,t) = 0$ for $x \in \Omega$ and $t > 0$. Actually, in this case it is easily inferred from the lower bound in (6.19) that there should be $a = 0$ in Ω. Therefore, Theorem 6.1 and the upper bound in (6.19) immediately imply $u \equiv 0$ in $\Omega \times (0,\infty)$. Furthermore, (6.18) also gives the convergence rate of the approximation

$$u(\cdot\,,t) - \frac{q_m}{\Gamma(1-\alpha_m)}\frac{\mathcal{A}^{-1}a}{t^{\alpha_m}} \to 0 \quad \text{in } H^2(\Omega) \text{ as } t \to \infty,$$

that is, $t^{-\min\{\alpha_{m-1},2\alpha_m\}}$.

6.3 Proofs of main results

In this section, we give proofs for the well-posedness results stated in Section 6.2.

In the discussion of single-term time-fractional diffusion equations, it turns out that the solutions can be explicitly represented by the usual Mittag-Leffler function (5.4), and it plays a remarkable role especially for obtaining estimates for the stability. Since explicit solutions to the multi-term case are also available by using a generalized form of (5.4) called the multinomial Mittag-Leffler function, we shall take advantage of several important properties of this generalization so that similar arguments are still feasible for multi-term time-fractional diffusion equations. Here we only state those properties as technical lemmata in this section and provide the proofs later in Section 6.5.

The multinomial Mittag-Leffler function is defined as (see Luchko and Gorenflo [104])

$$E_{(\beta_1,\dots,\beta_m),\beta_0}(z_1,\dots,z_m) := \sum_{k=0}^{\infty}\sum_{k_1+\cdots+k_m=k}\frac{(k;k_1,\dots,k_m)\prod_{j=1}^m z_j^{k_j}}{\Gamma(\beta_0+\sum_{j=1}^m\beta_j k_j)}, \tag{6.20}$$

where we assume $0 < \beta_0 < 2$, $0 < \beta_j < 1$ and $z_j \in \mathbb{C}$ $(j = 1,\dots,m)$. Here $(k;k_1,\dots,k_m)$ denotes the multinomial coefficient

$$(k;k_1,\dots,k_m) := \frac{k!}{k_1!\cdots k_m!} \quad \text{with } k = \sum_{j=1}^m k_j,$$

where k_j $(1 \le j \le m)$ are non-negative integers.

Concerning the relation between multinomial Mittag-Leffler functions with different parameters, we have the following lemma.

Lemma 6.1 *Let $0 < \beta_0 < 2$, $0 < \beta_j < 1$ $(j = 1,\dots,m)$ and $z_j \in \mathbb{C}$ $(j = 1,\dots,m)$ be fixed. Then*

$$\frac{1}{\Gamma(\beta_0)} + \sum_{j=1}^m z_j E_{(\beta_1,\dots,\beta_m),\beta_0+\beta_j}(z_1,\dots,z_m) = E_{(\beta_1,\dots,\beta_m),\beta_0}(z_1,\dots,z_m).$$

Concerning the regularity of the solution to a single-term time-fractional diffusion equation, the estimate (see [116, p. 35])

$$|E_{\alpha,\beta}(-\eta)| \le \frac{C}{1+\eta} \quad (\eta \ge 0)$$

is essential. Here we extend the above inequality to the multinomial case.

Lemma 6.2 *Let $0 < \beta < 2$ and $1 > \alpha_1 > \cdots > \alpha_m > 0$ be given. Assume that $\alpha_1\pi/2 < \mu < \alpha_1\pi$, $\mu \le |\arg(z_1)| \le \pi$ and there exists $K > 0$ such that $-K \le z_j < 0$ $(j = 2, \dots, m)$. Then there exists a constant $C > 0$ depending only on μ, K, α_j $(j = 1, \dots, m)$ and β such that*

$$|E_{(\alpha_1,\alpha_1-\alpha_2,\dots,\alpha_1-\alpha_m),\beta}(z_1, \dots, z_m)| \le \frac{C}{1+|z_1|}.$$

For later use, we adopt the abbreviation

$$E^{(n)}_{\boldsymbol{\alpha}',\beta}(t) := E_{(\alpha_1,\alpha_1-\alpha_2,\dots,\alpha_1-\alpha_m),\beta}(-\lambda_n t^{\alpha_1}, -q_2 t^{\alpha_1-\alpha_2}, \dots, -q_m t^{\alpha_1-\alpha_m}) \quad (t > 0), \tag{6.21}$$

where λ_n is the n-th eigenvalue of $\mathcal{A}$, $0 < \beta < 2$, and α_j, q_j are those positive constants in (6.1). Especially, regarding the derivative of $t^{\alpha_1} E^{(n)}_{\boldsymbol{\alpha}',1+\alpha_1}(t)$ with respect to $t > 0$, we state the following technical lemma.

Lemma 6.3 *Let $1 > \alpha_1 > \cdots > \alpha_m > 1$. Then*

$$\frac{\mathrm{d}}{\mathrm{d}t}\left\{t^{\alpha_1} E^{(n)}_{\boldsymbol{\alpha}',1+\alpha_1}(t)\right\} = t^{\alpha_1-1} E^{(n)}_{\boldsymbol{\alpha}',\alpha_1}(t) \quad (t > 0).$$

Now we are ready to employ the multinomial Mittag-Leffler functions to show the well-posedness results.

6.3.1 Proof of Theorem 6.1

When the source term F vanishes, it was shown in [103] that the explicit solution to (6.1)–(6.3) is given by

$$u(\cdot\,, t) = \sum_{n=1}^{\infty} \left(1 - \lambda_n t^{\alpha_1} E^{(n)}_{\boldsymbol{\alpha}',1+\alpha_1}(t)\right)(a, \varphi_n)\,\varphi_n, \tag{6.22}$$

where φ_n is the n-th eigenfunction of $\mathcal{A}$. With the aid of Lemmata 6.1–6.3, it is straightforward to give estimates for the solution by the initial value.

Completion of Proof of Theorem 6.1. Let $a \in \mathcal{D}(\mathcal{A}^\gamma)$ with some fixed $\gamma \in [0, 1]$. In this proof, $C > 0$ denotes generic positive constants depending at most on $\Omega, T, \boldsymbol{\alpha}, \boldsymbol{q}, \mathcal{A}$ but independent of the initial value a, which may vary from line by line.

(a) First, a direct application of Lemma 6.2 yields

$$\left|1 - \lambda_n t^{\alpha_1} E^{(n)}_{\boldsymbol{\alpha}',1+\alpha_1}(t)\right| \le 1 + \lambda_n t^{\alpha_1} \frac{C}{1+\lambda_n t^{\alpha_1}} \le C.$$

Thus, we take advantage of (6.22) to derive

$$\|u(\cdot\,, t)\|_{L^2(\Omega)} = \left\{\sum_{n=1}^{\infty} \left|1 - \lambda_n t^{\alpha_1} E^{(n)}_{\boldsymbol{\alpha}',1+\alpha_1}(t)\right|^2 |(a, \varphi_n)|^2\right\}^{1/2} \le C\|a\|_{L^2(\Omega)}$$

for $0 < t \le T$, where we use the fact that $\{\varphi_n\}$ forms an orthonormal basis of $L^2(\Omega)$. Since the summation in (6.22) converges in $L^2(\Omega)$ uniformly in $t \in [0,T]$, we get $u \in C([0,T];L^2(\Omega))$ or (6.5). Furthermore, by the definition of $\mathcal{D}(\mathcal{A})$, we see

$$\|u(\cdot\,,t)\|^2_{\mathcal{D}(\mathcal{A})} = \sum_{n=1}^{\infty} \left(\lambda_n \left|1 - \lambda_n t^{\alpha_1} E^{(n)}_{\boldsymbol{\alpha}',1+\alpha_1}(t)\right|\right)^2 |(a,\varphi_n)|^2.$$

In order to treat the term $1 - \lambda_n t^{\alpha_1} E^{(n)}_{\boldsymbol{\alpha}',1+\alpha_1}(t)$, we substitute

$$\beta_0 = 1, \quad \beta_1 = \alpha_1, \quad z_1 = -\lambda_n t^{\alpha_1}, \quad \beta_j = \alpha_1 - \alpha_j \text{ and } z_j = -q_j t^{\alpha_1-\alpha_j} \ (j = 2,\dots,m)$$

in Lemma 6.1 and then utilize Lemma 6.2 to deduce

$$\begin{aligned}\left|1 - \lambda_n t^{\alpha_1} E^{(n)}_{\boldsymbol{\alpha}',1+\alpha_1}(t)\right| &= \left|E^{(n)}_{\boldsymbol{\alpha}',1}(t) + \sum_{j=2}^{m} q_j t^{\alpha_1-\alpha_j} E^{(n)}_{\boldsymbol{\alpha}',1+\alpha_1-\alpha_j}(t)\right| \\ &\le \left|E^{(n)}_{\boldsymbol{\alpha}',1}(t)\right| + C\sum_{j=2}^{m} t^{\alpha_1-\alpha_j}\left|E^{(n)}_{\boldsymbol{\alpha}',1+\alpha_1-\alpha_j}(t)\right| \le C\sum_{j=1}^{m}\frac{t^{\alpha_1-\alpha_j}}{1+\lambda_n t^{\alpha_1}}.\end{aligned}$$

Therefore, for $0 < t \le T$, we estimate

$$\begin{aligned}\|u(\cdot\,,t)\|^2_{\mathcal{D}(\mathcal{A})} &= \sum_{n=1}^{\infty}\left|\lambda_n^{1-\gamma}\left(1 - \lambda_n t^{\alpha_1} E^{(n)}_{\boldsymbol{\alpha}',1+\alpha_1}(t)\right)\right|^2 |\lambda_n^{\gamma}(a,\varphi_n)|^2 \\ &\le C^2\sum_{n=1}^{\infty}\left(\sum_{j=1}^{m}\frac{\lambda_n^{1-\gamma}t^{\alpha_1-\alpha_j}}{1+\lambda_n t^{\alpha_1}}\right)^2 |\lambda_n^{\gamma}(a,\varphi_n)|^2 \\ &\le C^2\sum_{n=1}^{\infty}\left(\sum_{j=1}^{m}\frac{(\lambda_n t^{\alpha_1})^{1-\gamma}}{1+\lambda_n t^{\alpha_1}}t^{\alpha_1\gamma-\alpha_j}\right)^2 |\lambda_n^{\gamma}(a,\varphi_n)|^2 \\ &\le C^2\left(\sum_{j=1}^{m} t^{\alpha_1\gamma-\alpha_j}\right)^2\sum_{n=1}^{\infty}|\lambda_n^{\gamma}(a,\varphi_n)|^2 \le \left(C\|a\|_{\mathcal{D}(\mathcal{A}^\gamma)}t^{\alpha_1(\gamma-1)}\right)^2,\end{aligned}$$

where we use the fact

$$\frac{(\lambda_n t^{\alpha_1})^{1-\gamma}}{1+\lambda_n t^{\alpha_1}} \le \left\{\begin{aligned}&\frac{1}{1+\lambda_n t^{\alpha_1}} \text{ if } \lambda_n t^{\alpha_1} \le 1\\ &\frac{\lambda_n t^{\alpha_1}}{1+\lambda_n t^{\alpha_1}} \text{ if } \lambda_n t^{\alpha_1} \ge 1\end{aligned}\right\} \le 1$$

in the third inequality. This, together with the fact $\mathcal{D}(\mathcal{A}) \subset H^2(\Omega)$, yield the estimate (6.6). Furthermore, it follows immediately from (6.6) and $\alpha_1 < 1$ that $u \in L^{\frac{1}{1-\gamma}}(0,T;H^2(\Omega)\cap H_0^1(\Omega))$.

(b) In order to investigate the asymptotic behavior near $t = 0$, first we have

$$\|u(\cdot\,,t) - a\|^2_{\mathcal{D}(\mathcal{A}^\gamma)} = \sum_{n=1}^{\infty}\left|\lambda_n t^{\alpha_1} E^{(n)}_{\boldsymbol{\alpha}',1+\alpha_1}(t)\right|^2 |\lambda_n^{\gamma}(a,\varphi_n)|^2 \le \left(C\|a\|_{\mathcal{D}(\mathcal{A}^\gamma)}\right)^2 < \infty$$

for $0 \le t \le T$ by a direct calculation and Lemma 6.2. On the other hand, in view of Lemma 6.1, the term $\lambda_n t^{\alpha_1} E^{(n)}_{\boldsymbol{\alpha}',1+\alpha_1}(t)$ can be rewritten as

$$\lambda_n t^{\alpha_1} E^{(n)}_{\boldsymbol{\alpha}',1+\alpha_1}(t) = -(E^{(n)}_{\boldsymbol{\alpha}',1}(t) - 1) - \sum_{j=2}^{m} q_j t^{\alpha_1-\alpha_j} E^{(n)}_{\boldsymbol{\alpha}',1+\alpha_1-\alpha_j}(t).$$

Thanks to the fact that $\lim_{t\to 0}(E^{(n)}_{\boldsymbol{\alpha}',1}(t)-1)=0$ and the boundedness of $E^{(n)}_{\boldsymbol{\alpha}',1+\alpha_1-\alpha_j}$ $(j=2,\dots,m)$ by Lemma 6.2 for each $n=1,2,\dots$, the above observation implies

$$\lim_{t\to 0}(\lambda_n t^{\alpha_1}E^{(n)}_{\boldsymbol{\alpha}',1+\alpha_1}(t))=0 \quad (\forall\, n=1,2,\dots).$$

Therefore, (6.7) follows immediately from Lebesgue's dominated convergence theorem.

(c) In order to deal with $\partial_t u$, we make use of Lemma 6.3 to obtain

$$\partial_t u(\,\cdot\,,t)=-t^{\alpha_1-1}\sum_{n=1}^{\infty}\lambda_n E^{(n)}_{\boldsymbol{\alpha}',\alpha_1}(t)(a,\varphi_n)\varphi_n.$$

Then a similar argument to that for (6.6) indicates

$$\begin{aligned}\|\partial_t u(\,\cdot\,,t)\|^2_{L^2(\Omega)}&=t^{2(\alpha_1-1)}\sum_{n=1}^{\infty}\left|\lambda_n^{1-\gamma}E^{(n)}_{\boldsymbol{\alpha}',\alpha_1}(t)\right|^2|\lambda_n^{\gamma}(a,\varphi_n)|^2\\&\le C^2t^{2(\alpha_1-1)}\sum_{n=1}^{\infty}\left(\frac{(\lambda_n t^{\alpha_1})^{1-\gamma}}{1+\lambda_n t^{\alpha_1}}t^{\alpha_1(\gamma-1)}\right)^2|\lambda_n^{\gamma}(a,\varphi_n)|^2\\&\le\left(C\|a\|_{\mathcal{D}(\mathcal{A}^\gamma)}t^{\alpha_1\gamma-1}\right)^2\quad(0<t\le T)\end{aligned}$$

or (6.8). This implies $\partial_t u\in C((0,T];L^2(\Omega))$ immediately.

(d) Finally, to give estimates for $\partial_t^\beta u$ with $0<\beta<1$ when $\gamma>0$, we employ (6.8) and turn to the definition of the Caputo derivative to obtain

$$\begin{aligned}\|\partial_t^\beta u(\,\cdot\,,t)\|_{L^2(\Omega)}&=\frac{1}{\Gamma(1-\beta)}\left\|\int_0^t\frac{\partial_s u(\,\cdot\,,s)}{(t-s)^\beta}\,\mathrm{d}s\right\|_{L^2(\Omega)}\le C\int_0^t\frac{\|\partial_s u(\,\cdot\,,s)\|_{L^2(\Omega)}}{(t-s)^\beta}\,\mathrm{d}s\\&\le C\|a\|_{\mathcal{D}(\mathcal{A}^\gamma)}\int_0^t s^{\alpha_1\gamma-1}(t-s)^{-\beta}\,\mathrm{d}s\le C\|a\|_{\mathcal{D}(\mathcal{A}^\gamma)}t^{\alpha_1\gamma-\beta}\quad(0<t\le T),\end{aligned}$$

that is, (6.9), where the first inequality follows from Minkowski's inequality for integrals. Especially, as long as $\beta\le\alpha_1$, there holds $\alpha_1\gamma-\beta>\gamma-1$ and obviously $\partial_t^\beta u\in L^{\frac{1}{1-\gamma}}(0,T;L^2(\Omega))$.

Collecting all the results above, we complete the proof of Theorem 6.1. □

6.3.2 Proof of Theorem 6.2

In order to construct an explicit solution when the initial value a vanishes, we apply the eigenfunction expansion method. In other words, we seek for a solution to (6.1)–(6.3) of the particular form

$$u(\,\cdot\,,t)=\sum_{n=1}^{\infty}T_n(t)\varphi_n\quad(0<t\le T),\tag{6.23}$$

where φ_n is the n-th eigenfunction of $\mathcal{A}$. The substitution of (6.23) into (6.1) yields

$$\sum_{n=1}^{\infty}\left(\sum_{j=1}^{m}q_j\partial_t^{\alpha_j}T_n(t)\right)\varphi_n=-\sum_{n=1}^{\infty}\lambda_n T_n(t)\varphi_n+\sum_{n=1}^{\infty}(F(\,\cdot\,,t),\varphi_n)\varphi_n.$$

Therefore, it is readily seen from the orthogonality of $\{\varphi_n\}$ and the homogeneous initial condition (6.3) that T_n satisfies an initial value problem for an ordinary differential equation

$$\begin{cases}\displaystyle\sum_{j=1}^{m}q_j\partial_t^{\alpha_j}T_n(t)+\lambda_n T_n(t)=(F(\,\cdot\,,t),\varphi_n)\quad(0<t\le T),\\ T_n(0)=0.\end{cases}$$

Then it follows from [104, Theorem 4.1] that

$$T_n(t) = \int_0^t s^{\alpha_1-1} E^{(n)}_{\boldsymbol{\alpha}',\alpha_1}(s)(F(\,\cdot\,,t-s),\varphi_n)\,\mathrm{d}s,$$

implying that the solution takes the form of a convolution

$$u(\,\cdot\,,t) = \int_0^t U(s)F(\,\cdot\,,t-s)\,\mathrm{d}s, \tag{6.24}$$

where

$$U(t)f := t^{\alpha_1-1}\sum_{n=1}^{\infty} E^{(n)}_{\boldsymbol{\alpha}',\alpha_1}(t)(f,\varphi_n)\varphi_n. \tag{6.25}$$

Before proceeding to the proof, we introduce a key lemma for showing Theorem 6.2(a).

Lemma 6.4 (see [59, Theorem 3.2]) *The function $t^{\alpha_1-1}E^{(n)}_{\boldsymbol{\alpha}',\alpha_1}(t)$ is positive for $t>0$.*

Completion of Proof of Theorem 6.2. Let $F \in L^p(0,T;\mathcal{D}(\mathcal{A}^\gamma))$ with some fixed $p\in[1,\infty]$ and $\gamma\in[0,1]$. In this proof, $C>0$ denotes generic positive constants depending at most on $\Omega, T, \boldsymbol{\alpha}, \boldsymbol{q}, \mathcal{A}$ but independent of F and the choice of ϵ.

(a) Let $p=2$. According to the expression (6.24)–(6.25), formally we write

$$\|u(\,\cdot\,,t)\|^2_{\mathcal{D}(\mathcal{A})} = \sum_{n=1}^{\infty}\lambda_n^2\left(\int_0^t s^{\alpha_1-1}E^{(n)}_{\boldsymbol{\alpha}',\alpha_1}(s)(F(\,\cdot\,,t-s),\varphi_n)\,\mathrm{d}s\right)^2.$$

Using Young's inequality for convolutions, we estimate

$$\begin{aligned}\|u\|^2_{L^2(0,T;\mathcal{D}(\mathcal{A}))} &= \sum_{n=1}^{\infty}\lambda_n^2\left\|\int_0^t s^{\alpha_1-1}E^{(n)}_{\boldsymbol{\alpha}',\alpha_1}(s)(F(\,\cdot\,,t-s),\varphi_n)\,\mathrm{d}s\right\|^2_{L^2(0,T)}\\ &\le \sum_{n=1}^{\infty}\left(\lambda_n\int_0^T t^{\alpha_1-1}|E^{(n)}_{\boldsymbol{\alpha}',\alpha_1}(t)|\,\mathrm{d}t\right)^2\|(F(\,\cdot\,,t),\varphi_n)\|^2_{L^2(0,T)}.\end{aligned}$$

By Lemma 6.4, we can remove the absolute value of $E^{(n)}_{\boldsymbol{\alpha}',\alpha_1}(t)$ and apply Lemma 6.3 to derive

$$\int_0^T t^{\alpha_1-1}|E^{(n)}_{\boldsymbol{\alpha}',\alpha_1}(t)|\,\mathrm{d}t = \int_0^T t^{\alpha_1-1}E^{(n)}_{\boldsymbol{\alpha}',\alpha_1}(t)\,\mathrm{d}t = T^{\alpha_1}E^{(n)}_{\boldsymbol{\alpha}',1+\alpha_1}(T).$$

Consequently, we use Lemma 6.2 to conclude

$$\begin{aligned}\|u\|^2_{L^2(0,T;H^2(\Omega))} &\le C^2\|u\|^2_{L^2(0,T;\mathcal{D}(\mathcal{A}))} \le C^2\sum_{n=1}^{\infty}\left(\lambda_n T^{\alpha_1}E^{(n)}_{\boldsymbol{\alpha}',1+\alpha_1}(T)\right)^2\|(F(\,\cdot\,,t),\varphi_n)\|^2_{L^2(0,T)}\\ &\le C^2\sum_{n=1}^{\infty}\|(F(\,\cdot\,,t),\varphi_n)\|^2_{L^2(0,T)} = \left(C\|F\|_{L^2(\Omega\times(0,T))}\right)^2.\end{aligned}$$

(b) Fix $\epsilon\in(0,1]$ arbitrarily. First we give an estimate for (6.25) with $f\in\mathcal{D}(\mathcal{A}^\gamma)$. Similarly to the proof of Theorem 6.1, we apply Lemma 6.2 to deduce

$$\begin{aligned}\|U(t)f\|^2_{\mathcal{D}(\mathcal{A}^{\gamma+1-\epsilon})} &= t^{2(\alpha_1-1)}\sum_{n=1}^{\infty}\left|\lambda_n^{1-\epsilon}E^{(n)}_{\boldsymbol{\alpha}',\alpha_1}\right|^2|\lambda_n^\gamma(f,\varphi_n)|^2\\ &\le C^2t^{2(\alpha_1-1)}\sum_{n=1}^{\infty}\left(\frac{(\lambda_n t^{\alpha_1})^{1-\epsilon}}{1+\lambda_n t^{\alpha_1}}t^{\alpha_1(\epsilon-1)}\right)^2|\lambda_n^\gamma(f,\varphi_n)|^2\end{aligned}$$

$$\leq \big(C\|f\|_{\mathcal{D}(\mathcal{A}^\gamma)}t^{\alpha_1\epsilon-1}\big)^2 \quad (0<t\leq T).$$

Using (6.24) and Minkowski's inequality for integrals, formally we have

$$\begin{aligned}\|u(\,\cdot\,,t)\|_{\mathcal{D}(\mathcal{A}^{\gamma+1-\epsilon})} &= \left\|\int_0^t U(s)F(\,\cdot\,,t-s)\,\mathrm{d}s\right\|_{\mathcal{D}(\mathcal{A}^{\gamma+1-\epsilon})}\\ &\leq \int_0^t \|U(s)F(\,\cdot\,,t-s)\|_{\mathcal{D}(\mathcal{A}^{\gamma+1-\epsilon})}\,\mathrm{d}s\\ &\leq C\int_0^t \|F(\,\cdot\,,t-s)\|_{\mathcal{D}(\mathcal{A}^\gamma)}s^{\alpha_1\epsilon-1}\,\mathrm{d}s \quad (0<t\leq T). \end{aligned} \tag{6.26}$$

Finally, it follows from Young's inequality for convolutions that

$$\begin{aligned}\|u\|_{L^p(0,T;\mathcal{D}(\mathcal{A}^{\gamma+1-\epsilon}))} &\leq C\left\|\int_0^t \|F(\,\cdot\,,t-s)\|_{\mathcal{D}(\mathcal{A}^\gamma)}s^{\alpha_1\epsilon-1}\,\mathrm{d}s\right\|_{L^p(0,T)}\\ &\leq C\|F\|_{L^p(0,T;\mathcal{D}(\mathcal{A}^\gamma))}\int_0^T t^{\alpha_1\epsilon-1}\,\mathrm{d}t \leq \frac{C}{\epsilon}\|F\|_{L^p(0,T;\mathcal{D}(\mathcal{A}^\gamma))}.\end{aligned}$$

This completes the verification of (6.10).

(c) Assume $\alpha_1 p>1$ and fix $\kappa\in(0,\gamma+1-\frac{1}{\alpha_1 p})$ arbitrarily. To investigate the asymptotic behavior near $t=0$, we apply Hölder's inequality to (6.26) with $\epsilon=\gamma+1-\kappa$ to see

$$\|u(\,\cdot\,,t)\|_{\mathcal{D}(\mathcal{A}^\kappa)} \leq C\|F\|_{L^p(0,t;\mathcal{D}(\mathcal{A}^\gamma))}\left(\int_0^t s^{(\alpha_1(\gamma+1-\kappa)-1)p'}\,\mathrm{d}s\right)^{1/p'},$$

where p' is the conjugate number of p, i.e. $1/p+1/p'=1$. Since $\kappa<\gamma+1-\frac{1}{\alpha_1 p}$, we see $(\alpha_1(\gamma+1-\kappa)-1)p'>-1$ and then $\lim_{t\to0}\int_0^t s^{(\alpha_1(\gamma+1-\kappa)-1)p'}\,\mathrm{d}s=0$, indicating (6.11) immediately. □

6.3.3 Proof of Theorem 6.3 and Corollary 6.1

As a direct application of Theorems 6.1–6.2, it is straightforward to show the Lipschitz stability of the solution with respect to various coefficients.

Proof of Theorem 6.3. Let $a\in\mathcal{D}(\mathcal{A}^\gamma)$ with some fixed $\gamma\in(0,1]$. In this proof, $C>0$ denotes general constants depending at most on $\Omega,T,\|a\|_{\mathcal{D}(\mathcal{A}^\gamma)},\mathcal{U},\mathcal{V},\mathcal{W}$ but independent of the specific choices of the coefficients and $\epsilon\in(0,1]$.

First, a direct application of Theorem 6.1 immediately yields $u\in L^p(0,T;H^2(\Omega)\cap H_0^1(\Omega))$ and $\partial_t^\beta u\in L^p(0,T;L^2(\Omega))$ for $0<\beta\leq\alpha_1$, where we abbreviate $p:=\frac{1}{1-\gamma}$. More precisely, there exists $C>0$ such that

$$\|u\|_{L^p(0,T;H^2(\Omega))}\leq C,\quad \|\partial_t^\beta u\|_{L^p(0,T;L^2(\Omega))}\leq C\ (0<\beta\leq\alpha_1). \tag{6.27}$$

On the other hand, by taking the difference of systems (6.13) and (6.12), it turns out that the system for $v:=\widetilde{u}-u$ reads

$$\begin{cases}\displaystyle\sum_{j=1}^m \widetilde{q}_j\partial_t^{\widetilde{\alpha}_j}v = L_{\widetilde{D}}v+F & \text{in } \Omega\times(0,T],\\ v=0 & \text{in } \Omega\times\{0\},\\ v=0 & \text{on } \partial\Omega\times(0,T],\end{cases}$$

where we set

$$F := \sum_{j=1}^{m} \widetilde{q}_j(\partial_t^{\alpha_j} u - \partial_t^{\widetilde{\alpha}_j} u) + \sum_{j=2}^{m} (q_j - \widetilde{q}_j)\partial_t^{\alpha_j} u + L_{\widetilde{D}-D} u.$$

Without loss of generality, we assume $\alpha_1 \geq \widetilde{\alpha}_1$, or otherwise we investigate $v := u - \widetilde{u}$ instead. Therefore, together with $D, \widetilde{D} \in C^1(\overline{\Omega})$, we see $F \in L^p(0,T;L^2(\Omega))$ from (6.27). Now it is straightforward to employ Theorem 6.2(b) to obtain

$$\|u - \widetilde{u}\|_{L^p(0,T;\mathcal{D}(\mathcal{A}^{1-\epsilon}))} = \|v\|_{L^p(0,T;\mathcal{D}(\mathcal{A}^{1-\epsilon}))} \leq \frac{C}{\epsilon}\|F\|_{L^p(0,T;L^2(\Omega))}. \tag{6.28}$$

Especially, if $\gamma \geq \frac{1}{2}$, we see $p = \frac{1}{1-\gamma} \geq 2$ and hence $L^p(\Omega \times (0,T)) \subset L^2(0,T;L^2(\Omega))$. It then follows from Theorem 6.2(a) that

$$\|u - \widetilde{u}\|_{L^2(0,T;H^2(\Omega))} \leq C\|F\|_{L^2(\Omega\times(0,T))} \leq C\|F\|_{L^p(0,T;L^2(\Omega))}. \tag{6.29}$$

Therefore, it suffices to dominate $\|F\|_{L^p(0,T;L^2(\Omega))}$ by the difference of coefficients.

To this end, first it is readily seen from (6.27) that

$$\begin{aligned}
\|F\|_{L^p(0,T;L^2(\Omega))} &\leq \sum_{j=1}^{m} \widetilde{q}_j \|\partial_t^{\alpha_j} u - \partial_t^{\widetilde{\alpha}_j} u\|_{L^p(0,T;L^2(\Omega))} + \sum_{j=2}^{m} |q_j - \widetilde{q}_j| \|\partial_t^{\alpha_j} u\|_{L^p(0,T;L^2(\Omega))} \\
&\quad + C\|D - \widetilde{D}\|_{C^1(\overline{\Omega})} \|u\|_{L^p(0,T;H^2(\Omega))} \\
&\leq C\left(\sum_{j=1}^{m} \|\partial_t^{\alpha_j} u - \partial_t^{\widetilde{\alpha}_j} u\|_{L^p(0,T;L^2(\Omega))} + \sum_{j=2}^{m} |q_j - \widetilde{q}_j| + \|D - \widetilde{D}\|_{C^1(\overline{\Omega})} \right).
\end{aligned}$$

To give an estimate for $\partial_t^{\alpha_j} u - \partial_t^{\widetilde{\alpha}_j} u$ by $|\alpha_j - \widetilde{\alpha}_j|$, we adopt a similar treatment as that in [96, Proposition 1] and decompose it by definition as

$$\begin{aligned}
\partial_t^{\alpha_j} u(\,\cdot\,,t) - \partial_t^{\widetilde{\alpha}_j} u(\,\cdot\,,t) &= \frac{1}{\Gamma(1-\alpha_j)} \int_0^t \frac{\partial_s u(\,\cdot\,,s)}{(t-s)^{\alpha_j}}\,\mathrm{d}s - \frac{1}{\Gamma(1-\widetilde{\alpha}_j)} \int_0^t \frac{\partial_s u(\,\cdot\,,s)}{(t-s)^{\widetilde{\alpha}_j}}\,\mathrm{d}s \\
&= I_j^1(\,\cdot\,,t) + I_j^2(\,\cdot\,,t),
\end{aligned}$$

where

$$\begin{aligned}
I_j^1(\,\cdot\,,t) &:= \frac{\Gamma(1-\widetilde{\alpha}_j) - \Gamma(1-\alpha_j)}{\Gamma(1-\widetilde{\alpha}_j)} \partial_t^{\alpha_j} u(\,\cdot\,,t), \\
I_j^2(\,\cdot\,,t) &:= \frac{1}{\Gamma(1-\widetilde{\alpha}_j)} \int_0^t \{(t-s)^{-\alpha_j} - (t-s)^{-\widetilde{\alpha}_j}\} \partial_s u(\,\cdot\,,s)\,\mathrm{d}s.
\end{aligned}$$

Since $\alpha_j, \widetilde{\alpha}_j \in [\underline{\alpha}, \overline{\alpha}]$ and the Gamma function is Lipschitz continuous in $[1-\overline{\alpha}, 1-\underline{\alpha}]$, it follows from (6.27) that

$$\|I_j^1\|_{L^p(0,T;L^2(\Omega))} = \frac{|\Gamma(1-\widetilde{\alpha}_j) - \Gamma(1-\alpha_j)|}{\Gamma(1-\widetilde{\alpha}_j)} \|\partial_t^{\alpha_j} u\|_{L^p(0,T;L^2(\Omega))} \leq C|\alpha_j - \widetilde{\alpha}_j|. \tag{6.30}$$

In order to treat I_j^2, we recall the estimate (6.8) for $\partial_t u$ and utilize Minkowski's inequality for integrals to deduce

$$\begin{aligned}
\|I_j^2(\,\cdot\,,t)\|_{L^2(\Omega)} &= \frac{1}{\Gamma(1-\widetilde{\alpha}_j)} \left\| \int_0^t \{(t-s)^{-\alpha_j} - (t-s)^{-\widetilde{\alpha}_j}\} \partial_s u(\,\cdot\,,s)\,\mathrm{d}s \right\|_{L^2(\Omega)} \\
&\leq \int_0^t |(t-s)^{-\alpha_j} - (t-s)^{-\widetilde{\alpha}_j}| \|\partial_s u(\,\cdot\,,s)\|_{L^2(\Omega)}\,\mathrm{d}s
\end{aligned}$$

$$\leq C \int_0^t |(t-s)^{-\alpha_j} - (t-s)^{-\widetilde{\alpha}_j}|\, s^{\alpha_1\gamma-1}\,\mathrm{d}s$$
$$= C \int_0^t |s^{-\alpha_j} - s^{-\widetilde{\alpha}_j}|\, (t-s)^{\alpha_1\gamma-1}\,\mathrm{d}s.$$

Using the mean value theorem, we have

$$|s^{-\alpha_j} - s^{-\widetilde{\alpha}_j}| = |\ln s|\, s^{-\widehat{\alpha}_j(s)} |\alpha_j - \widetilde{\alpha}_j|,$$

where $\widehat{\alpha}_j(s)$ is a parameter depending on s such that

$$\min\{\alpha_j, \widetilde{\alpha}_j\} \leq \widehat{\alpha}_j(s) \leq \max\{\alpha_j, \widetilde{\alpha}_j\} \leq \alpha_1$$

by the assumption $\alpha_1 \geq \widetilde{\alpha}_1$. Henceforth, we assume $T > 1$ without lose of generality. We prove separately in the cases $0 < t \leq 1$ and $1 < t \leq T$. First, let $0 < t \leq 1$. Then there holds $0 < s < 1$ and hence

$$s^{-\widehat{\alpha}_j(s)} \leq s^{-\alpha_1} = s^{\varepsilon} s^{-\alpha_1-\varepsilon},$$

where $\varepsilon > 0$ is sufficiently small such that $\alpha_1(1-\gamma) + \varepsilon < 1 - \gamma$. Since $|\ln s|\, s^{\varepsilon} \leq C$ for $0 < s < 1$, we obtain

$$\begin{aligned}
\|I_j^2(\,\cdot\,,t)\|_{L^2(\Omega)} &\leq C|\alpha_j - \widetilde{\alpha}_j| \int_0^t |\ln s|\, s^{-\widehat{\alpha}_j(s)} (t-s)^{\alpha_1\gamma-1}\,\mathrm{d}s \\
&\leq C|\alpha_j - \widetilde{\alpha}_j| \int_0^t (|\ln s|\, s^{\varepsilon}) s^{-\alpha_1-\varepsilon} (t-s)^{\alpha_1\gamma-1}\,\mathrm{d}s \\
&\leq C|\alpha_j - \widetilde{\alpha}_j|\, t^{-\alpha_1(1-\gamma)-\varepsilon} \quad (0 < t \leq 1),
\end{aligned} \tag{6.31}$$

where we apply the boundedness of the Beta function $B(1-\alpha_1-\varepsilon, \alpha_1\gamma)$ and $\gamma > 0$. Second, let $1 < t \leq T$. Then it is readily seen that $t - s > 1 - s$ for $0 < s < 1$ and $|\ln s|\, s^{-\widehat{\alpha}_j(s)} \leq C$ for $1 \leq s < t$. These observation, together with the inequality (6.31) for $t = 1$, indicate

$$\begin{aligned}
\|I_j^2(\,\cdot\,,t)\|_{L^2(\Omega)} &\leq C|\alpha_j - \widetilde{\alpha}_j| \left(\int_0^1 + \int_1^t \right) |\ln s|\, s^{-\widehat{\alpha}_j(s)} (t-s)^{\alpha_1\gamma-1}\,\mathrm{d}s \\
&\leq C|\alpha_j - \widetilde{\alpha}_j| \left(\int_0^1 |\ln s|\, s^{-\widehat{\alpha}_j(s)} (1-s)^{\alpha_1\gamma-1}\,\mathrm{d}s + C \int_1^t (t-s)^{\alpha_1\gamma-1}\,\mathrm{d}s \right) \\
&\leq C|\alpha_j - \widetilde{\alpha}_j| \quad (1 < t \leq T).
\end{aligned} \tag{6.32}$$

The combination of (6.31) and (6.32) immediately yields

$$\|I_j^2(\,\cdot\,,t)\|_{L^2(\Omega)} \leq C|\alpha_j - \widetilde{\alpha}_j|\, t^{-\alpha_1(1-\gamma)-\varepsilon} \quad (0 < t \leq T)$$

and thus $\|I_j^2\|_{L^p(0,T;L^2(\Omega))} \leq C|\alpha_j - \widetilde{\alpha}_j|$ because $\alpha_1(1-\gamma) + \varepsilon < 1 - \gamma = 1/p$. Consequently, collecting the estimate (6.30) for I_j^1, we conclude

$$\begin{aligned}
\|F\|_{L^p(0,T;L^2(\Omega))} &\leq C \left(\sum_{j=1}^m \|I_j^1 + I_j^2\|_{L^p(0,T;L^2(\Omega))} + \sum_{j=2}^m |q_j - \widetilde{q}_j| + \|D - \widetilde{D}\|_{C^1(\overline{\Omega})} \right) \\
&\leq C \left(\sum_{j=1}^m |\alpha_j - \widetilde{\alpha}_j| + \sum_{j=2}^m |q_j - \widetilde{q}_j| + \|D - \widetilde{D}\|_{C^1(\overline{\Omega})} \right),
\end{aligned}$$

implying (6.15) and (6.16) with the aid of (6.28) and (6.29) respectively. □

On the basis of Theorem 6.3, we can immediately show Corollary 6.1 by a minimizing sequence argument.

Proof of Corollary 6.1. Fix $a \in L^2(\Omega)$. First, by the assumption $p > d$, it follows from the embedding relation (see Adams [1])

$$W^{2,p}(\Omega) \subset C^{1,1-d/p}(\overline{\Omega}) \subset\subset C^1(\overline{\Omega})$$

that the embedding $W^{2,p}(\Omega) \subset C^1(\overline{\Omega})$ is compact. Especially, we have $\widetilde{\mathcal{W}} \subset \mathcal{W}$ (see the definitions (6.14) and (6.17) for $\mathcal{W}, \widetilde{\mathcal{W}}$). Therefore, for any triples $(\boldsymbol{\alpha}, \boldsymbol{q}, D), (\widetilde{\boldsymbol{\alpha}}, \widetilde{\boldsymbol{q}}, \widetilde{D}) \in \mathcal{U} \times \mathcal{V} \times \widetilde{\mathcal{W}}$, the trace theorem and Theorem 6.3 with $\gamma = 0, \epsilon = 1/4$ imply

$$\begin{aligned}
&\left\| \partial_\nu u(\boldsymbol{\alpha}, \boldsymbol{q}, D) - \partial_\nu u(\widetilde{\boldsymbol{\alpha}}, \widetilde{\boldsymbol{q}}, \widetilde{D}) \right\|_{L^1(0,T;L^2(\Sigma))} \\
&\le C \left\| u(\boldsymbol{\alpha}, \boldsymbol{q}, D) - u(\widetilde{\boldsymbol{\alpha}}, \widetilde{\boldsymbol{q}}, \widetilde{D}) \right\|_{L^1(0,T;\mathcal{D}(\mathcal{A}^{3/4}))} \\
&\le C \left(\sum_{j=1}^m |\alpha_j - \widetilde{\alpha}_j| + \sum_{j=2}^m |q_j - \widetilde{q}_j| + \|D - \widetilde{D}\|_{C^1(\overline{\Omega})} \right). \qquad (6.33)
\end{aligned}$$

On the other hand, fixing the partial boundary observation data $w \in L^1(0,T;L^2(\Sigma))$, we set

$$\delta_0 := \inf_{(\boldsymbol{\alpha}, \boldsymbol{q}, D) \in \mathcal{U} \times \mathcal{V} \times \widetilde{\mathcal{W}}} \|\partial_\nu u(\boldsymbol{\alpha}, \boldsymbol{q}, D) - w\|_{L^1(0,T;L^2(\Sigma))}$$

and pick a minimizing sequence $\{(\boldsymbol{\alpha}^{(\ell)}, \boldsymbol{q}^{(\ell)}, D^{(\ell)})\}_{\ell=1}^\infty \subset \mathcal{U} \times \mathcal{V} \times \widetilde{\mathcal{W}}$ such that

$$\lim_{\ell \to \infty} \left\| \partial_\nu u(\boldsymbol{\alpha}^{(\ell)}, \boldsymbol{q}^{(\ell)}, D^{(\ell)}) - w \right\|_{L^1(0,T;L^2(\Sigma))} = \delta_0. \qquad (6.34)$$

As $\mathcal{U}, \mathcal{V}, \widetilde{\mathcal{W}}$ are bounded and closed in respective reflexible spaces, we can extract a subsequence, still denoted by $\{(\boldsymbol{\alpha}^{(\ell)}, \boldsymbol{q}^{(\ell)}, D^{(\ell)})\}$, such that

$$\begin{aligned}
&\boldsymbol{\alpha}^{(\ell)} \to \boldsymbol{\alpha}^* \in \mathcal{U} \text{ and } \boldsymbol{q}^{(\ell)} \to \boldsymbol{q}^* \in \mathcal{V} \text{ in } \mathbb{R}^m, \\
&D^{(\ell)} \rightharpoonup D^* \in \widetilde{\mathcal{W}} \text{ weakly in } W^{2,p}(\Omega)
\end{aligned} \quad \text{as } \ell \to \infty. \qquad (6.35)$$

Using the compactness of the embedding $W^{2,p}(\Omega) \subset C^1(\overline{\Omega})$, we have

$$D^{(\ell)} \to D^* \text{ strongly in } C^1(\overline{\Omega}) \quad \text{as } \ell \to \infty. \qquad (6.36)$$

Now it suffices to verify that $(\boldsymbol{\alpha}^*, \boldsymbol{q}^*, D^*)$ is indeed a minimizer. Actually, it follows from (6.33) that

$$\begin{aligned}
\|\partial_\nu u(\boldsymbol{\alpha}^*, \boldsymbol{q}^*, D^*) - w\|_{L^1(0,T;L^2(\Sigma))} &\le \left\| \partial_\nu u(\boldsymbol{\alpha}^*, \boldsymbol{q}^*, D^*) - \partial_\nu u(\boldsymbol{\alpha}^{(\ell)}, \boldsymbol{q}^{(\ell)}, D^{(\ell)}) \right\|_{L^1(0,T;L^2(\Sigma))} \\
&\quad + \left\| \partial_\nu u(\boldsymbol{\alpha}^{(\ell)}, \boldsymbol{q}^{(\ell)}, D^{(\ell)}) - w \right\|_{L^1(0,T;L^2(\Sigma))} \\
&\le C \left(\sum_{j=1}^m \left| \alpha_j^* - \alpha_j^{(\ell)} \right| + \sum_{j=2}^m \left| q_j^* - q_j^{(\ell)} \right| + \|D^* - D^{(\ell)}\|_{C^1(\overline{\Omega})} \right) \\
&\quad + \left\| \partial_\nu u(\boldsymbol{\alpha}^{(\ell)}, \boldsymbol{q}^{(\ell)}, D^{(\ell)}) - w \right\|_{L^1(0,T;L^2(\Sigma))}.
\end{aligned}$$

Passing $\ell \to \infty$ and applying (6.34)–(6.36), we conclude

$$\|\partial_\nu u(\boldsymbol{\alpha}^*, \boldsymbol{q}^*, D^*) - w\|_{L^2(0,T;L^2(\Sigma))} \le \delta_0,$$

indicating that $(\boldsymbol{\alpha}^*, \boldsymbol{q}^*, D^*)$ is the desired minimizer by definition. □

6.4 Proof of Theorem 6.4

Independently of the previous section, now we study the long-time asymptotic behavior of the solution u to (6.1)–(6.3) with $F = 0$ by a Laplace transform argument. In this section, $C > 0$ denotes generic constants depending at most on $\Omega, \boldsymbol{\alpha}, \boldsymbol{q}, \mathcal{A}$ but independent of the initial value a.

Although an explicit representation (6.22) is available in this case, we write the solution in form of

$$u(\,\cdot\,,t) = \sum_{n=1}^{\infty} u_n(t)\varphi_n \quad (t > 0) \tag{6.37}$$

by use of the eigensystem $\{(\lambda_n, \varphi_n)\}$ of $\mathcal{A}$, where a direct calculation and the orthogonality of $\{\varphi_n\}$ yield

$$\begin{cases} \displaystyle\sum_{j=1}^{m} q_j \partial_t^{\alpha_j} u_n(t) + \lambda_n u_n(t) = 0 \quad (t > 0), \\ u_n(0) = (a, \varphi_n), \end{cases} \qquad n = 1, 2, \ldots. \tag{6.38}$$

The proof of Theorem 6.4 relies on the following lemma.

Lemma 6.5 *Let u_n $(n = 1, 2, \ldots)$ solve the initial value problem* (6.38)*. Then there exists a constant $C > 0$ such that*

$$\left| u_n(t) - \frac{q_m}{\lambda_n \Gamma(1-\alpha_m)} \frac{(a, \varphi_n)}{t^{\alpha_m}} \right| \le \frac{C|(a, \varphi_n)|}{\lambda_n t^{\min\{\alpha_{m-1}, 2\alpha_m\}}} \quad (t \gg 1). \tag{6.39}$$

Proof. We abbreviate $a_n := (a, \varphi_n)$ for simplicity. Applying the Laplace transform

$$(\mathcal{L}f)(s) := \int_0^{\infty} \mathrm{e}^{-st} f(t)\,\mathrm{d}t$$

to (6.38) and using the formula

$$\mathcal{L}(\partial_t^{\beta} f)(s) = s^{\beta}\mathcal{L}(f)(s) - s^{\beta-1} f(0+) \quad (0 < \beta < 1),$$

we are led to the transformed algebraic equation

$$\mathcal{L}(u_n)(s) = \frac{a_n}{w(s)} \sum_{j=1}^{m} q_j s^{\alpha_j - 1}, \quad w(s) := \sum_{j=1}^{m} q_j s^{\alpha_j} + \lambda_n.$$

Noting that the Laplace transform of u_n has a branch point zero, we should cut off the negative part of the real axis so that the function $w(s)$ does not vanish in the main sheet of the Riemann surface including its boundaries on the cut. In fact, for $s = r\,\mathrm{e}^{\mathrm{i}\theta}$, we see that $\sin(\alpha_j\theta)$ $(j = 1, \cdots, m)$ share the same signal and thus $\mathrm{Im}(w(s)) = \sum_{j=1}^{m} q_j r^{\alpha_j} \sin(\alpha_j\theta) \neq 0$ since $q_j > 0$. Therefore, the inverse Laplace transform of $\mathcal{L}(u_n)$ can be represented by an integral on the Hankel path $\mathrm{Ha}(0+)$ (i.e., the loop constituted by a small circle $|s| = \varepsilon$ with $\varepsilon \to 0$ and by the two borders of the cut negative real axis). Actually, it suffices to consider the following integral

$$\frac{1}{2\pi\,\mathrm{i}} \int_{\mathcal{C}} \mathcal{L}(u_n)(s)\,\mathrm{e}^{st}\,\mathrm{d}s \tag{6.40}$$

and estimate each

$$H_\ell(t; R) := \int_{\mathcal{C}_\ell} \mathcal{L}(u_n)(s)\,\mathrm{e}^{st}\,\mathrm{d}s \quad (\ell = 1, \cdots, 5),$$

where the loop $\mathcal{C}$ and its partitions $\mathcal{C}_\ell$ $(\ell = 1, \ldots, 5)$ are illustrated in Figure 6.1.

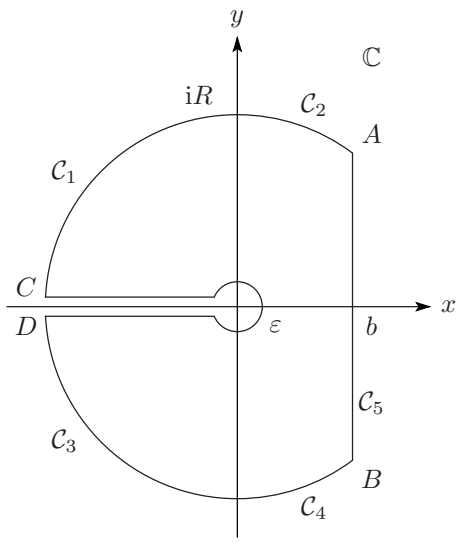

Figure 6.1: The loop $\mathcal{C}$ and its partition.

For $H_1(t;R)$, noting that $|s| = R > 1$ and using a change of variable, we have

$$\begin{aligned}|H_1(t;R)| &= \left|\int_{\mathcal{C}_1} \mathcal{L}(u_n)(s)\,\mathrm{e}^{st}\,\mathrm{d}s\right| \le C|a_n| \int_{\pi/2}^{\pi} R^{\alpha_m}\,\mathrm{e}^{Rt\cos\theta}\,\mathrm{d}\theta \\ &= C|a_n|R^{\alpha_m}\int_{-1}^{0} \frac{\mathrm{e}^{Rt\eta}}{\sqrt{1-\eta^2}}\,\mathrm{d}\eta \quad (t>0).\end{aligned}$$

Furthermore, we break up the above integral in $[-1,0]$ into two parts and calculate their bounds respectively as

$$\begin{aligned}R^{\alpha_m}\int_{-1}^{0} \frac{\mathrm{e}^{Rt\eta}}{\sqrt{1-\eta^2}}\,\mathrm{d}\eta &= R^{\alpha_m}\left(\int_{-1}^{-1/2} + \int_{-1/2}^{0}\right)\frac{\mathrm{e}^{Rt\eta}}{\sqrt{1-\eta^2}}\,\mathrm{d}\eta \\ &\le R^{\alpha_m}\,\mathrm{e}^{-Rt/2}\int_{-1}^{-1/2}\frac{\mathrm{d}\eta}{\sqrt{1-\eta^2}} + CR^{\alpha_m}\int_{-1/2}^{0}\mathrm{e}^{Rt\eta}\,\mathrm{d}\eta \\ &\le CR^{\alpha_m}\,\mathrm{e}^{-Rt/2} + CR^{\alpha_m-1}\frac{1-\mathrm{e}^{-Rt/2}}{t} \to 0 \quad \text{as } R\to\infty\ (t>0).\end{aligned}$$

Therefore, for any $t>0$, we see that $H_1(t;R)\to 0$ as $R\to\infty$. Similarly to the calculation of $H_1(t;R)$, we have $H_3(t;R)\to 0$ as $R\to\infty$ for any $t>0$. On the other hand, since $R\cos\theta \le b$ for all $\theta\in[\theta_R,\pi/2]$ where θ_R denotes the argument of point A, we have

$$\begin{aligned}|H_2(t;R)| &\le C|a_n|R^{\alpha_m}\int_{\theta_R}^{\pi/2}\mathrm{e}^{Rt\cos\theta}\,\mathrm{d}\theta \le C|a_n|R^{\alpha_m}\,\mathrm{e}^{bt}\left(\frac{\pi}{2}-\theta_R\right) \\ &= C|a_n|R^{\alpha_m}\,\mathrm{e}^{bt}\left(\frac{\pi}{2}-\arccos\frac{1}{R}\right)\to 0 \quad \text{as } R\to\infty.\end{aligned}$$

Therefore, since $w(s)$ has no zero in the main sheet of the Riemann surface including the boundaries on the cut, the integral in (6.40) vanishes. By Fourier-Mellin formula (see, e.g., [124]), we have

$$u_n(t) = \lim_{M\to\infty}\frac{1}{2\pi\,\mathrm{i}}\int_{b-\mathrm{i}M}^{b+\mathrm{i}M}\mathcal{L}(u_n)(s)\,\mathrm{e}^{st}\,\mathrm{d}s = \frac{1}{2\pi\,\mathrm{i}}\int_{\mathrm{Ha}(\varepsilon)}\mathcal{L}(u_n)(s)\,\mathrm{e}^{st}\,\mathrm{d}s.$$

Here the integral is taken on the segment from $b-\mathrm{i}M$ to $b+\mathrm{i}M$, and $\mathrm{Ha}(\varepsilon)$ denotes the Hankel path in $\mathbb{C}$ defined as

$$\mathrm{Ha}(\varepsilon) := \{s \in \mathbb{C};\, \arg s = \pm\pi,\ |s| \geq \varepsilon\} \cup \{s \in \mathbb{C};\, -\pi \leq \arg s \leq \pi,\ |s| = \varepsilon\}.$$

By a similar argument as above, we find

$$\frac{1}{\Gamma(1-\alpha_m)\, t^{\alpha_m}} = \lim_{M\to\infty} \frac{1}{2\pi\,\mathrm{i}} \int_{b-\mathrm{i}M}^{b+\mathrm{i}M} s^{\alpha_m - 1}\, \mathrm{e}^{st}\, \mathrm{d}s = \frac{1}{2\pi\,\mathrm{i}} \int_{\mathrm{Ha}(\varepsilon)} s^{\alpha_m - 1}\, \mathrm{e}^{st}\, \mathrm{d}s.$$

It is now straightforward to show that the contribution from the Hankel path $\mathrm{Ha}(\varepsilon)$ as $\varepsilon \to 0$ is provided by

$$u_n(t) - \frac{q_m a_n}{\lambda_n \Gamma(1-\alpha_m)\, t^{\alpha_m}} = a_n \int_0^\infty H(r, \lambda_n)\, \mathrm{e}^{-rt}\, \mathrm{d}r, \quad \text{where} \tag{6.41}$$

$$H(r, \lambda_n) := -\frac{1}{\pi} \operatorname{Im} \left\{ \left(\frac{1}{w(s)} \sum_{j=1}^m q_j s^{\alpha_j - 1} - \frac{q_m}{\lambda_n} s^{\alpha_m - 1} \right) \Bigg|_{s = r\,\mathrm{e}^{\mathrm{i}\pi}} \right\}.$$

To give the desired estimate (6.39), we observe that $|w(s)| \geq C\lambda_n$ as long as $r = |s| \leq \varepsilon_0 \lambda_n$, where $\varepsilon_0 > 0$ is sufficiently small. This indicates

$$\begin{aligned} |H(r, \lambda_n)| &\leq \left| \frac{\lambda_n \sum_{j=1}^{m-1} q_j s^{\alpha_j - 1} - \sum_{j=1}^m q_j q_m s^{\alpha_j + \alpha_m - 1}}{\lambda_n (\sum_{j=1}^m q_j s^{\alpha_j} + \lambda_n)} \right| \\ &\leq \frac{C|a_n|}{\lambda_n} \left(\sum_{j=1}^{m-1} |s|^{\alpha_j - 1} + \sum_{j=1}^m |s|^{\alpha_j + \alpha_m - 1} \right) \quad (\forall\, |s| \leq \varepsilon_0 \lambda_n). \end{aligned}$$

Meanwhile, for any $s = r\,\mathrm{e}^{\pm\mathrm{i}\pi}$ with $r \geq \varepsilon_0 \lambda_n$, we know that

$$|H(r, \lambda_n)| \leq \frac{\sum_{j=1}^{m-1} q_j r^{\alpha_j - 1}}{|\operatorname{Im} \sum_{j=1}^m q_j s^{\alpha_j}|} + \frac{\sum_{j=1}^m q_j q_m r^{\alpha_j + \alpha_m - 1}}{\lambda_n |\operatorname{Im} \sum_{j=1}^m q_j s^{\alpha_j}|} \leq C.$$

Using these estimates, we break up the integral in (6.41) into two parts and give respective bounds as

$$\begin{aligned} \left| \int_0^{\varepsilon_0 \lambda_n} H(r, \lambda_n)\, \mathrm{e}^{-rt}\, \mathrm{d}r \right| &\leq \frac{C}{\lambda_n} \int_0^\infty \left(\sum_{j=1}^{m-1} r^{\alpha_j - 1} + \sum_{j=1}^m r^{\alpha_j + \alpha_m - 1} \right) \mathrm{e}^{-rt}\, \mathrm{d}r \\ &\leq \frac{C}{\lambda_n} \left(\sum_{j=1}^{m-1} \frac{1}{t^{\alpha_j}} + \sum_{j=1}^m \frac{1}{t^{\alpha_j + \alpha_m}} \right), \\ \left| \int_{\varepsilon_0 \lambda_n}^\infty H(r, \lambda_n)\, \mathrm{e}^{-rt}\, \mathrm{d}r \right| &\leq C \int_{\varepsilon_0 \lambda_n}^\infty \mathrm{e}^{-rt}\, \mathrm{d}r = \frac{C}{t\, \mathrm{e}^{\varepsilon_0 \lambda_n t}} \leq \frac{C}{\lambda_n t^2}. \end{aligned}$$

Collecting the above two estimates, we obtain (6.39) for sufficiently large t. □

Proof of Theorem 6.4. Let u take the form of (6.37) which solves (6.1)–(6.3) with $a \in L^2(\Omega)$ and $F = 0$, and fix any $T > 0$ sufficiently large. For all $t \geq T$, it immediately follows from Lemma 6.5 and the eigenfunction expansion that

$$\left\| u(\,\cdot\,, t) - \frac{q_m}{\Gamma(1-\alpha_m)} \frac{\mathcal{A}^{-1} a}{t^{\alpha_m}} \right\|_{H^2(\Omega)} \leq C \left\| \sum_{n=1}^\infty \left(u_n(t) - \frac{q_m}{\lambda_n \Gamma(1-\alpha_m)} \frac{(a, \varphi_n)}{t^{\alpha_m}} \right) \varphi_n \right\|_{\mathcal{D}(\mathcal{A})}$$

$$
\begin{aligned}
&= C\left(\sum_{n=1}^{\infty}\left|\lambda_n u_n(t) - \frac{q_m}{\Gamma(1-\alpha_m)}\frac{(a,\varphi_n)}{t^{\alpha_m}}\right|^2\right)^{1/2}\\
&\le \frac{C}{t^{\min\{\alpha_{m-1},2\alpha_m\}}}\left(\sum_{n=1}^{\infty}|(a,\varphi_n)|^2\right)^{1/2}\\
&= \frac{C\|a\|_{L^2(\Omega)}}{t^{\min\{\alpha_{m-1},2\alpha_m\}}},
\end{aligned}
$$

implying $u \in C([T,\infty); H^2(\Omega)\cap H_0^1(\Omega))$. On the other hand, since Theorem 6.1(a) guarantees $u \in C([0,T]; L^2(\Omega))\cap C((0,T]; H^2(\Omega)\cap H_0^1(\Omega))$, the proof is finished by combining the regularity results in the finite and infinite time spans. □

Remark 6.3 If some q_{j_0} is negative, then we cannot obtain the asymptotic estimate for the solution u of the initial-boundary value problem (6.1)–(6.3). In fact, for some $n \in \mathbb{N}$ sufficiently large, we study the following problem

$$
\begin{cases}
\partial_t^{1/2}u - 3\lambda_n\partial_t^{1/4}u + \mathcal{A}u = 0 & \text{in } \Omega\times(0,\infty),\\
u = a_n\varphi_n = (a,\varphi_n)\varphi_n & \text{in } \Omega\times\{0\},\\
u = 0 & \text{on } \partial\Omega\times(0,\infty),
\end{cases}
$$

where (λ_n,φ_n) is the n-th pair in the eigensystem of the elliptic operator $\mathcal{A}$, and $a \in L^2(\Omega)$. The Laplace transform of the solution reads

$$
\mathcal{L}(u)(s) = \frac{a_n}{w(s)}\left(s^{-1/2} - 3\lambda_n s^{-3/4}\right)\varphi_n, \quad w(s) := s^{1/2} - 3\lambda_n s^{1/4} + \lambda_n.
$$

We see that $\{s;\, w(s) = 0\}$ is a finite set with all of the zero points having finite multiplicities in the main sheet of the Riemann surface, and there is no zero point on the negative part of the real axis since λ_n is sufficiently large. Furthermore, we can prove that there exist zeros of $w(s)$ having positive real parts. In fact, obviously

$$
r_\pm := \frac{3\lambda_n \pm \sqrt{9\lambda_n^2 - 4\lambda_n}}{2} > 0
$$

solves $w(r_\pm) = 0$, and we have

$$
w'(r_\pm) = \frac{1}{2}r_\pm^{-1/2} - \frac{3\lambda_n}{4}r_\pm^{-3/4} \ne 0.
$$

Note that

$$
\frac{1}{2\pi\,\mathrm{i}}\int_{\mathcal{C}}\mathcal{L}(u)(s)\,\mathrm{e}^{st}\,\mathrm{d}s = \sum \mathrm{Res}\{\mathcal{L}(u)(s)\,\mathrm{e}^{st},\mathcal{C}\},
$$

where $\mathcal{C}$ is defined in Figure 6.1, $\mathrm{Res}\{f,\mathcal{C}\}$ denotes the residue of function f in the domain enclosed by $\mathcal{C}$, and the sum is taken over all the poles of $\mathcal{L}(u)(s)\,\mathrm{e}^{st}$ in this domain. Repeating the argument in the proof of Lemma 6.5, we deduce

$$
u(t) = \lim_{M\to\infty}\frac{1}{2\pi\,\mathrm{i}}\int_{b-\mathrm{i}M}^{b+\mathrm{i}M}\mathcal{L}(u)(s)\,\mathrm{e}^{st}\mathrm{d}s = \sum \mathrm{Res}\{\mathcal{L}(u)(s)\,\mathrm{e}^{st}\} + \frac{1}{2\pi\,\mathrm{i}}\int_{\mathrm{Ha}(0+)}\mathcal{L}(u)(s)\,\mathrm{e}^{st}\,\mathrm{d}s.
$$

Here the sum is taken over all the poles of $\mathcal{L}(u)(s)\,\mathrm{e}^{st}$ lying on the left-hand side of the line $\{z = b + \mathrm{i}\,M;\, M \in \mathbb{R}\}$ with $b > r_+$, and there are only finite terms in this summation since $w(s)$ only has a finite number of zero points including multiplicities in the main sheet of the Riemann surface cutting of the negative axis. We can easily see that

$$
\mathrm{Res}\{(\mathcal{L}(u)(s)\,\mathrm{e}^{st})|_{s=r_\pm}\} = \frac{r_\pm^{-1/2} - 3\lambda_n r_\pm^{-3/4}}{w'(r_\pm)}\,\mathrm{e}^{r_\pm t}a_n\varphi_n.
$$

Of course $\mathrm{e}^{r_\pm t}$ tend to infinity as $t\to\infty$ since $r_\pm > 0$, indicating that the asymptotic behavior in Theorem 6.4 does not hold for this case.

6.5 Proofs of Lemmata 6.1–6.3

This section is devoted to the verifications of the technical lemmata regarding several important properties of the multinomial Mittag-Leffler functions in Section 6.3. To this end, first we recall the following formula for multinomial coefficients (see Berge [61])

$$\sum_{j=1}^{m}(k-1;k_1,\dots,k_{j-1},k_j-1,k_{j+1},\dots,k_m)=(k;k_1,\dots,k_m). \tag{6.42}$$

If some k_{j_0} vanishes, we understand $(k-1;k_1,\dots,k_{j_0-1},k_{j_0}-1,k_{j_0+1},\dots,k_m)=0$ and (6.42) degenerates to its lower dimensional version.

Proof of Lemma 6.1. According to definition (6.20), we directly calculate

$$\begin{aligned}
&\sum_{j=1}^{m} z_j E_{(\beta_1,\dots,\beta_m),\beta_0+\beta_j}(z_1,\dots,z_m)\\
&=\sum_{j=1}^{m}\sum_{k=0}^{\infty}\sum_{k_1+\cdots+k_m=k}\frac{(k;k_1,\dots,k_m)\,z_j\prod_{\ell=1}^{m}z_\ell^{k_\ell}}{\Gamma(\beta_0+\beta_j+\sum_{\ell=1}^{m}\beta_\ell k_\ell)}\\
&=\sum_{k=0}^{\infty}\sum_{j=1}^{m}\left\{\frac{z_j^{k+1}}{\Gamma(\beta_0+\beta_j(k+1))}+\sum_{\substack{k_1+\cdots+k_m=k\\ k_j<k}}\frac{(k;k_1,\dots,k_m)\,z_j\prod_{\ell=1}^{m}z_\ell^{k_\ell}}{\Gamma(\beta_0+\beta_j+\sum_{\ell=1}^{m}\beta_\ell k_\ell)}\right\} \qquad (6.43)\\
&=\sum_{k=0}^{\infty}\sum_{j=1}^{m}\left\{\frac{z_j^{k+1}}{\Gamma(\beta_0+\beta_j(k+1))}+\sum_{\substack{k_1+\cdots+k_m=k+1\\ 0<k_j<k+1}}\frac{(k;k_1,\dots,k_{j-1},k_j-1,k_{j+1},\dots,k_m)\prod_{\ell=1}^{m}z_\ell^{k_\ell}}{\Gamma(\beta_0+\sum_{\ell=1}^{m}\beta_\ell k_\ell)}\right\}\\
&=\sum_{k=0}^{\infty}\left\{\sum_{j=1}^{m}\frac{z_j^{k+1}}{\Gamma(\beta_0+\beta_j(k+1))}+\sum_{\substack{k_1+\cdots+k_m=k+1\\ k_\ell<k+1\ (\forall\,\ell)}}\frac{(k+1;k_1,\dots,k_m)\prod_{\ell=1}^{m}z_\ell^{k_\ell}}{\Gamma(\beta_0+\sum_{\ell=1}^{m}\beta_\ell k_\ell)}\right\} \qquad (6.44)\\
&=\sum_{k=0}^{\infty}\sum_{k_1+\cdots+k_m=k+1}\frac{(k+1;k_1,\dots,k_m)\prod_{\ell=1}^{m}z_j^{k_j}}{\Gamma(\beta_0+\sum_{\ell=1}^{m}\beta_\ell k_\ell)}\\
&=\sum_{k=1}^{\infty}\sum_{k_1+\cdots+k_m=k}\frac{(k;k_1,\dots,k_m)\prod_{\ell=1}^{m}z_\ell^{k_\ell}}{\Gamma(\beta_0+\sum_{\ell=1}^{m}\beta_\ell k_\ell)}=E_{(\beta_1,\dots,\beta_m),\beta_0}(z_1,\dots,z_m)-\frac{1}{\Gamma(\beta_0)},
\end{aligned}$$

where we apply formula (6.42) to obtain (6.44). In (6.43), we distill the case $k_j=k$ in the j-th term and substitute k_j+1 with k_j for the others to proceed to the next equality. □

Next, to give an estimate for the multinomial Mittag-Leffler function, we turn to a complex variable argument which is motivated by a similar treatment in [104].

Proof of Lemma 6.2. Let α_j, z_j $(j=1,\dots,m)$ and β be assumed as that in the statement of Lemma 6.2 and introduce the notation

$$E_{\boldsymbol{\alpha}',\beta}(z_1,\dots,z_m):=E_{(\alpha_1,\alpha_1-\alpha_2,\dots,\alpha_1-\alpha_m),\beta}(z_1,\dots,z_m).$$

In the sequel, we denote by C a general positive constant depending at most on μ, K, α_j $(j=1,\dots,m)$ and β. First we rewrite the multinomial Mittag-Leffler function (6.20) in an

alternative form with the aid of the contour integral representation of $1/\Gamma(z)$ (see [116, §1.1.6]) that

$$\frac{1}{\Gamma(z)} = \frac{1}{2\alpha_1\pi\,\mathrm{i}}\int_{\Upsilon(R,\theta)} \exp(\zeta^{1/\alpha_1})\zeta^{(1-z-\alpha_1)/\alpha_1}\,\mathrm{d}\zeta,$$

where $R>0$ is a constant to be determined later and $\alpha_1\pi/2<\theta<\mu$. Here $\gamma(R,\theta)$ denotes the contour

$$\Upsilon(R,\theta) := \{\zeta\in\mathbb{C};\ |\zeta|=R,\ |\arg(\zeta)|\le\theta\}\cup\{\zeta\in\mathbb{C};\ |\zeta|>R,\ |\arg(\zeta)|=\pm\theta\}.$$

Then it follows from the multinomial formula that

$$\begin{aligned}
&E_{\boldsymbol{\alpha}',\beta}(z_1,\dots,z_m)\\
&= \frac{1}{2\alpha_1\pi\,\mathrm{i}}\sum_{k=0}^{\infty}\sum_{k_1+\cdots+k_m=k}(k;k_1,\dots,k_m)\prod_{j=1}^{m} z_j^{k_j}\\
&\qquad\qquad\times\left\{\int_{\Upsilon(R,\theta)}\exp(\zeta^{1/\alpha_1})\zeta^{(1-\beta-\alpha_1(k+1)-\alpha_2k_2-\cdots-\alpha_mk_m)/\alpha_1}\,\mathrm{d}\zeta\right\}\\
&= \frac{1}{2\alpha_1\pi\,\mathrm{i}}\int_{\Upsilon(R,\theta)}\exp(\zeta^{1/\alpha_1})\zeta^{(1-\beta)/\alpha_1-1}\\
&\qquad\qquad\times\sum_{k=0}^{\infty}\left\{\sum_{k_1+\cdots+k_m=k}(k;k_1,\dots,k_m)\left(\frac{z_1}{\zeta}\right)^{k_1}\prod_{j=2}^{m}\left(\frac{z_j}{\zeta^{1-\alpha_j/\alpha_1}}\right)^{k_j}\right\}\mathrm{d}\zeta\\
&= \frac{1}{2\alpha_1\pi\,\mathrm{i}}\int_{\Upsilon(R,\theta)}\exp(\zeta^{1/\alpha_1})\zeta^{(1-\beta)/\alpha_1-1}\sum_{k=0}^{\infty}\left(\frac{z_1}{\zeta}+\sum_{j=2}^{m}\frac{z_k}{\zeta^{1-\alpha_j/\alpha_1}}\right)^{k}\mathrm{d}\zeta.
\end{aligned}$$

In order to guarantee the convergence of the summation with respect to k, it is required that

$$\left|\frac{z_1}{\zeta}+\sum_{j=2}^{m}\frac{z_j}{\zeta^{1-\alpha_j/\alpha_1}}\right|<1,\quad\forall\,\zeta\in\Upsilon(R,\theta).$$

Since $|z_j|\le K$ for $j=2,\dots,m$, the above inequality is achieved by taking R such that

$$R>|z_1|+K\sum_{j=2}^{m}R^{\alpha_j/\alpha_1}.$$

Moreover, if we restrict, for example, $|z_1|\le K$, then R can be fixed as a constant depending only on K and α_j $(j=1,\dots,m)$. Now we deduce for $|z_j|\le K$ $(j=1,\dots,m)$ that

$$E_{\boldsymbol{\alpha}',\beta}(z_1,\dots,z_m) = \frac{1}{2\alpha_1\pi\,\mathrm{i}}\int_{\Upsilon(R,\theta)}\frac{\exp(\zeta^{1/\alpha_1})\zeta^{(1-\beta)/\alpha_1}}{\zeta-z_1-\sum_{j=2}^{m}z_j\zeta^{\alpha_j/\alpha_1}}\,\mathrm{d}\zeta. \tag{6.45}$$

Next we fix $z_2,\dots,z_m$ as negative parameters and regard both sides of (6.45) as functions of the single complex variable z_1, which allows the application of the principle of analytic continuation to extend equality (6.45) to a domain including $\{z_1\in\mathbb{C};\ \mu\le|\arg(z_1)|\le\pi\}$ (see Figure 6.2).

For $|z_1|>R$, we investigate the denominator of the integrand in (6.45). Since $z_j<0$ and $\alpha_j<\alpha_1$ for $j=2,\dots,m$, it turns out that the curve $\zeta-\sum_{j=2}^{m}z_j\zeta^{\alpha_j/\alpha_1}$ $(\zeta\in\Upsilon(R,\theta))$ locates on the right-hand side of $\Upsilon(R,\theta)$; that is, $\Upsilon(R,\theta)$ is shifted by the term $-\sum_{j=2}^{m}z_j\zeta^{\alpha_j/\alpha_1}$ to the positive direction. This observation immediately implies

$$\min_{\zeta\in\Upsilon(R,\theta)}\left|\zeta-z_1-\sum_{j=2}^{m}z_j\zeta^{\alpha_j/\alpha_1}\right|\ge\min_{\zeta\in\Upsilon(R,\theta)}|\zeta-z_1|\ge|z_1|\sin(\mu-\theta).$$

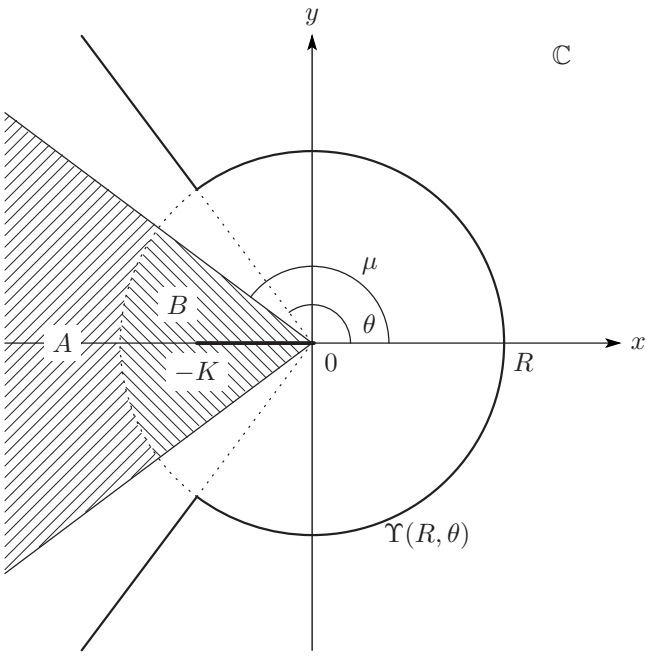

Figure 6.2: Settings of Lemma 6.2 and the contour $\Upsilon(R,\theta)$. If z_1 is located in the shaded domain A, we employ the principle of analytic continuation and the contour integral representation (6.45). When z_1 is in the shaded domain B, it suffices to argue by definition (6.20).

Therefore, we come up with the estimate

$$\begin{aligned}|E_{\boldsymbol{\alpha}',\beta}(z_1,\dots,z_m)| &= \frac{1}{2\alpha_1\pi}\left|\int_{\Upsilon(R,\theta)} \frac{\exp(\zeta^{1/\alpha_1})\zeta^{(1-\beta)/\alpha_1}}{\zeta - z_1 - \sum_{j=2}^m z_j\zeta^{\alpha_j/\alpha_1}}\,\mathrm{d}\zeta\right| \\ &\le \left(\frac{1}{2\alpha_1\pi\sin(\mu-\theta)}\int_{\Upsilon(R,\theta)} |\exp(\zeta^{1/\alpha_1})||\zeta^{(1-\beta)/\alpha_1}|\,\mathrm{d}\zeta\right)\frac{1}{|z_1|}.\end{aligned}$$

The integral along $\Upsilon(R,\theta)$ converges, because for ζ such that $\arg(\zeta) = \pm\theta$ and $|\zeta| > R$, there holds

$$|\exp(\zeta^{1/\alpha_1})| = \exp(|\zeta|^{1/\alpha_1}\cos(\theta/\alpha_1)) \quad \text{with } \cos(\theta/\alpha_1) < 0,$$

while the integral on the arc $\{\zeta\in\mathbb{C};\ |\zeta| = R,\ |\arg(\zeta)|\le\theta\}$ is a constant. Consequently

$$|E_{\boldsymbol{\alpha}',\beta}(z_1,\dots,z_m)| \le \frac{C}{|z_1|}, \quad \mu \le |\arg(z_1)| \le \pi,\ |z_1| > R. \tag{6.46}$$

For $\mu \le |\arg(z_1)| \le \pi$ such that $|z_1| \le R$, it is directly verified that

$$\begin{aligned}|E_{\boldsymbol{\alpha}',\beta}(z_1,\dots,z_m)| &= \left|\sum_{k=0}^\infty \sum_{k_1+\cdots+k_m=k} \frac{(k;k_1,\dots,k_m)\prod_{j=1}^m z_j^{k_j}}{\Gamma(\beta+\alpha_1 k - \sum_{j=2}^m \alpha_j k_j)}\right| \\ &\le \sum_{k=0}^\infty \sum_{k_1+\cdots+k_m=k} \frac{(k;k_1,\dots,k_m)\prod_{j=1}^m |z_j|^{k_j}}{\Gamma(\beta+\alpha_1 k - \sum_{j=2}^m \alpha_j k_j)} \\ &\le C\sum_{k=0}^\infty \sum_{k_1+\cdots+k_m=k} \frac{(k;k_1,\dots,k_m)\prod_{j=1}^m |z_j|^{k_j}}{\Gamma(\beta+(\alpha_1-\alpha_2)k)} \\ &= C\sum_{k=0}^\infty \frac{1}{\Gamma(\beta+(\alpha_1-\alpha_2)k)}\left(\sum_{j=1}^m |z_j|\right)^k \le C\sum_{k=0}^\infty \frac{(R+(m-1)K)^k}{\Gamma(\beta+(\alpha_1-\alpha_2)k)} \le C,\end{aligned}$$

which, together with (6.46), finishes the proof. □

Finally, we treat Lemma 6.3. Here we recall the abbreviation $E^{(n)}_{\boldsymbol{\alpha}',\beta}(t)$ in (6.21).

Proof of Lemma 6.3. By definition, we carry out a direct differentiation and utilize the formula $\Gamma(s) = \Gamma(s+1)/s$ to derive

$$\begin{aligned}
&\frac{\mathrm{d}}{\mathrm{d}t}\left\{t^{\alpha_1}E^{(n)}_{\boldsymbol{\alpha}',1+\alpha_1}(t)\right\}\\
&= \frac{\mathrm{d}}{\mathrm{d}t}\left\{\sum_{k=0}^{\infty}\sum_{k_1+\cdots+k_m=k}\frac{(k;k_1,\dots,k_m)(-\lambda_n)^{k_1}\prod_{j=2}^m(-q_j)^{k_j}t^{\alpha_1(k+1)-\alpha_2k_2-\cdots-\alpha_mk_m}}{\Gamma(1+\alpha_1(k+1)-\sum_{j=2}^m\alpha_jk_j)}\right\}\\
&= \sum_{k=0}^{\infty}\sum_{k_1+\cdots+k_m=k}\frac{(k;k_1,\dots,k_m)(-\lambda_n)^{k_1}\prod_{j=2}^m(-q_j)^{k_j}t^{\alpha_1(k+1)-\alpha_2k_2-\cdots-\alpha_mk_m-1}}{\Gamma(\alpha_1(k+1)-\sum_{j=2}^m\alpha_jk_j)}\\
&= t^{\alpha_1-1}\sum_{k=0}^{\infty}\sum_{k_1+\cdots+k_m=k}\frac{(k;k_1,\dots,k_m)(-\lambda_nt^{\alpha_1})^{k_1}\prod_{j=2}^m(-q_jt^{\alpha_1-\alpha_j})^{k_j}}{\Gamma(\alpha_1+\alpha_1k_1+\sum_{j=2}^m(\alpha_1-\alpha_j)k_j)}\\
&= t^{\alpha_1-1}E^{(n)}_{\boldsymbol{\alpha}',\alpha_1}(t).
\end{aligned}$$

Here we use the fact that $t^{\alpha_1}E^{(n)}_{\boldsymbol{\alpha}',1+\alpha_1}(t)$ is real analytic for $t>0$ so that termwise differentiations are available. □

6.6 Concluding remarks

We summarize this chapter by providing several concluding remarks. Concerning the initial-boundary value problem (6.1)–(6.3) for multi-term time-fractional diffusion equations, we mainly investigate the well-posedness and the long-time asymptotic behavior of the solution, which turn out to be mostly parallel to those of the single-term prototype. On the basis of the representation of solutions and a careful analysis of multinomial Mittag-Leffler functions, we succeed in dominating the solutions by the initial value a and the source term F. Although uniqueness and stability also follow from the maximum principle developed in [103], we carry out various estimates so that regularity and short-time asymptotic behaviors of the solutions are directly connected with the regularity of a and F (see Theorems 6.1–6.2). Furthermore, in Theorem 6.3 we establish the Lipschitz stability of the solution with respect to α_j, q_j and the diffusion coefficient, which is not only important by itself but also applicable to the corresponding inverse coefficient problem when treated by a minimization approach (see [96, Theorem 5]).

Simultaneously, we also obtain an extended version of [121, Corollary 2.6] in Theorem 6.4, which asserts that, if the solution does not vanish identically, then its decay rate cannot be faster than $t^{-\alpha_m}$, where α_m is the minimum order of fractional time-derivative. It is a remarkable property of fractional diffusion equations because the classical diffusion equation admits non-zero solutions decaying exponentially. This characterizes the slow diffusion in contrast to the classical one.

In the formulation of the initial-boundary value problem, we emphasize that the coefficients q_j of the time derivatives are positive constants because this assumption is obligatory not only to acquire explicit solutions but also to apply the Laplace transform in time, which are essential in the discussions of well-posedness and asymptotic behavior, respectively. On the other hand, if q_j are space-dependent, then explicit solutions are not available so that one should rely on a fixed point argument for the unique existence of solution, and the improvement of regularity

in space is strictly less than 2 orders (see [60, Theorem 2]). On the other hand, if some q_{j_0} is negative, then one may construct a counterexample in which the asymptotic property fails (see Remark 6.3).

However, in view of practical applications and theoretical interests, the linear non-symmetric diffusion equation with positive variable coefficients of Caputo derivatives in time can be regarded as a more feasible model equation than that we have studied in this chapter, but it will be definitely more challenging. Though still under consideration, we expect to establish parallel results for this more generalized case.

Chapter 7

The Galerkin Finite Element Method for Multi-Term Time-Fractional Diffusion Equations

Based on the theoretical results obtained in the previous chapter, here we consider the numerical treatments for the initial-boundary value problem for a multi-term time-fractional diffusion equation on a bounded convex polyhedral domain. We analyze a space semidiscrete scheme based on the standard Galerkin finite element method using continuous piecewise linear functions. Nearly optimal error estimates for both cases of initial data and inhomogeneous term are derived, which cover both smooth and nonsmooth data. Further we develop a fully discrete scheme based on a finite difference discretization of the time-fractional derivatives, and discuss its stability and error estimate. Extensive numerical experiments for one- and two-dimensional problems confirm the theoretical convergence rates.

7.1 Introduction

In this chapter, we consider the following initial-boundary value problem for a multi-term time fractional diffusion equation

$$\begin{cases} \displaystyle\sum_{j=1}^{m} q_j \partial_t^{\alpha_j} u(x,t) = \triangle u(x,t) + F(x,t) & (x \in \Omega,\ 0 < t \le T), \\ u(x,0) = a(x) & (x \in \Omega), \\ u(x,t) = 0 & (x \in \partial\Omega,\ 0 < t \le T), \end{cases} \tag{7.1}$$

where $T > 0$, Ω is a bounded convex polygonal domain in $\mathbb{R}^d$ ($d = 1, 2, 3$) with a boundary $\partial\Omega$, and $\partial_t^{\alpha_j} u$ denotes the Caputo derivative (see [86, p. 91]). The above problem is a special case of (6.1)–(6.3) investigated in the previous chapter, that is, the operator $\mathcal{A} = -\triangle$ instead of a general symmetric elliptic operator. Here we inherit the assumptions on the positive coefficients α_j and q_j ($j = 1, 2, \ldots, m$), that is, $1 > \alpha_1 > \cdots > \alpha_m > 0$ and $q_1 = 1$. For later convenience, we abbreviate $\boldsymbol{\alpha} = (\alpha_1, \ldots, \alpha_m)$ and $\boldsymbol{q} = (q_1, \ldots, q_m)$.

In the case of $m = 0$, the model (7.1) reduces to its single-term counterpart

$$\partial_t^{\alpha} u = \triangle u + F \quad \text{in } \Omega \times (0, T]. \tag{7.2}$$

This model has been studied extensively from different aspects due to its extraordinary capability of modeling anomalous diffusion phenomena in highly heterogeneous aquifers and complex viscoelastic materials [58, 114]. It is the fractional analogue of the classical diffusion equation: with $\alpha = 1$, it recovers the latter, and thus inherits some of its analytical properties. However, it differs considerably from the latter in the sense that, due to the presence of the nonlocal fractional derivative term, it has limited smoothing property in space and slow asymptotic decay in time [121], which in turn also impacts related numerical analysis [81] and inverse problems [83, 121].

The model (7.1) was developed to improve the modeling accuracy of the single-term model (7.2) for describing anomalous diffusion. For example, in [125], a two-term fractional-order diffusion model was proposed for the total concentration in solute transport, in order to distinguish explicitly the mobile and immobile status of the solute using fractional dynamics. The kinetic equation with two fractional derivatives of different orders appears also quite naturally when describing subdiffusive motion in velocity fields [110]; see also [85] for discussions on the model for wave-type phenomena.

There are very few mathematical studies on the model (7.1). Luchko [103] established a maximum principle for problem (7.1), and constructed a generalized solution for the case $F \equiv 0$ using the multinomial Mittag-Leffler function. Jiang et al. [77] derived formal analytical solutions for the diffusion equation with fractional derivatives in both time and space. Li and Yamamoto [94] established the existence, uniqueness, and the Hölder regularity of the solution using a fixed point argument for problem (7.1) with variable coefficients $\{q_j\}$. Very recently, Li et al. [88] showed the uniqueness and continuous dependence of the solution on the initial value a and the source term F, by exploiting several properties of the multinomial Mittag-Leffler function.

The potential applications of the model (7.1) motivate the design and analysis of numerical schemes that have optimal (with respect to data regularity) convergence rates. Such schemes are especially valuable for problems where the solution has low regularity. The case $m = 0$, i.e., the single-term model (7.2), has been extensively studied, and stability and error estimates were provided; see [97, 126, 131] for the finite difference method, [90, 91, 130] for the spectral method, [79–81,92,107,112,113] for the finite element method, and [62,69] for meshfree methods based on radial basis functions, to name a few. In particular, in [79–81], the authors established almost optimal error estimates with respect to the regularity of the initial data a and the right-hand side F for a semidiscrete Galerkin scheme. These studies include the interesting case of very weak data, i.e., $a \in \mathcal{D}(\mathcal{A}^\gamma)$ and $F \in L^\infty(0, T; \mathcal{D}(\mathcal{A}^\gamma))$ for $-1/2 < \gamma < 0$ (see Subsection 7.2.1 for the definition of the fractional power $\mathcal{A}^\gamma$ and the domain $\mathcal{D}(\mathcal{A}^\gamma)$).

Numerical methods for the multi-term case for an ordinary differential equation were considered in [68,84]. In [133], a scheme based on the finite element method in space and a specialized finite difference method in time was proposed for (7.1), and error estimates were derived. We also refer to [98] for a numerical scheme based on a fractional predictor.corrector method for the multi-term time fractional wave-diffusion equation. The error analysis in these works is done under the assumption that the solution is sufficiently smooth and therefore it excludes the case of low regularity solutions. This is the main goal of the present study. However, the derivation of optimal with respect to the regularity error estimates requires additional analysis of the properties of problem (7.1), e.g., stability, asymptotic behavior for $t \downarrow 0$. Relevant results of this type have recently been obtained in [88], which, however, are not enough for the analysis of the semidiscrete Galerkin scheme, and hence in Section 7.2, we make the necessary extensions.

Now we describe the semidiscrete Galerkin scheme. Let $\{\mathcal{T}_h\}_{0<h<1}$ be a family of shape regular and quasi-uniform partitions of the domain Ω into d-simplexes, called finite elements, with a maximum diameter h. The approximate solution u_h is sought in the finite element space X_h of continuous piecewise linear functions over the triangulation $\mathcal{T}_h$

$$X_h = \left\{ f \in H_0^1(\Omega);\ f \text{ is linear over } \omega,\ \forall\, \omega \in \mathcal{T}_h \right\}.$$

The semidiscrete Galerkin FEM for problem (7.1) is: find $u_h(t) \in X_h$ such that

$$\begin{cases} \displaystyle\sum_{j=1}^{m} q_j \left(\partial_t^{\alpha_j} u_h(t), v_h\right) + (\nabla u_h(t), \nabla v_h) = (F_h(t), v_h) \quad (\forall\, v_h \in X_h,\ 0 < t \le T), \\ u_h(0) = a_h, \end{cases} \tag{7.3}$$

where a_h and $F_h(t)$ are appropriate approximations of the initial data a and the source term $F(\,\cdot\,, t)$ whose choice will depend on their smoothness. We shall study the convergence of the semidiscrete Galerkin FEM (7.3) for the case of initial data $a \in \mathcal{D}(\mathcal{A}^\gamma)$, $-1/2 < \gamma \le 1$, and right-hand side $F \in L^\infty(0, T; \mathcal{D}(\mathcal{A}^\gamma))$, $-1/2 < \gamma \le 1/2$. The case of nonsmooth data, i.e., $-1/2 < \gamma < 0$, is very common in inverse problems and optimal control (see [83, 121]); see also [64, 82] for the parabolic counterpart.

The goal of this chapter is to develop a numerical scheme based on the finite element approximation for the model (7.1), and provide a complete error analysis. We derive error estimates optimal with respect to the data regularity for the semidiscrete scheme, and a convergence rate $\mathcal{O}(h^2 + \tau^{2-\alpha_1})$ for the fully discrete scheme in case of a smooth solution, where τ is the step size in time, and α_1 is the highest order of the Caputo derivatives in (7.1). Specifically, our essential contributions are as follows. First, we generalize the regularity results in the previous chapter by allowing less regular initial value and source term (see Theorems 7.1–7.3). Second, we derive nearly optimal error estimates for a semidiscrete Galerkin scheme for both homogeneous and inhomogeneous problems (see Theorems 7.4–7.7, which cover both smooth and nonsmooth data. Third, we develop a fully discrete scheme based on a finite difference method in time, and establish its stability and error estimates (see Theorem 7.8). We note that the derived error estimate for the fully discrete scheme holds only for smooth solutions.

The rest of the chapter is organized as follows. In Section 7.2, we first recall properties of Mittag-Leffler functions introduced in Chapter 6, and then refine the well-posedness results to cover lower regularity cases. The readers not interested in the analysis may proceed directly to Section 7.3, where almost optimal error estimates for their semidiscrete Galerkin finite element approximations are given. Then a fully discrete scheme based on a finite difference approximation of the Caputo fractional derivatives is given in Section 7.4, and an error analysis is also provided. Finally, extensive numerical experiments are presented to illustrate the accuracy and efficiency of the Galerkin scheme, and to verify the convergence theory. In the sequel, we denote by C a generic constant, which may differ at different occurrences, but always independent of the mesh size h and time step size τ.

7.2 Well-posedness and refined estimates

This section is concerned with the well-posedness of problem (7.1). We generalize and refine the regularity results obtained in the previous chapter for the homogeneous and inhomogeneous problems.

7.2.1 Preliminary

For the sake of self-containedness, we recall the general notations and the multinomial Mittag-Leffler functions for the solution representation, which were introduced in Chapter 6.

Let $L^2(\Omega)$ be the usual L^2-space equipped with the inner produce $(\,\cdot\,,\,\cdot\,)$. Denote by $H_0^1(\Omega)$, $H^{-1}(\Omega)$, etc. the Sobolev spaces (see, e.g., Adams [1]). For simplicity, $(\,\cdot\,,\,\cdot\,)$ will also refer to the pairing between $H^{-1}(\Omega)$ and $H_0^1(\Omega)$ throughout this chapter. Let $\{\lambda_n, \varphi_n\}_{n=1}^{\infty}$ be the eigensystem of $\mathcal{A} = -\triangle$ such that $0 < \lambda_1 < \lambda_2 \le \cdots$, $\lambda_n \to \infty$ as $n \to \infty$ and $\{\varphi_n\} \subset H^2(\Omega) \cap H_0^1(\Omega)$ forms an orthonormal basis of $L^2(\Omega)$. Then the fractional power $\mathcal{A}^\gamma$ is well-defined for $\gamma \ge -1/2$ (see, e.g., Pazy [115]) with

$$\mathcal{D}(\mathcal{A}^\gamma) = \left\{ f \in H^{-1}(\Omega);\ \sum_{n=1}^{\infty} |\lambda_n^\gamma (f, \varphi_n)|^2 \le \infty \right\}, \quad \mathcal{A}^\gamma f := \sum_{n=1}^{\infty} \lambda_n^\gamma (f, \varphi_n)\varphi_n,$$

and $\mathcal{D}(\mathcal{A}^\gamma)$ is a Hilbert space with the norm

$$\|f\|_{\mathcal{D}(\mathcal{A}^\gamma)} = \left(\sum_{n=1}^{\infty} |\lambda_n^\gamma (f, \varphi_n)|^2 \right)^{1/2}.$$

We know that $\{\lambda_n^{1/2}\varphi_n\}_{n=1}^{\infty}$ forms an orthonormal basis in $H^{-1}(\Omega)$, and $\|\cdot\|_{\mathcal{D}(\mathcal{A}^{-1/2})} \sim \|\cdot\|_{H^{-1}(\Omega)}$ is the norm in $H^{-1}(\Omega)$. Further, it is easy to verify that $\|f\|_{\mathcal{D}(\mathcal{A}^{1/2})} = \|\nabla f\|_{L^2(\Omega)}$ is also the norm in $H_0^1(\Omega)$, and $\|f\|_{\mathcal{D}(\mathcal{A})} = \|\triangle f\|_{L^2(\Omega)}$ is equivalent to the norm in $H^2(\Omega) \cap H_0^1(\Omega)$ (see [127, Lemma 3.1]). Note that $\{\mathcal{D}(\mathcal{A}^\gamma)\}_{\gamma \ge -1/2}$ forms a Hilbert scale of interpolation spaces, and $\mathcal{D}(\mathcal{A}^\gamma) \subset H^{2\gamma}(\Omega)$ for $\gamma > 0$. For $1 \le p \le \infty$, we say that $f \in L^p(0, T; \mathcal{D}(\mathcal{A}^\gamma))$ provided

$$\|f\|_{L^p(0,T;\mathcal{D}(\mathcal{A}^\gamma))} := \left\{ \begin{array}{ll} \displaystyle\left(\int_0^T \|f(\,\cdot\,, t)\|_{\mathcal{D}(\mathcal{A}^\gamma)}^p \, \mathrm{d}t \right)^{1/p} & \text{if } 1 \le p < \infty \\ \displaystyle\operatorname*{ess\,sup}_{0<t<T} \|f(\,\cdot\,, t)\|_{\mathcal{D}(\mathcal{A}^\gamma)} & \text{if } p = \infty \end{array} \right\} < \infty.$$

In order to represent the solution to (7.1), we shall utilize the multinomial Mittag-Leffler function defined as (see Luchko and Gorenflo [104])

$$E_{(\beta_1,\ldots,\beta_m),\beta_0}(z_1, \ldots, z_m) := \sum_{k=0}^{\infty} \sum_{k_1+\cdots+k_m=k} \frac{(k; k_1, \ldots, k_m) \prod_{j=1}^m z_j^{k_j}}{\Gamma(\beta_0 + \sum_{j=1}^m \beta_j k_j)}.$$

Here $0 < \beta_0 < 2$, $0 < \beta_j < 1$, $z_j \in \mathbb{C}$ $(j = 1, \ldots, m)$, and $(k; k_1, \ldots, k_m)$ denotes the multinomial coefficiet

$$(k; k_1, \ldots, k_m) := \frac{k!}{k_1! \cdots k_m!} \quad \text{with } k = \sum_{j=1}^m k_j,$$

where k_j $(j = 1, \ldots, m)$ are non-negative integers.

Concerning the properties of the multinomial Mittag-Leffler functions, we recall the following lemmata proved in Chapter 6, which will play important roles in refining the regularity results.

Lemma 7.1 *Let $0 < \beta_0 < 2$, $0 < \beta_j < 1$ $(j = 1, \ldots, m)$ and $z_j \in \mathbb{C}$ $(j = 1, \ldots, m)$ be fixed. Then*

$$\frac{1}{\Gamma(\beta_0)} + \sum_{j=1}^m z_j E_{(\beta_1,\ldots,\beta_m),\beta_0+\beta_j}(z_1, \ldots, z_m) = E_{(\beta_1,\ldots,\beta_m),\beta_0}(z_1, \ldots, z_m).$$

Lemma 7.2 *Let $0 < \beta < 2$ and $1 > \alpha_1 > \cdots > \alpha_m > 0$ be given. Assume that $\alpha_1\pi/2 < \mu < \alpha_1\pi$, $\mu \le |\arg(z_1)| \le \pi$ and there exists $K > 0$ such that $-K \le z_j < 0$ $(j = 2, \dots, m)$. Then there exists a constant $C > 0$ depending only on μ, K, α_j $(j = 1, \dots, m)$ and β such that*

$$|E_{(\alpha_1,\alpha_1-\alpha_2,\dots,\alpha_1-\alpha_m),\beta}(z_1, \dots, z_m)| \le \frac{C}{1 + |z_1|}.$$

For later use, we adopt the same abbreviation

$$E^{(n)}_{\boldsymbol{\alpha}',\beta}(t) := E_{(\alpha_1,\alpha_1-\alpha_2,\dots,\alpha_1-\alpha_m),\beta}(-\lambda_n t^{\alpha_1}, -q_2 t^{\alpha_1-\alpha_2}, \dots, -q_m t^{\alpha_1-\alpha_m}) \quad (t > 0)$$

as (6.21), where λ_n is the n-th eigenvalue of $\mathcal{A}$, $0 < \beta < 2$, and α_j, q_j are those positive constants in (7.1). To treat the inhomogeneous case, i.e., the source term $F \neq 0$, we need the following key lemma.

Lemma 7.3 *For each $n = 1, 2, \dots$, the function $t^{\alpha_1-1}E^{(n)}_{\boldsymbol{\alpha}',\alpha_1}(t)$ is completely monotone. Moreover, there exists a constant $C = C(\boldsymbol{\alpha}) > 0$ such that*

$$\int_0^t \left| s^{\alpha_1-1} E^{(n)}_{\boldsymbol{\alpha}',\alpha_1}(s) \right| \mathrm{d}s \le \frac{C}{\lambda_n} \quad (t > 0).$$

According to the previous chapter, we can write the explicit solution to (7.1) by using the multinomial Mittag-Leffler functions and the eigensystem $\{\lambda_n, \varphi_n\}$ as

$$u(\,\cdot\,, t) = \sum_{n=1}^{\infty} \left(1 - \lambda_n t^{\alpha_1} E^{(n)}_{\boldsymbol{\alpha}',1+\alpha_1}(t)\right)(a, \varphi_n)\varphi_n + \int_0^t U(s)F(\,\cdot\,, t-s)\,\mathrm{d}s \quad (0 < t \le T), \quad (7.4)$$

where

$$U(t)f := t^{\alpha_1-1} \sum_{n=1}^{\infty} E^{(n)}_{\boldsymbol{\alpha}',\alpha_1}(t)(f, \varphi_n)\varphi_n \quad (f \in \mathcal{D}(\mathcal{A}^{-1/2})). \quad (7.5)$$

The operator $U(t)$ has the following smoothing property.

Lemma 7.4 *Fix $f \in \mathcal{D}(\mathcal{A}^\gamma)$ with some $\gamma \in (-1/2, 1]$. Then for any $0 < t \le T$, there exists a constant $C = C(\Omega, T, \boldsymbol{\alpha}, \boldsymbol{q}) > 0$ such that for $0 \le \kappa - \gamma \le 1$, there holds*

$$\|U(t)f\|_{\mathcal{D}(\mathcal{A}^\kappa)} \le C\|f\|_{\mathcal{D}(\mathcal{A}^\gamma)} t^{\alpha_1(1+\gamma-\kappa)-1}.$$

Proof. The definition (7.5) of $U(t)$ and Lemma 7.2 immediately yield

$$\begin{aligned}
\|U(t)\|^2_{\mathcal{D}(\mathcal{A}^\kappa)} &= t^{2(\alpha_1-1)} \sum_{n=1}^{\infty} \left| \lambda_n^\kappa E^{(n)}_{\boldsymbol{\alpha}',\alpha_1}(t)(f, \varphi_n) \right|^2 \\
&= t^{2(\alpha_1(1+\gamma-\kappa)-1)} \sum_{n=1}^{\infty} \left| (\lambda_n t^{\alpha_1})^{\kappa-\gamma} E^{(n)}_{\boldsymbol{\alpha}',\alpha_1}(t) \right|^2 |\lambda_n^\gamma (f, \varphi_n)|^2 \\
&\le \left(C\, t^{\alpha_1(1+\gamma-\kappa)-1} \right)^2 \sum_{n=1}^{\infty} \left| \frac{(\lambda_n t^{\alpha_1})^{\kappa-\gamma}}{1 + \lambda_n t^{\alpha_1}} \right|^2 |\lambda_n^\gamma (f, \varphi_n)|^2 \\
&\le \left(C\, t^{\alpha_1(1+\gamma-\kappa)-1} \right)^2 \sum_{n=1}^{\infty} |\lambda_n^\gamma (f, \varphi_n)|^2 = \left(C\|f\|_{\mathcal{D}(\mathcal{A}^\gamma)} t^{\alpha_1(1+\gamma-\kappa)-1} \right)^2,
\end{aligned}$$

where in the second inequality we use the fact

$$\frac{(\lambda_n t^{\alpha_1})^{\kappa-\gamma}}{1 + \lambda_n t^{\alpha_1}} \le \left\{ \begin{array}{l} \dfrac{1}{1 + \lambda_n t^{\alpha_1}} \text{ if } \lambda_n t^{\alpha_1} \le 1 \\ \dfrac{\lambda_n t^{\alpha_1}}{1 + \lambda_n t^{\alpha_1}} \text{ if } \lambda_n t^{\alpha_1} \ge 1 \end{array} \right\} \le 1$$

since $0 \le \kappa - \gamma \le 1$. □

7.2.2 Solution regularity

First we recall known regularity results. In [94], Li and Yamamoto investigated the same problem under a more general setting of variable coefficients, namely, $q_j = q_j(x)$ $(j = 2, \dots, m)$. It reveals that the unique mild solution u satisfies

$$u \in \begin{cases} C((0,T]; \mathcal{D}(\mathcal{A}^{1-\epsilon})) \cap C([0,T]; L^2(\Omega)), & \text{when } a \in L^2(\Omega),\ F = 0, \\ C([0,T]; \mathcal{D}(\mathcal{A}^{1-\epsilon})) \cap L^\infty(0,T; H^2(\Omega) \cap H_0^1(\Omega)), & \text{when } a = 0,\ F \in L^\infty(0,T; L^2(\Omega)), \end{cases}$$

where $\epsilon > 0$ can be arbitrarily small. In Chapter 6, these results were refined for the case of constant coefficients, i.e., problem (6.1)–(6.3). In particular, it was shown that for $a \in \mathcal{D}(\mathcal{A}^\gamma)$ with $\gamma \in [0,1]$ and $F = 0$, there holds $u \in L^{1/(1-\gamma)}(0,T; H^2(\Omega) \cap H_0^1(\Omega))$. For $a = 0$ and $F \in L^p(0,T; \mathcal{D}(\mathcal{A}^\gamma))$ with $p \in [1,\infty], \gamma \in [0,1]$, there holds $u \in L^p(0,T; \mathcal{D}(\mathcal{A}^{\gamma+1-\epsilon}))$ for arbitrarily small $\epsilon > 0$. Here we follow the same approach and extend these results to a slightly more general setting, namely $a \in \mathcal{D}(\mathcal{A}^\gamma)$ and $F \in L^2(0,T; \mathcal{D}(\mathcal{A}^\gamma))$ with $\gamma \in (-1/2, 1]$. The nonsmooth case, i.e., $\gamma < 0$, arises commonly in related inverse problems and optimal control problems.

As before, we shall separate the cases of $F = 0$ and $a = 0$ to derive the regularities of the solutions, respectively. These results will be essential for the error analysis of the space semidiscrete Galerkin scheme (7.3) in Section 7.3. First we consider the homogeneous problem with initial data $a \in \mathcal{D}(\mathcal{A}^\gamma)$ with $\gamma \in (-1/2, 1]$.

Theorem 7.1 *Let u be the solution to problem (7.1) with $F \equiv 0$ and $a \in \mathcal{D}(\mathcal{A}^\gamma)$ $(\gamma \in (-1/2, 1])$. Then there exists a constant $C = C(\Omega, T, \boldsymbol{\alpha}, \boldsymbol{q}) > 0$ such that for $0 \le \kappa - \gamma \le 1$, there holds*

$$\|u(\cdot\,,t)\|_{\mathcal{D}(\mathcal{A}^\kappa)} \le C\|a\|_{\mathcal{D}(\mathcal{A}^\gamma)} t^{\alpha_1(\gamma-\kappa)} \quad (0 < t \le T).$$

Proof. Taking $F = 0$ in (7.4) immediately gives

$$u(\cdot\,,t) = \sum_{n=1}^\infty \left(1 - \lambda_n t^{\alpha_1} E^{(n)}_{\boldsymbol{\alpha}',1+\alpha_1}(t)\right)(a,\varphi_n)\varphi_n.$$

Then by Lemma 7.2, we have for $0 \le \kappa - \gamma \le 1$ that

$$\|u(\cdot\,,t)\|^2_{\mathcal{D}(\mathcal{A}^\kappa)} = \sum_{n=1}^\infty \left(\lambda_n^{\kappa-\gamma} \left|1 - \lambda_n t^{\alpha_1} E^{(n)}_{\boldsymbol{\alpha}',1+\alpha_1}(t)\right|\right)^2 |\lambda_n^\gamma (a,\varphi_n)|^2.$$

To treat the term $1 - \lambda_n t^{\alpha_1} E^{(n)}_{\boldsymbol{\alpha}',1+\alpha_1}(t)$, we utilize Lemma 7.1 and apply Lemma 7.2 to deduce

$$\begin{aligned} \left|1 - \lambda_n t^{\alpha_1} E^{(n)}_{\boldsymbol{\alpha}',1+\alpha_1}(t)\right| &= \left|E^{(n)}_{\boldsymbol{\alpha}',1}(t) + \sum_{j=2}^m q_j t^{\alpha_1-\alpha_j} E^{(n)}_{\boldsymbol{\alpha}',1+\alpha_1-\alpha_j}(t)\right| \\ &\le \left|E^{(n)}_{\boldsymbol{\alpha}',1}(t)\right| + C\sum_{j=2}^m t^{\alpha_1-\alpha_j} \left|E^{(n)}_{\boldsymbol{\alpha}',1+\alpha_1-\alpha_j}(t)\right| \le C\sum_{j=1}^m \frac{t^{\alpha_1-\alpha_j}}{1+\lambda_n t^{\alpha_1}}. \end{aligned}$$

Therefore, we estimate for $0 < t \le T$ that

$$\begin{aligned} \|u(\cdot\,,t)\|^2_{\mathcal{D}(\mathcal{A}^\kappa)} &\le C^2 \sum_{n=1}^\infty \left(\sum_{j=1}^m \frac{\lambda_n^{\kappa-\gamma} t^{\alpha_1-\alpha_j}}{1+\lambda_n t^{\alpha_1}}\right)^2 |\lambda_n^\gamma (a,\varphi_n)|^2 \\ &= C^2 \sum_{n=1}^\infty \left(\frac{(\lambda_n t^{\alpha_1})^{\kappa-\gamma}}{1+\lambda_n t^{\alpha_1}} t^{\alpha_1(1+\gamma-\kappa)-\alpha_j}\right)^2 |\lambda_n^\gamma (a,\varphi_n)|^2 \end{aligned}$$

$$\le C^2 \left(\sum_{j=1}^{m} t^{\alpha_1(1+\gamma-\kappa)-\alpha_j} \right)^2 \sum_{n=1}^{\infty} |\lambda_n^\gamma(a,\varphi_n)|^2 \le \left(C\|a\|_{\mathcal{D}(\mathcal{A}^\gamma)} t^{\alpha_1(\gamma-\kappa)} \right)^2.$$

The proof of $\lim_{t\downarrow 0} \|u(\,\cdot\,,0)-a\|_{\mathcal{D}(\mathcal{A}^\gamma)} = 0$ coincides with that for Theorem 6.1(b) and we omit the details here. □

Now we turn to the inhomogeneous problem with a nonsmooth right-hand side and the homogeneous initial condition.

Theorem 7.2 *Let u be the solution to* (7.1) *with $a = 0$ and $F \in L^\infty(0,T;\mathcal{D}(\mathcal{A}^\gamma))$ ($\gamma \in (-1/2, 1/2]$). Then $u \in L^\infty(0,T;\mathcal{D}(\mathcal{A}^{\gamma+1-\epsilon}))$ for any $\epsilon \in (0,1]$. Furthermore, there exists a constant $C = C(\Omega,T,\boldsymbol{\alpha},\boldsymbol{q}) > 0$ such that*

$$\|u(\,\cdot\,,t)\|_{\mathcal{D}(\mathcal{A}^{\gamma+1-\epsilon})} \le \frac{C}{\epsilon} \|F\|_{L^\infty(0,t;\mathcal{D}(\mathcal{A}^\gamma))} t^{\alpha_1\epsilon}. \tag{7.6}$$

Hence, it is a solution to problem (7.1) *with the homogeneous initial condition in the sense that $\lim_{t\downarrow 0} \|u(\,\cdot\,,t)\|_{\mathcal{D}(\mathcal{A}^{\gamma+1-\epsilon})} = 0$ for arbitrarily small $\epsilon > 0$.*

Proof. Fix $\epsilon \in (0,1]$ arbitrarily. Taking $a = 0$ in (7.4) and applying Lemma 7.4, we immediately obtain

$$\begin{aligned} \|u(\,\cdot\,,t)\|_{\mathcal{D}(\mathcal{A}^{\gamma+q-\epsilon})} &= \left\| \int_0^t U(s)F(\,\cdot\,,t-s)\,\mathrm{d}s \right\|_{\mathcal{D}(\mathcal{A}^{\gamma+1-\epsilon})} \le \int_0^t \|U(s)F(\,\cdot\,,t-s)\|_{\mathcal{D}(\mathcal{A}^{\gamma+1-\epsilon})}\,\mathrm{d}s \\ &\le C \int_0^t s^{-1+\alpha_1\epsilon} \|F(\,\cdot\,,t-s)\|_{\mathcal{D}(\mathcal{A}^\gamma)}\,\mathrm{d}s \le \frac{C}{\epsilon} \|F\|_{L^\infty(0,t;\mathcal{D}(\mathcal{A}^\gamma))} t^{\alpha_1\epsilon}, \end{aligned}$$

which shows the desired estimate. □

Next we extend Theorem 7.2 to allow less regular right-hand sides $F \in L^2(0,T;\mathcal{D}(\mathcal{A}^\gamma))$ with $-1/2 < \gamma \le 1$. Similarly to Theorem 6.2(a), it will be verified that the solution u satisfies the governing equation as an element in the space $L^2(0,T;\mathcal{D}(\Omega^{\gamma+1}))$. However, it may happen that the satisfaction of the homogeneous initial condition becomes meaningless in the usual sense. In Remark 7.1 below, we argue that the weakest class of the source term that produces a legitimate weak solution of (7.1) is $F \in L^p(0,T;\mathcal{D}(\mathcal{A}^\gamma))$ with $p > 1/\alpha_1$ and $-1/2 < \gamma \le 1$. Obviously, for $1/2 < \alpha < 1$, it does give a solution $u \in L^2(0,T;\mathcal{D}(\mathcal{A}^{\gamma+1}))$.

Theorem 7.3 *Let u be the solution to* (7.1) *with $a = 0$ and $F \in L^2(0,T;\mathcal{D}(\mathcal{A}^\gamma))$ ($\gamma \in (-1/2, 1/2]$). Then $u \in L^2(0,T;\mathcal{D}(\mathcal{A}^{\gamma+1}))$, and there exists a constant $C = C(\Omega,T,\boldsymbol{\alpha},\boldsymbol{q}) > 0$ such that*

$$\|u\|_{L^2(0,t;\mathcal{D}(\mathcal{A}^{\gamma+1}))} \le C\|F\|_{L^2(0,t;\mathcal{D}(\mathcal{A}^\gamma))} \quad (0 < t \le T).$$

Proof. Now we substitute the explicit form (7.5) of $U(t)$ into (7.4) to formally write

$$\|u(\,\cdot\,,t)\|^2_{\mathcal{D}(\mathcal{A}^{\gamma+1})} = \sum_{n=1}^{\infty} \lambda_n^2 \left(\int_0^t s^{\alpha_1-1} E^{(n)}_{\boldsymbol{\alpha}',\alpha_1}(s)\, \lambda_n^\gamma(F(\,\cdot\,,t-s),\varphi_n)\,\mathrm{d}s \right)^2.$$

Using Young's inequality for convolutions along with Lemma 7.3, we deduce

$$\begin{aligned} \|u\|^2_{L^2(0,t;\mathcal{D}(\mathcal{A}^{\gamma+1}))} &= \sum_{n=1}^{\infty} \lambda_n^2 \left\| \int_0^s r^{\alpha_1-1} E^{(n)}_{\boldsymbol{\alpha}',\alpha_1}(r)\, \lambda_n^\gamma(F(\,\cdot\,,s-r),\varphi_n)\,\mathrm{d}r \right\|^2_{L^2(0,t)} \\ &\le \sum_{n=1}^{\infty} \left(\lambda_n \int_0^t s^{\alpha_1-1} E^{(n)}_{\boldsymbol{\alpha}',\alpha_1}(s)\,\mathrm{d}s \right)^2 \|\lambda_n^\gamma(F(\,\cdot\,,s),\varphi_n)\|^2_{L^2(0,t)} \end{aligned}$$

$$\le C^2 \sum_{n=1}^{\infty} \|\lambda_n^\gamma (F(\cdot\,,s),\varphi_n)\|_{L^2(0,t)}^2 = \big(C\|F\|_{L^2(0,t;\mathcal{D}(\mathcal{A}^\gamma))}\big)^2 .$$

This completes the proof. □

Remark 7.1 The condition $F \in L^\infty(0,T;\mathcal{D}(\mathcal{A}^\gamma))$ in Theorem 7.2 can be weakened to $F \in L^p(0,T;\mathcal{D}(\mathcal{A}^\gamma))$ with $p > 1/\alpha_1$. In fact, it follows from Lemma 7.4 and Hölder's inequality that

$$\begin{aligned}\|u(\cdot\,,t)\|_{\mathcal{D}(\mathcal{A}^\gamma)} &\le \int_0^t \|U(s)F(\cdot\,,t-s)\|_{\mathcal{D}(\mathcal{A}^\gamma)}\,\mathrm{d}s \le C\int_0^t s^{\alpha_1-1}\|F(\cdot\,,t-s)\|_{\mathcal{D}(\mathcal{A}^\gamma)}\,\mathrm{d}s \\ &\le C\|F\|_{L^p(0,t;\mathcal{D}(\mathcal{A}^\gamma))}\left(\int_0^t s^{p'(\alpha_1-1)}\,\mathrm{d}s\right)^{1/p'} = C\|F\|_{L^p(0,t;\mathcal{D}(\mathcal{A}^\gamma))}t^{\alpha_1-1/p},\end{aligned}$$

where p' is the conjugate number of p, and we easily infer $p'(\alpha_1-1) = \frac{p(\alpha_1-1)}{p-1} > -1$ from $p > 1/\alpha_1$. Then it is obvious that the initial condition $u(\cdot\,,0) = 0$ holds in the sense that $\lim_{t\downarrow 0}\|u(\cdot\,,t)\|_{\mathcal{D}(\mathcal{A}^\gamma)} = 0$. Hence for any $\alpha \in (1/2,1)$ the solution remains a legitimate solution under the weaker condition $F \in L^2(0,T;\mathcal{D}(\mathcal{A}^\gamma))$.

7.3 Error estimates for semidiscrete Galerkin scheme

Now we derive and analyze the space semidiscrete Galerkin FEM scheme (7.3). First we describe the semidiscrete scheme, and then derive almost optimal error estimates for the homogeneous and inhomogeneous problems separately. In the analysis we essentially use the technique developed in [81] and improved in [79, 80].

7.3.1 Semidiscrete scheme

To describe the scheme, we need the $L^2(\Omega)$ projection $P_h : L^2(\Omega) \to X_h$ and Ritz projection $R_h : H_0^1(\Omega) \to X_h$, respectively, defined by

$$(P_h f, g_h) = (f, g_h), \quad (\nabla R_h f, \nabla g_h) = (\nabla f, \nabla g_h) \quad (\forall g_h \in X_h).$$

The operators R_h and P_h satisfy the following approximation property.

Lemma 7.5 (see [127]) *Let $f \in \mathcal{D}(\mathcal{A}^\gamma)$ with $1/2 \le \gamma \le 1$. Then the operator R_h satisfies*

$$\|R_h f - f\|_{L^2(\Omega)} + h\|\nabla(R_h f - f)\|_{L^2(\Omega)} \le C\,h^{2\gamma}\|f\|_{\mathcal{D}(\mathcal{A}^\gamma)}.$$

Further, for $\kappa \in [0,1/2]$ we have

$$\|P_h f - f\|_{\mathcal{D}(\mathcal{A}^\kappa)} \le \begin{cases} C\,h^{2(1-\kappa)}\|f\|_{\mathcal{D}(\mathcal{A})} & (\forall\, f \in \mathcal{D}(\mathcal{A})), \\ C\,h^{1-2\kappa}\|f\|_{\mathcal{D}(\mathcal{A}^{1/2})} & (\forall\, f \in \mathcal{D}(\mathcal{A}^{1/2})). \end{cases}$$

By interpolation, the operator P_h is also bounded on $\mathcal{D}(\mathcal{A}^\kappa)$, $-1/2 \le \kappa \le 0$.

Now we can describe the semidiscrete Galerkin scheme. Introducing the discrete Laplacian $\triangle_h : X_h \to X_h$ defined by

$$-(\triangle_h f_h, g_h) = (\nabla f_h, \nabla g_h) \quad (f_h, g_h \in X_h)$$

and setting $F_h(t) := P_h F(\,\cdot\,, t)$, we may write the spatially discrete problem (7.3) as

$$\begin{cases} \displaystyle\sum_{j=1}^{m} q_j \partial_t^{\alpha_j} u_h(t) - \triangle_h u_h(t) = F_h(t) \quad (0 < t \le T), \\ u_h(0) = a_h, \end{cases} \tag{7.7}$$

where $a_h \in X_h$ is an approximation to the initial data a. Next, by using the eigensystem $\{\lambda_n^h, \varphi_n^h\}_{n=1}^N$ of the discrete Laplacian $-\triangle_h$, we can give a solution representation of (7.7) as

$$u_h(t) = \sum_{n=1}^{N} \left(1 - \lambda_n^h t^{\alpha_1} E^{(n,h)}_{\boldsymbol{\alpha}', 1+\alpha_1}(t)\right) (a_h, \varphi_n^h)\varphi_n^h + \int_0^t U_h(s) F_h(t-s)\,\mathrm{d}s, \quad \text{where} \tag{7.8}$$

$$U_h(t) f_h := t^{\alpha_1 - 1} \sum_{n=1}^{N} E^{(n,h)}_{\boldsymbol{\alpha}', \alpha_1}(t)(f_h, \varphi_n^h)\varphi_n^h, \quad f_h \in X_h, \tag{7.9}$$

$$E^{(n,h)}_{\boldsymbol{\alpha}', \beta}(t) := E_{(\alpha_1, \alpha_1 - \alpha_2, \ldots, \alpha_1 - \alpha_m), \beta}(-\lambda_n^h t^{\alpha_1}, -q_2 t^{\alpha_1 - \alpha_2}, \ldots, -q_m t^{\alpha_1 - \alpha_m}).$$

On the finite element space X_h, we introduce the discrete norm

$$|||f_h|||_{\mathcal{D}(\mathcal{A}^\gamma)} := \left(\sum_{n=1}^{N} \left|(\lambda_n^h)^\gamma (f_h, \varphi_n^h)\right|^2\right)^{1/2} \qquad (f_h \in X_h).$$

The norm $|||\cdot|||_{\mathcal{D}(\mathcal{A}^\gamma)}$ is well defined for all $\gamma \in \mathbb{R}$. Clearly, $|||f_h|||_{\mathcal{D}(\mathcal{A}^{1/2})} = \|f_h\|_{\mathcal{D}(\mathcal{A}^{1/2})}$ and $|||f_h|||_{\mathcal{D}(\mathcal{A}^0)} = \|f_h\|_{L^2(\Omega)}$ for any $f_h \in X_h$. Further, the following inverse inequality holds (see [81]): if the mesh $\mathcal{T}_h$ is quasi-uniform, then for any $\kappa > \gamma$,

$$|||f_h|||_{\mathcal{D}(\mathcal{A}^\kappa)} \le C\, h^{2(\gamma-\kappa)} |||f_h|||_{\mathcal{D}(\mathcal{A}^\gamma)} \quad (\forall\, f_h \in X_h). \tag{7.10}$$

Lemma 7.6 *Assume that the mesh $\mathcal{T}_h$ is quasi-uniform. Let $u_h(t)$ satisfy (7.8) with $F = 0$. Then for any $a_h \in X_h$, there exists a constant $C = C(\Omega, T, \boldsymbol{\alpha}, \boldsymbol{q}) > 0$ such that for $0 \le \kappa - \gamma \le 1$, there holds*

$$|||u_h(t)|||_{\mathcal{D}(\mathcal{A}^\kappa)} \le C |||a_h|||_{\mathcal{D}(\mathcal{A}^\gamma)} t^{\alpha_1(\gamma-\kappa)} \quad (0 < t \le T).$$

Proof. By the representation (7.8) , we have for $0 \le \kappa - \gamma \le 1$ that

$$|||u_h(t)|||^2_{\mathcal{D}(\mathcal{A}^\kappa)} = \sum_{n=1}^{N} \left((\lambda_n^h)^{\kappa-\gamma} \left|1 - \lambda_n^h t^{\alpha_1} E^{(n,h)}_{\boldsymbol{\alpha}', 1+\alpha_1}(t)\right|\right)^2 \left|(\lambda_n^h)^\gamma (a_h, \varphi_n^h)\right|^2.$$

By the same argument as that in the proof of Theorem 7.1, we apply Lemmata 7.1–7.2 to deduce

$$\left|1 - \lambda_n^h t^{\alpha_1} E^{(n,h)}_{\boldsymbol{\alpha}', 1+\alpha_1}(t)\right| \le C \sum_{j=1}^{m} \frac{t^{\alpha_1 - \alpha_j}}{1 + \lambda_n^h t^{\alpha_1}},$$

which yields

$$\begin{aligned} |||u_h(t)|||^2_{\mathcal{D}(\mathcal{A}^\kappa)} &\le C^2 \sum_{n=1}^{N} \left(\sum_{j=1}^{m} \frac{(\lambda_n^h)^{\kappa-\gamma} t^{\alpha_1 - \alpha_j}}{1 + \lambda_n^h t^{\alpha_1}}\right)^2 \left|(\lambda_n^h)^\gamma (a_h, \varphi_n^h)\right|^2 \\ &\le \left(C\, t^{\alpha_1(\gamma-\kappa)}\right)^2 \sum_{n=1}^{N} \left(\frac{(\lambda_n^h t^{\alpha_1})^{\kappa-\gamma}}{1 + \lambda_n^h t^{\alpha_1}}\right)^2 \left|(\lambda_n^h)^\gamma (a_h, \varphi_n^h)\right|^2 \\ &\le \left(C |||a_h|||_{\mathcal{D}(\mathcal{A}^\gamma)} t^{\alpha_1(\gamma-\kappa)}\right)^2 \end{aligned}$$

for $0 < t \le T$. ∎

The next result is a discrete analogue to Lemma 7.4.

Lemma 7.7 *Let $U_h(t)$ be defined by (7.9) and $f_h \in X_h$. Then there exists a constant $C = C(\Omega, T, \boldsymbol{\alpha}, \boldsymbol{q}) > 0$ such that*

$$|||U_h(t) f_h|||_{\mathcal{D}(\mathcal{A}^\kappa)} \le \begin{cases} C|||f_h|||_{\mathcal{D}(\mathcal{A}^\gamma)} t^{\alpha_1(1+\gamma-\kappa)-1}, & 0 \le \kappa - \gamma \le 1, \\ C|||f_h|||_{\mathcal{D}(\mathcal{A}^\gamma)} t^{\alpha_1 - 1}, & \kappa < \gamma. \end{cases}$$

Proof. The proof for the case $0 \le \kappa - \gamma \le 1$ is similar to that of Lemma 7.4. The another assertion follows from the fact that $\{\lambda_n^h\}_{n=1}^N$ are bounded from zero independent of h. □

In view of the superposition principle, again we separate the discussions on the homogeneous and inhomogeneous problems, that is, the cases of $F = 0$ and $a = 0$ respectively. In the sequel, we abbreviate $u(t) := u(\cdot\,, t)$ for simplicity.

7.3.2 Error estimates for the homogeneous problem

To derive error estimates for the homogeneous problem, first we consider the case of smooth initial data, i.e., $a \in \mathcal{D}(\mathcal{A})$. To this end, we split the error $u_h(t) - u(t)$ into two terms as

$$u_h - u = (u_h - R_h u) + (R_h u - u) =: \vartheta + \varrho.$$

By Lemma 7.5 and Theorem 7.1, we have

$$\|\varrho(t)\|_{L^2(\Omega)} + h\|\nabla \varrho(t)\|_{L^2(\Omega)} \le C\, h^2 \|u(t)\|_{\mathcal{D}(\mathcal{A})} \le C\, h^2 \|a\|_{\mathcal{D}(\mathcal{A})} \quad (0 < t \le T). \tag{7.11}$$

So it suffices to get proper estimates for $\vartheta(t)$, which is given below.

Lemma 7.8 *Let $F = 0$, $a \in \mathcal{D}(\mathcal{A})$, $a_h = R_h a$ and $\vartheta(t) := u_h(t) - R_h u(t)$. Then there exists a constant $C = C(\Omega, T, \boldsymbol{\alpha}, \boldsymbol{q}) > 0$ such that for $\kappa = 0, 1/2$, there holds*

$$\|\vartheta(t)\|_{\mathcal{D}(\mathcal{A}^\kappa)} \le C\, h^{2(1-\kappa)} \|a\|_{\mathcal{D}(\mathcal{A})} \quad (0 < t \le T).$$

Proof. Using the identity $\triangle_h R_h = P_h \triangle$, we note that ϑ satisfies

$$\begin{cases} \displaystyle\sum_{j=1}^m q_j \partial_t^{\alpha_j} \vartheta(t) - \triangle_h \vartheta(t) = -P_h \left(\sum_{j=1}^m q_j \partial_t^{\alpha_j} \varrho(t) \right) & (0 < t \le T), \\ \vartheta(0) = 0. \end{cases}$$

By the representation (7.8), we have

$$\vartheta(t) = -\int_0^t U_h(s)\, P_h \left(\sum_{j=1}^m q_j \partial_t^{\alpha_j} \varrho(t-s) \right) \mathrm{d}s.$$

Then by Lemma 7.7, Lemma 7.5 and Theorem 7.1, we deduce for $\kappa = 0, 1/2$ and $0 < t \le T$ that

$$\begin{aligned} \|\vartheta(t)\|_{\mathcal{D}(\mathcal{A}^\kappa)} &\le \int_0^t \left\| U_h(s)\, P_h \left(\sum_{j=1}^m q_j \partial_t^{\alpha_j} \varrho(t-s) \right) \right\|_{\mathcal{D}(\mathcal{A}^\kappa)} \mathrm{d}s \\ &\le C \int_0^t s^{\alpha_1(1-\kappa)-1} \left\| P_h \left(\sum_{j=1}^m q_j \partial_t^{\alpha_j} \varrho(t-s) \right) \right\|_{L^2(\Omega)} \mathrm{d}s \end{aligned}$$

$$
\begin{aligned}
&\le C\int_0^t (t-s)^{\alpha_1(1-\kappa)-1}\left\|\sum_{j=1}^m q_j\partial_t^{\alpha_j}\varrho(s)\right\|_{L^2(\Omega)}\,\mathrm{d}s\\
&\le C\,h^{2(1-\kappa)}\int_0^t (t-s)^{\alpha_1(1-\kappa)-1}\left\|\sum_{j=1}^m q_j\partial_t^{\alpha_j}u(s)\right\|_{\mathcal{D}(\mathcal{A}^{1-\kappa})}\,\mathrm{d}s\\
&\le C\,h^{2(1-\kappa)}\int_0^t (t-s)^{\alpha_1(1-\kappa)-1}\|u(s)\|_{\mathcal{D}(\mathcal{A}^{2-\kappa})}\,\mathrm{d}s\\
&\le C\,h^{2(1-\kappa)}\|a\|_{\mathcal{D}(\mathcal{A})}\int_0^t (t-s)^{\alpha_1(1-\kappa)-1}s^{\alpha_1(\kappa-1)}\,\mathrm{d}s \le C\,h^{2(1-\kappa)}\|a\|_{\mathcal{D}(\mathcal{A})},
\end{aligned}
$$

where we use the fact that $\sum_{j=1}^m q_j\partial_t^{\alpha_j}u = \triangle u$ in the fifth inequality. □

Using (7.11), Lemma 7.8 and the triangle inequality, we arrive at our first estimate, which is formulated in the following theorem.

Theorem 7.4 *Let $F = 0$, $a \in \mathcal{D}(\mathcal{A})$ and u, u_h be the solutions to (7.1) and (7.3) with $a_h = R_h a$, respectively. Then there exists a constant $C = C(\Omega, T, \boldsymbol{\alpha}, \boldsymbol{q}) > 0$ such that*

$$
\|u_h(t) - u(t)\|_{L^2(\Omega)} + h\|\nabla(u_h(t) - u(t))\|_{L^2(\Omega)} \le C\,h^2\|a\|_{\mathcal{D}(\mathcal{A})} \quad (0 < t \le T).
$$

Now we turn to the nonsmooth case, i.e., $a \in \mathcal{D}(\mathcal{A}^\gamma)$ with $-1/2 < \gamma \le 1/2$. Since the Ritz projection R_h is not well-defined for nonsmooth data, we use instead the $L^2(\Omega)$-projection $a_h = P_h a$ and split the error $u_h(t) - u(t)$ into two terms as

$$
u_h - u = (u_h - P_h u) + (P_h u - u) =: \widetilde{\vartheta} + \widetilde{\varrho}. \tag{7.12}
$$

By Lemma 7.5 and Theorem 7.1, we have for $-1/2 < \gamma \le 1/2$ that

$$
\begin{aligned}
\|\widetilde{\varrho}(t)\|_{L^2(\Omega)} + h\|\nabla\widetilde{\varrho}(t)\|_{L^2(\Omega)} &\le C\,h^{2(1+\min(0,\gamma))}\|u(t)\|_{\mathcal{D}(\mathcal{A}^{1+\min(0,\gamma)})}\\
&\le C\,h^{2(1+\min(0,\gamma))}t^{\alpha_1(\max(\gamma,0)-1)}\|a\|_{\mathcal{D}(\mathcal{A}^\gamma)} \quad (0 < t \le T).
\end{aligned}
$$

Thus, we only need to estimate the term $\widetilde{\vartheta}(t)$, which is stated in the following lemma.

Lemma 7.9 *Let $F = 0$, $a \in \mathcal{D}(\mathcal{A}^\gamma)$ with $-1/2 < \gamma \le 1/2$, $a_h = P_h a$ and $\widetilde{\vartheta}(t) := u_h(t) - P_h u(t)$. Then there exists a constant $C = C(\Omega, T, \boldsymbol{\alpha}, \boldsymbol{q}) > 0$ such that for $\kappa = 0, 1/2$, there holds*

$$
\|\widetilde{\vartheta}(t)\|_{\mathcal{D}(\mathcal{A}^\kappa)} \le C\,h^{2(1+\min(\gamma,0)-\kappa)}\sigma_h\,\|a\|_{\mathcal{D}(\mathcal{A}^\gamma)}t^{\alpha_1(\max(\gamma,0)-1)} \quad (0 < t \le T),
$$

where $\sigma_h = |\ln h|$.

Proof. Using the identities

$$
P_h\left(\sum_{j=1}^m q_j\partial_t^{\alpha_j}\widetilde{\varrho}\right) = \sum_{j=1}^m q_j\partial_t^{\alpha_j}P_h(P_h u - u) = 0
$$

and $\triangle_h R_h = P_h\triangle$, we see that $\widetilde{\vartheta}$ satisfies

$$
\begin{cases}
\displaystyle\sum_{j=1}^m q_j\partial_t^{\alpha_j}\widetilde{\vartheta}(t) - \triangle_h\widetilde{\vartheta}(t) = -\triangle_h(R_h u - P_h u)(t) \quad (0 < t \le T),\\
\widetilde{\vartheta}(0) = 0.
\end{cases} \tag{7.13}
$$

By the representation (7.8), we have

$$\widetilde{\vartheta}(t) = -\int_0^t U_h(s)\,\triangle_h(R_h u - P_h u)(t-s)\,\mathrm{d}s. \tag{7.14}$$

Then by Lemma 7.6, there holds for $\kappa = 0, 1/2$ and arbitrarily small $\epsilon > 0$ that

$$\begin{aligned}\|U_h(s)\,\triangle_h(R_h u - P_h u)(t-s)\|_{\mathcal{D}(\mathcal{A}^\kappa)} &\le C\,s^{\alpha_1\epsilon-1}|||\triangle_h(R_h u - P_h u)(t-s)|||_{\mathcal{D}(\mathcal{A}^{\kappa-1+\epsilon})}\\ &\le C\,s^{\alpha_1\epsilon-1}|||(R_h u - P_h u)(t-s)|||_{\mathcal{D}(\mathcal{A}^{\kappa+\epsilon})}.\end{aligned}$$

Moreover, by (7.10), Theorem 7.1 and Lemma 7.5, we have for $-1/2 < \gamma \le 1/2$ that

$$\begin{aligned}&\|U_h(s)\,\triangle_h(R_h u - P_h u)(t-s)\|_{\mathcal{D}(\mathcal{A}^\kappa)}\\ &\le C\,h^{2(1+\min(\gamma,0)-\kappa-\epsilon)}\,s^{\alpha_1\epsilon-1}\|u(t-s)\|_{\mathcal{D}(\mathcal{A}^{1+\min(\gamma,0)})}\\ &\le C\,h^{2(1+\min(\gamma,0)-\kappa-\epsilon)}\|a\|_{\mathcal{D}(\mathcal{A}^\gamma)}s^{\alpha_1\epsilon-1}(t-s)^{\alpha_1(\max(\gamma,0)-1)} \quad (\kappa = 0, 1/2).\end{aligned}$$

Then we plug the above estimate back into (7.14) to obtain

$$\begin{aligned}\|\widetilde{\vartheta}(t)\|_{\mathcal{D}(\mathcal{A}^\kappa)} &\le C\,h^{2(1+\min(\gamma,0)-\kappa-\epsilon)}\|a\|_{\mathcal{D}(\mathcal{A}^\gamma)}\int_0^t s^{\alpha_1\epsilon-1}(t-s)^{\alpha_1(\max(\gamma,0)-1)}\,\mathrm{d}s\\ &\le C\,\epsilon^{-1}h^{2(1+\min(\gamma,0)-\kappa-\epsilon)}\|a\|_{\mathcal{D}(\mathcal{A}^\gamma)}t^{\alpha_1(\max(\gamma,0)-1)} \quad (\kappa = 0, 1/2,\ 0 < t \le T),\end{aligned}$$

where the last inequality follows from the fact that

$$\int_0^t s^{\alpha_1\epsilon-1}(t-s)^{\alpha_1(\max(\gamma,0)-1)}\,\mathrm{d}s = t^{\alpha_1(\epsilon+\max(\gamma,0)-1)}\frac{\Gamma(\alpha_1\epsilon)\Gamma(1+\alpha_1(\max(\gamma,0)-1))}{\Gamma(1+\alpha_1(\epsilon+\max(\gamma,0)-1))}$$

and the estimate $\Gamma(\alpha_1\epsilon) = \Gamma(1+\alpha_1\epsilon)/(\alpha_1\epsilon) \le C\,\epsilon^{-1}$. Now with the choice $\epsilon = 1/\sigma_h$ and the fact that $h^{-1/|\ln h|}$ is uniformly bounded for $h > 0$, we obtain the desired estimate. □

Now the triangle inequality yields an error estimate for the case of a nonsmooth initial data.

Theorem 7.5 *Let $F = 0$, $a \in \mathcal{D}(\mathcal{A}^\gamma)$ with $-1/2 < \gamma \le 1/2$, and u, u_h be the solutions of (7.1) and (7.3) with $a_h = P_h a$, respectively. Then there exists a constant $C = C(\Omega, T, \boldsymbol{\alpha}, \boldsymbol{q}) > 0$ such that*

$$\|u_h(t) - u(t)\|_{L^2(\Omega)} + h\|\nabla(u_h(t) - u(t))\|_{L^2(\Omega)} \le C\,h^{2(1+\min(\gamma,0))}\sigma_h\,\|a\|_{\mathcal{D}(\mathcal{A}^\gamma)}t^{\alpha_1(\max(\gamma,0)-1)}$$

for $0 < t \le T$, where $\sigma_h = |\ln h|$.

7.3.3 Error estimates for the inhomogeneous problem

Now we derive error estimates for Galerkin approximations of the inhomogeneous problem with $a = 0$ and $F \in L^\infty(0,T;\mathcal{D}(\mathcal{A}^\gamma))$ $(-1/2 < \gamma \le 0)$ in both L^2- and L^∞-norms in time. The case $F \in L^\infty(0,T;\mathcal{D}(\mathcal{A}^\gamma))$, $0 < \gamma \le 1/2$ is simpler and can be treated analogously. To this end, we appeal again to the splitting (7.12). By Theorem 7.2 and Lemma 7.5, the following estimate holds for $\widetilde{\varrho}$:

$$\begin{aligned}\|\widetilde{\varrho}(t)\|_{L^2(\Omega)} + h\|\nabla\widetilde{\varrho}(t)\|_{L^2(\Omega)} &\le C\,h^{2(1+\gamma-\epsilon)}\|u(t)\|_{\mathcal{D}(\mathcal{A}^{1+\gamma-\epsilon})}t^{-\alpha_1\epsilon}\\ &\le C\,\epsilon^{-1}h^{2(1+q-\epsilon)}\|F\|_{L^\infty(0,t;\mathcal{D}(\mathcal{A}^\gamma))} \quad (0 < t \le T).\end{aligned}$$

Now the choice $\sigma_h = |\ln h|$ and $\epsilon = 1/\sigma_h$ yields

$$\|\widetilde{\varrho}(t)\|_{L^2(\Omega)} + h\|\nabla\widetilde{\varrho}(t)\|_{L^2(\Omega)} \le C\,h^{2(1+\gamma)}\sigma_h\,\|F\|_{L^\infty(0,t;\mathcal{D}(\mathcal{A}^\gamma))} \quad (0 < t \le T).$$

Thus, it suffices to bound the term $\widetilde{\vartheta}$.

Lemma 7.10 *Let $a = 0$, $F \in L^\infty(0,T;\mathcal{D}(\mathcal{A}^\gamma))$ with $-1/2 < \gamma \le 0$ and $\widetilde{\vartheta}(t)$ be defined by (7.14). Then there exists a constant $C = C(\Omega, T, \boldsymbol{\alpha}, \boldsymbol{q}) > 0$ such that*

$$\|\widetilde{\vartheta}(t)\|_{L^2(\Omega)} + h\|\nabla\widetilde{\vartheta}(t)\|_{L^2(\Omega)} \le C\, h^{2(1+\gamma)}\sigma_h^2\, \|F\|_{L^\infty(0,t;\mathcal{D}(\mathcal{A}^\gamma))} \quad (0 < t \le T).$$

where $\sigma_h = |\ln h|$.

Proof. By (7.8) and Lemma 7.7, we deduce for $\kappa = 0, 1/2$ that

$$\begin{aligned}\|\widetilde{\vartheta}(t)\|_{\mathcal{D}(\mathcal{A}^\kappa)} &\le \int_0^t \|U_h(s)\triangle_h(R_hu - P_hu)(t-s)\|_{\mathcal{D}(\mathcal{A}^\kappa)}\,\mathrm{d}s\\ &\le C\int_0^t s^{\alpha_1\epsilon-1}\|\!|\triangle_h(R_hu - P_hu)(t-s)|\!\|_{\mathcal{D}(\mathcal{A}^{\kappa-1+\epsilon})}\,\mathrm{d}s\\ &\le C\int_0^t s^{\alpha_1\epsilon-1}\|\!|(R_hu - P_hu)(t-s)|\!\|_{\mathcal{D}(\mathcal{A}^{\kappa+\epsilon})}\,\mathrm{d}s \quad (0 < t \le T).\end{aligned}$$

Further, using (7.10) and Lemma 7.5, we deduce

$$\begin{aligned}\|\widetilde{\vartheta}(t)\|_{\mathcal{D}(\mathcal{A}^\kappa)} &\le C\, h^{-\epsilon}\int_0^t s^{\alpha_1\epsilon-1}\|(R_hu - P_hu)(t-s)\|_{\mathcal{D}(\mathcal{A}^\kappa)}\,\mathrm{d}s\\ &\le C\, h^{2(1+\gamma-\kappa-\epsilon)}\int_0^t s^{\alpha_1\epsilon-1}\|u(t-s)\|_{\mathcal{D}(\mathcal{A}^{1+\gamma-\epsilon})}\,\mathrm{d}s \quad (\kappa = 0, 1/2,\ 0 < t \le T).\end{aligned}$$

Now by (7.6) and the choice $\epsilon = 1/\sigma_h$, we get for $\kappa = 0, 1/2$ and $0 < t \le T$ that

$$\begin{aligned}\|\widetilde{\vartheta}(t)\|_{\mathcal{D}(\mathcal{A}^\kappa)} &\le C\,\epsilon^{-1}h^{2(1+\gamma-\kappa-\epsilon)}\|F\|_{L^\infty(0,t;\mathcal{D}(\mathcal{A}^\gamma))}\int_0^t s^{\alpha_1\epsilon-1}(t-s)^{\alpha_1\epsilon}\,\mathrm{d}s\\ &\le C\,\epsilon^{-2}h^{2(1+\gamma-\kappa-\epsilon)}\|F\|_{L^\infty(0,t;\mathcal{D}(\mathcal{A}^\gamma))} \le C\, h^{2(1+\gamma-\kappa)}\sigma_h^2\,\|F\|_{L^\infty(0,t;\mathcal{D}(\mathcal{A}^\gamma))},\end{aligned}$$

where the second inequality follows from

$$\int_0^t s^{\alpha_1\epsilon-1}(t-s)^{\alpha_1\epsilon}\,\mathrm{d}s \le t^{\alpha_1\epsilon}\int_0^t s^{\alpha_1\epsilon-1}\,\mathrm{d}s = \frac{2}{\alpha_1\epsilon}t^{\alpha_1\epsilon} \le C\,\epsilon^{-1}.$$

This completes the proof of the lemma. □

An inspection of the proof of Lemma 7.10 indicates that for $0 < \gamma \le 1/2$, one can get rid of the factor σ_h. Now we can state an error estimate in L^∞-norm in time.

Theorem 7.6 *Let $a = 0$, $F \in L^\infty(0,T;\mathcal{D}(\mathcal{A}^\gamma))$ with $-1/2 < \gamma \le 0$, and u, u_h be the solutions of (7.1) and (7.3) with $F_h = P_hF$, respectively. Then there exists a constant $C = C(\Omega, T, \boldsymbol{\alpha}, \boldsymbol{q}) > 0$ such that*

$$\|u_h(t) - u(t)\|_{L^2(\Omega)} + h\|\nabla(u_h(t) - u(t))\|_{L^2(\Omega)} \le C\, h^{2(1+\gamma)}\sigma_h^2\,\|F\|_{L^\infty(0,t;\mathcal{D}(\mathcal{A}^\gamma))} \quad (0 < t \le T),$$

where $\sigma_h = |\ln h|$.

Finally, we derive an error estimates in L^2-norm in time. To this end, we need a discrete analogue of Theorem 7.3, whose proof follows identically and hence is omitted here.

Lemma 7.11 *Let u_h be the solution of (7.3) with $a_h = 0$. Then for arbitrary $\gamma > -1/2$, there exists a constant $C = C(\Omega, T, \boldsymbol{\alpha}, \boldsymbol{q}) > 0$ such that*

$$\int_0^t \|\!|u_h(s)|\!\|^2_{\mathcal{D}(\mathcal{A}^{\gamma+1})}\,\mathrm{d}s \le C\int_0^t \|\!|F_h(s)|\!\|^2_{\mathcal{D}(\mathcal{A}^\gamma)}\,\mathrm{d}s \quad (0 < t \le T).$$

Theorem 7.7 *Let $a = 0$, $F \in L^\infty(0,T;\mathcal{D}(\mathcal{A}^\gamma))$ with $-1/2 < \gamma \le 0$, and u, u_h be the solutions of (7.1) and (7.3) with $F_h = P_h F$, respectively. Then there exists a constant $C = C(\Omega, T, \boldsymbol{\alpha}, \boldsymbol{q}) > 0$ such that*

$$\|u_h - u\|_{L^2(0,t;L^2(\Omega))} + h\|\nabla(u_h - u)\|_{L^2(0,t;L^2(\Omega))} \le C\, h^{2(1+\gamma)} \|F\|_{L^2(0,t;\mathcal{D}(\mathcal{A}^\gamma))} \quad (0 < t \le T).$$

Proof. We use again the splitting (7.12). By Theorem 7.3 and Lemma 7.5,

$$\begin{aligned} \|\widetilde{\varrho}\|_{L^2(0,t;L^2(\Omega))} + h\|\nabla\widetilde{\varrho}\|_{L^2(0,t;L^2(\Omega))} &\le C\, h^{2(1+\gamma)} \|u\|_{L^2(0,t;\mathcal{D}(\mathcal{A}^{1+\gamma}))} \\ &\le C\, h^{2(1+\gamma)} \|F\|_{L^2(0,t;\mathcal{D}(\mathcal{A}^\gamma))} \quad (0 < t \le T). \end{aligned}$$

By (7.8), (7.13), Lemma 7.11 and Lemma 7.5, we have for $\kappa = 0, 1/2$ that

$$\begin{aligned} \int_0^t \|\widetilde{\vartheta}(s)\|^2_{\mathcal{D}(\mathcal{A}^\kappa)}\,\mathrm{d}s &\le C \int_0^t \|\!|\triangle_h (R_h u - P_h u)(s)|\!\|^2_{\mathcal{D}(\mathcal{A}^{\kappa-1})}\,\mathrm{d}s \\ &\le C \int_0^t \|(R_h u - P_h u)(s)\|^2_{\mathcal{D}(\mathcal{A}^\kappa)}\,\mathrm{d}s \le \Big(C\, h^{2(1+\gamma-\kappa)} \|u\|_{L^2(0,t;\mathcal{D}(\mathcal{A}^{1+\gamma}))}\Big)^2 \\ &\le \Big(C\, h^{2(1+\gamma-\kappa)} \|F\|_{L^2(0,t;\mathcal{D}(\mathcal{A}^\gamma))}\Big)^2 \quad (0 < t \le T). \end{aligned}$$

Combing the above two estimates yields the desired assertion. □

7.4 A fully discrete scheme

Now we describe a fully discrete scheme for problem (7.1) based on the finite difference method introduced in [97]. To discretize the time-fractional derivatives, we divide the interval $[0,T]$ uniformly with a time step size $\tau = T/N_t$ ($N_t \in \mathbb{N}$). For $\beta \in (0,1)$, we perform the discretization at each knot $t_\ell = \ell\,\tau$ ($\ell = 1, \dots, N_t$) as

$$\begin{aligned} \partial_t^\beta f(t_\ell) &= \frac{1}{\Gamma(1-\beta)} \sum_{i=1}^{\ell} \int_{t_{i-1}}^{t_i} \frac{f'(s)}{(t_\ell - s)^\beta}\,\mathrm{d}s \approx \frac{1}{\Gamma(1-\beta)} \sum_{i=1}^{\ell} \frac{f(t_i) - f(t_{i-1})}{\tau} \int_{t_{i-1}}^{t_i} \frac{\mathrm{d}s}{(t_\ell - s)^\beta} + R_\ell^{\beta,\tau} \\ &= \frac{1}{\Gamma(2-\beta)} \sum_{i=1}^{\ell} d_i^\beta \frac{f(t_{\ell-i+1}) - f(t_{\ell-i})}{\tau^\beta} + R_\ell^{\beta,\tau}, \end{aligned}$$

where $d_i^\beta := i^{1-\beta} - (i-1)^{1-\beta}$ ($i = 1, 2, \dots$), and $R_\ell^{\beta,\tau}$ denotes the local truncation error. Lin and Xu [97, Lemma 3.1] (see also [126, Lemma 4.1]) showed that $R_\ell^{\beta,\tau}$ can be bounded as

$$|R_\ell^{\beta,\tau}| \le C\, \tau^{2-\beta} \max_{0 \le t \le T} |f''(t)| \quad (f \in C^2[0,T],\ \ell = 1, 2, \dots, N_t). \tag{7.15}$$

Then the multi-term fractional derivative $\sum_{j=1}^m q_j \partial_t^{\alpha_j} u(x,t)$ at $t = t_\ell$ in (7.1) can be discretized by

$$\sum_{j=1}^m q_j \partial_t^{\alpha_j} u(x, t_\ell) = P_\tau(\partial_t) u(x, t_\ell) + R_\ell^\tau(x), \tag{7.16}$$

where the discrete differential operator $P_\tau(\partial_t)$ is defined by

$$P_\tau(\partial_t) u(x, t_\ell) := \frac{1}{\Gamma(2-\alpha_1)} \sum_{i=1}^{\ell} P_i \frac{u(x, t_{\ell-i+1}) - u(x, t_{\ell-i})}{\tau^{\alpha_1}},$$

and the coefficients P_i ($i = 1, 2, \dots$) are defined by

$$P_i = \sum_{j=1}^m \frac{\Gamma(2-\alpha_1)\, q_j\, d_i^{\alpha_j}\, \tau^{\alpha_1 - \alpha_j}}{\Gamma(2-\alpha_j)}.$$

Then by (7.15), the local truncation error $R_\ell^\tau(x)$ of the approximation $P_\tau(\partial_t)u(x,t_\ell)$ is bounded by

$$|R_\ell^\tau(x)| \le C\sum_{j=1}^{m} q_j \tau^{2-\alpha_j} \max_{0\le t\le T} |\partial_t^2 u(x,t)| \le C\,\tau^{2-\alpha_1} \max_{0\le t\le T} |\partial_t^2 u(x,t)|. \tag{7.17}$$

By the monotonicity and convergence of $\{d_i^\beta\}$ (see [97, Eqn. (13)]), we know that

$$P_0 > P_1 > \ldots > 0 \quad \text{and} \quad P_i \to 0 \text{ as } i \to \infty. \tag{7.18}$$

Now we are ready to propose the following fully discrete scheme: find $u_h^\ell \in X_h$ ($\ell = 1,\ldots,N_t$) such that

$$(P_\tau(\partial_t)u_h^\ell, v_h) + (\nabla u_h^\ell, \nabla v_h) = (F^\ell, v_h) \quad (\forall\, v_h \in X_h), \tag{7.19}$$

where $F^\ell = F(\,\cdot\,,t_\ell)$. By setting $\eta = \Gamma(2-\alpha_1)\,\tau^{\alpha_1}$, the fully discrete scheme (7.19) is equivalent to finding $u_h^\ell \in X_h$ such that for all $v_h \in X_h$ and $\ell = 1,\ldots,N_t$,

$$P_0(u_h^\ell, v_h) + \eta(\nabla u_h^\ell, \nabla v_h) = \sum_{i=1}^{\ell-1}(P_{i-1}-P_i)(u_h^{\ell-i}, v_h) + P_{\ell-1}(u_h^0, v_h) + \eta(F^\ell, v_h). \tag{7.20}$$

The next result gives the stability of the fully discrete scheme.

Lemma 7.12 *The fully discrete scheme* (7.20) *is unconditionally stable, i.e., there exists a constant* $C = C(\Omega, T, \boldsymbol{\alpha}, \boldsymbol{q}) > 0$ *such that*

$$\|u_h^\ell\|_{L^2(\Omega)} \le \|u_h^0\|_{L^2(\Omega)} + C \max_{1\le i\le \ell} \|F^i\|_{L^2(\Omega)} \quad (\ell = 1,\ldots,N_t).$$

Proof. The case $\ell = 1$ is trivial, and we proceed by induction. By observing the monotone decreasing property of the sequence $\{P_i\}$ from (7.18) and choosing $v_h = u_h^\ell$ in (7.20), we deduce

$$\begin{aligned} P_0\|u_h^\ell\|_{L^2(\Omega)} &\le \sum_{i=1}^{\ell-1}(P_{i-1}-P_i)\|u_h^{\ell-i}\|_{L^2(\Omega)} + P_{\ell-1}\|u_h^0\|_{L^2(\Omega)} + \eta\|F^\ell\|_{L^2(\Omega)} \\ &\le \sum_{i=1}^{\ell-1}(P_{i-1}-P_i)\|u_h^{\ell-i}\|_{L^2(\Omega)} + P_{\ell-1}\|u_h^0\|_{L^2(\Omega)} + \eta \max_{1\le i\le \ell}\|F^i\|_{L^2(\Omega)} \\ &\le P_0\|u_h^0\|_{L^2(\Omega)} + (C(P_0-P_{\ell-1}) + \eta) \max_{1\le i\le \ell}\|F^i\|_{L^2(\Omega)}. \end{aligned}$$

Using the monotonicity of $\{P_i\}$ again gives

$$C(P_0 - P_{\ell-1}) + \eta \le C\,P_0 - (C\,P_{N_t} - \eta).$$

It suffices to choose a constant C such that $C\,P_{N_t} - \eta > 0$. Recalling $\tau = T/N_t$ and noting the concavity of the function $b(\tau) = (T+\tau)^{1-\alpha_1}$, we get $b(\tau) - b(0) \le b'(0)\tau$, i.e., $(T+\tau)^{1-\alpha_1} - T^{1-\alpha_1} \le (1-\alpha_1)T^{-\alpha_1}\tau$, and thus

$$d_{N_t+1}^{\alpha_1} = (N+1)^{1-\alpha_1} - N^{1-\alpha_1} = \big((T+\tau)^{1-\alpha_1} - T^{1-\alpha_1}\big)\,\tau^{\alpha_1-1} \le (1-\alpha_1)\,T^{-\alpha_1}\tau^{\alpha_1}.$$

Hence

$$P_{N_t} \le \sum_{j=1}^{m} \frac{\Gamma(2-\alpha_1)\,q_j\,(1-\alpha_j)\,T^{\alpha_1-\alpha_j}}{\Gamma(2-\alpha_j)} T^{-\alpha_1}\tau^{\alpha_1} =: C_0\,T^{-\alpha_1}\tau^{\alpha_1}.$$

Thus by choosing $C = T^{\alpha_1}/C_0$, we obtain

$$P_0\|u_h^\ell\|_{L^2(\Omega)} \le P_0\|u_h^0\|_{L^2(\Omega)} + C\,P_0 \max_{1\le i\le \ell}\|F^i\|_{L^2(\Omega)}.$$

The desired result follows by dividing both sides by P_0. □

Next we state an error estimate for the fully discrete scheme. In order to analyze the temporal discretization error, we assume that the solution is sufficiently smooth.

Theorem 7.8 *Let $a \in \mathcal{D}(\mathcal{A})$ and $F \in L^\infty(0,T;\mathcal{D}(\mathcal{A}^{1/2}))$. Suppose that the solution u is sufficiently smooth, and let $\{u_h^\ell\}_{\ell=0}^{N_t} \subset X_h$ be the solution to the fully discrete scheme* (7.20) *with u_h^0 satisfying $\|u_h^0 - a\|_{L^2(\Omega)} \le C\,h^2\|a\|_{\mathcal{D}(\mathcal{A})}$. Then there exists a constant $C = C(\Omega, T, \boldsymbol{\alpha}, \boldsymbol{q}) > 0$ such that*

$$\|u_h^\ell - u(t_\ell)\|_{L^2(\Omega)} \le C\left\{h^2\left(\|a\|_{\mathcal{D}(\mathcal{A})} + \|F\|_{L^\infty(0,t_\ell;\mathcal{D}(\mathcal{A}^{1/2}))} + \max_{0\le t\le t_\ell}\|\partial_t u(t)\|_{\mathcal{D}(\mathcal{A})}\right)\right.$$
$$\left. + \tau^{2-\alpha_1}\max_{0\le t\le t_\ell}\|\partial_t^2 u(t)\|_{L^2(\Omega)}\right\} \quad (\ell = 1,\dots,N_t).$$

Proof. We split the error $e^\ell := u(t_\ell) - u_h^\ell$ into two terms as

$$e^\ell = (u(t_\ell) - R_h u(t_\ell)) + \left(R_h u(t_\ell) - u_h^\ell\right) =: \varrho^\ell + \vartheta^\ell.$$

Here ϱ^ℓ is a special case of $\varrho(t) := u(t) - R_h u(t)$ with $t = t_\ell$. Applying Lemma 7.5, we have

$$\|\varrho(t)\|_{L^2(\Omega)} \le C\,h^2\|u(t)\|_{\mathcal{D}(\mathcal{A})} \le C\,h^2\left(\|a\|_{\mathcal{D}(\mathcal{A})} + \|F\|_{L^\infty(0,T;\mathcal{D}(\mathcal{A}^{1/2}))}\right), \tag{7.21}$$
$$\|\partial_t\varrho(t)\|_{L^2(\Omega)} \le C\,h^2\|\partial_t u(t)\|_{\mathcal{D}(\mathcal{A})}. \tag{7.22}$$

It suffices to bound the term ϑ^n. By comparing (7.1) and (7.19), we derive the error equation

$$\begin{cases}(P_\tau(\partial_t)\vartheta^n, v_h) + (\nabla\vartheta^n, \nabla v_h) = (\xi^n, v_h) \quad (\forall\, v_h \in X_h,\ 1 \le \ell \le N_t),\\ \vartheta^0 = R_h a - u_h^0,\end{cases} \tag{7.23}$$

where the right-hand side ξ^n is given by

$$\xi^n = P_\tau(\partial_t)R_h u(t_\ell) - \sum_{j=1}^m q_j\partial_t^{\alpha_j}u(t_\ell) = -P_\tau(\partial_t)\varrho^\ell - R_\ell^\tau =: \xi_1^\ell + \xi_2^\ell,$$

and the truncation error R_ℓ^τ is defined in (7.16). Using the identity

$$\varrho^i - \varrho^{i-1} = \int_{t_{i-1}}^{t_j}\partial_t\varrho(t)\,\mathrm{d}t$$

and the inequality (7.22), we can bound the term ξ_1^ℓ by

$$\begin{aligned}\|\xi_1^\ell\|_{L^2(\Omega)} &\le C\left\|\sum_{i=1}^\ell \frac{\varrho(t_i) - \varrho(t_{i-1})}{\tau}\sum_{j=1}^m q_j\int_{t_{i-1}}^{t_i}\frac{\mathrm{d}s}{(t_\ell - s)^{\alpha_j}}\right\|_{L^2(\Omega)}\\ &\le \frac{C}{\tau}\sum_{i=1}^\ell\int_{t_{i-1}}^{t_i}\|\partial_t\varrho(t)\|_{L^2(\Omega)}\,\mathrm{d}t\sum_{j=1}^m q_j\int_{t_{i-1}}^{t_i}\frac{\mathrm{d}s}{(t_\ell - s)^{\alpha_j}}\\ &\le C\,h^2\max_{0\le t\le t_\ell}\|\partial_t u(t)\|_{\mathcal{D}(\mathcal{A})}\sum_{j=1}^m q_j\int_0^{t_\ell}\frac{\mathrm{d}s}{(t_\ell - s)^{\alpha_j}} \le C\,h^2\max_{0\le t\le t_\ell}\|\partial_t u(t)\|_{\mathcal{D}(\mathcal{A})}.\end{aligned}$$

Meanwhile, the second term ξ_2^ℓ can be bounded using (7.17). Then by the stability from Lemma 7.12 for the error equation (7.23), we obtain

$$\|\vartheta^\ell\|_{L^2(\Omega)} \le C\left(\|\vartheta^0\|_{L^2(\Omega)} + \max_{1\le i\le\ell}\|\xi_1^i\|_{L^2(\Omega)} + \max_{1\le i\le\ell}\|\xi_2^i\|_{L^2(\Omega)}\right)$$

$$\leq C \left\{ h^2 \left(\|a\|_{\mathcal{D}(\mathcal{A})} + \max_{0\leq t\leq t_\ell} \|\partial_t u(t)\|_{\mathcal{D}(\mathcal{A})} \right) + \tau^{2-\alpha_1} \max_{0\leq t\leq t_\ell} \|\partial_t^2 u(t)\|_{L^2(\Omega)} \right\}, \quad (7.24)$$

where ϑ^0 is estimated by the choice of u_h^0 and Lemma 7.5 as

$$\|\vartheta^0\|_{L^2(\Omega)} = \|R_h a - u_h^0\|_{L^2(\Omega)} \leq \|R_h a - a\|_{L^2(\Omega)} + \|a - u_h^0\|_{L^2(\Omega)} \leq C\, h^2 \|a\|_{\mathcal{D}(\mathcal{A})}.$$

The combination of (7.21) and (7.24) immediately yields the desired error estimate. □

Remark 7.2 The error estimate in Theorem 7.8 holds only if the solution u is sufficiently smooth u. There seems no known error estimate expressed in terms of the initial data (and right-hand side) only for fully discrete schemes for nonsmooth initial data even for the single-term time-fractional diffusion equation with a Caputo fractional derivative.

7.5 Numerical experiments

In this section, we present one-and two-dimensional numerical experiments to verify the error estimates in Sections 7.3 and 7.4. We shall discuss the cases of a homogeneous problem and an inhomogeneous problem separately. Without lose of generality, we consider the following initial-boundary value problem for a fractional diffusion equation with two Caputo derivatives in time throughout this section

$$\begin{cases} \partial_t^\alpha u + \partial_t^\beta u = \triangle u + F & \text{in } \Omega \times (0,T], \\ u = a & \text{in } \Omega \times \{0\}, \\ u = 0 & \text{on } \partial\Omega \times (0,T], \end{cases} \quad (7.25)$$

where we basically fix $\alpha = 0.5$ and $\beta = 0.2$. Only in Subsection 7.5.1 and Example 7.1, we choose various α to compare the numerical performances.

7.5.1 The case of a smooth solution

Here we consider the one-dimensional case of (7.25) on the unit interval $\Omega = (0,1)$. In order to verify the estimate in Theorem 7.8, we first check the situation that the solution u is sufficiently smooth. Set

$$a(x) = x - x^2, \quad F(x,t) = 2\left(\frac{t^{2-\alpha}}{\Gamma(3-\alpha)} + \frac{t^{2-\beta}}{\Gamma(3-\beta)} \right)(x - x^2) + 2(1+t^2).$$

Then the exact solution u is given by $u(x,t) = (1+t^2)(x-x^2)$, which is very smooth.

In our computation, we divide the unit interval $\Omega = (0,1)$ into N_x equidistant subintervals with the mesh size $h = 1/N_x$. Similarly, the time span is also equally partitioned with a step length τ. Here we choose N_x large enough so that the space discretization error is negligible, and the time discretization error dominates. We evaluate the accuracy of the numerical approximation u_h^ℓ by the normalized errors $\|u_h^\ell - u(t_\ell)\|_{L^2(\Omega)}/\|a\|_{L^2(\Omega)}$. In Table 7.1, we show the temporal convergence rates, indicated under the column "Rate" (the number in bracket is the theoretical rate), for three different α values, which fully confirms the theoretical result. See also Figure 7.1 for the plot of the convergence rates.

Table 7.1: Numerical results for the case with a smooth solution at $t = 1$ with $\beta = 0.2$ and $\alpha = 0.25, 0.5, 0.95$, discretized on a uniform mesh of mesh size $h = 2^{-10}$ and $\tau = 0.2 \times 2^{-k}$ $(k = 1, \ldots, 5)$.

α	Norm	$\tau = 1/10$	$\tau = 1/20$	$\tau = 1/40$	$\tau = 1/80$	$\tau = 1/160$	Rate
0.25	L^2	5.58e-4	1.73e-4	5.25e-5	1.51e-5	3.90e-6	≈ 1.81 (1.75)
0.5	L^2	1.45e-3	5.11e-4	1.78e-4	6.17e-5	2.08e-5	≈ 1.55 (1.50)
0.95	L^2	7.92e-3	3.79e-3	1.82e-3	8.73e-4	4.20e-4	≈ 1.06 (1.05)

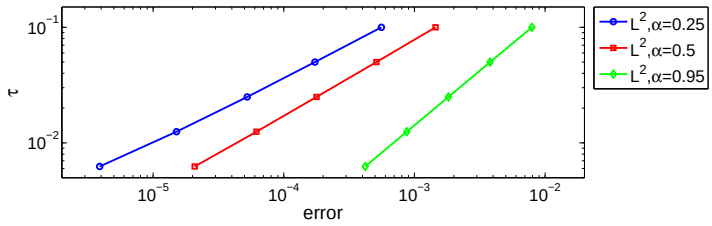

Figure 7.1: Numerical results for the case with a smooth solution at $t = 1$ with $\beta = 0.2$ and $\alpha = 0.25, 0.5, 0.95$.

7.5.2 Homogeneous problems

In this subsection, we present numerical results to illustrate the spatial convergence rates in section 7.3 in case of $F = 0$ in (7.25). We performed numerical tests for initial data with different smoothness. In order to check the convergence rate of the semidiscrete scheme, we discretize the fractional derivatives with a tiny time step, and thus the temporal discretization error is negligible. For each example, we evaluate the error $e(t) = u(t) - u_h(t)$ by the normalized errors $\|e(t)\|_{L^2(\Omega)}/\|a\|_{L^2(\Omega)}$ and $\|\nabla e(t)\|_{L^2(\Omega)}/\|a\|_{L^2(\Omega)}$. The normalization enables us to observe the behavior of the error with respect to time in case of nonsmooth initial data. For simplicity, we still consider the one-dimensional case with $\Omega = (0, 1)$.

Example 7.1 We first choose a smooth initial value $a(x) = \sin(2\pi x)$ which belongs to $H^2(\Omega) \cap H_0^1(\Omega)$, and perform the tests with $\beta = 0.2$ and $\alpha = 0.25, 0.5, 0.95$. The numerical results show that for all three different values of α, the convergence rates in L^2- and H^1-norms of the error turn out to be $\mathcal{O}(h^2)$ and $\mathcal{O}(h)$ respectively (see Figure 7.2). As the value of α increases from 0.25 to 0.95, the error at $t = 1$ decreases accordingly, which resembles that for the single-term case in [81].

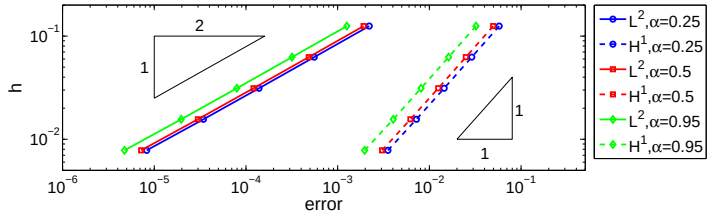

Figure 7.2: Numerical results for Example 7.1 at $t = 1$ with $\beta = 0.2$ and $\alpha = 0.25, 0.5, 0.95$, discretized on a uniform mesh $h = 2^{-k}$ $(k = 3, \ldots, 7)$ and $\tau = 2 \times 10^{-5}$.

Example 7.2 Next, we choose a nonsmooth initial value $a(x) = \chi_{(0,1/2]}(x)$, that is, the characterization function of $(0, 1/2]$. It is known that $a \in \mathcal{D}(\mathcal{A}^{1/4-\epsilon})$ for arbitrarily small $\epsilon > 0$.

Here we are particularly interested in the errors for t close to zero, and thus we also present the errors at $t = 0.01$ and $t = 0.001$ in Table 7.2. The numerical results fully confirm the theoretically predicted rates for the nonsmooth initial data. Further, in Table 7.3 we show the L^2-norm of the error for fixed $h = 2^{-6}$ as $t \downarrow 0$. We observe that the error deteriorates as $t \downarrow 0$. Noting that a almost belongs to $\mathcal{D}(\mathcal{A}^{1/4})$, it follows from Theorem 7.5 that the error grows like $\mathcal{O}(t^{-3\alpha_1/4})$, which is in excellent agreement with the numerical experiments in Table 7.3.

Table 7.2: Numerical results for Example 7.2 at $t = 1, 0.01, 0.001$, discretized on a uniform mesh $h = 2^{-k}$ $(k = 3, \ldots, 7)$ and $\tau = t/(5 \times 10^4)$.

t	Norm	$k=3$	$k=4$	$k=5$	$k=6$	$k=7$	Rate
1	L^2	1.86e-3	4.64e-4	1.16e-4	2.87e-5	6.88e-6	≈ 2.02 (2.00)
	H^1	4.89e-2	2.44e-2	1.22e-2	6.07e-3	2.96e-3	≈ 1.01 (1.00)
0.01	L^2	8.04e-3	2.00e-3	5.01e-4	1.24e-4	2.98e-5	≈ 2.03 (2.00)
	H^1	2.31e-1	1.16e-1	5.79e-2	2.88e-2	1.40e-2	≈ 1.01 (1.00)
0.001	L^2	1.65e-2	4.14e-3	1.03e-3	2.56e-4	6.18e-4	≈ 2.01 (2.00)
	H^1	5.15e-1	2.58e-1	1.29e-1	6.41e-2	3.13e-2	≈ 1.01 (1.00)

Table 7.3: L_2-error with $h = 2^{-6}$ as $t \downarrow 0$ in Example 7.2.

t	1e-3	1e-4	1e-5	1e-6	1e-7	1e-8	Rate
L^2-norm	2.56e-4	5.39e-4	1.15e-3	2.91e-3	6.77e-3	1.55e-2	≈ -0.37 $(\approx -3/8)$

Example 7.3 In this example, we choose a nonsmooth initial value with even lower regularity as $a(x) = \delta_{1/2}(x)$, that is, a Dirac function concentrating at $x = 1/2$. Actually, $a \in \mathcal{D}(\mathcal{A}^{-1/4-\epsilon})$ for arbitrarily small $\epsilon > 0$. The numerical results show a superconvergence with a rate of $\mathcal{O}(h^2)$ in the L^2-norm and a rate of $\mathcal{O}(h)$ in the H^1-norm (see Figure 7.3(a)). This is attributed to the fact that in one spatial dimension, the solution with a Dirac function as the initial data is smooth from both sides of the support point, and the finite element spaces X_h possess a good approximation property. When the singular point $x = 1/2$ is not aligned with the grid, Figure 7.3(b) indicates an $\mathcal{O}(h^{3/2})$ and $\mathcal{O}(h^{1/2})$ convergence rate for the L^2- and H^1-norm of the error respectively, which agrees with our theoretical results.

7.5.3 Inhomogeneous problems

Now we consider the inhomogeneous problem with $a = 0$ in (7.25) on the unit interval $\Omega = (0, 1)$. Similarly to the previous subsection, we adjust the smoothness of data to test their influence upon the numerical performance.

Example 7.4 We first choose $F(x, t) = \chi_{[0,1,2]}(x)\,(\chi_{[1/2,1]}(t)+1)$, which belongs to $L^\infty(0, T; \mathcal{D}(\mathcal{A}^{1/4-\epsilon})$ for arbitrarily small $\epsilon > 0$. Since Theorem 7.6 guarantees a time-independent error estimate, we only present the errors $\|e(t)\|_{L^2(\Omega)}$ and $\|\nabla e(t)\|_{L^2(\Omega)}$. In Table 7.4, we present the L^2- and H^1-errors at $t = 1, 0.01, 0.001$. The numerical results agree well with our theoretical predictions, i.e., $\mathcal{O}(h^2)$ and $\mathcal{O}(h)$ convergence rates for the L^2- and H^1-norms of the error, respectively.

Example 7.5 In this example, we choose $F(x, t) = \delta_{1/2}(x)\,(\chi_{[1/2,1]}(t) + 1)$, which involves a Dirac function concentrating at $x = 1/2$ in space and then $F \in L^\infty(0, T; \mathcal{D}(\mathcal{A}^{-1/4-\epsilon})$ for arbitrarily small $\epsilon > 0$. In Table 7.6, we show the error and convergence rates at $t = 1, 0.01, 0.001$. Here the mesh size h is chosen as $h = 1/(2^k + 1)$ $(k = 3, \ldots, 7)$, and thus the support of

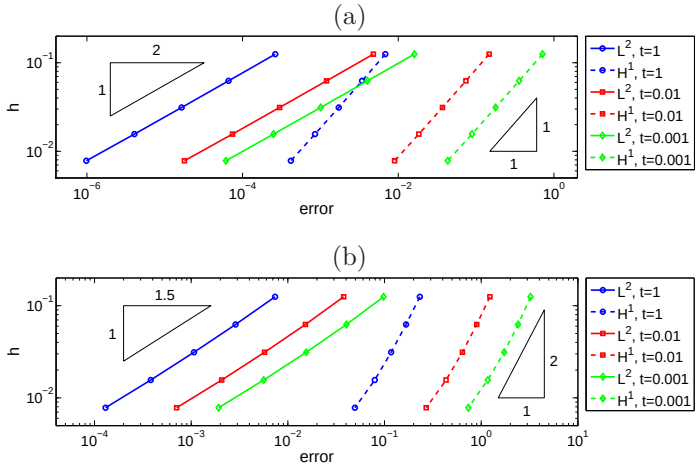

Figure 7.3: Numerical results for Example 7.3 at $t = 0.005, 0.01, 1$ with the step length $\tau = t/(5 \times 10^4)$ in time. (a) $x = 1/2$ aligns with the grid when $h = 2^{-k}$ $(k = 3, \ldots, 7)$. (b) $x = 1/2$ does not align with the grid for $h = 1/(2^k + 1)$ $(k = 3, \ldots, 7)$.

Table 7.4: Numerical results for Example 7.4 at $t = 1, 0.01, 0.001$, discretized on a uniform mesh $h = 2^{-k}$ $(k = 3, \ldots, 7)$ and $\tau = t/(5 \times 10^4)$.

t	Norm	$k = 3$	$k = 4$	$k = 5$	$k = 6$	$k = 7$	Rate
1	L^2	1.76e-3	4.40e-4	1.10e-4	2.71e-5	6.53e-6	≈ 2.01 (2.00)
	H^1	4.72e-2	2.36e-2	1.18e-2	5.86e-3	2.86e-3	≈ 1.01 (1.00)
0.01	L^2	6.34e-4	1.59e-4	3.96e-5	9.82e-6	2.38e-6	≈ 2.01 (2.00)
	H^1	1.89e-2	9.46e-3	4.72e-3	2.35e-3	1.15e-3	≈ 1.01 (1.00)
0.001	L^2	4.55e-4	1.15e-4	2.88e-5	1.15e-6	1.73e-6	≈ 2.02 (2.00)
	H^1	1.45e-2	7.31e-3	3.66e-3	1.82e-3	8.88e-4	≈ 1.01 (1.00)

the Dirac function does not align with the grid. The results indicate an $\mathcal{O}(h^{1/2})$ and $\mathcal{O}(h^{3/2})$ convergence rate for the H^1- and L^2-norm of the error respectively, which agrees well with the theoretical prediction. However, if the Dirac function is supported at a grid point, both L^2- and H^1-norm of the error exhibit a superconvergence phenomenon, namely, order $\mathcal{O}(h^2)$ and $\mathcal{O}(h)$ respectively, which are one half order higher than theoretical ones (see Table 7.5). This superconvergence still awaits theoretical justifications.

Table 7.5: Numerical results for Example 7.5 at $t = 0.1, 0.01, 0.001$, discretized on a uniform mesh $h = 1/(2^k + 1)$ $(k = 3, \ldots, 7)$ and $\tau = t/(5 \times 10^4)$.

t	Norm	$k=3$	$k=4$	$k=5$	$k=6$	$k=7$	Rate
1	L^2	1.02e-2	4.01e-3	1.49e-3	5.35e-4	1.82e-4	≈ 1.49 (1.50)
	H^1	3.24e-1	2.35e-1	1.65e-1	1.11e-1	6.94e-2	≈ 0.50 (0.50)
0.01	L^2	4.66e-3	1.91e-3	7.29e-4	2.64e-4	9.02e-5	≈ 1.45 (1.50)
	H^1	1.54e-1	1.14e-1	8.16e-2	5.54e-2	3.47e-2	≈ 0.55 (0.50)
0.001	L^2	4.30e-3	1.83e-3	7.12e-4	2.61e-4	8.97e-5	≈ 1.45 (1.50)
	H^1	1.47e-1	1.11e-1	8.05e-2	5.50e-2	3.45e-2	≈ 0.55 (0.50)

Table 7.6: Numerical results for Example 7.5 at $t = 1, 0.01, 0.001$, discretized on a uniform mesh $h = 2^{-k}$ $(k = 3, \ldots, 7)$ and $\tau = t/(5 \times 10^4)$.

t	Norm	$k=3$	$k=4$	$k=5$	$k=6$	$k=7$	Rate
1	L^2	5.35e-4	1.34e-4	3.35e-5	8.31e-6	2.01e-6	≈ 2.01 (1.50)
	H^1	1.49e-2	7.48e-3	3.74e-3	1.86e-3	9.07e-4	≈ 1.01 (0.50)
0.01	L^2	6.67e-4	1.67e-4	4.17e-5	1.04e-5	2.52e-6	≈ 2.03 (1.50)
	H^1	2.56e-2	1.29e-2	6.44e-3	3.20e-3	1.56e-3	≈ 1.02 (0.50)
0.001	L^2	8.19e-4	2.08e-4	5.22e-5	1.30e-5	3.19e-6	≈ 2.02 (1.50)
	H^1	3.96e-2	2.00e-2	1.00e-3	4.98e-3	2.45e-3	≈ 1.01 (0.50)

7.5.4 Two-dimensional examples

Finally, we present three two-dimensional examples with various choices of initial value and right-hand side on the unit square $\Omega = (0,1)^2$.

(a) Nonsmooth initial data $a = \chi_{(0,1/2)\times(0,1)}$ and $F = 0$.

(b) Nonsmooth initial data with lower regularity $a = \delta_\Gamma$ and $F = 0$. Here Γ denotes the union of $\{1/4\} \times [1/4, 3/4] \cup [1/4, 3/4] \times \{3/4\}$ clockwise and $[1/4, 3/4] \times \{1/4\} \cup \{3/4\} \times [1/4, 3/4]$ counterclockwise. The duality is defined by $\langle \delta_\Gamma, v \rangle = \int_\Gamma v(s)\,\mathrm{d}s$. By Hölder's inequality and the continuity of the trace operator from $\mathcal{D}(\mathcal{A}^{1/4+\epsilon})$ to $L^2(\Gamma)$ for any $\epsilon > 0$ (see [1]), we deduce $\delta_\Gamma \in \mathcal{D}(\mathcal{A}^{-1/4-\epsilon})$ for arbitrarily small $\epsilon > 0$.

(c) Nonsmooth right-hand side $F(x,t) = \chi_{(0,1/2)\times(0,1)}(x)\,(\chi_{[1/20,1/10]}(t) + 1)$ and $a = 0$.

To discretize the problem, we divide the each direction into $N_x = 2^k$ equally spaced subintervals with a mesh size $h = 1/N_x$, so that the domain $[0,1]^2$ is divided into N_x^2 small squares. We get a symmetric mesh by connecting the diagonal of each small square.

The numerical results for example (a) are shown in Tables 7.7, which agree well with the theoretical rate in Theorem 7.5, with a rate $\mathcal{O}(h^2)$ and $\mathcal{O}(h)$ respectively for the L^2- and H^1-norm of the errors. Interestingly, for example (b), both the L^2-norm and H^1-norm of the errors

exhibit superconvergence (see Table 7.8). The numerical results for example (c) confirm the theoretical results (see Table 7.9). The solution profiles for examples (b) and (c) at $t = 0.1$ are shown in Figure 7.4, from which the nonsmooth region of the solution can be clearly observed.

Table 7.7: Numerical results for example (a) at $t = 0.1, 0.01, 0.001$, discretized on a uniform mesh $h = 2^{-k}$ $(k = 3, \ldots, 7)$ and $\tau = t/10^4$.

t	Norm	$k=3$	$k=4$	$k=5$	$k=6$	$k=7$	Rate
0.1	L^2	5.25e-3	1.35e-3	3.38e-4	8.24e-5	1.98e-5	≈ 2.06 (2.00)
	H^1	9.10e-2	4.53e-2	2.25e-2	1.09e-2	4.99e-3	≈ 1.04 (1.00)
0.01	L^2	1.25e-2	3.23e-3	8.09e-4	1.97e-4	4.65e-5	≈ 2.05 (2.00)
	H^1	2.18e-1	1.08e-1	5.35e-2	2.62e-2	1.27e-2	≈ 1.05 (1.00)
0.001	L^2	3.02e-2	7.84e-3	1.97e-3	4.81e-4	1.16e-4	≈ 2.03 (2.00)
	H^1	5.30e-1	2.64e-1	1.31e-1	6.38e-2	3.14e-2	≈ 1.04 (1.00)

Table 7.8: Numerical results for example (b) at $t = 0.1, 0.01, 0.001$, discretized on a uniform mesh $h = 2^{-k}$ $(k = 3, \ldots, 7)$ and $\tau = t/10^4$.

t	Norm	$k=3$	$k=4$	$k=5$	$k=6$	$k=7$	Rate
0.1	L^2	1.18e-2	3.18e-3	8.41e-4	2.18e-4	5.41e-5	≈ 1.92 (1.50)
	H^1	2.25e-1	1.13e-1	6.60e-2	3.40e-2	1.66e-2	≈ 0.92 (0.50)
0.01	L^2	2.82e-2	7.62e-3	2.28e-3	5.26e-4	1.25e-4	≈ 1.95 (2.00)
	H^1	5.66e-1	3.09e-1	1.65e-1	8.52e-2	4.19e-2	≈ 0.94 (1.00)
0.001	L^2	6.65e-2	1.83e-3	4.98e-3	1.33e-3	3.30e-4	≈ 1.91 (2.00)
	H^1	1.66e0	8.93e-1	4.75e-1	2.43e-1	1.21e-1	≈ 0.95 (1.00)

Table 7.9: Numerical results for example (c) at $t = 0.1, 0.01, 0.001$, discretized on a uniform mesh $h = 2^{-k}$ $(k = 3, \ldots, 7)$ and $\tau = t/10^4$.

t	Norm	$k=3$	$k=4$	$k=5$	$k=6$	$k=7$	Rate
0.1	L^2	2.28e-3	5.86e-4	1.47e-4	3.58e-5	7.91e-6	≈ 2.07 (2.00)
	H^1	3.97e-2	1.97e-2	9.77e-3	4.76e-3	2.13e-3	≈ 1.06 (1.00)
0.01	L^2	1.06e-3	2.73e-4	6.86e-5	1.67e-6	3.70e-7	≈ 2.06 (2.00)
	H^1	1.85e-2	9.18e-3	4.56e-3	2.22e-3	9.94e-4	≈ 1.06 (1.00)
0.001	L^2	8.66e-4	2.28e-4	5.75e-5	1.40e-6	3.11e-7	≈ 2.04 (2.00)
	H^1	1.56e-2	7.82e-3	3.88e-3	1.90e-3	8.47e-4	≈ 1.05 (1.00)

7.6 Concluding remarks

In this chapter, we have developed a simple numerical scheme based on the Galerkin finite element method for a multi-term time fractional diffusion equation which involves multiple Caputo fractional derivatives in time. A complete error analysis of the space semidiscrete Galerkin scheme is provided. The theory covers the practically very important case of nonsmooth initial data and right-hand side. The analysis relies essentially on some refined regularity results of the multi-term time fractional diffusion equation. Further, we have developed a fully discrete scheme based on a finite difference discretization of the Caputo fractional derivatives. The stability and error estimate of the fully discrete scheme were established, provided that the solution is smooth. The extensive numerical experiments in one-and two-dimension fully con-

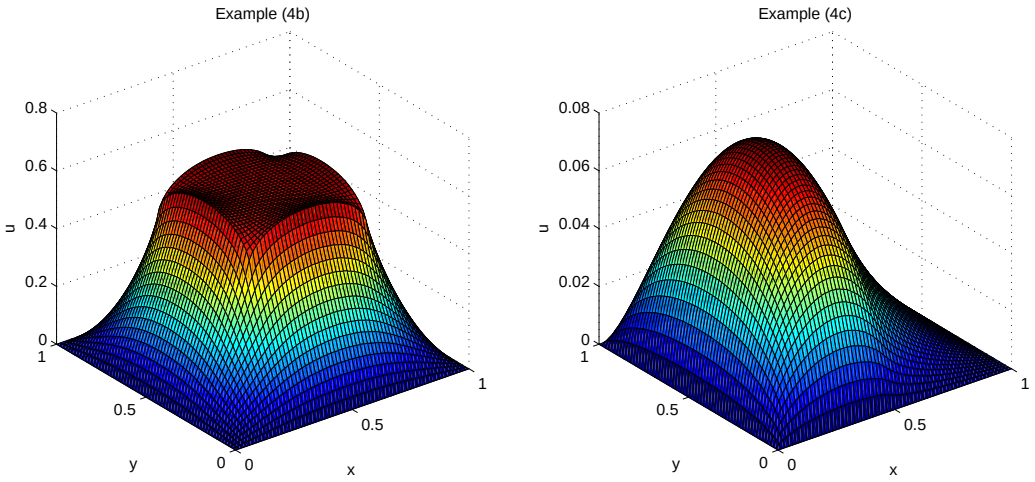

Figure 7.4: Numerical solutions of examples (b) and (c) with $h = 2^{-6}$ at $t = 0.1$.

firmed our convergence analysis: the empirical convergence rates agree well with the theoretical predictions for both smooth and nonsmooth data.

References for Part II

[58] Adams E E and Gelhar L W 1992 Field study of dispersion in a heterogeneous aquifer 2. Spatial moments analysis *Water Resources Res.* **28** 3293–307

[59] Bazhlekova E 2013 Properties of the fundamental and the impulse-response solutions of multi-term fractional differential equations *Complex Analysis and Applications '13 (Proc. Intern. Conf., Sofia, 2013)* ed V Kiryakova (Bulg. Acad. Sci. Sofia) pp 55–64

[60] Beckers S and Yamamoto M 2013 Regularity and unique existence of solution to linear diffusion equation with multiple time-fractional derivatives *Control and Optimization with PDE Constraints* ed K Bredies, C Clason, K Kunisch and G von Winckel (Basel: Birkhäuser) pp 45–56

[61] Berge C 1971 *Principles of Combinatorics* (New York: Academic Press)

[62] Brunner H, Ling L and Yamamoto M 2010 Numerical simulations of 2D fractional subdiffusion problems *J. Comput. Phys.* **229** 6613–22

[63] Cannon J R and Esteva S P 1986 An inverse problem for the heat equation *Inverse Problems* **2** 395–403

[64] Casas E, Clason C and Kunisch K 2013 Parabolic control problems in measure spaces with sparse solutions *SIAM J. Control Optim.* **51** 28–63

[65] Cheng J, Nakagawa J, Yamamoto M and Yamazaki T 2009 Uniqueness in an inverse problem for a one-dimensional fractional diffusion equation *Inverse Problems* **25** 115002

[66] Courant R and Hilbert D 1953 *Methods of Mathematical Physics* (New York: Interscience)

[67] Diethelm K 2010 *The Analysis of Fractional Differential Equations: An Application-Oriented Exposition Using Differential Operators of Caputo Type* (Berlin: Springer)

[68] El-Sayed A M A, El-Kalla I L and Ziada E A A 2010 Analytical and numerical solutions of multi-term nonlinear fractional orders differential equations *Appl. Numer. Math.* **60** 788–97

[69] Fu Z-J, Chen W and Yang H-T 2013 Boundary particle method for Laplace transformed time fractional diffusion equations *J. Comput. Phys.* **235** 52–66

[70] Fujishiro K 2014 Approximate controllability for fractional diffusion equations by dirichlet boundary control arXiv:1404.0207v2

[71] Fujishiro K and Yamamoto M 2014 Approximate controllability for fractional diffusion equations by interior control *Appl. Anal.* **93** 1793–1810

[72] Ginoa M, Cerbelli S amd Roman H E 1992 Fractional diffusion equation and relaxation in complex viscoelastic materials *Phys. A* **191** 449–53

[73] Gorenflo R, Luchko Y and Yamamoto M 2014 Operator theoretic approach to the Caputo derivative and the fractional diffusion equations arXiv:1411.7289

[74] Gorenflo R, Luchko Y and Zabrejko P P 1999 On solvability of linear fractional differential equations in Banach spaces *Frac. Calc. Appl. Anal.* **2** 163–76

[75] Gorenflo R and Mainardi F 1997 Fractional calculus: Integral and differential equations of fractional order *Fractals and Fractional Calculus in Continuum Mechanics* ed A Carpinteri and F Mainardi (New York: Springer-Verlag) pp 223–76

[76] Hatano Y and Hatano N 1998 Dispersive transport of ions in column experiments: an explanation of long-tailed profiles *Water Resources Res.* **34** 1027–33

[77] Jiang H, Liu F, Turner I and Burrage K 2012 Analytical solutions for the multi-term time-space Caputo-Riesz fractional advection-diffusion equations on a finite domain *J. Math. Anal. Appl.* **389** 1117–27

[78] Jin B, Lazarov R, Liu Y and Zhou Z 2015 The Galerkin finite element method for a multi-term time-fractional diffusion equation *J. Comput. Phys.* **281** 825–43

[79] Jin B, Lazarov R, Pasciak J and Zhou Z 2013 Error analysis of semidiscrete finite element methods for inhomogeneous time-fractional diffusion *IMA J. Numer. Anal.* in press

[80] Jin B, Lazarov R, Pasciak J and Zhou Z 2013 Galerkin FEM for fractional order parabolic equations with initial data in H^{-s}, $0 \leq s \leq 1$ *Proc. 5th Conf. Numer. Anal. Appl.* (Berlin: Springer) pp 24–37

[81] Jin B, Lazarov R and Zhou Z 2013 Error estimates for a semidiscrete finite element method for fractional order parabolic equations *SIAM J. Numer. Anal.* **51** 445–66

[82] Jin B and Lu X 2012 Numerical identification of a Robin coefficient in parabolic problems *Math. Comp.* **81** 1369–98

[83] Jin B and Rundell W 2012 An inverse problem for a one-dimensional time-fractional diffusion problem *Inverse Problems* **28** 075010

[84] Katsikadelis J 2009 Numerical solution of multi-term fractional differential equations *Z. Angew. Math. Mech.* **89** 593–608

[85] Kelly J F, McGough R J and Meerschaert M M 2008 Analytical time-domain Green's functions for power-law media *J. Acoust. Soc. Am.* **124** 2861–72

[86] Kilbas A A, Srivastava H M and Trujillo J J 2006 *Theory and Applications of Fractional Differential Equations* (Amsterdam: Elsevier)

[87] Li Z, Imanuvilov O Y and Yamamoto M 2014 Uniqueness in inverse boundary value problems for fractional diffusion equations arXiv:1404.7024

[88] Li Z, Liu Y and Yamamoto M 2014 Initial-boundary value problems for multi-term time-fractional diffusion equations with positive constant coefficients *Appl. Math. Comput.* in press

[89] Li Z, Luchko Y and Yamamoto M 2014 Asymptotic estimates of solutions to initial-boundary-value problems for distributed order time-fractional diffusion equations *Fract. Calc. Appl. Anal.* **17** 1114–1136

[90] Li X and Xu C 2009 A space-time spectral method for the time fractional diffusion equation *SIAM J. Numer. Anal.* **47** 2108–31

[91] Li X and Xu C 2010 Existence and uniqueness of the weak solution of the space-time fractional diffusion equation and a spectral method approximation *Commun. Comput. Phys.* **8** 1016–51

[92] Li L and Xu D 2014 Alternating direction implicit Galerkin finite element method for the two-dimensional time fractional evolution equation *Numer. Math. Theory Methods Appl.* **7** 41–57

[93] Li Z and Yamamoto M 2013 Some inverse source problems for linear diffusion equation with multiple time-fractional derivatives (preprint)

[94] Li Z and Yamamoto M 2013 Initial-boundary value problems for linear diffusion equations with multiple time-fractional derivatives arXiv:1306.2778v2

[95] Li Z and Yamamoto M 2014 Uniqueness for inverse problems of determining orders of multi-term time-fractional derivatives of diffusion equation *Appl Anal.* in press

[96] Li G, Zhang D, Jia X and Yamamoto M 2013 Simultaneous inversion for the space-dependent diffusion coefficient and the fractional order in the time-fractional diffusion equation *Inverse Problems* **29** 065014

[97] Lin Y and Xu C 2007 Finite difference/spectral approximations for the time-fractional diffusion equation *J. Comput. Phys.* **225** 1533–52

[98] Liu F, Meerschaert M M, McGough R J, Zhuang P and Liu X 2013 Numerical methods for solving the multi-term time-fractional wave-diffusion equation *Frac. Cal. Appl. Anal.* **16** 9–25

[99] Liu F, Zhuang P, Anh V, Turner I and Burrage K 2007 Stability and convergence of the difference methods for the space-time fractional advection-diffusion equation *Appl. Math. Comput.* **191** 12–20

[100] Luchko Y 2008 Initial-boundary value problems for the generalized time-fractional diffusion equation *Proceedings of 3rd IFAC Workshop on Fractional Differentiation and Its Applications (FDA08)* Ankara, Turkey, 05–07 November 2008.

[101] Luchko Y 2009 Maximum principle for the generalized time-fractional diffusion equation *J. Math. Anal. Appl.* **351** 218–23

[102] Luchko Y 2010 Some uniqueness and existence results for the initial-boundary value problems for the generalized time-fractional diffusion equation *Comput. Math. Appl.* **59** 1766–72

[103] Luchko Y 2011 Initial-boundary-value problems for the generalized multi-term time-fractional diffusion equation *J. Math. Anal. Appl.* **374** 538–48

[104] Luchko Y and Gorenflo R 1999 An operational method for solving fractional differential equations with the Caputo derivatives *Acta Math. Vietnam* **24** 207–33

[105] Luchko Y, Rundell W, Yamamoto M and Zuo L 2013 Uniqueness and reconstruction of an unknown semilinear term in a time-fractional reaction.diffusion equation *Inverse Problems* **29** 065019

[106] Mainardi F, Mura A, Pagnini G and Gorenflo R 2008 Time-fractional diffusion of distributed order *J. Vib. Control* **14** 1267–90

[107] McLean W and Thomee V 2010 Maximum-norm error analysis of a numerical solution via Laplace transformation and quadrature of a fractional-order evolution equation *IMA J. Numer. Anal.* **30** 208–30

[108] Meerschaert M M and Tadjeran C 2004 Finite difference approximations for fractional advection-dispersion flow equations *J. Comput. Appl. Math.* **172** 65–77

[109] Metzler R and Klafter J 2000 The random walk's guide to anomalous diffusion: a fractional dynamics approach *Phys. Rep.* **339** 1–77

[110] Metzler R, Klafter J and Sokolov I M 1998 Anomalous transport in external fields: continuous time random walks and fractional diffusion equations extended *Phys. Rev. E* **58** 1621–33

[111] Miller L and Yamamoto M 2013 Coefficient inverse problem for a fractional diffusion equation *Inverse Problems* **29** 075013

[112] Mustapha K 2011 An implicit finite-difference time-stepping method for a sub-diffusion equation, with spatial discretization by finite elements *IMA J. Numer. Anal.* **31** 719–39

[113] Mustapha K and McLean W 2013 Superconvergence of a discontinuous Galerkin method for fractional diffusion and wave equations *SIAM J. Numer. Anal.* **51** 491–515

[114] Nigmatullin R R 1986 The realization of the generalized transfer equation in a medium with fractal geometry *Phys. Stat. Sol. B* **133** 425–30

[115] Pazy A 1983 *Semigroups of Linear Operators and Applications to Partial Differential Equations* (Berlin: Springer-Verlag)

[116] Podlubny I 1999 *Fractional Differential Equations* (San Diego: Academic Press)

[117] Prüss J 1993 *Evolutionary Integral Equations and Applications* (Basel: Birkhäuser)

[118] Rundell W, Xu X and Zuo L The determination of an unknown boundary condition in a fractional diffusion equation *Appl. Anal.* **92** 1511–1526

[119] Saitoh S, Tuan V K and Yamamoto M 2002 Reverse convolution inequalities and applications to inverse heat source problems *JIPAM. J. Inequal. Pure Appl. Math.* **3** Article 80

[120] Saitoh S, Tuan V K and Yamamoto M 2003 Convolution inequalities and applications *JIPAM. J. Inequal. Pure Appl. Math.* **4** Article 50

[121] Sakamoto K and Yamamoto M 2011 Initial value/boundary value problems for fractional diffusion-wave equations and applications to some inverse problems *J. Math. Anal. Appl.* **382** 426–47

[122] Sakamoto K and Yamamoto M 2011 Inverse source problem with a final overdetermination for a fractional diffusion equation *Math. Control Relat. Fields* **1** 509–518

[123] Samko S G, Kilbas A A and Marichev O I 1993 *Fractional Integrals and Derivatives* (Philadelphia: Gordon and Breach Science Publishers)

[124] Schiff J L 1991 *The Laplace Transform: Theory and Applications* (New York: Springer-Verlag)

[125] Schumer R, Benson D A, Meerschaert M M and Baeumer B 2003 Fractal mobile/immobile solute transport *Water Res. Research* **39** 1296

[126] Sun Z-Z and Wu X 2006 A fully discrete difference scheme for a diffusion-wave system *Appl. Numer. Math.* **56** 193–209

[127] Thomee V 2006 *Galerkin Finite Element Methods for Parabolic Problems (Springer Series in Computational Mathematics vol 25)* (Berlin: Springer-Verlag)

[128] Titchmarsh E C 1926 The zeros of certain integral functions *Proc. London Math. Soc.* **2** 283–302

[129] Yamamoto M and Zhang Y 2012 Conditional stability in determining a zeroth-order coefficient in a half-order fractional diffusion equation by a Carleman estimate *Inverse Problems* **28** 105010

[130] Zayernouri M and Karniadakis G E 2014 Exponentially accurate spectral and spectral element methods for fractional ODEs *J. Comput. Phys.* **257** 460–80

[131] Zhang Y-N, Sun Z-Z and Wu H-W 2011 Error estimates of Crank-Nicolson-type difference schemes for the subdiffusion equation *SIAM J. Numer. Anal.* **49** 2302–22

[132] Zhang Y and Xu X 2011 Inverse source problem for a fractional diffusion equation *Inverse Problems* **27** 035010

[133] Zhao J, Xiao J and Xu Y 2013 Stability and convergence of an effective finite element method for multiterm fractional partial differential equations *Abstr. Appl. Anal.* 857205

[134] Zhou Y 2014 *Basic Theory of Fractional Differential Equations* (Singapore: World Scientific)